Title
Naturally Occurring Melanin Synthesis Regulators and Their Modes of Action

Author
Satooka, Hiroki

Publication Date
2011

Peer reviewed|Thesis/dissertation

Naturally Occurring Melanin Synthesis Regulators and Their Modes of Action

By

Hiroki Satooka

A dissertation submitted in partial satisfaction of the

requirements for the degree of

Doctor of Philosophy

in

Molecular Toxicology

in the

Graduate Division

of the

University of California, Berkeley

Committee in charge:

Professor Isao Kubo, Chair
Professor Leonard F. Bjeldanes
Assistant Professor Jen-Chywan (Wally) Wang
Professor Terry Machen

Fall 2011

Naturally Occurring Melanin Synthesis Regulators and
Their Modes of Action

by

Hiroki Satooka

Abstract

Naturally Occurring Melanin Synthesis Regulators and
Their Modes of Action

by

Hiroki Satooka

Doctor of Philosophy in Molecular Toxicology

University of California, Berkeley

Professor Isao Kubo, Chair

The effect of various naturally occurring and structurally related chemical compounds on mushroom tyrosinase and B16-F10 melanoma cells were examined. For each natural product or related compound, the detailed mechanism of regulatory effect on tyrosinase-catalyzed melanin synthesis was elucidated, and occasionally, the optimal mechanism of cytotoxicity on B16 melanoma cells exhibited by chemical compounds are evaluated. Arbutin (hydroquinone-o-β-D-glucopyranoside), a well-known depigmenting reagent, was oxidized by tyrosinase to the corresponding *o*-quinone with an extremely slow rate, and this reactive metabolite caused melanocytotoxicity, resulting in the antimelanogenic effect. Another monophenol derivative, thymol (5-methyl-2-isopropylphenol), on the other hand, did not act as either a substrate or an inhibitor, but it acted as a redox inhibitor, due to its prooxidative property, to disrupt the melanin formation. This prooxidant effect also triggered the prooxidative-related toxicity on melanoma cells. In the case of cardols (5-alkylresorcinol), naturally occurring resorcinolic lipid, hydrophilic head, and hydrophobic tail concept was applied to the mechanism of both tyrosinase inhibition and cytotoxicity. More specifically, resorcinol moiety *quickly* and *reversibly* bound to binuclear copper of tyrosinase, and then, hydrophobic tail portion *slowly* and *irreversibly* interacted with the hydrophobic portions proximate to the active site of the enzyme. However, this inhibitory mechanism was only observed when the hydrophobic alkyl chain was long enough to interact with the hydrophobic portion of the enzyme. In the case of cellular effect, cardol ($C_{15:3}$) preferentially acted as a surfactant to disrupt the function of cellular membrane while cardol ($C_{5:0}$) produced prooxidant-related toxicity. Alkyl-3,5-dihydroxybenzoate and 3,5-dihydroxyphenyl alkanoate with various lengths of alkyl chain were examined to clarify the effect of the lengths of alkyl chain on inhibitory and toxic effect. In the cases of both alkyl-3,5-dihydroxybenzoate and 3,5-dihydroxyphenyl alkanoate, basically, both compounds with alkyl chain longer than C9 caused a two-step inactivation on mushroom tyrosinase. In addition, alkyl-3,5-dihydroxybenzoate acted as a surfactant to cause cytotoxicity while 3,5-dihydroxyphenyl

alkanoate were decomposed in the growth medium. Alkyl-3,5-dihydroxybenzoate, interestingly and importantly, inhibited melanogenesis without affecting any cell growth, which is due to the combined effect of the two-step tyrosinase inactivation and surfactant activity. Finally, the effect of polyphenolic compounds, resveratrol and luteolin, were subjects to elucidate their effect on tyrosinase and B16 melanoma cells. In both cases, tyrosinase oxidized them to the corresponding *o*-quinone. However, in the case of resveratrol (*trans*-3,5,4'-trihydroxystilbene), the corresponding *o*-quinone irreversibly interacted with tyrosinase, indicating that k_{cat} type (suicide) inhibition was the mechanism of inhibition. Resveratrol did not show any toxicity up to 200 μM, and at 200 μM, melanogenesis was suppressed with the addition of resveratrol. Luteolin (2-(3,4-Dihydroxyphenyl)-5,7-dihydroxy-4-chromenone), on the other hand, the corresponding *o*-quinone did not inhibit tyrosinase but did act as a redox cycler, which oxidized leukodopachrome to dopachrome when luteolin was coexisted L-DOPA and tyrosinase. In the case of luteolin, luteolin *o*-quinone was also an active principle for the toxicity. Through the investigation, the biological significance of each molecule was observed. Based on the dynamic perspective and the biological significance, the possible utilization of these chemicals was also discussed.

This dissertation is dedicated to
my parents, Yoshihiro and Fujiko
and
my grandfathers, Kageyoshi and Masatoshi

TABLE OF CONTENTS

LIST OF FIGURES, TABLES, AND SCHEMES

Introduction

Chapter 1

Chapter 2

Chapter 3

ACKNOWLEDGEMENT

I would like to express my deep thanks to Professor Isao Kubo for his support and mentoring. I am grateful for him for giving me the opportunity to, first, work in his lab since 2007 when I was an undergraduate student, and then pursue into my Ph.D. work at UC Berkeley. I am always inspired by him and his approach to science. These invaluable experiences will be a fundamental background for my future journey. Again, I appreciate Professor Isao Kubo deeply.

I thank Professor Leonard F. Bjeldanes, Assistant Professor Wally Wang, and Professor Terry Machen for their advices, encouragements, and for many hours of contribution to meaningful discussions; especially, for the qualifying examination and further dissertation progress.

I would like to thank Dr. Kuniyoshi Shimizu for his significant contribution to GC-MS measurements of thyme oil and fruitful discussion of tyrosinase inhibitory mechanism of cardols. I also thank Dr. Ken-ichi Nihei for the synthesis of all resorcinolic lipids including alkyl-3,5-dihydroxybenzoate, 3,5-dihydroxyphenyl alkanoate, alkyl-3-dihydroxybenzoate, and alkyl-2,4-dihydroxybenzoate. I would also like to thank Dr. Shimizu, Dr. Nihei, and Dr. Teruhiko Nitoda for their significant effort to preliminary data of luteolin against tyrosinase and B16 melanoma cells collected during their postdoctoral training at UC Berkeley. Many thanks go to Andrew Yang for assistance with Fluorescence spectrometer for DFCH-DA assays. I also thank Yui Kitamura for a significant contribution to checking grammatical errors of my dissertation.

I also offer many thanks to my friends in U.S. and Japan for the various journeys outside the lab. Lastly, I sincerely thank my family in Japan for their encouragements and supports in many ways. I appreciate everything they have done for me in my entire life.

Introduction

Melanin and Melanogenesis

Melanin is a biopigment, which is a polymer of oxidized products of L-tyrosine. There are two types of melanin; namely, eumelanin and pheomelanin. Eumelanin is a black/brown pigmented molecule which is a cross-linked polymer molecule of 5,6-dihydroxyindole (DHI) and 5,6-dihydroxyindole-2-carboxylic acid (DHICA) while pheomelanin, composed of benzothiaine, is a colored one (*1*). Even though the entire function of melanin in human has not been identified yet, several biological functions of melanin have been reported previously: a redox buffer (free radical scavenger), a cation binding material, and a radiation sink (photoprotection and photosensitization to protect from UV radiation) (*2*). In other organisms such as a fungus or insect (except spiders), melanin also has important roles as pigments (*3*). Thus, melanin biosynthesis is one of the ubiquitous biochemical processes in nature.

Melanogenesis is the process of melanin production in melanocytes, which is located in the bottom layer of the epidermis in the skin. Melanocytes are also located in hair follicles, eyes or even brain. In melanocytes, there are special organelles called melanosomes, and they are derived from Golgi or early endosome through cellular surface (*4*). Melanosomes are highly mobile, and their actions are controlled by hormonal signals. They are tracked by microtubules and motor proteins to transfer to the periphery of the cells (*5*). This tracking mechanism of melanosomes helps the insoluble (insoluble in water-based or organic solvent) polymer compound, melanin, to be transferable to other cells such as keratinocytes or brain cells, from melanocytes. Seiberg *et al*. previously reported that skin lightening effect resulted from the inhibition of melanosome transfer (*6*). Interestingly, different racial skin colors are primarily determined by difference in the number, size, and the distribution of melanosomes. Hence, melanin is the key factor of skin, hair and eyes colors. (*7, 8*). Furthermore, dopamine, one of the most important neurotransmitters in organisms is also synthesized from L-tyrosine and L-DOPA within melanosomes, and it is transferred to neuronal cells (*9*). Therefore, melanogenesis is a significantly important process in most living organisms.

Tyrosinase

Melanogenesis is mediated by several enzymes such as tyrosinase (EC 1.14.18.1), tyrosinase-related protein-1 and -2 (TRP-1 and TRP-2) (*10*). In melanin biosynthesis, tyrosinase is the key enzyme. This copper-containing multi-functional oxidase catalyzes two reactions (Eqn. **a** and **b**). Monophenolase activity of tyrosinase catalyzes the *ortho*-hydroxylation of L-tyrosine to L-dihydroxyphenylalanine (L-DOPA) (Eqn. **a**), and diphenolase (or catecholase) activity of that catalyzes the oxidation of L-DOPA to dopaquinone (Eqn. **b**) (*11*).

$$\text{monophenol} + 1/2\ O_2 \rightarrow \textit{ortho}\text{-diphenol} + H_2O \quad (\mathbf{a})$$

$$\textit{ortho}\text{-diphenol} + 1/2\ O_2 \rightarrow \textit{ortho}\text{-quinone} + H_2O \quad (\mathbf{b})$$

The reaction from the dopaquinone to dopachrome is proceeded non-enzymatically. The relatively stable intermediate compound, dopachrome, then undergoes chemical and enzymatic processes to form eumelanin (*12, 13*). Subsequently, dopaquinone is also

reacted with thiols such as L-cysteine or glutathione to be a pheomelanin (*13*). This series of reaction are known as the Raper-Mason Pathway (Figure 1) (*14, 15*). The first two steps, L-tyrosine to L-DOPA and L-DOPA to dopaquinone, are the rate-limiting steps in melanogenesis. Hence, the regulation of these two reactions significantly impacts on the melanin biosynthesis, respectively (*15, 16*). In Figure 1, the addition of hydroxyl group on *ortho*-position of L-tyrosine is relatively an unfavorable reaction rather than the oxidation of catechol to *ortho*-quinone; hence, the first catalysis (L-tyrosine to L-DOPA) is usually much slower than the latter case. Thus, in the reaction of monophenolase, the induction phase (lag phase) is usually observed (*17*). The rate of tyrosinase-catalyzed monophenol oxidation is enhanced with the addition of cofactors, which is observed as a disappearance of the lag phase. The well-known cofactors are L-DOPA and L-ascorbic acid (vitamin C) (*18, 19*). The proton donation of cofactors to tyrosinase active site seems to change its conformation from resting to active form. This conformational change is one key feature of tyrosinase activity and of its regulatory mechanisms (*20, 21*).

Various diversities of tyrosinase have been discovered and studied including bacteria, fungi, plants, crustaceans, insects, vertebrates, and mammals (*22*). Mushroom tyrosinase isolated from *Agaricus bisporus* (known as a common mushroom) has been studied extensively for its kinetics, inhibitors, and so on, due to its availability and convenience. Because of the high degree of hydrophobicity of tyrosinase, the X-ray crystallization of the enzyme has not been reported yet. However, bacterial tyrosinase was recently isolated for its X-ray crystal structure (*23, 24*). The crystal structure of tyrosinase gave the information to understanding the metal complex and the role of amino acid residues surrounding in its active site; however, many questions still have been unclear.

Binuclear copper of tyrosinase active site is μ-η^2:η^2-peroxodicopper(II) active site coordination (Type III Copper) (Figure 2) (*11, 25*). As well as tyrosinase, hemocyanin and catechol oxidase are type III copper enzymes, and share the same bridging mode. This μ-η^2:η^2 side-on peroxo complex reacts very differently from other types of binuclear peroxo-dicopper(II) complexes (*26*). Depending on the oxidation states of this binuclear copper coordination, tyrosinase allows three different conformations, namely E_{met}, E_{deoxy} and E_{oxy} (Figure 3) (*27*). Each state of tyrosinase has a unique coordination and corresponding catalytic functions. The oxidation of monophenol to *o*-diphenol and *o*-diphenol to *o*-quinone are dependent on several factors: the oxidation states of copper, structural arrangement of copper and oxygen and contribution of imidazole provided by histidine (and maybe other amino acids residue surrounded) in tyrosinase active site (*23, 24, 28-30*).

Monophenolase activity of tyrosinase is quite unique and powerful. However, the mechanism is still unclear and debatable. Figure 4 shows the possible mechanism of monophenolase and diphenolase activities of tyrosinase activity. To activate molecular oxygen for monophenol hydroxylation, dioxygen has to be bound to deoxy form, containing Cu(I), of tyrosinase. This binding event activates binuclear copper to form

oxy-tyrosinase with Cu(II) state. During the reaction, monophenol substrate has to be bound to copper-dioxygen complex and oxygen atom is transferred to *ortho*-position to the hydroxyl group of monophenol bound to active site. In *oxy* state of tyrosinase, one copper (CuA) exhibits a tetragonal-pyramidal geometry, with two binding of hydroxide and two histidine residues in equatorial and one histidine residue in an axial position (*23, 31*). The other copper (CuB) also holds similar geometry. Decker and his colleagues importantly indicated that *trans*-position to axial histidine of CuA (and also CuB) is freely accessible from the substrate binding pocket (*32*). Thus, as a substrate binding, a monophenol substrate approaches towards the *trans*-position to axial histidine of CuA in oxy-tyrosinase with the preorientation through a hydrophobic interaction to the equatorial histidine residue of CuA (or CuB). For the hydroxylation of monophenol substrate, the O-O axis in the active site rotates to point toward the phenolic ring, and then electrophilic attack on the aromatic ring (*31*). The electrophilic substitution mechanism was further supported by Itoh and Fukuzaki. They found that "neutral" phenol substrates gave C-C or C-O coupling dimer as products rather than catechol (actual product of tyrosinase reaction) when they were treated with μ-η^2:η^2-peroxodicopper(II) complex as a model system. This suggests that oxygenation of "neutral" phenol involves radical mechanism; the peroxo complex of tyrosinase acts as a one-electron oxidant to produce a phenoxy radical. However, the oxygenation reaction of "phenolate" (deprotonated form of phenol) by the side-on peroxo complex involves neither electron transfer nor hydrogen atom transfer but proceeds via an ionic mechanism such as "an electrophilic aromatic substitution mechanism." In this case, successful C-O bond was generated (Figure 5). In the case of "phenolate," formation of the phenoxy radial is prohibited due to the energetic uphill while the anionic reaction is preferred (*29*). Hence, the state of the substrate (Neutral vs. Phenolate) gives dramatic difference in products, and active site environment has great importance for the catalytic activity of tyrosinase. Several mechanisms of hydroxylation have been also proposed; however, the mechanism of the step is still under investigation.

Molecular Mechanism of Melanogenesis

Transcription of melanogenic enzymes is often controlled by hormonal signals (*33*). Melanocyte stimulating hormone (MSH) is one of the peptide hormones, synthesized and secreted from the proopiomelanocortin (POMC) gene promoter in keratinocytes cells or opiomelanotropinergic cells of the pair intermediate of the pituitary gland and by neurons in the central nervous system (*34*). α-MSH, one class of MSH, stimulates melanocortin-1 receptor (MC1R), located at the melanocytic plasma membrane. It leads to the activation of adenylyl cyclase to increase the level of cAMP, followed by the activation of protein kinase A (PKA). In downstream event, PKA induces the transcription of microphthalmia-associated transcription factor (MITF). MITF is fully activated by MAP kinase cascade, which leads to the activation of the transcription of melanogenic proteins. The synthesized melanin and melanosomes are transported to initially stimulating keratinocytes (Figure 6) (*35*).

UV B radiation is directly absorbed by DNA molecules, leading to DNA damage. This DNA damage (or other stress factors) also stimulates melanogenesis. Treatment of melanocytes with the agents that cause excessive DNA damage, enhances melanogenesis (*36, 37*). UV-induced melanocytes or melanoma is in the absence of high α-MSH level; however, they show a strong melanogenic response. Moreover, UV induced DNA damage induces H_2O_2, known as a p53 activator. Previous study shows that p53 also stimulates tyrosinase transcription. Hence, these pathways may have a critical role in the induction of melanogenesis in UV-irradiated melanocytes (*38, 39*).

Mammalian tyrosinase is the copper containing glycoprotein which is located on the melanosomal membrane. The catalytic domain is faced toward the inner melanosomal domain, and two serine residues in the cytoplasmic domain of melanosome. The activation of this enzyme requires phosphorylation of these two serine residues by a PKC-β_α, followed by the activation through the ligand-activated cell surface receptors and UV radiation (*35*). Thus, the regulation of melanogenesis is highly regulated in the molecular and enzymatic level.

Lastly, melanosomes are "tissue-specific lysosome-related organelles," synthesized in the endosomal reticulum. Matured melanosomes are translocated along the microtubule to keratinocytes. This translocation is facilitated by both dynein and kinesin motor proteins, and also other peripheral proteins. Several molecular machineries involve the sorting process of melanosomes. The sorting is highly regulated and the protein complex called BLOC-1 exhibits a role of the regulator. The mechanism of the regulation of melanosome sorting is complex; however, the advances in understanding the melanosome biology may allow for a new sight of understand in other cell-specific lysosome organelles (*4*).

Applications of Melanogenesis Regulators

Alterations in melanin synthesis occur in many disease states such as melanoma, melasma, or Parkinson's disease, because of the various functions of melanin in living systems. Melanoma is one of the most commonly diagnosed diseases (*40, 41*) and its incidence is raising a world-wide concern (*42*). Melanoma is less common than other types of skin cancer; however, it causes the highest rate of death in skin cancer (*43*). During melanoma neoplasia, the pigmentation is uncontrolled, and the over-expression of melanin causes irregulared skin color. Melanoma is cured in most cases by surgery, but once the metastatic phase developed, it is almost always fatal. Systemic chemotherapy is often the only viable treatment, but the lack of selective cytotoxicity often leads to intolerable side effects (*44*). Moreover, melanoma has one of the worst response rates to chemotherapy of all neoplasisas (*45*). Thus, understanding the regulatory mechanism of melanogenesis plays a critical role in developing the treatment of melanin-related disorders.

Melanogenesis regulators (inhibitors or activators) can be used for many other purposes. As described, in various living systems, melanin is responsible for pigmentation and other functions such as chelation. However, undesirable browning is a

considerable problem in food industries or for cosmetic users. Furthermore, toxic oxidized products are commonly generated in the melanin synthetic pathway; for instance, high lipid content fruits such as avocado develop the toxic oxide products in the browning process (*46*). Thus, antibrowning reagents are frequently used. Previously most widely spread method for antibrowning was the use of sulfiting agents (*47*), but Food and Drug Administration has banned sulfate agent for fruits and vegetables (*48*). As the purpose of applications, naturally occurring substances are usually more favorable than synthetic ones. The most common natural antibrowning agent is ascorbic acid. However, the effect of ascorbic acid against enzymatic oxidation is temporary since it is chemically oxidized to non-functional form, dehydroascorbic acid (*49*). Hence, immediate finding for a replacement of antibrowning reagents is essential. On the other hand, melanogenesis activators can also be used in a different sense since melanins play a crucial role in the absorption of free radicals generated within the cytoplasm and in shielding the host from various types of ionizing radicals, including UV irradiation. This role unfortunately seems destined to become even more critical due to the alarming predicted increases in incident UV at the Earth's surface by recent stratospheric ozone depletion. In fact, light-skinned people usually have a lower level of melanin, especially eumelanin (*33*), and have a lower level of protection against UV radiation than dark-skinned people. Those people who absorb a high level of UV radiation are easier to get skin tumors such as melanoma. Hence, the melanogenic activators from natural products are possibly used as major active components of UV-blocker reagents or sun-tanning oils, which reduce the risk of skin cancers. These problems and aspects prompt us to search safer and more stable melanin formation regulators from natural sources.

Finally, the clear explanations of their toxic mechanism (if they show toxicity) are also required as long as they are used for the general application. Furthermore, because melanogenesis is one type of defense systems of skin, the advance in melanogenesis regulations may allow us to better understand other defense systems such as apoptosis or stress response. However, the regulatory mechanism of melanogenesis has been poorly understood. The basic concepts how small molecules involve in the regulatory systems, give the detailed picture of the biological functions/mechanisms.

Natural Products

Natural product science has a long history. Even though anthropogenic chemicals have been heavily used in many fields, naturally occurring compounds still have played many roles in agriculture, medicine, and nutrition; many naturally occurring chemicals are discovered and developed as medicines, pesticides, or food preservatives. Especially, nowadays, the underestimation of the safety, due to poor understanding of newly synthesized chemicals, becomes more critical (*50*). On the other hand, the advantage of utilization of natural products rather than synthetic chemicals is the enormous amount of data collected for hundreds of thousands of years, which is a fundamental resource for current pharmacology, medicinal chemistry and many other fields. For instance, many chemotherapeutic drugs are commonly designed based on the

functions of natural products. Thus, linking to modern biological science/technology offers the development of new fields of natural product utilization.

FIGURES

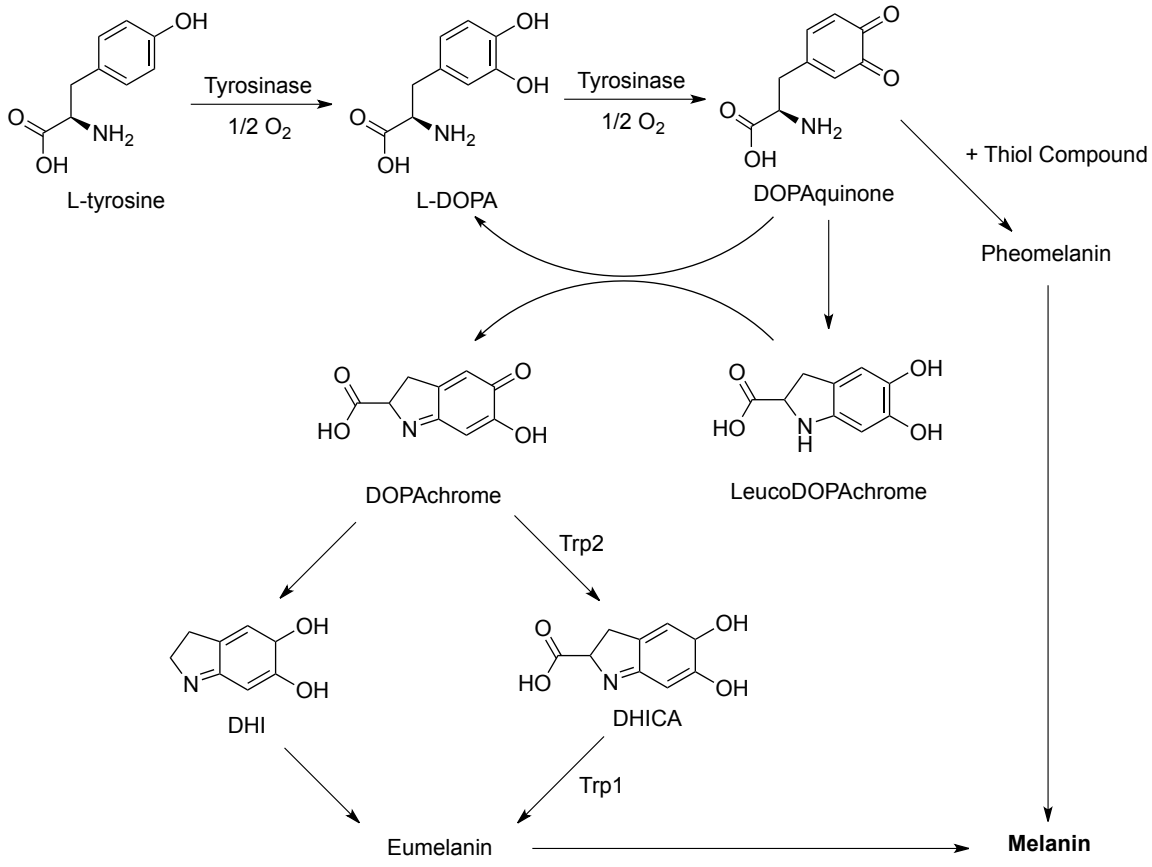

Figure 1. Raper-Mason melanin synthetic pathway.

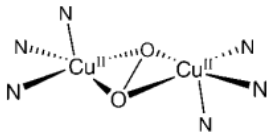

Figure 2. Structure of μ-η^2:η^2-peroxodicopper(II) complex of tyrosinase.

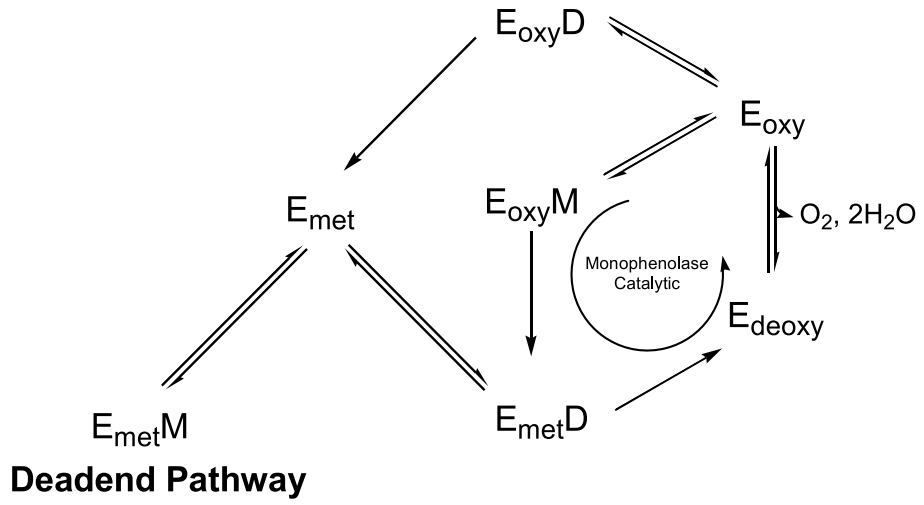

Figure 3. Three different states of tyrosinase and the conformational change pathway.

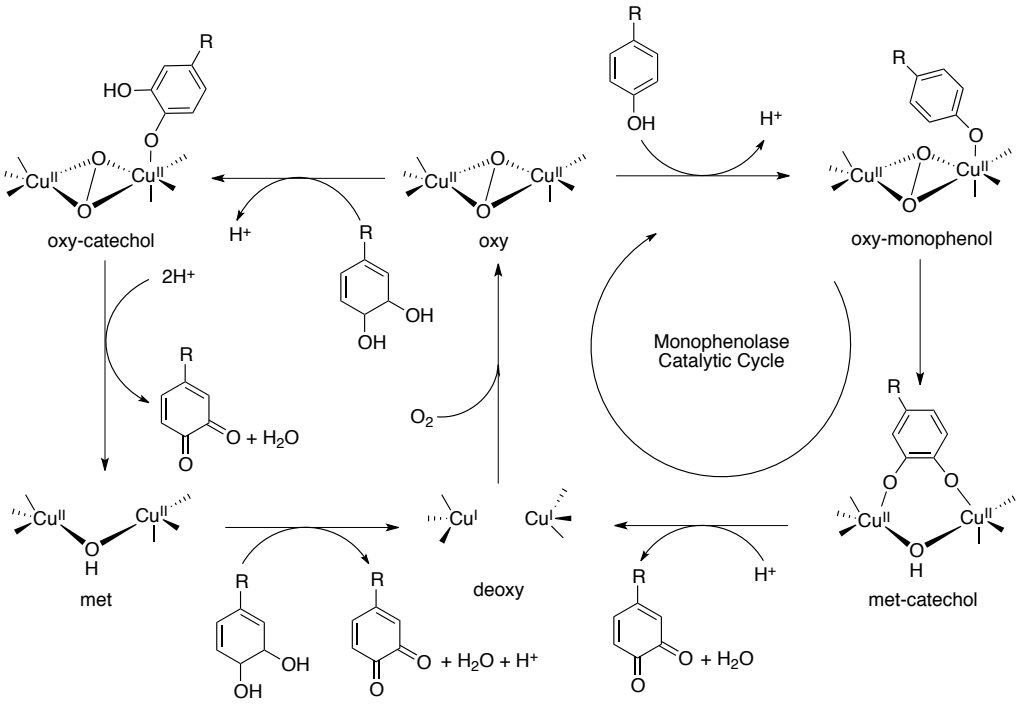

Figure 4. Catalytic cycles of tyrosinase. Right cycle represents monophenol catalytic acaction.

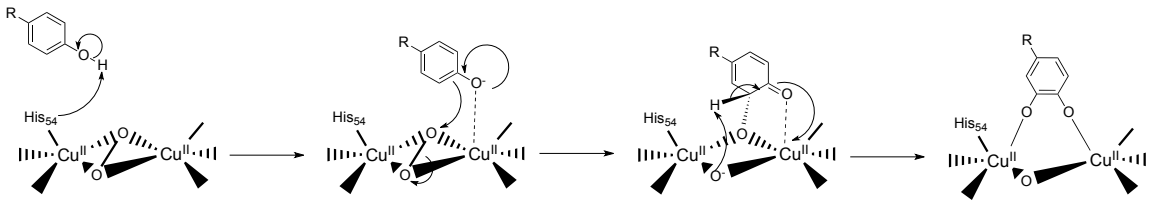

Figure 5. Formation of C-O bridge between phenol substrate and μ-η^2:η^2-peroxodicopper(II) complex by electrophilic aromatic substitution reaction.

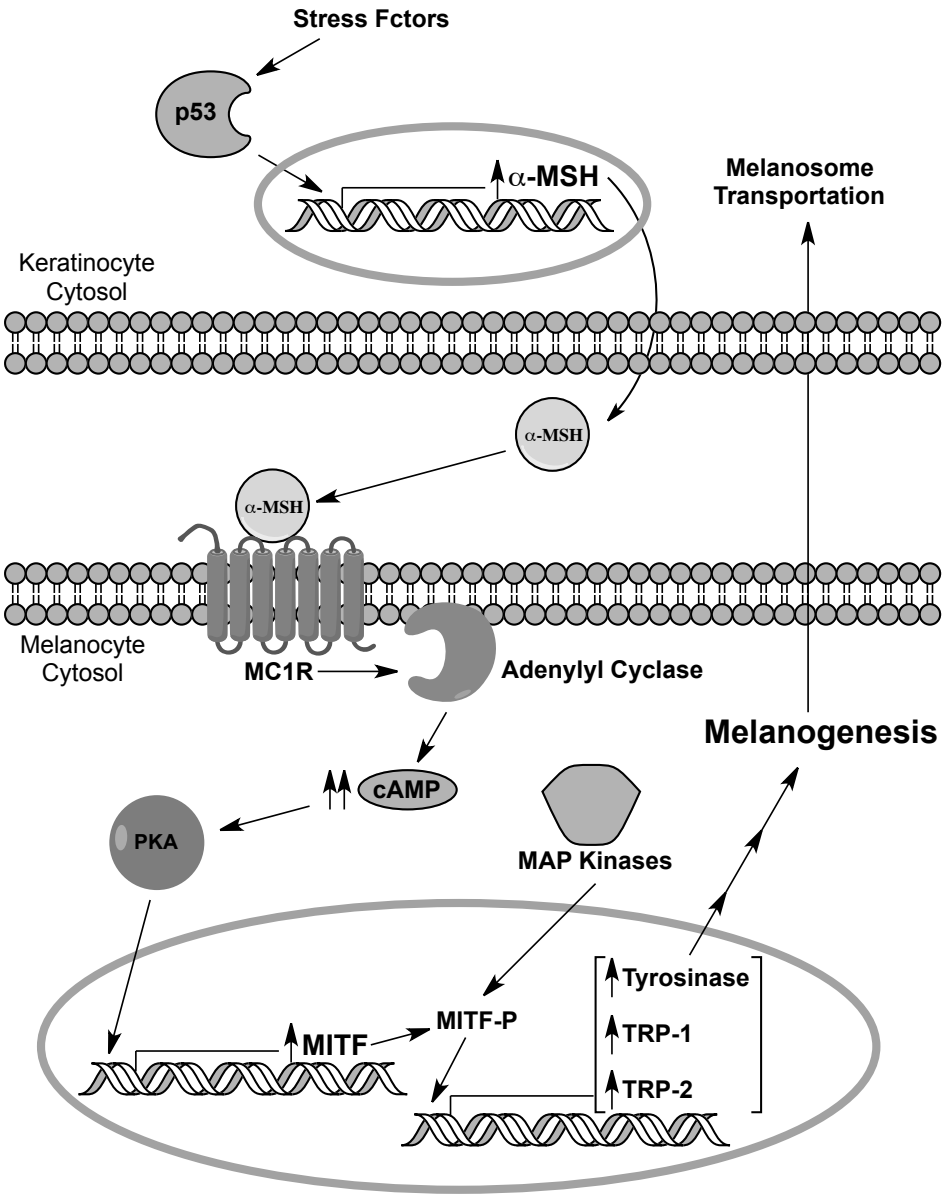

Figure 6. Molecular Mechanism of regulation of melanogenic enzymes.

REFERENCES

1. Ito, S.; Wakamatsu, K., Chemistry of mixed melanogenesis - Pivotal roles of dopaquinone. *Photochem. Photobiol.* **2008,** 84, (3), 582-592.
2. Riley, P. A., Melanogenesis and melanoma. *Pigm. Cell Res.* **2003,** 16, (5), 548-552.
3. Oxford, G.; Gillespie, R., Evolution and ecology of spider coloration. *Ann. Rev. Entomol.* **1998,** 43, (1), 619-643.
4. Raposo, G.; Marks, M. S., Melanosomes — dark organelles enlighten endosomal membrane transport. *Nat. Rev. Mol. Cell Biol.* **2007,** 8, (10), 786-797.
5. Virador, V. M.; Muller, J.; Wu, X.; Abdel-Malek, Z. A.; Yu, Z. X.; Ferrans, V. J.; Kobayashi, N.; Wakamatsu, K.; Ito, S.; Hammer, J. A., Influence of α-melanocyte-stimulating hormone and ultraviolet radiation on the transfer of melanosomes to keratinocytes. *FASEB J.* **2002,** 16, (1), 105.
6. Seiberg, M.; Paine, C.; Sharlow, E.; Andrade-Gordon, P.; Costanzo, M.; Eisinger, M.; Shapiro, S. S., Inhibition of Melanosome Transfer Results in Skin Lightening1. *J. Invest. Dermatol.* **2000,** 115, (2), 162-167.
7. Gerson, D. E.; Szabó, G., The effects of single gene substitution on the mammalian melanocyte system—a qualitative and quantitative histological study in the C57BL and DBL mice. *Am. J. Phys. Anthropol.* **1969,** 31, (3), 363-381.
8. Thong, H. Y.; Jee, S. H.; Sun, C. C.; Boissy, R., The patterns of melanosome distribution in keratinocytes of human skin as one determining factor of skin colour. *Brit. J. Dermatol.* **2003,** 149, (3), 498-505.
9. Elsworth, J. D.; Roth, R. H., Dopamine Synthesis, Uptake, Metabolism, and Receptors: Relevance to Gene Therapy of Parkinson's Disease* 1. *Exp. Neurol.* **1997,** 144, (1), 4-9.
10. Kippenberger, S.; Loitsch, S.; Solano, F.; Bernd, A.; Kaufmann, R., Quantification of tyrosinase, TRP-1, and TRP-2 transcripts in human melanocytes by reverse transcriptase-competitive multiplex PCR-regulation by steroid hormones. *J. Invest. Dermatol.* **1998,** 110, (4), 364-367.
11. Kitajima, N.; Moro-oka, Y., μ-η^2:η^2-Peroxide in Biological Systems. *J. Chem. Soc. Dalton.* **1993**, 2665-2671.
12. Sanchez-Ferrer, A.; Rodriguez-Lopez, J.; Garcia-Canovas, F.; Garcia-Carmona, F., Tyrosinase: a comprehensive review of its mechanism. *BBA-Protein Struct. M.* **1995,** 1247, (1), 1-11.
13. Seo, S.; Sharma, V.; Sharma, N., Mushroom tyrosinase: Recent prospects. *J. Agr. Food Chem.* **2003,** 51, (10), 2837-2853.
14. Sarangarajan, R.; Apte, S. P., The polymerization of melanin: a poorly understood phenomenon with egregious biological implications. *Melanoma Res.* **2006,** 16, (1), 3.
15. Raper, H., The aerobic oxidases. *Physiol. Rev.* **1928,** 8, (2), 245-282.

16. Hearing, V. J., Mammalian monophenol monooxygenase (tyrosinase): Purification, properties, and reactions catalyzed. *Methods Enzymol.* **1987,** 142, 154-165.
17. Falguera, V.; Gatius, F.; Pagán, J.; Ibarz, A., Kinetic analysis of melanogenesis by means of Agaricus bisporus tyrosinase. *Food Res. Int.* **2010,** 43, (4), 1174-1179.
18. Hearing Jr, V. J.; Ekel, T. M.; Montague, P. M.; Nicholson, J. M., Mammalin tyrosinase. Stoichiometry and measurement of reaction products. *BBA-Enzymol.* **1980,** 611, (2), 251-268.
19. Ros, J.; Rodriguez-Lopez, J.; Garcia-Canovas, F., Effect of L-ascorbic acid on the monophenolase activity of tyrosinase. *Biochem. J.* **1993,** 295, (Pt 1), 309.
20. Devi, C. C.; Ramaiah, A.; Tripathi, R. K., pH-dependent interconvertible allosteric forms of murine melanoma tyrosinase. *Eur. J. Biochem.* **1987,** 166, (3), 705-711.
21. Espín, J. C.; Wichers, H. J., Kinetics of activation of latent mushroom (*Agaricus bisporus*) tyrosinase by benzyl alcohol. *J. Agr. Food Chem.* **1999,** 47, (9), 3503-3508.
22. Solomon, E.; Sundaram, U.; Machonkin, T., Multicopper oxidases and oxygenases. *Chem. Rev.* **1996,** 96, (7), 2563-2605.
23. Matoba, Y.; Kumagai, T.; Yamamoto, A.; Yoshitsu, H.; Sugiyama, M., Crystallographic evidence that the dinuclear copper center of tyrosinase is flexible during catalysis. *J. Biol. Chem.* **2006,** 281, (13), 8981-8990.
24. Osako, T.; Ohkubo, K.; Taki, M.; Tachi, Y.; Fukuzumi, S.; Itoh, S., Oxidation Mechanism of Phenols by Dicopper-Dioxygen (Cu2/O2) Complexes. *J. Am. Chem. Soc.* **2003,** 125, (36), 11027-11033.
25. Kitajima, N.; Fujisawa, K.; Morooka, Y.; Toriumi, K., .mu.-.eta.2:.eta.2-Peroxo binuclear copper complex, [Cu(HB(3,5-(Me2CH)2pz)3)]2(O2). *J. Am. Chem. Soc.* **1989,** 111, (24), 8975-8976.
26. Hatcher, L. Q.; Karlin, K. D., Oxidant types in copper–dioxygen chemistry: the ligand coordination defines the Cu_n-O 2 structure and subsequent reactivity. *J. Biol. Inorg. Chem.* **2004,** 9, (6), 669-683.
27. Jolley, R. L.; Evans, L. H.; Makino, N.; Mason, H. S., Oxytyrosinase. *J. Biol. Chem.* **1974,** 249, (2), 335.
28. Itoh, S.; Kumei, H.; Taki, M.; Nagatomo, S.; Kitagawa, T.; Fukuzumi, S., Oxygenation of Phenols to Catechols by A (μ-η^2:η^2-Peroxo)dicopper (II) Complex: Mechanistic Insight into the Phenolase Activity of Tyrosinase. *J. Am. Chem. Soc.* **2001,** 123, (27), 6708-6709.
29. Itoh, S.; Fukuzumi, S., Monooxygenase Activity of Type 3 Copper Proteins. *Acc. Chem. Res.* **2007,** 40, (7), 592-600.
30. Pfiffner, E.; Lerch, K., Histidine at the active site of Neurospora tyrosinase. *Biochemistry* **1981,** 20, (21), 6029-6035.
31. Decker, H.; Schweikardt, T.; Tuczek, F., The First Crystal Structure of Tyrosinase: All Questions Answered? *Angew. Chem. Int. Edit.* **2006,** 45, (28), 4546-4550.

32. Decker, H.; Tuczek, F., Tyrosinase/catecholoxidase activity of hemocyanins: structural basis and molecular mechanism. *Trends Biochem. Sci.* **2000,** 25, (8), 392-397.
33. Montagna, W.; Prota, G.; Kenney, J., J. A. , *Black Skins*. Academic Press, Inc: 1993.
34. O'Donohue, T. L.; Dorsa, D. M., The opiomelanotropinergic neuronal and endocrine systems. *Peptides* **1982,** 3, (3), 353-395.
35. Park, H. Y.; Kosmadaki, M.; Yaar, M.; Gilchrest, B. A., Cellular mechanisms regulating human melanogenesis. *Cell. Mol. Life Sci.* **2009,** 66, (9), 1493-1506.
36. Gilchrest, B. A.; Zhai, S.; Eller, M. S.; Yarosh, D. B.; Yaar, M., Treatment of human melanocytes and S91 melanoma cells with the DNA repair enzyme T4 endonuclease V enhances melanogenesis after ultraviolet irradiation. *J. Invest. Dermatol.* **1993,** 101, (5), 666-672.
37. Eller, M. S.; Ostrom, K.; Gilchrest, B. A., DNA damage enhances melanogenesis. *P. Natl. Acad. Sci.* **1996,** 93, (3), 1087.
38. Nylander, K.; Bourdon, J. C.; Bray, S. E.; Gibbs, N. K.; Kay, R.; Hart, I.; Hall, P. A., Transcriptional activation of tyrosinase and TRP-1 by p53 links UV irradiation to the protective tanning response. *J. Pathol.* **2000,** 190, (1), 39-46.
39. Khlgatian, M. K.; Hadshiew, I. M.; Asawanonda, P.; Yaar, M.; Eller, M. S.; Fujita, M.; Norris, D. A.; Gilchrest, B. A., Tyrosinase gene expression is regulated by p53. *J. Invest. Dermatol.* **2002,** 118, (1), 126-132.
40. Siegel, R.; Ward, E.; Brawley, O.; Jemal, A., Cancer statistics, 2011. *CA-Cancer J. Clin.* **2011**.
41. Holme, S.; Malinovsky, K.; Roberts, D. L., Malignant melanoma in South Wales: changing trends in presentation (1986–98). *Clin. Exp. Dermatol.* **2001,** 26, (6), 484-489.
42. Morton, D. L.; Barth, A., Vaccine therapy for malignant melanoma. *CA-Cancer J. Clin.* **1996,** 46, (4), 225-244.
43. Jerant, A. F.; Johnson, J. T.; Sheridan, C. D.; Caffrey, T. J., Early detection and treatment of skin cancer. *Am. Fam. Physician* **2000,** 62, (2), 357-368.
44. Anderson, D. M.; Johnson, L.; Glaccum, M. B.; Copeland, N. G.; Gilbert, D. J.; Jenkins, N. A.; Valentine, V.; Kirstein, M. N.; Shapiro, D. N.; Morris, S. W., Chromosomal assignment and genomic structure of Il15. *Genomics* **1995,** 25, (3), 701-706.
45. Schadendorf, D.; Kern, M. A.; Artuc, M.; Pahl, H. L.; Rosenbach, T.; Fichtner, I.; Nürnberg, W.; Stüting, S.; Von Stebut, E.; Worm, M., Treatment of melanoma cells with the synthetic retinoid CD437 induces apoptosis via activation of AP-1 in vitro, and causes growth inhibition in xenografts in vivo. *J. Cell Biol.* **1996,** 135, (6), 1889.
46. Raju, P. S.; Bawa, A. S., *Food additives in fruit processing.* Blackwell Publishing: Oxford, U.K., 2007.
47. Iyengar, R.; McEvily, A. J., Anti-browning agents: alternatives to the use of sulfites in foods. *Trends Food Sci. Tech.* **1992,** 3, 60-64.

48. Food and Drug Administration, *Chemicalpreservatives*. In Code of Federal Regulations; U.S. GPO: Washington, DC, 1987; Title 21 part.
49. Komthong, P.; Igura, N.; Shimoda, M., Effect of ascorbic acid on the odours of cloudy apple juice. *Food Chem.* **2007,** 100, (4), 1342-1349.
50. Wilson, M. P.; Schwarzman, M. R., Toward a new US chemicals policy: rebuilding the foundation to advance new science, green chemistry, and environmental health. *Environ. Health Persp.* **2009,** 117, (8), 1202.

Chapter 1

Monophenol Derivatives

1.1 Effect of Arbutin on Mushroom Tyrosinase and B16 Melanoma Cells

1.1.1 INTRODUCTION

Arbutin, hydroquinone-o-β-D-glucopyranoside (**1**; see Figure 7 for the structure), has been used as a depigmenting agent in cosmetics in recent years. In our continuing search of melanin formation regulators from plant sources, arbutin was previously characterized from the fresh fruits of California buckeye, *Aesculus californica* (*1*). In spite of the wide usage of arbutin as a depigmenting reagent, the detailed molecular mechanism of depigmenting has not been fully understood. This hydroquinone glucoside was previously reported to show a dose-dependent competitive inhibitory effect on the oxidation of L-DOPA catalyzed by mushroom tyrosinase with IC_{50} of 8.4 mM (*2*). However, our recent finding shows that arbutin actually acts as a poor substrate on tyrosinase (*3*); hence, a common kinetic study does not apply to the case of arbutin. E_{oxy}, the active form of tyrosinase, slowly oxidizes arbutin to release the corresponding *o*-diol. Further oxidation allows releasing corresponding *o*-quinone. The result indicates alternative clues on how arbutin acts as a depigmenting agent. Therefore, further study of arbutin to gain new insight into the biological activities is prompted.

1.1.2 RESULTS

Effect of Arbutin on Mushroom Tyrosinase

Tyrosinase (EC 1.14.18.1) is a key enzyme in melanin synthesis and therefore, tyrosinase inhibitors are expected to inhibit melanin production. Hence, their effects on tyrosinase activity were tested. In our preliminary cell free experiments using mushroom tyrosinase, arbutin (**1**) inhibited the tyrosinase catalyzed oxidation of L-tyrosine. Inhibitory action on tyrosinase activity was measured using UV-vis spectrum and oxygen consumption assays (Figure 8 A and B). In both measurements, tyrosinase activity was dose-dependently inhibited. Furthermore, direct inhibitory interaction of arbutin with tyrosinase was monitored using *N*-acetyl-L-tyrosine. Because of the blockage of intracyclization of *N*-acetyldopaquinone, only the tyrosinase-catalyzed reaction step in melanin synthesis can be examined with *N*-acetyl- L-tyrosine. Arbutin suppressed oxidation of *N*-acetyl-L-tyrosine in the 60 min of reaction period (Figure 9). Typical lag phases due to monophenol oxidation were observed in both control and sample cases. The rate of consumption of *N*-acetyl-L-tyrosine was significantly slowed down with addition of 100 μM arbutin. Interestingly, about 45% of the inhibitory effect by arbutin (the difference of the substrate consumption between control and arbutin sample) was maximized at 35 min, and it was reduced to 35 % at the end of the reaction. This suggested that tyrosinase activity was not completely inactivated by arbutin, but the inhibitory effect was slowly diminished. In fact, the oxidation of substrate such as L-tyrosine was suppressed due to an extremely slow rate of oxidation of arbutin by

tyrosinase (*3*). As a result, the inhibition by arbutin on tyrosinase was reduced when arbutin was slowly oxidized. Thus, it is logical to conclude that arbutin is not a "true" inhibitor.

Cellular Degradation of Arbutin

According to tyrosinase assay results and the previous study (*3*) arbutin could be intracellularly metabolized by tyrosinase. Hence, the experiment was further extended to determine whether arbutin is oxidized intracellularly or not. Cellular homogenate was prepared with the method described in the Materials and Methods section. Briefly, B16-F10 melanoma cells were homogenated using a sonic homogenizer with a designated buffer. Corrected cell lysate was incubated with DMSO or arbutin for 6 hr. For each 2 hr interval, the reaction mixture was corrected in order to be analyzed with reverse-phase HPLC system. In Figure 10, arbutin (peak ***a***; t_R = 10.0 min) was time-dependently decreased. About 15-20 % of arbutin in peak height was degraded after 6 hrs of incubation. It should be noted that the degradation of arbutin was observed *in vitro* experiment with using mushroom tyrosinase, but not with using horseradish peroxidase, which is one of the enzymes corresponding with the xenobiotic metabolism (data not shown). On the basis of cell-free experiments, arbutin was enzymatically modified its structure and this modification could affect cellular functions. Thus, the experiment of arbutin was extended to test for their effects on murine B16-F10 melanoma cells.

Degradation of Arbutin in DMEM

The investigation began with checking the stability of arbutin in Dulbecco's modified Eagle's medium (DMEM). Some molecules had high degradability in this growth medium since the pH of fresh DMEM was relatively basic, and was about pH 9. Arbutin was a subject to test its degradability in this medium since the ester linkage between hydroquinone to glucose might be unstable in this pH range. Hence, the stability of arbutin in DMEM was tested with HPLC analysis (Figure 11). After 60 min of incubation in DMEM, any consumption/decrease of arbutin (peak ***a***; t_R = 14.0 min) was not observed. Thus, arbutin was stable in this medium and it is readily used for the cellular assays.

Effects of Arbutin on B16-F10 Melanoma Cells

The initial goal was to test whether arbutin inhibits melanogenesis in cultured melanocytes without affecting cell growth. Hence, their cell viability was examined first. In this regard, cell viability was determined on the third day for melanocytes using both trypan blue dye exclusion and 3-(4,5-dimethylthiazole-2-yl)-2,5-diphenyltetrazolium bromide (MTT) colorimetric assays. The same result was usually observed by both assays, but the concentration leading to 50 % viable cells lost (IC_{50}) was established by trypan blue assay for steady comparison purpose. The specificity of melanogenesis inhibition was assessed by dividing the melanin content by the number of cells determined by tyrpan blue exclusion. The appropriated concentrations of the test

chemicals were selected by microscopic observation of the preliminary cell viability assay.

The effect of arbutin on B16 melanoma cells was examined first. Highest examined concentration of arbutin was 200 μM. Arbutin dose-dependently suppressed cell viability (Figure 12A), and observed IC_{50} was 105 μM. The cell viability above 12.5 μM was significantly different ($P < 0.01$) from the control. Total melanin production was significantly suppressed ($P < 0.01$) up to 200 μM in a concentration-dependent manner (Figure 12B). It came out that the total melanin production was reduced with the decline of cell viability; that is to say, there is positive correlation between cytotoxic and depigmentation effects. Interestingly, arbutin showed inhibitory effect on cellular melanin production (Figure 12C). At the concentration between 12.5 μM and 50 μM, the cellular melanin synthesis was significantly suppressed ($P < 0.01$). As expected from the previous reports, arbutin showed potent depigmenting effects; however, at the same time, the inhibitory effect was corresponding to the cytotoxic effects.

Hydroquinone and Structurally-related Compounds

Various hydroquinone derivatives and structurally related compounds were tested for the structure activity relationship (SAR) study (all data not shown). Among the tested compounds, hydroquinone (**2**; See Figure 7 for the structure) showed the most potent cytotoxic and antimelanogenic effect on B16-F10 melanoma cells. The effects of hydroquinone on cells had similar patterns to that of arbutin. Observed IC_{50} was 6 μM. Other hydroquinone-related compounds, 4-hydroxyanisole (**3**), and 4-*tert*-butylcatechol (**4**) also showed similar effects; both compounds also showed potent toxicity and dose-dependent antimelanogenic effect up to 200 μM. Observed IC_{50} of 4-hydroxyanisole and 4-*tert*-butylcatechol were 24 μM and 32.5 μM, respectively. Depigmenting effects of all three compounds were positively correlated to their cytotoxic effects as well as arbutin.

Effects of Vitamin C, GSH, BHA and L-cysteine on Arbutin-treated Cells

Surprisingly, observed cytotoxicity of arbutin at 100 μM (approximately equivalent to IC_{50}) was suppressed by 40 % in cell viability with addition of L-ascorbic acid (vitamin C) up to 400 μM (Figure 13A). It is possible for vitamin C to act as a two-electron reductant or a radical scavenger to reduce the toxicity of arbutin. Additionally, glutathione (GSH) was also tested in the same manner. GSH is a major intracellular antioxidant molecule to eliminate oxidative stress, or it also acts as a nucleophile to eliminate reactive electrophiles such as quinones. GSH suppressed the toxic effect of arbutin by 10 % in cell viability on B16-F10 melanoma cells (data not shown). According to the results, it seemed that arbutin toxicity was due to either the transformation of arbutin to toxic oxide by intracellular oxidation or the generation of free radicals (prooxidant effect). In order to determine this postulate, a single electron scavenger, butylated hydroxyanisole (BHA) was also tested for a comparison. As a result, BHA showed no reversed effect on arbutin-treated melanoma cells (Figure 13B). Thus, *o*-quinone formation was involved in the arbutin toxicity. For further confirmation of the involvement of formation of *o*-quinone, L- cysteine was also used. L-cysteine does not

act as either a reducing agent or a radical scavenger but rather acts as a nucleophile to react with a Michael-addition receptor such as quinone-related compounds. Cytotoxicity of arbutin on B16-F10 melanoma cells were reversed by 13 % in cell viability with a treatment of L-cysteine (data not shown). Therefore, arbutin was intracellularly oxidized to convert to corresponding *o*-quinone molecule.

This result was further confirmed with 2',7'-dichlorodihydrofluorescin diacetate (DCFH-DA) assay. After 1hr of incubation with arbutin and DCFH-DA, B16-F10 melanoma cells were assayed to measure intracellular ROS. Up to 200 μM, the total ROS did not show any change as well as cellular viability (data not shown). Thus, ROS per cells also did not change. The primary mechanism of arbutin toxicity, at least, was not due to prooxidative effect in this concentration range.

Morphological Change of B16 Melanoma Cells

Cellular morphological changes of arbutin-treated melanoma cells were microscopically observed. Figure 14A and B represent the cellular morphology of control (DMSO treated) cells and arbutin treated cells, respectively. As seen in the Figures, the density of melanoma cells was significantly reduced by addition of 100 μM arbutin. Further, the dendrites of individual arbutin- treated cell were extended compared to DMSO treatment. Interestingly, after a treatment of equivalent concentration of vitamin C to arbutin-treated cells (100 μM), the morphological change of arbutin-treated cells became similar to that of the control (Figure 14C). As expected; however, this phenomenon was not observed with a treatment of 100 μM of BHA (Figure 14D).

1.1.3 DISCUSSION

Several antibrowning reagents are developed and discovered nowadays. Hydroquinone is one of the most potent depigmenting reagents, studied for long decades. Depigmenting effect of hydroquinone, as previously reported, is due to the potent toxic action to kill the melanin synthetic cells (*4*). In addition to hydroquinone, other two tested hydroquinone-related compounds (4-hydroxyanisole, and 4-*tert*-butylcatechol) are subject to be oxidized by tyrosinase, which leads to cytotoxic and depigmenting effects on the cells (*4-6*). According to our cell-free and cellular experimental data, it is logical to conclude that arbutin is intracellularly oxidized and is converted to corresponding *o*-quinone. The antibrowning effect of arbutin is mainly due to this cytotoxic effect resulting in the formation of *o*-quinone as well as the case of hydroquinone. A previous report and our new findings explain that this corresponding *o*-quinone formation is specifically due to tyrosinase (*3*). Quinone-related compounds are known to cause damage on cellular macromolecules such as DNA, RNA and proteins. Subsequently, a correlation between depletion of glutathione level and antimelanogenesis is previously reported (*7*). Some potent depigmenting reagents such as hydroquinone show their action through depletion of glutathione. (*8, 9*). Thus, there is no doubt that the formation of arbutin-*o*-quinone through two-oxidation reactions of tyrosinase causes

melanocytotoxicity, and then further antimelanogenic effect is possible. (Scheme 1). It is true that tyrosinase activity was inhibited by addition of arbutin in short period (<5 min) *in vitro*; however, arbutin was slowly degraded. Hence, based on the cell- free and cellular experimental results, for the long term effect, the primary mechanism of depigmentation of arbutin is the formation of *o*-quinone but not the inhibition of tyrosinase.

Arbutin showed moderate cytotoxicity on B16-F10 melanoma cells (IC_{50} = 105 μM); several biological reasons lead this "moderate" toxicity of arbutin on cells. One is the very slow rate of oxidation of arbutin by tyrosinase (*3*). This implies that only a small portion of arbutin is oxidized to release *o*-quinone. The secondary reason of moderate toxicity is low absorbing rate of arbutin into the cells. In general, high hydrophilic molecules are less membrane permeable. Thus, because of high hydrophilicity due to glucose molecules in arbutin, there is no doubt that arbutin is poorly absorbed into cells. All of these suggest that arbutin toxicity is much lower than that of hydroquinone.

Safety is a primary concern for many purposes including chemotherapy and cosmetic products. As shown, arbutin showed adverse effects on melanoma cell line. Thus, it is hazardous to use arbutin at high doses; especially, large caution is required for the usage of stale arbutin products, which may contain oxidized arbutin. Many of biological effects of arbutin remain to be defined. Further investigation including cell free experiments and human cell lines, is still under the projects.

DISCLOSURE

The cellular work of arbutin was presented in part at the Poster Session for the 2009 AAAS National Meeting in Chicago, IL.

1.1.4 FIGURES & TABLES

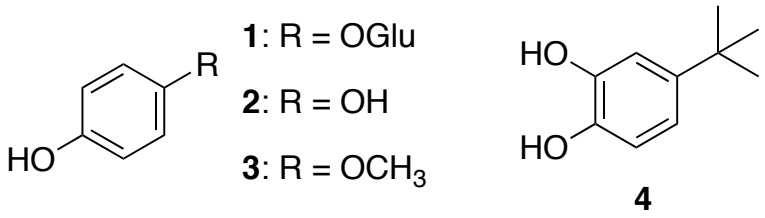

Figure 7. Structure of arbutin (**1**), hydroquinone (**2**), 4-hydroxyanisole (**3**), and 4-*tert*-butylcatechol (**4**).

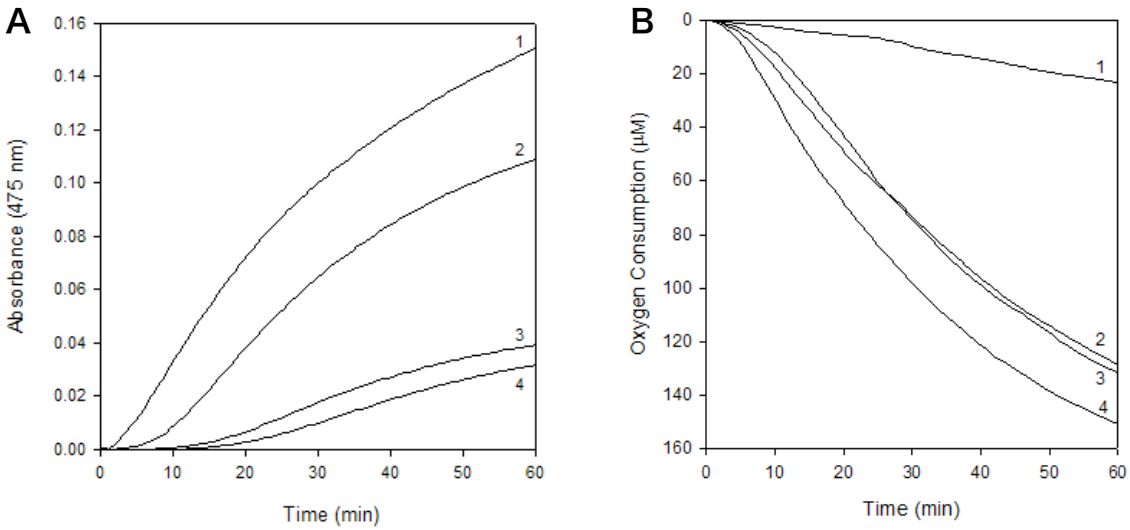

Figure 8. (**A**) UV-Vis spectra at 475 nm obtained in oxidation of 100 µM of L-tyrosine by mushroom tyrosinase in presence of arbutin for 60 min. Concentrations of arbutin were selected at 50 µM (2), 100 µM (3) and 200 µM (4). Line 1 represents oxidation of L-tyrosine by mushroom tyrosinase in absence of arbutin. (**B**) Oxygen consumption of 100 µM of L-tyrosine oxidation by mushroom tyrosinase in presence of arbutin for 60 min. Concentrations of arbutin was selected at 200 µM (1), 100 µM (3) and 50 µM (2). Line 4 represents oxidation of L-tyrosine by mushroom tyrosinase in absence of arbutin.

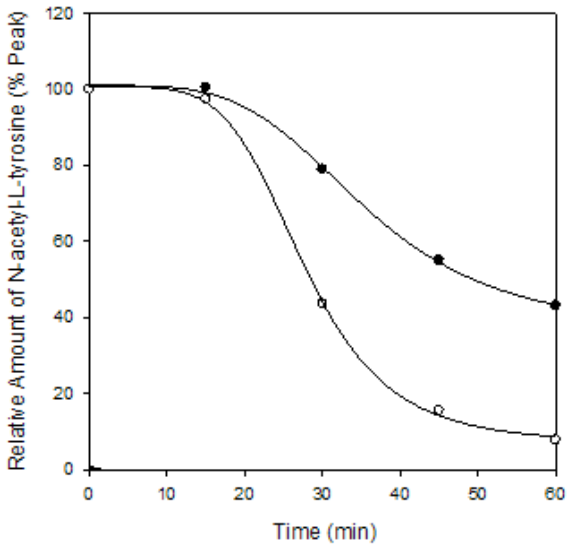

Figure 9. HPLC analysis of *N*-acetyl-L-tyrosine (100 μM) oxidation by tyrosinase in absence (○) or presence (●) of arbutin (100 μM). Sampling time was chosen at 0 min, 15 min, 30 min, 45 min and 60 min. HPLC operating conditions were as follows; Deverosil ODS-UG-5 (Nomura Chemical, CO., LTD., Seto-Shi, Aichi, Japan). Solvent; 12 % MeCN/H_2O containing 0.2 % TFA, Flow rate 1.0 mL/ min, detection; UV at 280 nm, 0.02 range, injected amount; 25 μL. Curve fitting is done with SigmaPlot (Systat Software, Inc.).

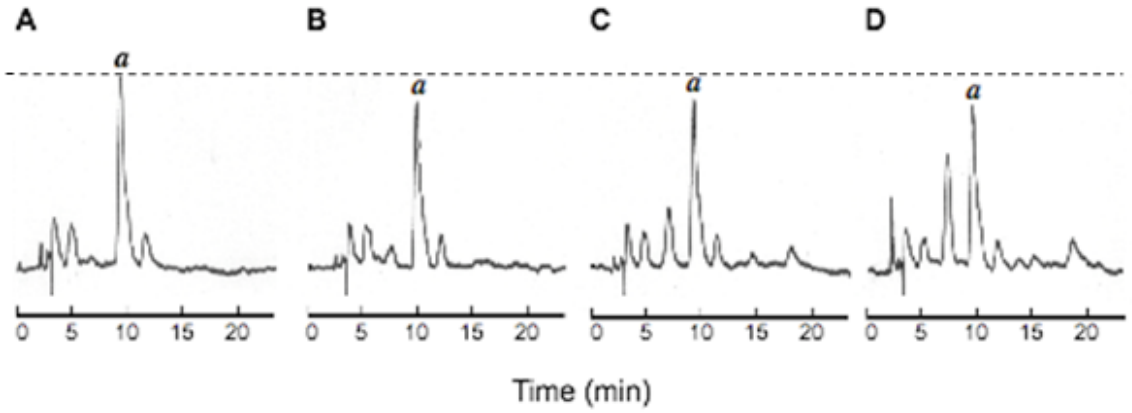

Figure 10. HPLC analysis of the reaction mixture with arbutin (100 μM) and B16 melanoma cell lysate. Sampling times were chosen at 0 h (**A**), 2 h (**B**), 4 h (**C**) and 6 h (**D**). HPLC operating conditions were as follows; Deverosil ODS-UG-5 (Nomura Chemical, CO., LTD., Seto-Shi, Aichi, Japan). Solvent; 1.0 % MeCN/H_2O containing 0.2 % TFA, Flow rate 1.0 mL/min, detection; UV at 280 nm, injected amount; 25 μL. Peak ***a*** represents arbutin.

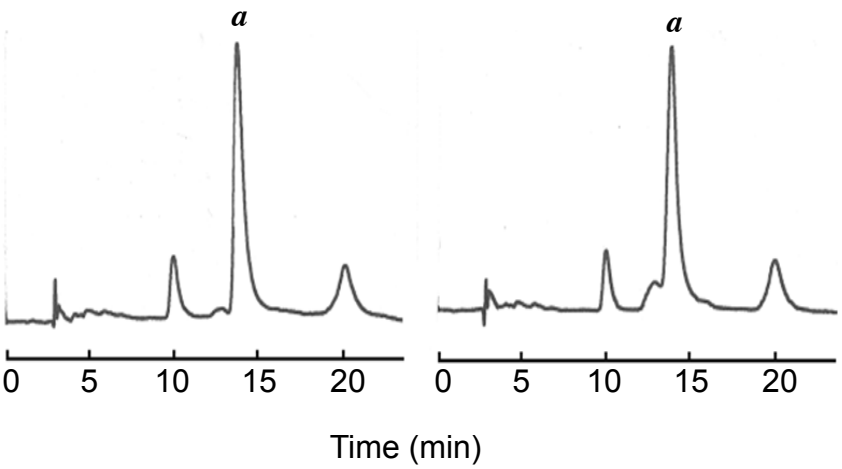

Figure 11. HPLC analysis of DMEM with arbutin (400μM). Sampling time was chosen at 0 min (left) and 60 min (right). HPLC operating conditions were as follows; Develosil ODS-UG-5 (Nomura Chemical, CO., LTD., Seto-Shi, Aichi, Japan). Solvent; 1.0 % MeCN/H_2O containing 0.2 % TFA, Flow rate 0.6 mL/min, detection; UV at 280 nm, injected amount; 25 μL. Peak ***a*** represents arbutin.

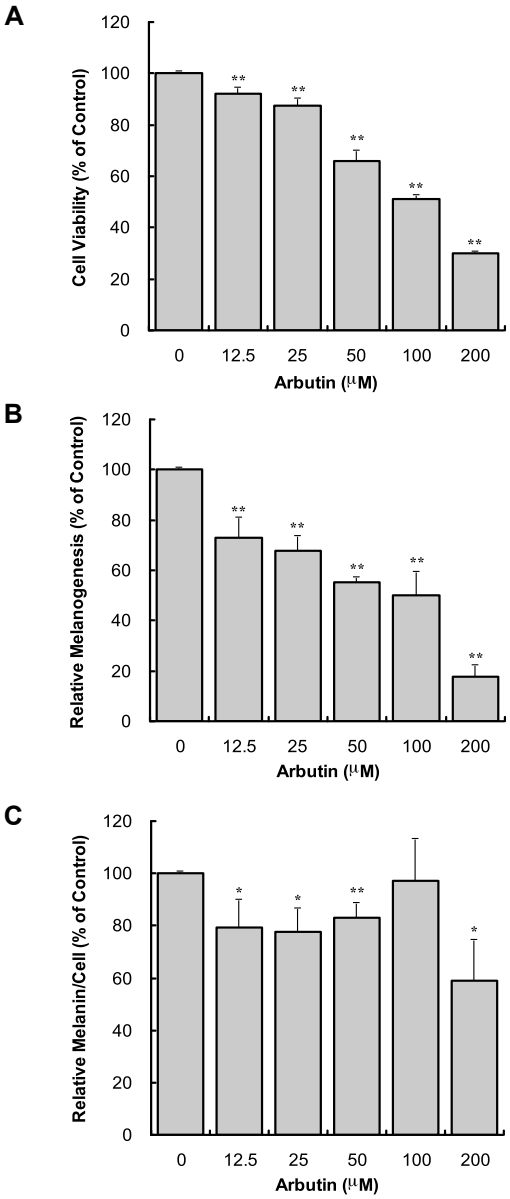

Figure 12. (**A**) Viabilities of B16-F10 melanoma cells following treatment with arbutin for 72hr; data are expressed as percentage of the number of viable cells observed with the control, and each column represents the mean ± S.D. of at least 4 determinations. (**B**) Total melanin content in B16 melanoma cells following treatment with arbutin for 72hr; data are expressed as percentage of melanin content per well observed with the control, and each column represents the mean ± S.D. of 4 determinations. (**C**) Cellular melanin content in B16 melanoma cells following treatment with arbutin for 72hr measured as percentage of melanin content per cell observed with the control, and each column represents the mean ± S.D. of 4 determinations. The statistical significance of differences was evaluated using Student's or Welch's *t*-test. Significantly different from the control value: **p*<0.05, ***p*<0.01.

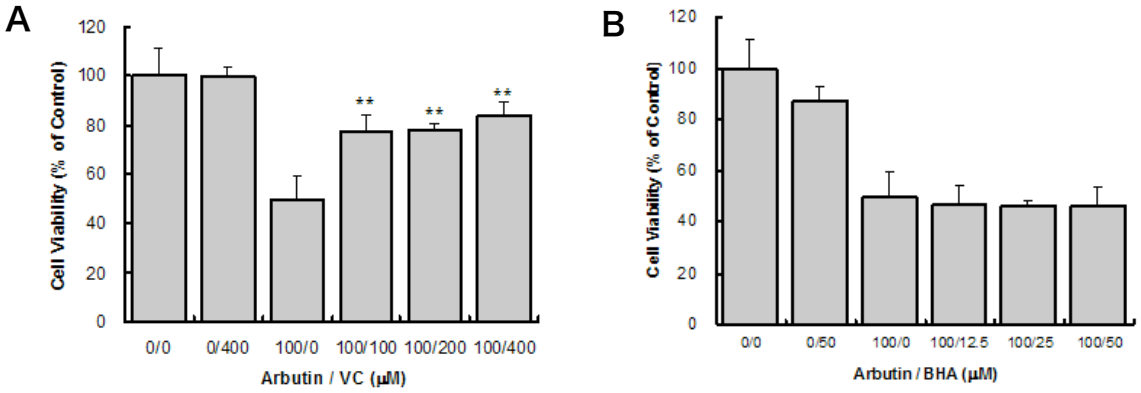

Figure 13. (**A**) Viabilities of B16 melanoma cells following treatment with 100 μM of arbutin in presence or absence of vitamin C (VC) for 72hr. The concentrations of vitamin C applied to arbutin treated cells were chosen at 0 μM (100/0), 100 μM (100/100), 200 μM (100/200) and 400 μM (100/400). Cells are also treated with 400μM of vitamin C without arbutin (0/400). Data are expressed as the percentage of the number of viable cells observed with arbutin control (100/0), and each column represents the mean ± S.D. of at least 4 determinations. (**B**) Viabilities of B16 melanoma cells following treatment with 100 μM of arbutin in presence or absence of butylated hydroxyanisole (BHA) for 72hr. The concentrations of butylated hydroxyanisole applied to arbutin treated cells were chosen at 0 μM (100/0), 12.5 μM (100/12.5), 25 μM (100/25) and 50 μM (100/50). Cells are also treated with 50 μM of butylated hydroxyanisole without arbutin (0/50). Data are expressed as the percentage of the number of viable cells observed with arbutin control (100/0), and each column represents the mean ± S.D. of at least 4 determinations. The statistical significance of differences was evaluated using Student's or Welch's *t*-test. Significantly different from arbutin control value: **p* <0.05, ***p* <0.01.

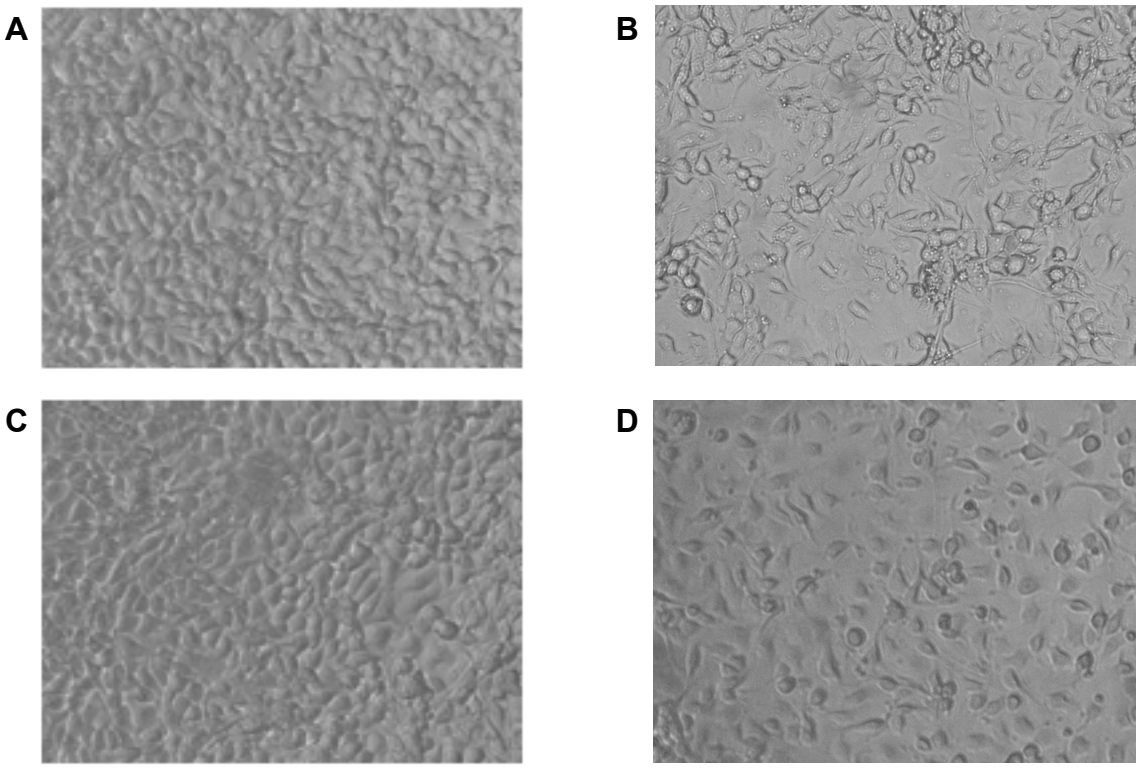

Figure 14. Cellular morphological change of B16-F10 melanoma cells. **A** represents cellular morphology of DMSO treated melanoma cells while **B** indicates morphological change of arbutin (100 μM) treated B16 melanoma cells. **C** shows that morphology of melanoma cells treated with arbutin (100 μM) and vitamin C (100 μM). **D** indicates that morphology of melanoma cells treated with arbutin (100 μM) and BHA (100 μM).

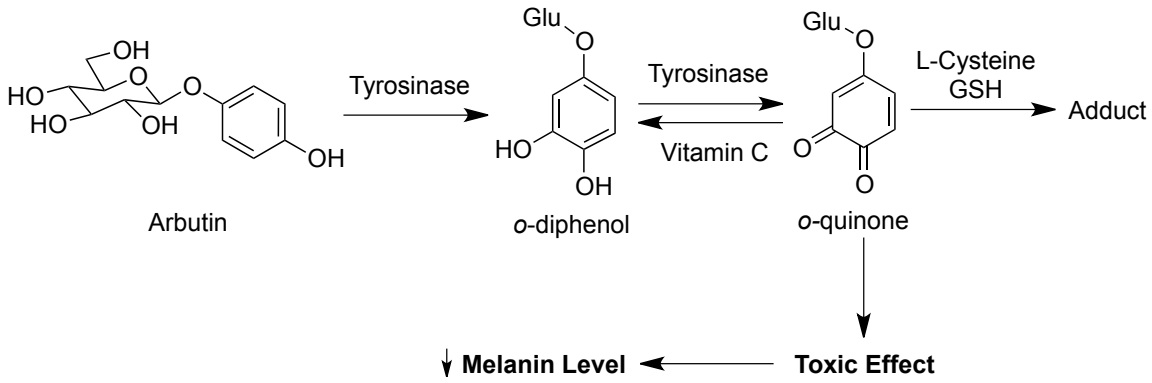

Scheme 1. Postulated mechanism of toxicity and antimelanogenic effects by arbutin.

1.2 Effect of Thymol on Mushroom Tyrosinase and B16 Melanoma Cells

1.2.1 INTRODUCTION

Aromatic monoterpenes, thymol (5-methyl-2-isopropylphenol) (**1**), carvacrol (5-isopropyl-2-methylphenol) (**2**) and *p*-cymene (1-methyl-4-(1-methylethyl)benzene) (**3**) (see Figure 15 for the structures) are found in the essential oil faction of thyme, *Thymus vulgaris* or *T. zygis* L. var. *gracilis* Boissir (Lamiaceae). The main constituents of thyme oil are thymol and carvacrol (up to 80 %). Thyme essential oil has been commercially available as a part of mouth washes for more than 100 years. Besides their odoriferous functions, thymol and carvacrol show antimicrobial activities (*10-12*). Thus, thymol and carvacrol are commonly used as meat preservatives or flavorings in the food industries. In addition to their broad antimicrobial activities, the antioxidant activity of thyme essential oils was previously reported (inhibit phospholipids peroxidation and lipid autoxidation without prooxidant effects), and it has been known to be due to the presence of thymol and carvacrol (*13-15*). As antioxidants, thymol and carvacrol protect food qualities and organisms from damage induced by oxidative stress. In contrast to these well-studied biological effects of thymol and carvacrol, their inhibitory actions on tyrosinase and melanin biosynthesis are poorly understood. The antibrowning effect in addition to the antimicrobial and antioxidant activities of thymol and carvacrol would help them to be considered as multifunctional additives. Hence, thymol was studied as a melanin formation inhibitor.

1.2.2 RESULTS

Effects of Thyme Oil on Mushroom Tyrosinase

The investigation began with thyme oil because it is commercially available and also found in food supplies. Thyme oil exhibited a concentration-dependent inhibitory effect on the tyrosinase-catalyzed oxidation of L-tyrosine with 60 min of reaction time (Figure 16) whereas there was no inhibition effect against the L-DOPA oxidation (data not shown). As the concentration of thyme oil increased, the formation of dopachrome decreased. Due to the solubility problem, the highest tested concentration of the oil was 66.6 μg/mL, and about 35 % of dopachrome formation was suppressed at this concentration. Typical lag phases were observed in all of the curves (Figure 16 curve 1-3). However, the extension of the lag phase, which is commonly observed with the effect of monophenol substrate analogues, was not observed with addition of thyme oil. The components of thyme oil were characterized by using a Gas Chromatography-Mass Spectrometry (GC-MS) system. The major component of thyme oil was thymol (75.71 %), and about 80 % of contents were thymol and carvacrol in thyme oil (data not shown). As described above, thymol and carvacrol are the bioactive compounds in thyme oil for

various biological activities. Hence, we concluded that, in thyme oil, thymol and carvacrol are the major bioactive compounds for melanogenesis inhibition.

Effects of Thymol on Tyrosinase

As well as thyme essential oil inhibits dopachrome formation, thymol exhibited a concentration-dependent inhibitory effect on the dopachrome formation (Figure 17A). At 475 nm, about 25 % of dopachrome formation was suppressed with 400 μM of thymol after the 60 min of the incubation. The consumption of oxygen was also inhibited dose-dependently with addition of thymol (Figure 17B). Any change in lag phase was not observed for all curves in both UV and oxygen consumption assays (Figure 17A & B curve 1-4). However, the inhibitory effect was not observed with L-DOPA in UV-vis and oxygen consumption assays (data not shown). Similar inhibitory effects of thymol were observed using carvacrol in both spectrophotometric and oxygen consumption assays (data not shown). Interestingly, this inhibitory effect on dopachrome synthesis (475nm) and oxygen consumption with L-tyrosine was not observed when thymol methyl ether (1-methyl-3-methoxy-4-isopropylbenzene) (**4**) was used (data not shown). Blocking the phenolic OH of thymol with methyl group diminished the inhibitory activity that is observed with thymol. This structure activity relationship (SAR) study suggests that the presence of the phenolic hydroxyl group of thymol or carvacrol is essential for the inhibition.

The consecutive UV-vis spectrum of L-tyrosine oxidation by tyrosinase in the presence of 400 μM of thymol was obtained. The evolution of the peak at 475 nm, corresponding to dopachrome formation, decreased with the addition of thymol (Figure 18). About 40 % of dopachrome formation was suppressed in the spectrophotometric assay. Furthermore, at 320 nm, the peak developed in both spectra, but there was less increase in Figure 18B. The evolution of the peak at this wavelength refers to the formation of a quinone product, dopaquinone in the melanin synthesis process. Basically, the same result was observed in both spectrophotometric assays at 475 nm and consecutive UV-vis assay.

Effect of Thymol on E_{oxy} State of Tyrosinase

The effect of thymol on the E_{oxy} state of tyrosinase was examined by the addition of 10 μM L-DOPA as a cofactor. Introduction of L-DOPA to tyrosinase reduces its state from E_{met} to E_{oxy}, which are resting and active form of tyrosinase, respectively. L-DOPA was preincubated with tyrosinase for 3 min in order to convert all of the enzyme to E_{oxy}, and then dopachrome formation was measured after the addition of 100 μM L-tyrosine with or without 400 μM thymol. Addition of a cofactor did not show any effect on the inhibition of dopachrome formation (Figure 19) compared to the measurement result without a cofactor (Figure 17). Furthermore, previous results showing that thymol (and thyme oil) did not affect the lag phase support this result. Thus, these suggest that thymol does not interact with the E_{oxy} state of tyrosinase, and it can be concluded that thymol does not act as a monophenol analogue.

Radical Scavenger and Thymol

Surprisingly, the inhibitory effect of thymol was masked with the application of a radical scavenger, butylated hydroxyanisole (BHA). As the concentration of BHA was increased to 100 μM, the inhibitory effect due to thymol on dopachrome formation was dose-dependently decreased (Figure 20). With 100 μM BHA and thymol, about 20 % of the inhibitory activity on dopachrome formation was suppressed. This suggests that BHA affected the antimelanogenic action of thymol; in other words, the phenoxy radical formation and proton donation of thymol are linked to the antimelanogenic activity of thymol. On the other hand, the inhibitory activity was enhanced when tyrosinase was preincubated with thymol for 10 min (data not shown). In this treatment, preincubation gives extra time for the proton to dissociate from the hydroxyl group of thymol to form of a phenoxy radical. Thus, the antioxidant effect of thymol is the key for inhibition of dopachrome formation.

Non-involvement of Thymol on Tyrosinase Activity

The involvement of thymol in enzymatic reactions in melanin synthesis was investigated with *N*-acetyl-L-tyrosine. Using *N*-acetyl-L-tyrosine as a substrate, tyrosinase oxidizes substrate to synthesize up to *N*-acetyldopaquinone. Because of the presence of an acetate group on the *N*-group of an amino acid, intracyclization of dopaquinone to leukodopachrome is blocked. Hence, only the tyrosinase-catalyzed reaction step in melanin synthesis process can be examined using this compound as a substrate. When *N*-acetyl-L-tyrosine is applied to tyrosinase in the presence of 400 μM thymol, the consumption of *N*-acetyl-L-tyrosine was no different from the control (Figure 21). This explains why thymol did not show any involvement in the enzymatic reactions. Thus, it appears that thymol is not a "tyrosinase" inhibitor.

Inhibition of Redox Reaction in Melanogenesis

The formation of dopachrome from dopaquinone is extremely rapid. Therefore, an alternative model of this reaction is required to test whether thymol affects this nonenzymatic process. L-DOPA and *p*-benzoquinone were used as models instead of leukodopachrome and dopaquinone, respectively. The consmption of *p*-benzoquinone was measured by using HPLC analysis. As thymol was incubated in this model system, the consumption of *p*-benzoquinone was decreased about 20 % in 10 min (Figure 22 Top). At the same time, the formation of hydroquinone was also measured in the same manner. About 20 % of hydroquinone formation was suppressed with the addition of 400 μM thymol (Figure 22 Bottom). These results suggest thymol quenched the redox reaction between L-DOPA and *p*-benzoquinone (Scheme 2). On the basis of these results, it is logical to assume that the inhibitory action of thymol on dopachrome formation is due to the suppression of conversion of leukodopachrome to dopachrome (Scheme 3).

Effects of Thyme Essential Oil on B16-F10 Melanoma Cells

On the basis of tyrosinase inhibitor activity, thymol did not interact with tyrosinase; however, thymol inhibited a redox reaction in the melanin synthesis pathway.

Tyrosinase-catalyzed dopachrome formation is a key step in melanogenesis and therefore, inhibitors of dopachrome formation are expected to inhibit cellular melanin production. Thus, the investigation was extended to test for the effects of thymol on murine B16-F10 melanoma cells. Carvacrol (**2**), *p*-cymene (**3**), thymol methyl ether (1-methyl-3-methoxy-4-isopropylbenzene) (**4**), menthol (**5**), and a well-known depigmenting agent, arbutin (**6**) were also examined for comparisons (see Figure 15 for the structures).

The investigation began with thyme essential oil since it contains thymol, and it is commercially available. The composition of thyme oil was characterized by using a GC-MS system. The major component of thyme oil was thymol (75.71 %), and about 80 % of the contents were thymol and carvacrol (5.47 %) in thyme oil (data not shown). The examined highest concentration of thyme oil was 100 μg/mL, and it was the maximal concentration tested due to a problem in solubility. Thyme oil concentration-dependently suppressed cell viability (Figure 23A), and estimated IC_{50} was about 150 μg/mL. The cell viability above 12.5 μg/mL was significantly different (P <0.01) from the control. Total melanin production was significantly suppressed (P <0.01), up to 100 μg/mL in a concentration-dependent manner (Figure 23B). However, thyme oil did not show any effect on cellular melanin production (Figure 23C). As described in the introduction, thymol is a bioactive compound in thyme oil for various biological activities; hence, the investigation was continued using one of the components of thyme oil, thymol.

Effects of Thymol & Carvacrol on B16-F10 Melanoma Cells

Both thymol and carvacrol were noted to exhibit moderate cytotoxicity when they were cultured with murine B16-F10 melanoma cells. The highest concentration of thymol was 1200 μM. Cell viability of thymol-treated cells was suppressed in a concentration-dependent manner (Figure 24A). Observed IC_{50} was 400 μM (60.09 μg/mL) and almost complete lethality was observed at 1200 μM. Cell viability above 75 μM was significantly different (P <0.01) compared to the control. Total melanin production was also suppressed in a concentration-dependent manner (Figure 24B) and this suppression above 300 μM was significant (P <0.01). The cellular melanin production was not suppressed but slightly increased (Figure 24C). In the case of carvacrol, similar results were obtained in cell viability and melanin assays (Table 1). Unfortunately, both thymol and carvacrol did not inhibit melanogenesis in cultured melanocytes even though they inhibited dopachrome formation. Maeda and Fukuda previously reported that a correlation was not seen between the inhibition of mushroom tyrosinase activity with that of cellular tyrosinase or melanin formation in cultured melanocytes (*2*). However, the toxicity mechanism of these monoterpenes is poorly understood, and clarification of the mechanism of toxicity is important for further usage of thymol as food additives and for scientific purposes. Thus, investigation was focused on identifying the mechanism of toxicity of thymol or carvacrol.

Toxic Effects of Thymol-Related Compounds

p-Cymene (**3**), thymol methyl ether (1-methyl-3-methoxy-4-isopropylbenzene) (**4**), and menthol (**5**) were tested for structure activity relationship (SAR) studies. Among

the tested compounds, none of the compounds showed any significant cytotoxicity on B16 melanoma cells up to designated concentrations (Table 1). It should be noted that thymol methyl ether had relatively less solubility; hence, the tested highest concentration of thymol methyl ether was 200 μM. The results suggested that the blocking or lacking of hydroxyl OH group in monoterpene phenol decreased cytotoxicity against B16-F10 melanoma cells. As concluded in a previous report, phenolic hydroxyl group of thymol or carvacrol is essential for biological activities (*16*). Subsequently, menthol also did not show significant toxicity up to 1000 μM. It indicates that the aromaticity was essential for the toxicity.

Recovery from Thymol Toxicity

Cytotoxicity of thymol observed at 400 μM (approximately equivalent to IC_{50}) was suppressed by 20 % in cell viability with the addition of an equivalent concentration of vitamin C (Figure 25A). As a result, intracellular transformation of thymol, to either a toxic oxide by intracellular oxidation or a stable phenoxy radical to generate oxidative stress, involved in the mechanism of toxicity of thymol. In order to examine this postulate, the effect of vitamin E was also tested. Vitamin E showed approximately 40 % of reversed effect in cell viability on the same thymol-treated melanoma cells (Figure 25B). Subsequently, butylated hydroxyanisole (BHA) and butylated hydroxytoluene (BHT), were examined. Both treatments reduced the cytotoxicity of thymol by 17 % and 11 % in cell viability, respectively (Table 2). Additionally, glutathione (GSH) was tested in the same manner. GSH is a major intracellular antioxidant molecule to eliminate radicals as well as vitamin E. GSH treatment suppressed the toxic effect of thymol by 22 % in cell viability on B16-F10 melanoma cells. Since vitamin E, BHA, BHT and GSH are well-known radical scavenger, their defensive effects against thymol toxicity on B16 melanoma cells explained that a radical-based toxicity was, at least, involved in the mechanism of thymol toxicity. A surprising result was observed with the treatment of L-cysteine on thymol-treated cells. Toxicity effect of thymol on B16-F10 melanoma cells were reduced 15 % by the treatment of L-cysteine (Table 2). In fact, L-cysteine does not act as either a reducing agent or a radical scavenger, but it acts as a nucleophile to react with a Michael-addition receptor such as quinone-related compounds. This result suggested that thymol was converted to reactive electrophilic compound(s) such as quinone. Thus, both radical formation and toxic oxide(s) formation involved in the mechanism of thymol toxicity.

Intracellular Oxidative Stress

Intracellular oxidative stress was measured with DCFH-DA assay. Intracellular ROS oxidized DCFH to a highly fluorescent compound, DCF, after esterase cleaves two acetate groups (*25*). After 1hr of incubation of B16-F10 melanoma cells with thymol and DCFH-DA, cells were assayed to measure intracellular ROS. Within 75 to 300 μM, the total ROS were increased even though cellular viability was decreased (Figure 26A and B). The cellular ROS generation above 75 μM was significantly increased ($P < 0.01$) in a concentration-dependent manner (Figure 26C). The highest increase of ROS was

observed when 600 μM of thymol was applied to the cells. About two times higher ROS was generated than the control . It appeared that thymol acted as a prooxidant above 75 μM rather than as an antioxidant. Thus, oxidative stress was generated with a high concentration of thymol, and involved in the mechanism of toxicity.

Morphological Change of Thymol-Treated Cells

Cellular morphological changes of thymol-treated melanoma cells were microscopically observed. Figure 27A represents the cellular morphology of control (DMSO treated) cells while Figure 27B is that of thymol treated cells (Figure 27A and B). As seen in these Figures, the density of melanoma cells was significantly reduced by the treatment of 400 μM of thymol. Further, the individual cells were enlarged compared to DMSO treatment. As expected, after the treatment of intracellular antioxidant, GSH, to thymol-treated cells, the morphological change of the cells was masked and became similar to that of controls (Figure 27C). It was difficult to represent how these morphological differences were related to the mode of action of thymol; the questions have still been under investigations.

1.2.3 DISCUSSION

On the basis of the data obtained, it may be logical to assume that thymol inhibits the redox reaction in melanin synthetic pathway, and this inhibition of melanin formation is due to the radical scavenging activity of thymol. Direct proton donation from thymol interrupts electron flow between dopaquinone and leukodopachrome. The electron-donating isopropyl and methyl groups in ortho position contribute to stability of phenoxy radical and their antioxidative activities, similar to previous reports (*17, 18*). Furthermore, various monophenol compounds are recognized by tyrosinase and sometimes act as monophenol substrate analogues (*19, 20*). However, steric hindrance due to methyl or isopropyl groups adjacent to hydroxyl groups prevents tyrosinase from recognizing thymol as a monophenol substrate. Thus, thymol is considered to be a unique melanin synthesis inhibitor, but not an enzyme inhibitor.

Antioxidants work in various ways including direct quenching of ROS, inhibition of enzymes involved in the production of the ROS, chelation of low valent metal ions such as Fe^{2+} or Cu^{2+}, and regeneration of membrane bound antioxidants such as α-tocophenol (*21*); however, antioxidant-related radicals are usually formed during the action. The fate of newly formed radicals from antioxidant action to humans is still unclear. Because of this property, antioxidants are also known as a double-edged sword. All of the obtained data suggested that thymol showed moderate toxicity without any effects on melanogenesis. The mechanism of thymol toxicity is due to the intracellular transformation to corresponding toxic phenoxy radical and quinone. Because of its lipophilicity and small structural feature, thymol passively dissolves into the cell through the lipid bilayer. Once inside the cell, thymol first acts as an antioxidant which scavenges free radicals from the environment (*13, 15, 22*). However, the phenoxy radical is newly

formed through this reaction. The contribution of the electron donating methyl or isopropyl group in the *ortho* position of the phenolic hydroxyl group helps thymol to form a relatively stable phenoxy radical (*17*). Moreover, the resonance due to the aromaticity also involved to the stabilization of phenoxy radical based on the non-toxicity data of menthol. This thymol-derived phenoxy radical oxidizes environmental oxygen to generate reactive oxygen species (ROS); at the same time, phenoxy radical itself is further oxidized to form quinone oxide-related compounds (Scheme 4). Excess level of free radicals and of quinone-related compounds are known to lead oxidative stress in cells, which causes serious damage, such as diabetes, mellitus and coronary arteriosclerosis (*23, 24*), as well as being linked with aging and carcinogenesis (*25*).

Now, it is logical to conclude that the oxidative stress-related toxicity mechanism is the major mechanism of thymol toxicity. The moderate cytotoxicity of thymol or thyme oil is, interestingly, non-specific to all organisms; for example, they show the cytotoxic effect against bacterial strains including *Escherichia coli, Aeromoans hydrophila* and *Staphylococcus aureus* (*26, 27*), or fungi strains such as *Candida albicans* and *Saccharomyces cerevisiae* (*28, 29*). For all organisms, from humans to microorganisms, the oxidative phosphorylation in mitochondria is an essential metabolic pathway to create energy for their activities; however, ROS such as superoxide and hydrogen peroxide are usually propagated in this process. Thus, the excess amounts of thymol administration leads to the excess level of proton-donating/radical-scavenging action in order to eliminate these ROS; this leads to the generation of toxic levels of phenoxy radical intermediates. Therefore, thymol acts as a prooxidant rather than an antioxidant at high concentrations.

In the case of thymol, the radical-scavenging effect of thymol depletes an active electron in melanin synthesis, but antioxidant-related phenoxy radicals are newly formed. From our experimental results, the inhibitory mechanism of thymol on melanogenesis is due to the inhibition of the redox reaction between dopaquinone and leukodopachrome without any interaction with tyrosinase. Thus, this antimelanogenic effect (directly link to the antioxidative effect) in addition to antimicrobial and antioxidant activities allows thymol to be a multifunctional additive. However, at the high concentration, thymol shows moderate oxidative toxicity due to this antioxidant property. The fate of radicals newly formed through the antioxidant action promotes further formation of ROS and new thymol-derived superoxide related ROS. Because of this property, antioxidants, the careful consideration is required for the usage of thymol. However, the concentration that shows the considerable toxicity by thymol is relatively high, but as food additives, the toxic effect of thymol may be negligible. Moreover, Kohlert et al. reported that most of the thymol (>90%) administrated orally is excreted as a conjugate with glucuronide or sulfate in 40 hrs (*30*). Therefore, at low concentration, thymol may be an alternate choice to non-natural food additives for the purpose of antibrowning. Despite its advantage as an additive, the site of action including the metabolism is still unclear. Even though the part of effect of thymol on tyrosinase and B16-F10 melanoma cells has been clarified in this study, there are various uncertainties for the purpose of the applications.

DISCLOSURE

The cell free experimental part was accepted in part at the General Paper Session in Division of Agricultural and Food Chemistry for the 241st ACS National Meeting in Anaheim, CA, USA, and published in the Journal of Agricultural and Food Chemistry (Satooka and Kubo, 2011). The cellular experimental part was presented in part at the General Paper Session in Division of Agricultural and Food Chemistry for the 237th ACS National Meeting in Salt Lake City, UT.

1.2.4 FIGURES & TABLES

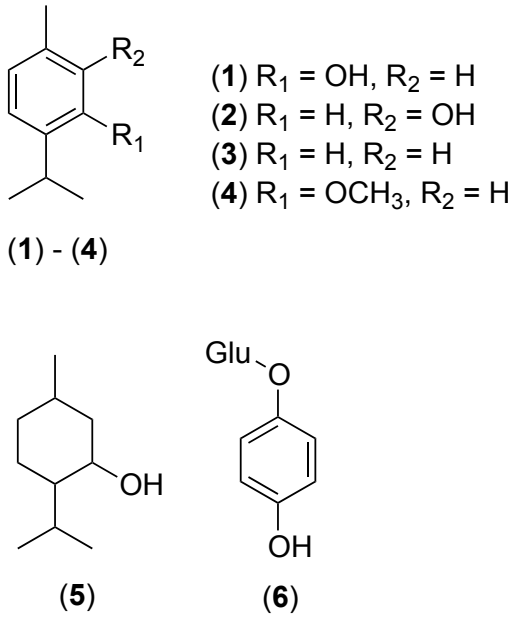

Figure 15. Chemical structures of thymol and related compounds.

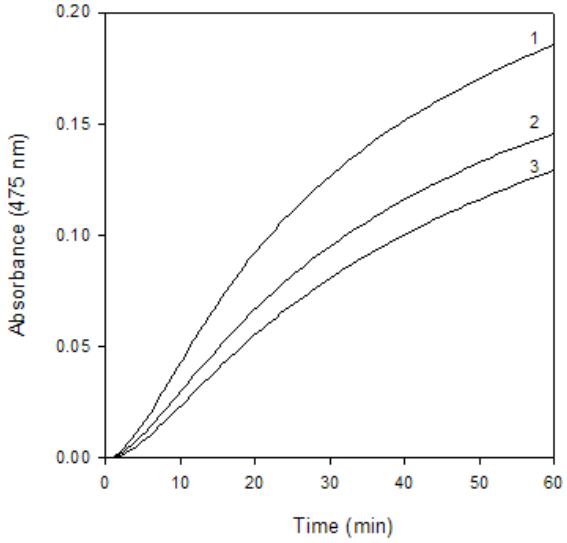

Figure 16. UV-Vis spectra at 475 nm obtained in oxidation of 100 μM of L-tyrosine by mushroom tyrosinase in presence or absence of thyme oil for 60 min. Concentrations of thyme oil were selected at 33.3 μg/mL (2) and 66.6 μg/mL (3). Line 1 represents oxidation of L-tyrosine by mushroom tyrosinase in absence of thyme oil.

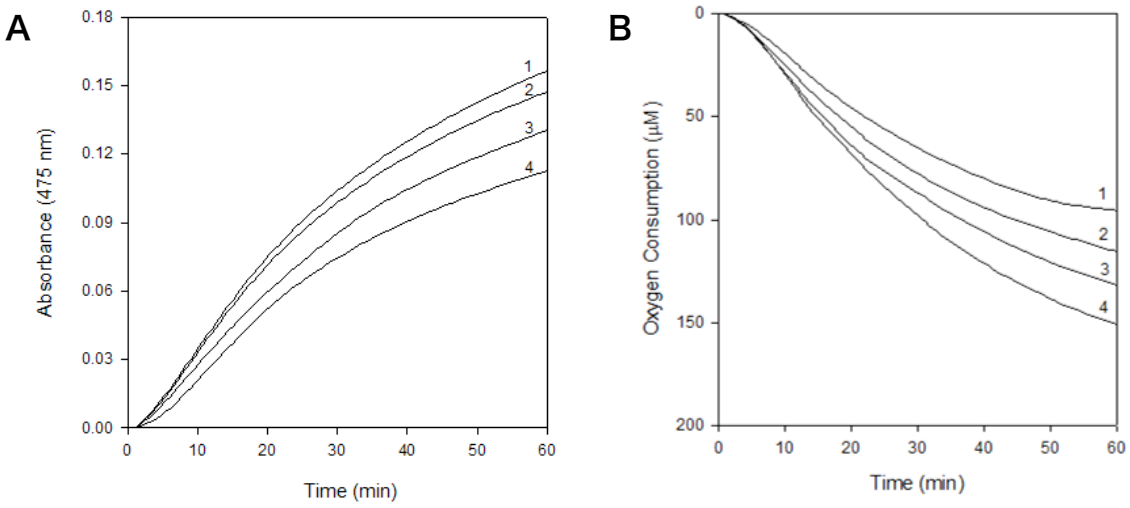

Figure 17. (**A**): UV-vis spectra at 475 nm obtained in oxidation of 100 µM of L-tyrosine by mushroom tyrosinase in presence or absence of thymol for 60 min. Concentrations of thymol were selected at 100 µM (2), 200 µM (3) and 400 µM (4). Line 1 represents oxidation of L-tyrosine by mushroom tyrosinase in absence of thymol. (**B**): Oxygen consumption of oxidation of L-tyrosine (100 µM) by mushroom tyrosinase in presence or absence of thymol for 60 min. The concentrations of thymol were 400 µM (1), 200 µM (3) and 100 µM (3). Line 4 represents the oxygen consumption of oxidation of 100 µM of L-tyrosine by mushroom tyrosinase in absence of thymol.

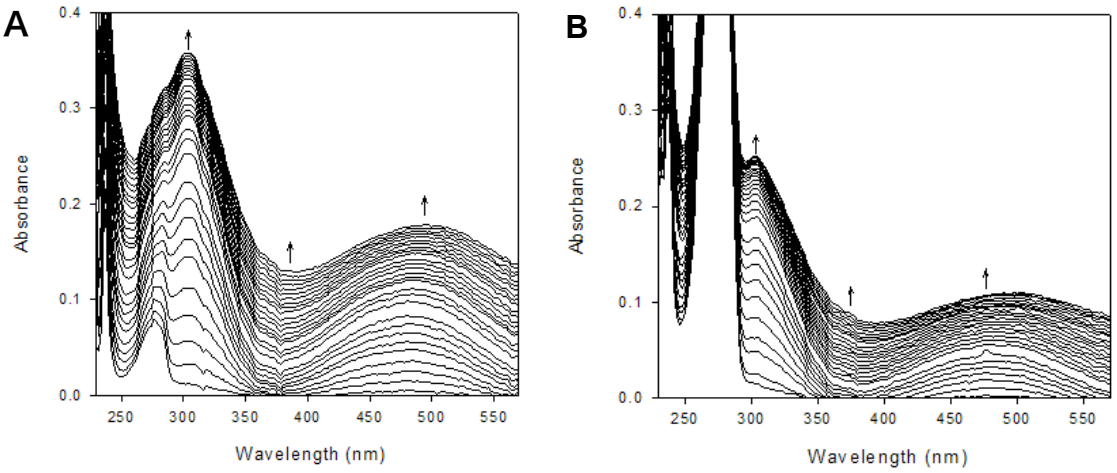

Figure 18. Consecutive UV-vis spectra obtained in the oxidation of 100 μM of L-tyrosine by mushroom tyrosinase in absence (**A**) or presence (**B**) of 400 μM of thymol for 60min. Scan speed was at 2 min intervals for 30 s. the arrows (↑) designate the evolution of the peak.

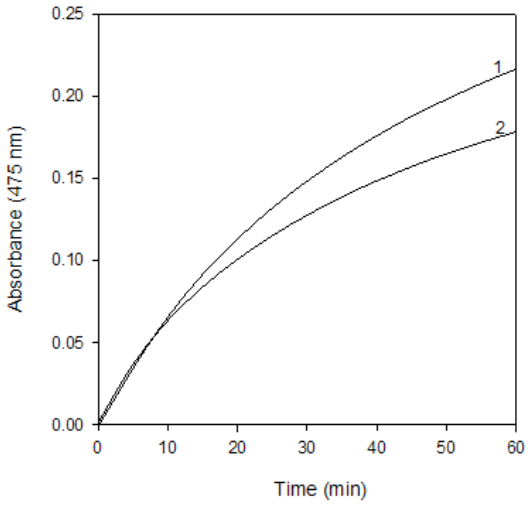

Figure 19. UV-vis spectra at 475 nm obtained in oxidation of 100 μM of L-tyrosine by mushroom tyrosinase in presence or absence of thymol and a cofactor for 60 min. Mushroom tyrosinase was preincubated with 10 μM of L-DOPA for 3min, and then L-tyrosine was added. Concentrations of thymol were selected at 400 μM (2). Line 1 represents oxidation of L-tyrosine by mushroom tyrosinase in absence of thymol.

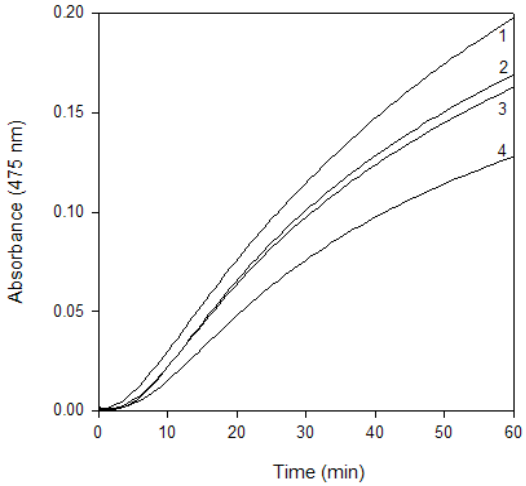

Figure 20. UV-vis spectra at 475 nm obtained in oxidation of 100 μM of L-tyrosine by mushroom tyrosinase in presence or absence of thymol and butylated hydroxyanisole mixture for 60 min. Concentration of thymol was 100 μM. Concentrations of butylated hydroxyanisole were selected at 100 μM (2), 50 μM (3) and 0 μM (4). Line 1 represents oxidation of L-tyrosine by mushroom tyrosinase in absence of both thymol and butylated hydroxyanisole.

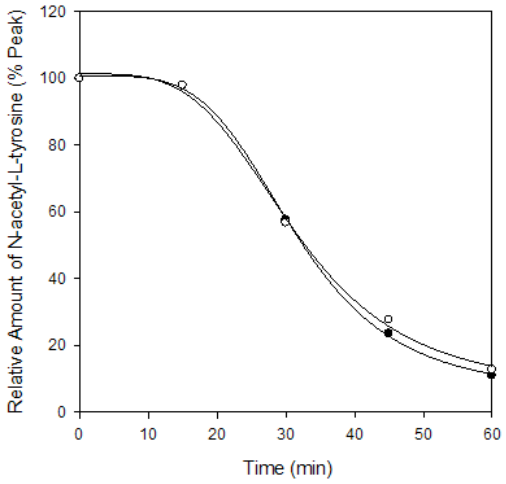

Figure 21. HPLC analysis of *N*-acetyl-L-tyrosine (100 μM) oxidation by tyrosinase in presence (○) or absence (●) of thymol (400 μM). Sampling time was chosen at 0 min, 15 min, 30 min, 45 min and 60 min. HPLC operating conditions were as follows; Develosil ODS-UG-5 (Nomura Chemical, CO., LTD., Seto-Shi, Aichi, Japan). Solvent; 15 % MeCN/H_2O containing 0.2 % TFA, Flow rate 1.0 mL/min, detection; UV at 280 nm, 0.02 range, injected amount; 25 μL. Curve fitting in order to connecting the points smoothly, is done with SigmaPlot (Systat Software, Inc.).

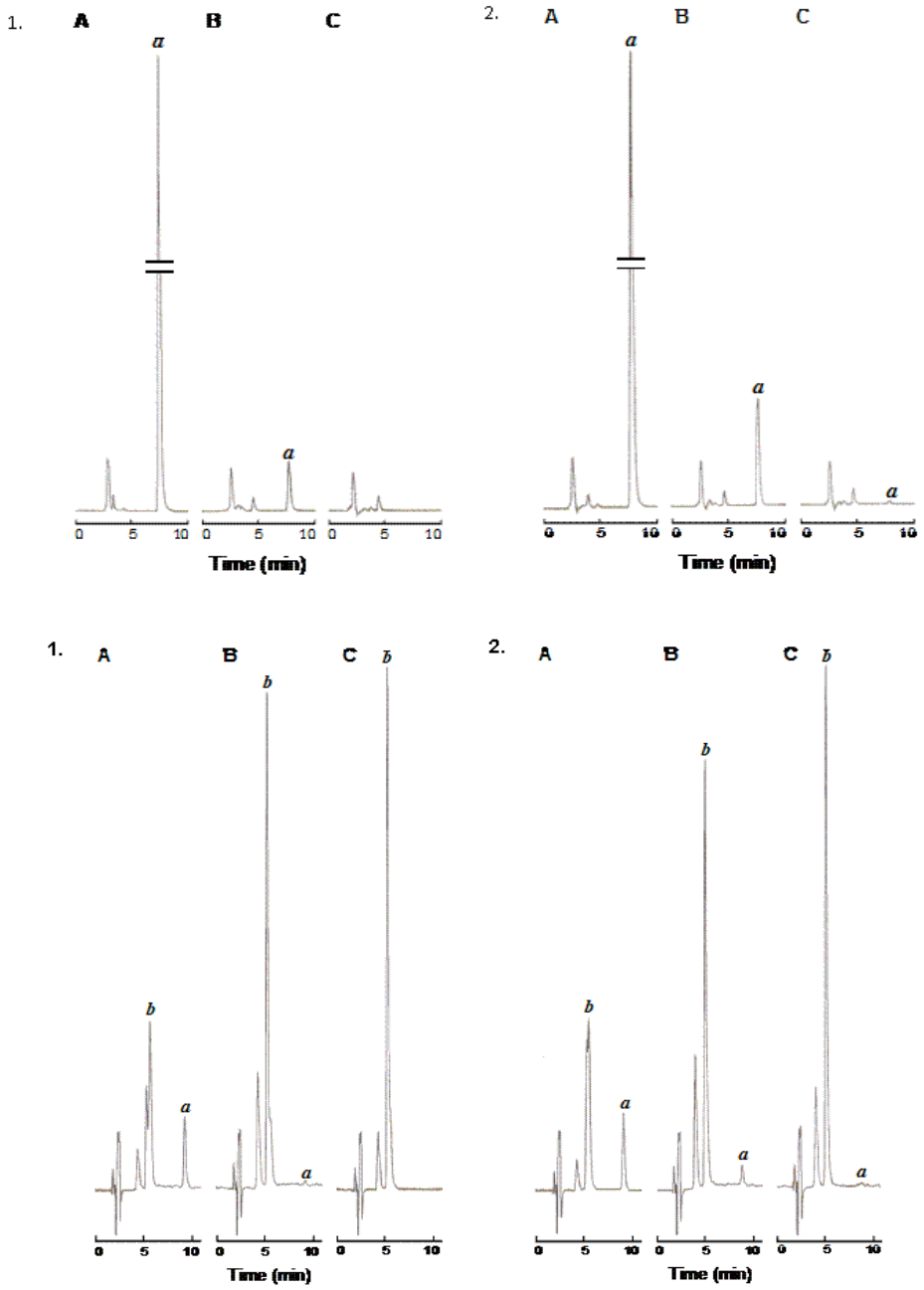

Figure 22. Top: HPLC analysis of the redox reaction of *p*-benzoquinone (400 μM) and L-DOPA (200 M) in absence (1) or presence (2) of 400 μM of thymol in buffer (without tyrosinase). Sampling time was chosen at 0 min (A), 10 min (B), and 20 min (C). HPLC operating conditions were as follows; Develosil ODS-UG-5 (Nomura Chemical, CO., LTD., Seto-Shi, Aichi, Japan). Solvent; 10 % MeCN/H_2O containing 0.2 % TFA, Flow rate 1.0 mL/min, detection; UV at 245 nm, 0.02 range, injected amount; 25 μL. Peak a represents *p*-benzoquinone. Bottom: HPLC analysis of L-DOPA (200 μM) oxidation by *p*-benzoquinone in absence (1) or presence (2) of 400 μM of thymol in buffer (without tyrosinase). Sampling time was chosen at 0 min (A), 10 min (B) and 20 min (C). HPLC operating conditions were as follows; Develosil ODS-UG-5 (Nomura Chemical, CO., LTD., Seto-Shi, Aichi, Japan). Solvent; 10 % MeCN/H_2O containing 0.2 % TFA, Flow rate 1.0 mL/min, detection; UV at 280 nm, 0.04 range, injected amount; 25 μL. Peak ***a*** and ***b*** represent *p*-benzoquinone and hydroquinone, respectively.

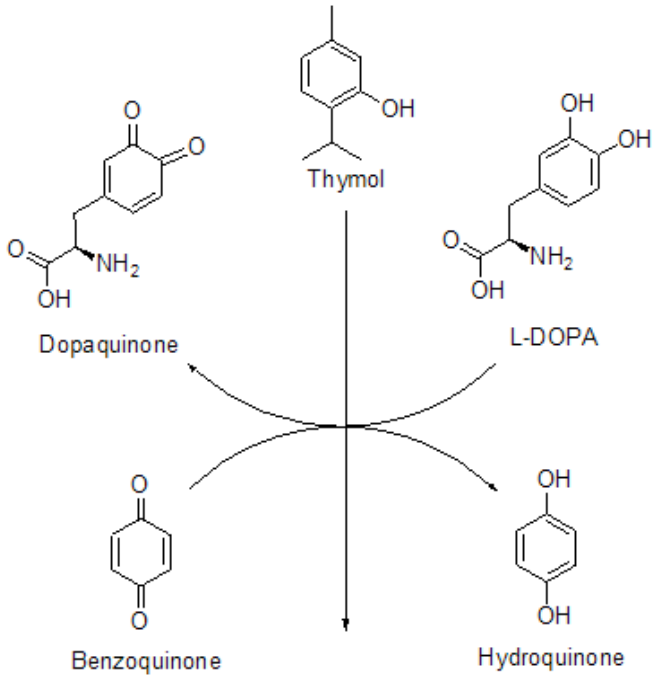

Scheme 2. The inhibitory effect of thymol on the redox reaction between *p*-benzoquinone and L-DOPA.

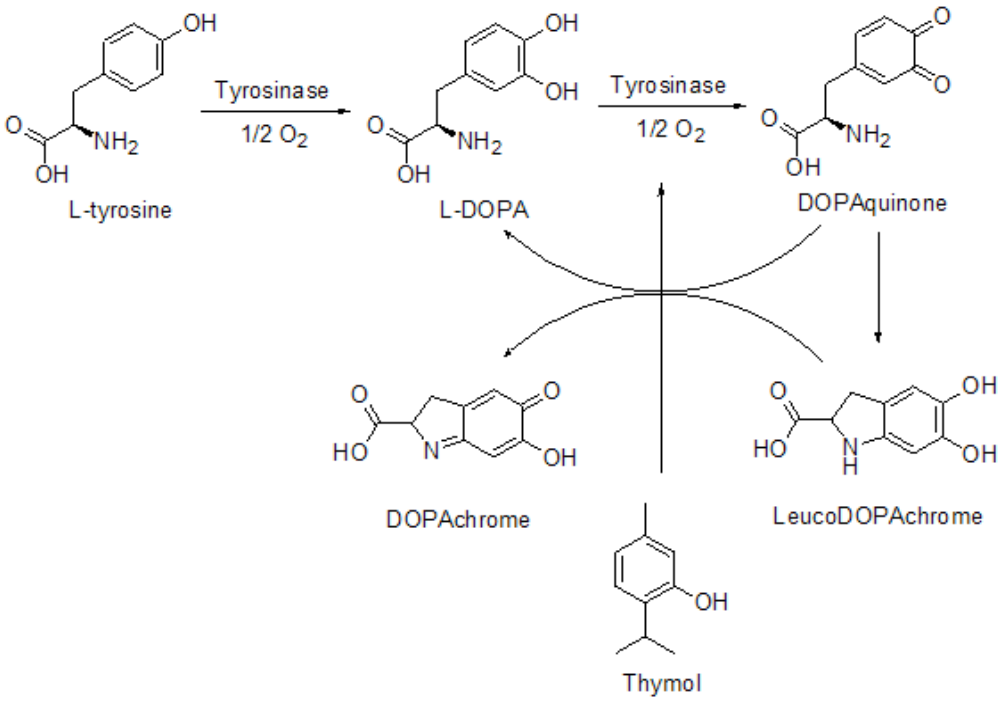

Scheme 3. Proposed scheme of inhibitory mechanism of melanin formation by thymol.

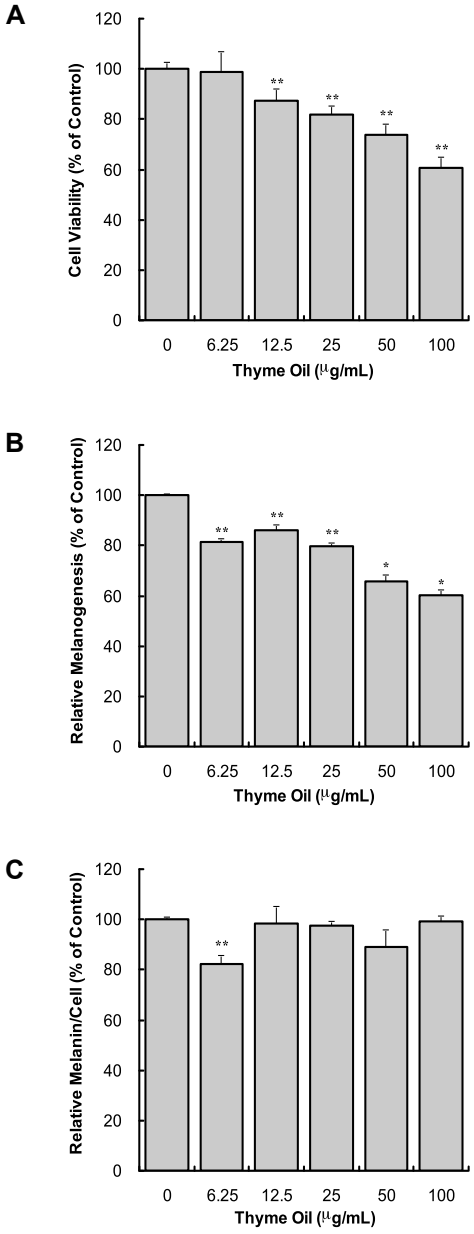

Figure 23. (**A**) Viabilities of B16-F10 melanoma cells following treatment with thyme oil for 72hr; data is expressed as a percentage of the number of viable cells observed with the control, and each column represents the mean ± S.D. of at least 4 determinations. (**B**) Total melanin content in B16 melanoma cells following treatment with thyme oil for 72hr; data is expressed as a percentage of melanin content per well observed with the control, and each column represents the mean ± S.D. of 4 determinations. (**C**) Cellular melanin content in B16 melanoma cells following treatment with thyme oil for 72hr measured as a percentage of melanin content per cell observed with the control, and each column represents the mean ± S.D. of 4 determinations. The statistical significance of differences was evaluated using Student's or Welch's *t*-test. Significantly different from the control value: **p* <0.05, ***p* <0.01.

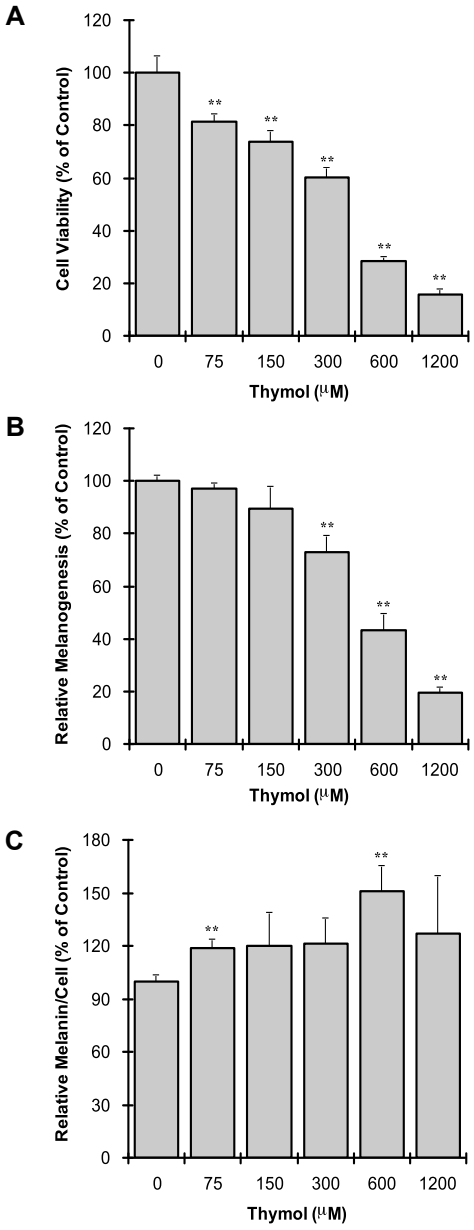

Figure 24. (**A**) Viabilities of B16-F10 melanoma cells following treatment with thymol for 72hr; data is expressed as a percentage of the number of viable cells observed with the control, and each column represents the mean ± S.D. of at least 4 determinations. (**B**) Total melanin content in B16 melanoma cells following treatment with thymol for 72hr; data is expressed as a percentage of melanin content per well observed with the control, and each column represents the mean ± S.D. of 4 determinations. (**C**) Cellular melanin content in B16 melanoma cells following treatment with thymol for 72hr measured as a percentage of melanin content per cell observed with the control, and each column represents the mean ± S.D. of 4 determinations. The statistical significance of differences was evaluated using Student's or Welch's *t*-test. Significantly different from the control value: $*p < 0.05$, $**p < 0.01$.

Table 1. Summary of the cytotoxic effect of thymol and of its related compounds

Tested Compounds	**IC_{50} (µg/mL)**	**Log*P*[a]**
Thyme Oil	N/A (~150)	N/A
Thymol	400 µM (60.09)	3.37
Carvacrol	550 µM (82.62)	3.37
Thymol Methyl Ether	>200 µM (>32.84)	3.63
p-Cymene	>1000 µM (>134.22)	3.76
Menthol	>1000 µM (>156.27)	2.75

[a]log*P* was calculated with ChemBioDraw Ultra 12

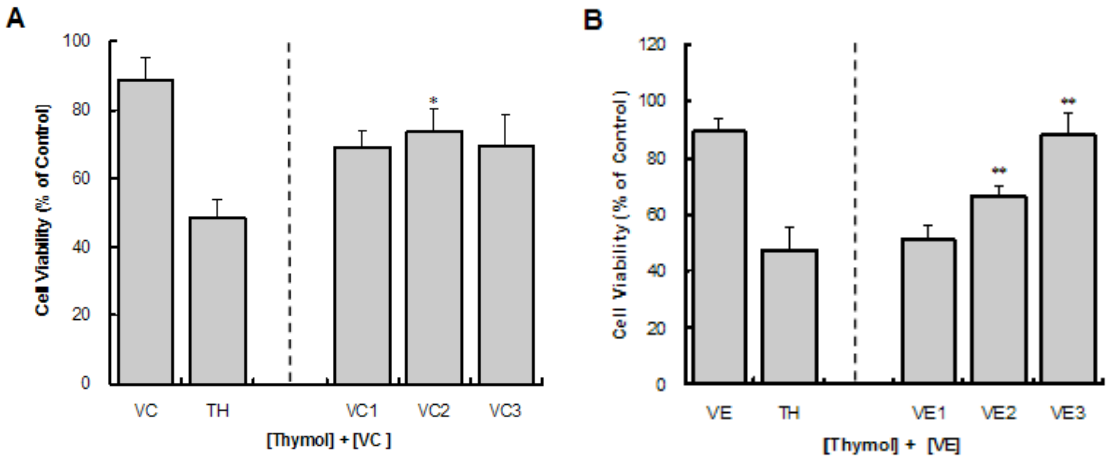

Figure 25. (**A**) Viabilities of B16 melanoma cells following treatment with 400 μM of thymol in the presence (VC1–VC3) or absence (TH) of vitamin C for 72hr. The concentrations of vitamin C applied to thymol treated cells were chosen at 200μM (VC1), 400μM (VC2) and 800μM (VC3). Cells are also treated with 800μM of vitamin C without thymol (VC). (**B**) Viabilities of B16 melanoma cells following treatment with 400 μM of thymol in the presence (VE1–VE3) or absence (TH) of vitamin E for 72hr. The concentrations of vitamin E applied to thymol treated cells were chosen at 100μM (VE1), 200μM (VE2) and 400μM (VE3). Cells are also treated with 400μM of vitamin E without thymol (VE). Data is expressed as a percentage of the number of viable cells observed with the TH control, and each column represents the mean ± S.D. of at least 4 determinations. The statistical significance of differences was evaluated using Student's or Welch's *t*-test. Significantly different from TH control value: **p* <0.05, ***p* <0.01.

Table 2. Summary table of the effect of tested treatment on thymol-applied B16 melanoma cells

Tested Treatments	Max. Recovery (%)	Mechanism [a]
Vitamin C	23	Two e^- Reduction/Radical Scavenging
Vitamin E	40	Radical Scavenging
BHA	17	Radical Scavenging
BHT	11	Radical Scavenging
GSH	22	Two e^- Reduction/Radical Scavenging
L-Cysteine	15	Nucleophilic Addition

[a]Possible mechanism to mask thymol cytotoxicity

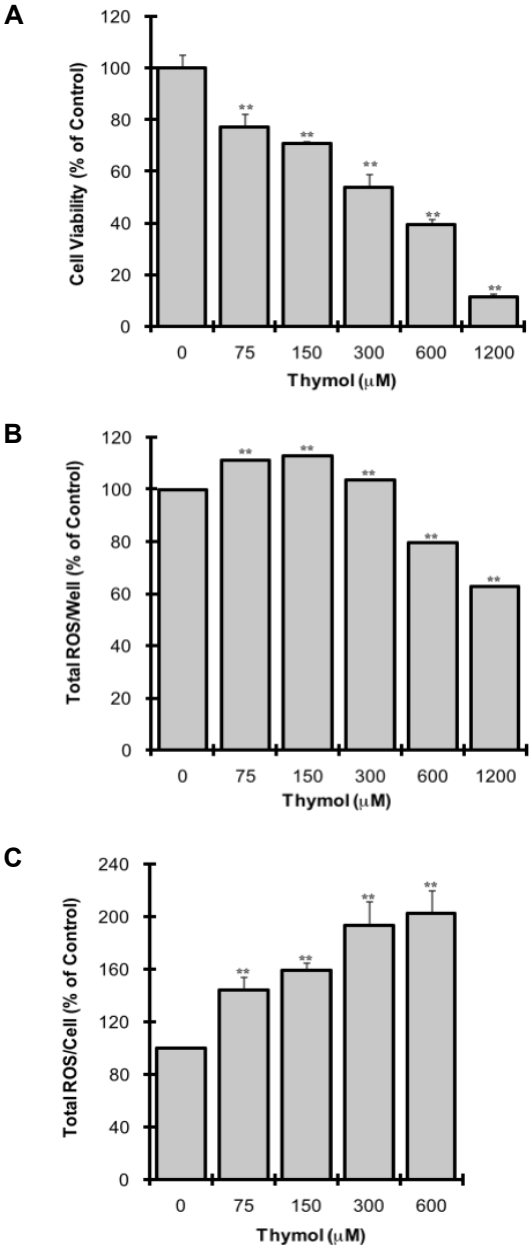

Figure 26. (**A**) Viabilities of B16-F10 melanoma cells following treatment with thymol for 1 hr; data is expressed as a percentage of the number of viable cells observed with the control, and each column represents the mean ± S.D. of at least 4 determinations. (**B**) Total ROS contents in B16 melanoma cells following treatment with thymol for 1 hr; data is expressed as a percentage of ROS content per well observed with the control, and each column represents the mean ± S.D. of 4 determinations. (**C**) Cellular ROS contents in B16 melanoma cells following treatment with thymol for 1 hr measured as a percentage of ROS contents per cell observed with the control, and each column represents the mean ± S.D. of 4 determinations. The statistical significance of differences was evaluated using Student's or Welch's *t*-test. Significantly different from the control value: $*p < 0.05$, $**p < 0.01$.

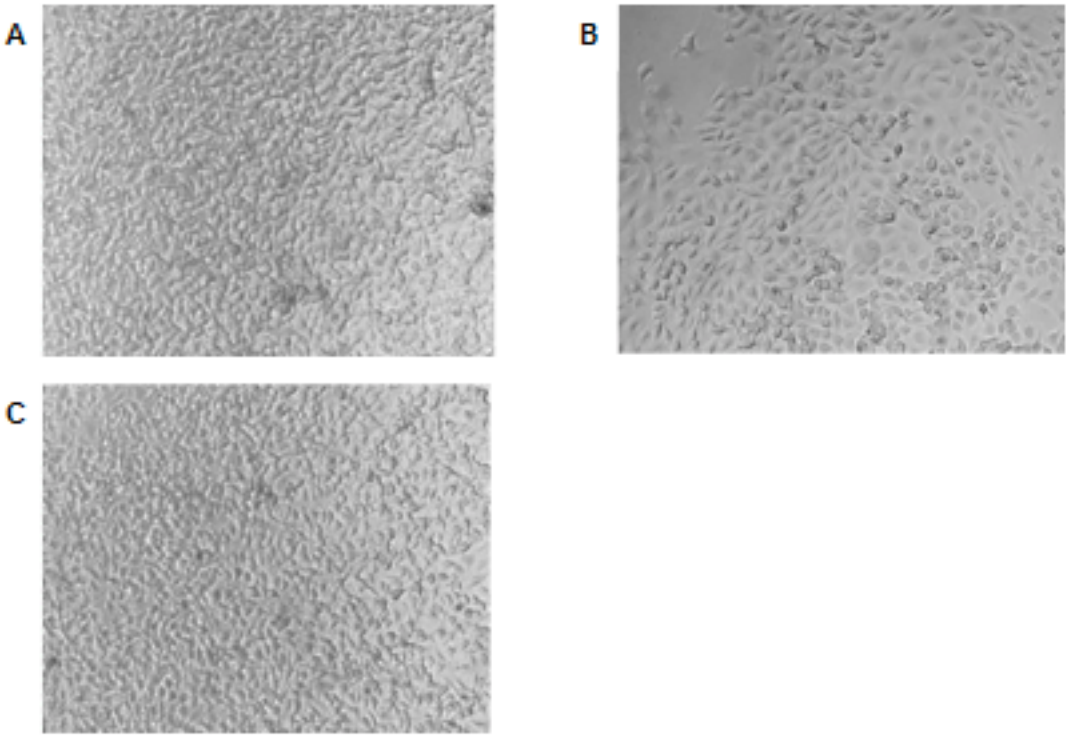

Figure 27. Cellular morphological change of B16-F10 melanoma cells. **A** represents cellular morphology of DMSO treated melanoma cells while **B** indicates morphological change of thymol (400 μM) treated B16 melanoma cells. **C** shows that morphology of melanoma cells treated with thymol (400 μM) and glutathione (400 μM).

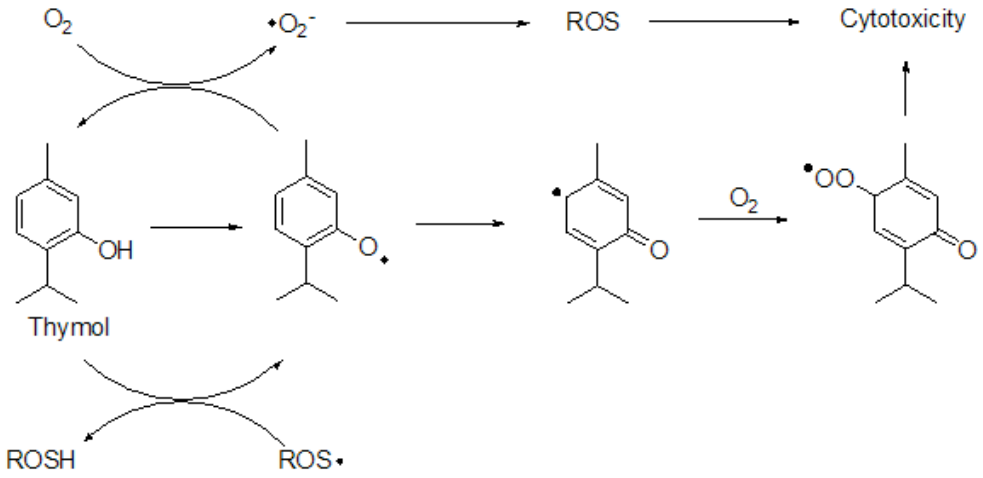

Scheme 4. Postulated mechanism of cytotoxicity of thymol on B16-F10 melanoma cells.

1.3 Conclusions and Remarks

Through the experiments with monophenol derivatives, the structural features of chemicals have a severe impact on tyrosinase-catalyzed melanin formation and the effect on B16-F10 melanoma cells. In the case of arbutin, it is a poor substrate of tyrosinase; however, because of the slow rate of oxidation of arbutin, tyrosinase activity was suppressed. The oxidation of arbutin conduces a further result; the corresponding *o*-quinone of arbutin is formed, and it leads to the melanocytotoxicity in B16 melanoma cells. As a result, cellular melanin content is reduced. On the other hand, thymol is not a substrate due to a problem in steric hinderance. In fact, thymol does not interact with tyrosinase; however, because of its antioxidative effect, thymol inhibits the redox reaction in melanogenesis. Moreover, in the case of thymol, the newly formed thymol-derived phenoxy radical causes prooxidative toxicity. As a result of cell free and cellular assays with arbutin and thymol, a small difference of the position and the types of functional groups causes a big impact on the difference in mechanism of action. In addition, the dynamic structural change through the enzymatic and chemical reactions may determine the cellular effects including cytotoxicity.

1.4 Materials and Methods

General

General procedures were the same in the previous work (*31-33*). The assays were performed in triplicate on separate occasions. Cells were viewed in 96-well plates approximately 72 hours after the chemical treatment.

Materials

Thyme oil, manufactured by NOW Foods (Bloomingdale, IL), was purchased at a local grocery store. Arbutin, thymol, carvacrol, menthol, *p*-cymene, 4-hydroxyanisole and hydroquinone were purchased from Aldrich Chemical Co. (Milwaukee, WI). L-Tyrosine, L-DOPA, L-cysteine, L-ascorbic acid (vitamin C), butylated hydroxyanisole, butylated hydorxytoluene, 2',7'-dichlorodihydrofluorescin diacetate (DCFH-DA), dimethyl sulfoxide (DMSO) and a protease inhibitor cocktail were purchased from Sigma Chemical Co. (St. Louis, MO). 1-methyl-3-methoxy-4-isopropylbenzene (thymol methyl ether) was purchased from SASF Supply Solutions (St. Louis, MO). α-tocophenol (vitamin E) was purchased from Lancaster Synthesis Inc. Pelham, NH). Glutathione was purchased from EASTMAN KODAK CO. (Rochester, N.Y.). 4-*tert*-butylcatechol was purchased from Fluka Chemika (Buchs, Switzerland). 1-methyl-3-methoxy-4-isopropylbenzene was purchased from SASF Supply Solutions (St. Louis, MO). *N*-acetyl-L-tyrosine was purchased from Tokyo Kasei Kogyo Co. Ltd. (Tokyo, Japan). Fatal bovine serum (FBS) and Dulbecco's modified Eagle's medium (DMEM), and 3-(4,5-dimethylthiazole-2-yl)-2,5-diphenyltetrazolium bromide (MTT) cell proliferation assay kit were purchased from ATCC (Manassas, VA, USA).

Instrumentation - Gas Chromatography-Mass Spectrometry (GC-MS)

The composition of thyme oil was analyzed by a GC-MS system (GC-17A/QP5050; Shimadzu Co., Ltd., Kyoto, Japan) equipped with a DB-5 column (30 m × 0.25 mm i.d., 0.25 μm film thickness; J & W Scientific Inc.). The temperature program was as follows: 45 °C for 8 min, followed by increases of 2.5 °C/min to 180 °C, and 10 °C/min to 250 °C, and holding for 3 min. The other parameters were as follows: injection temperature, 250 °C; ion source temperature, 250 °C; ionization energy, 70 eV; carrier gas, Helium (He) at 1.7 mL/min; injection volume, 1 μL (90 μg/mL Et_2O); split ratio, 1:20; mass range, m/z 50 to 450.

Enzyme/Spectrophotometric Assay

General procedures were the same as the previous works (*34, 35*) but slightly modified. All assays were performed in triplicate on separate occasions. The mushroom tyrosinase (EC 1.14.18.1) used for the bioassay was purchased from Sigma Chemical Co. and was purified by anion-exchange chromatography using DEAE-Sepharose Fast Flow (Pharmacia, Uppsala, Sweden) as previously described (*36*). The current experiment was subjected to use the purified tyrosinase. Although mushroom tyrosinase differs somewhat from those of other sources, this fungal enzyme was used for the entire experiment

because it is readily available. Throughout the experiment, L-DOPA or L-tyrosine was used as a substrate. In general, L-tyrosine was mainly used as a substrate since it is a natural substrate of tyrosinase. In a spectrophotometric experiment, the enzyme activity was monitored by dopachrome formation at 475 nm with a SpectraMAX Plus Microplate spectrophotometer (Molecular Devices, Sunnyvale, CA) at 30 °C. All samples were first dissolved in DMSO and used for the experiment after dilution. The final concentration of DMSO in the test solution was always 3.3%. The assay was performed as previously reported with slight modifications. First, 100 μL of a 3 mM L-DOPA or L-tyrosine aqueous solution was mixed with 2.1 mL of filtered distilled H_2O and 600 μL of 250 M phosphate buffer (pH 6.8) and incubated at 30 °C for 5 min. Then, 100 μL of the sample solution and 100 μL of the same phosphate buffer solution of the purified mushroom tyrosinase (1 μg/mL) were added in this order to the mixture. Results were expressed as in absorbance unit with appropriate wavelength (nm), and all data were processed with SigmaPlot 10 software (Systat Software Inc.).

Oxygen Consumption Assay

In general, procedure was previously described (*34, 35*). Briefly, 100 μL of a 3 mM L-DOPA or L-tyrosine aqueous solution was mixed with 2.1 mL of distilled H_2O, 600 μL of 67 mM phosphate buffer (pH 6.8) and 100 μL of sample-DMSO solution was incubated at 30 °C for 5 min. Then, 100 μL of the same phosphate buffer solution of the purified mushroom tyrosinase (1 μg/mL) was added and oxygen consumption was measured with an OBH 100 oxygen electrode and an oxygraph equipped with a water-jacket chamber of YSI 5300 (all from Yellow Springs Instruments Co., Yellow Springs, OH) maintained at 30 °C for 60 min. The results were expressed as the oxygen consumption in μM, and calibration of an oxygen electrode was performed by using 4-*tert*-butylcatechol and excess tyrosinase according to the previous report (*37*). All assays were performed in triplicate on separate occasions.

HPLC analysis

Time-dependent consumption of substrates and/or formation of products were monitored with HPLC analysis. The HPLC analysis was performed on an EYELA LPG-100 (Tokyo Rikakikai Co. Ltd., Tokyo, Japan) with an EYELA UV-7000 detector (Tokyo Rikakikai Co. Ltd., Tokyo, Japan) and Develosil ODS-UG-5 column (4.6 x 150 mm, Nomura Chemical Co., Ltd., Japan). In general, the operating conditions were as follows: solvent; 7% MeCN/H_2O containing 0.2 % TFA, flow rate; 1.0 mL/min, detection; UV at 280 nm, injected amount; 20 μL from above described 3 mL assay system. For analysis, samples were collected from the reaction mixtures described above at certain time points. The peak heights of each chromatographic peak were used to monitor the consumption of substrates and/or formation of products. In appropriate occasions, the results were expressed with the ratio of the height of sample peaks to that of control one, and then points were connected smoothly using the statistical software.

Cell culture

B16-F10 mouse melanoma cells (CRL-6475) were obtained from ATCC (Manassas, VA, USA), and cultured in continuous log phase growth in DMEM containing 10 % FBS. Cells were seeded in 96-well plates (2000 cells/well) and incubated at 37 °C in 5 % CO_2 for about 24 h before chemical treatment. Each chemical was applied in duplicate with a final content of 0.1% DMSO, and treated cells were cultured for 72 h before assays.

Melanin assay

The melanin content was determined as previously described (*38, 39*) with minor modifications. Cells were washed with PBS, harvested by trypsinization, and centrifuged for 10 min at 1500 x *g*. The cell pellets were then dissolved in 1.0 M NaOH containing 10 % DMSO during 2 h incubation at 80 °C. Melanin content was measured at 475 nm using a SpectraMax Plus spectrophotometer and SoftMax Pro software (Molecular Devices, Union City, CA, USA).

Cell viability assays

Cell viability was determined by trypan blue exclusion and MTT cell proliferation assays. Both bioassays basically provided the same results but the concentration leading to 50 % viable cells lost (IC_{50}) was established by trypan blue assay for steady comparison purpose. The appropriate concentrations of the test chemicals were selected by microscopic observation of the preliminary cell viability assay using a Nikon Diaphoto TMD (Nikon, Tokyo, Japan).

Trypan blue method

Cells were washed with PBS, and dispersed by trypsinization. An aliquot of the cells was mixed with a half volume of DMEM containing 10 % FBS, and then mixed with trypan blue solution (final content 0.1 %) at room temperature. Unstained cells (viable cells) were counted using a hemocytometer within 10 min after mixing with trypan blue solution.

MTT method

Cells were washed with PBS, and dispersed with trypsinization, and an aliquot of the cells was seeded in 96-well plates and incubated with DMEM containing 10 % FBS at 37 °C in 5 % CO_2 for 16 to 24 h. At the end of the period, 10 µl of MTT reagent were added to each well, which was then incubated at 37 °C in 5 % CO_2 for 4 h. Then, 100 µl of detergent reagent were added to each well. The plate was kept at room temperature in the dark for 2 h, and a relative amount of MTT reduction was determined based on the absorbance at 570 nm using a SpectraMax Plus spectrophotometer and SoftMax Pro software (Molecular Devices).

DCFH-DA method

The level of intracellular reactive oxygen species (ROS) in B16-F10 melanoma cells was measured by DCFH-DA method. Intracellular ROS oxidized the DCFH to a highly fluorescent compound, DCF, after esterase cleaves two acetate groups (*40*). General procedures are listed as previously described (*41, 42*) with minor modifications. Shortly, the cultured cells were incubated with the sample and DCFH-DA reagent for 60 min at 37 °C in the dark. After the incubation, cells were removed from the plate with trypsinization in order to measure fluorescent. The amount of formed DCF was measured using fluorolog-3 with DataMax (Instruments S.A., Inc. NJ, USA) with the excitation wavelength at 485 nm and the emission wavelength at 520 nm.

Cellular homogenate preparation

B16-F10 melanoma cells were cultured in flasks for 72 hrs for the designated concentration (~ 10^8 cells). On the day of the assay, cells were harvested with trypsinization in Ca/Mg free PBS. Buffer A (PBS with 1% of protease inhibitor cocktail) was added to stop further activity of typsin. Corrected cell mixture was centrifuged at 1,000 x g for 5 min at 4 °C. Corrected pellet was dissolved with buffer A, and was lysed with a sonic homogenizer for 30s. The mixture was centrifuged at 5,000 x g for 15 min at 4 °C. The corrected supernatant was used as cytosolic fraction for assays.

Statistical analysis

The statistical significance of differences was evaluated by either Student's or Welch's *t*-test after examining the variances using F test and $^{**}p < 0.01$ was considered to be statistically significant.

1.5 References

1. Kubo, I.; Bai-Ping, Y., Phenolic constituents of California buckeye fruit. *Phytochemistry* **1992,** 31, (11), 3793-3794.
2. Maeda, K.; Fukuda, M., Arbutin: mechanism of its depigmenting action in human melanocyte culture. *J. Pharmacol. Exp. Ther.* **1996,** 276, (2), 765-9.
3. Nihei, K.; Kubo, I., Identification of oxidation product of arbutin in mushroom tyrosinase assay system. *Bioorg. Med. Chem. Lett.* **2003,** 13, (14), 2409-2412.
4. Palumbo, A.; Dischia, M.; Misuraca, G.; Prota, G., Mechanism of inhibition of melanogenesis by hydroquinone. *Biochim. Biophys. Acta* **1991,** 1073, (1), 85-90.
5. Naish, S.; Holden, J. L.; Cooksey, C. J.; Riley, P. A., Major primary cytotoxic product of 4-hydroxyanisole oxidation by mushroom tyrosinase is 4-methoxy ortho benzoquinone. *Pigm. Cell Res.* **1988,** 1, (6), 382-5.
6. Palumbo, A.; Dischia, M.; Misuraca, G.; Prota, G., Skin depigmentation by hydroquinone - a chemical and biochemical insight. *Pigm. Cell Res.* **1992**, 299-303.
7. Jiménez-Cervantes, C.; Martínez-Esparza, M.; Pérez, C.; Daum, N.; Solano, F.; García-Borrón, J. C., Inhibition of melanogenesis in response to oxidative stress: transient downregulation of melanocyte differentiation markers and possible involvement of microphthalmia transcription factor. *J. Cell Sci.* **2001,** 114, (12), 2335.
8. Briganti, S.; Camera, E.; Picardo, M., Chemical and instrumental approaches to treat hyperpigmentation. *Pigm. Cell Res.* **2003,** 16, (2), 101-110.
9. Solano, F.; Briganti, S.; Picardo, M.; Ghanem, G., Hypopigmenting agents: an updated review on biological, chemical and clinical aspects. *Pigm. Cell Res.* **2006,** 19, (6), 550-571.
10. Kim, J.; Marshall, M.; Cornell, J.; Preston III, J.; Wei, C., Antibacterial activity of carvacrol, citral, and geraniol against Salmonella typhimurium in culture medium and on fish cubes. *J. Food Sci.* **1995,** 60, (6), 1364-1368.
11. Ultee, G., Bactericidal activity of carvacrol towards the food-borne pathogen Bacillus cereus. *J. Appl. Microbiol.* **1998,** 85, (2), 211-218.
12. Walsh, S. E.; Maillard, J. Y.; Russell, A.; Catrenich, C.; Charbonneau, D.; Bartolo, R., Activity and mechanisms of action of selected biocidal agents on Gram-positive and-negative bacteria. *J. Appl. Microbiol.* **2003,** 94, (2), 240-247.
13. Aeschbach, R.; Löliger, J.; Scott, B. C.; Murcia, A.; Butler, J.; Halliwell, B.; Aruoma, O. I., Antioxidant actions of thymol, carvacrol, 6-gingerol, zingerone and hydroxytyrosol. *Food Chem. Toxicol.* **1994,** 32, (1), 31-6.
14. Jukic, M.; Milos, M., Catalytic oxidation and antioxidant properties of thyme essential oils (*Thymus vulgarae* L.). *Croat. Chem. Acta* **2005,** 78, (1), 105-110.
15. Yanishlieva, N. V.; Marinova, E. M.; Gordon, M. H.; Raneva, V. G., Antioxidant activity and mechanism of action of thymol and carvacrol in two lipid systems. *Food Chem.* **1999,** 64, (1), 59-66.

16. Ultee, A.; Bennik, M.; Moezelaar, R., The phenolic hydroxyl group of carvacrol is essential for action against the food-borne pathogen Bacillus cereus. *Appl. Environ. Microbiol.* **2002,** 68, (4), 1561.
17. Amorati, R.; Pedulli, G. F.; Valgimigli, L.; Attanasi, O. A.; Filippone, P.; Fiorucci, C.; Saladino, R., Absolute rate constants for the reaction of peroxyl radicals with cardanol derivatives. *J. Chem. Soc. Perk. T. 2* **2001**, (11), 2142-2146.
18. Lee, S. J.; Umano, K.; Shibamoto, T.; Lee, K. G., Identification of volatile components in basil (*Ocimum basilicum* L.) and thyme leaves (*Thymus vulgaris* L.) and their antioxidant properties. *Food Chem.* **2005,** 91, (1), 131-137.
19. Kim, Y.; Uyama, H., Tyrosinase inhibitors from natural and synthetic sources: structure, inhibition mechanism and perspective for the future. *Cell Mol. Life Sci.* **2005,** 62, (15), 1707-1723.
20. Kubo, I.; Nihei, K.; Tsujimoto, K., Methyl *p*-coumarate, a melanin formation inhibitor in B16 mouse melanoma cells. *Bioorg. Med. Chem.* **2004,** 12, (20), 5349-5354.
21. Rice-Evans; Packer, C. A., In Flavonoids in Health and Disease. **1998**.
22. Haraguchi, H.; Saito, T.; Ishikawa, H.; Date, H.; Kataoka, S.; Tamura, Y.; Mizutani, K., Antiperoxidative Components of *Thymus vulgaris*. *Planta Med.* **1996,** 62, 217-221.
23. Sugawara, H.; Tobise, K.; Minami, H.; Uekita, K.; Yoshie, H.; Onodera, S., Diabetes mellitus and reperfusion injury increase the level of active oxygen-induced lipid peroxidation in rat cardiac membranes. *J. Clin. Exp. Med.* **1992,** 163, 237–238.
24. Kok, F. J.; Popple, G.; Melse, J.; Verheul, E.; Schouten, E. G.; Kruyssen, D. H. C. M.; Hofman, A., Do antioxidants and polyunsaturated fatty acids have a combined association with coronary arteriosclerosis? *Arteriosclerosis* **1991,** 86, 85–90.
25. Yagi, K., Lipid peroxides and human diseases. *Chem. Phys. Lipids* **1987,** 45, (2-4), 337-351.
26. Xu, J.; Zhou, F.; Ji, B.-P.; Pei, R.-S.; Xu, N., The antibacterial mechanism of carvacrol and thymol against Escherichia coli. *Lett. Appl. Microbiol.* **2008,** 47, (3), 174-179.
27. Dorman, H.; Deans, S., Antimicrobial agents from plants: antibacterial activity of plant volatile oils. *J. Appl. Microbiol.* **2000,** 88, (2), 308-316.
28. Braga, P. C.; Alfieri, M.; Culici, M.; Dal Sasso, M., Inhibitory activity of thymol against the formation and viability of Candida albicans hyphae. *Mycoses* **2007,** 50, (6), 502-506.
29. Bennis, S.; Chami, F.; Chami, N.; Bouchikhi, T.; Remmal, A., Surface alteration of Saccharomyces cerevisiae induced by thymol and eugenol. *Lett. Appl. Microbiol.* **2004,** 38, (6), 454-458.
30. Kohlert, C.; Schindler, G.; Marz, R. W.; Abel, G.; Brinkhaus, B.; Derendorf, H.; Grafe, E. U.; Veit, M., Systemic availability and pharmacokinetics of thymol in humans. *J. Clin. Pharmacol.* **2002,** 42, (7), 731.

31. Satooka, H.; Kubo, I., Effects of Thymol on Mushroom Tyrosinase-Catalyzed Melanin Formation. *J. Agr. Food Chem.* **2011,** 59, (16), 8908-8914.
32. Kubo, I.; Hori, I.; Nihei, K.; Satooka, H.; Cespedes, C. L.; Calderon, J. S., Insect Growth Inhibitory Activity and Cytotoxicity of Tannic Acid from Gallae Rhois. *Biopestic. Int.* **2008,** 4, (1), 6-14.
33. Nitoda, T.; Fan, M. D.; Kubo, I., Effects of cuminaldehyde on melanoma cells. *Phytother. Res.* **2008,** 22, (6), 809-813.
34. Kubo, I.; Kinst-Hori, I.; Yokokawa, Y., Tyrosinase inhibitors from *Anacardium occidentale* fruits. *J. Nat. Prod.* **1994,** 57, (4), 545-551.
35. Kubo, I.; Chen, Q.; Nihei, K.; Calderon, J.; Cespedes, C., Tyrosinase inhibition kinetics of anisic acid. *Z. Naturforsch. C.* **2003,** 58, (9-10), 713-718.
36. Espin, J. C.; Wichers, H. J., Slow-binding inhibition of mushroom (Agaricus bisporus) tyrosinase isoforms by tropolone. *J. Agric. Food Chem.* **1999,** 47, (7), 2638-2644.
37. Rodriguez-López, J. N.; Ros-Martínez, J. R.; Varón, R.; García-Cánovas, F., Calibration of a Clark-Type oxygen electrode by tyrosinase-catalyzed oxidation of 4-tert-butylcatechol. *Anal. Biochem.* **1992,** 202, (2), 356-60.
38. Kageyama, A.; Oka, M.; Nakamura, S.; Ueyama, T.; Saito, N.; Hearing, V. J.; Ichihashi, M.; Nishigori, C., Down-regulation of Melanogenesis by Phospholipase D2 through Ubiquitin Proteasome-mediated Degradation of Tyrosinase. *J. Biol. Chem.* **2004,** 279, (26), 27774-27780.
39. Venkatasamy, R.; Faas, L.; Young, A. R.; Raman, A.; Hider, R. C., Effects of piperine analogues on stimulation of melanocyte proliferation and melanocyte differentiation. *Bioorg. Med. Chem.* **2004,** 12, (8), 1905-1920.
40. Rhee, S. G.; Chang, T.-S.; Jeong, W.; Kang, D., Methods for detection and measurement of hydrogen peroxide inside and outside of cells. *Mol. Cells* **2010,** 29, (6), 539-549.
41. Galati, G.; Lin, A.; Sultan, A. M.; O'Brien, P. J., Cellular and in vivo hepatotoxicity caused by green tea phenolic acids and catechins. *Free Radical Bio. Med.* **2006,** 40, (4), 570-80.
42. Tsoncheva, V. L.; Milchev, G. I., Delayed reproductive death and ROS levels in the progeny of irradiated melanoma cells. *Z. Naturforsch, C* **2004,** 59, (3-4), 297-301.

Chapter 2

Resorcinolic Lipids

2.1 Effect of Cardols on Mushroom Tyrosinase and B16 Melanoma Cells

2.1.1 INTRODUCTION

Resorcinol moiety is one of the most abundant chemical functional groups in nature; many natural products including cardols, flavonoids, and stilbenoids contain the resorcinol moiety as a part of their structures. In our continuing search for a melanin formation inhibitor from natural sources, cardol triene, 5[8(Z),11(Z),14-pentadecatrienyl] resorcinol, cardol diene, 5[8(Z),14-pentadecadenyl]resorcinol, and cardol monoene, 5[8 (Z)-pentadecaeyl]resorcinol, were previously isolated from the cashew *Anacardium occidentale* L. (Anacardiaceae) in our previous studies (*1*), and in this paper, for simplicity, referred to as cardol ($C_{15:3}$) (**1**), cardol ($C_{15:2}$) (**2**) and cardol ($C_{15:1}$) (**3**) (see Figure 28 for the structures), respectively. Cardols are identified in many edible plants such as pistachio, *Pistacia vera*, macadamia, *Macademia ternifolia*, and mango, *Magifera indica* (*2*). Cashew nutshell liquid, a natural resin found in cashew nutshell, is also known to contain cardols (*3*). In addition, similar resorcinolic lipids were also characterized from grain plants such as wheat and rye (*4*). The biological significance, including antimicrobial and antioxidative activities of these cardols with cashew, has been extensively studied (*5*-*8*). In addition to these well-studied biological activities, cardols ($C_{15:3}$, $C_{15:2}$, and $C_{15:1}$) showed the competitive inhibition on the oxidation of L-DOPA in previous reports (*1*), and hence, they are expected to inhibit tyrosinase activity. 5-pentylresorcinol, commonly known as olivetol, is also a naturally occurring resorcinolic lipid. For the comparative simplicity, 5-pentylresorcinol is referred to as cardol ($C_{5:0}$) (**6**). Cardol ($C_{5:0}$) is characterized from some certain lichens such as oakmoss, *Evernia prunastri* (L) Ach. (*9*). As well as cardols ($C_{15:n}$), some biological activities of cardol ($C_{5:0}$) such as an antioxidative effect, are previously reported (*5*). In spite of the wide variety of biological outcome of cardols, the influence of these naturally occurring resorcinolic lipids on melanogenesis and toxicological action in mechanistic points of view are not fully understood. These aspects and questions prompt us to investigate cardols.

2.1.2 RESULTS

Effect of Cardols on L-tyrosine Oxidation

L-tyrosine oxidation is one of the key steps in Raper-Mason mealanin synthetic pathway. Hence, the inhibitory activity of cardols on the oxidation of L-tyrosine was examined first. Tyrosinase activity was monitored with three different methods: UV-Vis spectra at 475 nm, oxygen consumption, and high performance liquid chromatography (HPLC) analysis. Tyrosinase (1.0 μg/mL) was incubated with L-tyrosine (100 μM) and inhibitors for 60 min. Cardol ($C_{15:3}$) reduced dopachrome formation in a concentration-dependent manner with UV-Vis spectra assay (Figure 29A). The addition of cardol ($C_{15:3}$)

did not extend the lag phase. It should be noted that cardol ($C_{15:3}$) was highly lipophilic and is extremely difficult to be dissolved in the water-based solutions; hence, examined highest concentration was 2.5 μM (data not shown). In addition to that, cardol ($C_{15:3}$) was used rather than the other cardol ($C_{15:n}$). This is because there is no difference in inhibitory activity due to the presence of double bonding was observed in current or previous studies (data not shown) (*10, 11*). Hence, the most soluble compound, cardol ($C_{15:3}$) was place as a central for the assay. Oxygen consumption of L-tyrosine with the addition of cardol ($C_{15:3}$), surprisingly, was almost exactly the same as that of the control (Figure 29B). The results of UV-Vis and oxygen consumption assays were usually followed by each other. Thus, this difference in the results may be the key to clarify the mechanism of inhibition. Subsequently, the effect of cardol ($C_{5:0}$) or olivetol on tyrosinase-catalyzed L-tyrosine oxidation was also measured. With the UV-Vis assay, cardol ($C_{5:0}$) suppressed dopachrome formation in a dose-dependent manner (Figure 30A). The typical lag phase was observed and this lag phase was extended with the addition of a higher concentration of cardol ($C_{5:0}$). Interestingly, in the case of cardol ($C_{5:0}$), the concentration-dependent inhibitory activity was also observed with the oxygen consumption assay (Figure 30B). At this point, several differences in the results were observed, which implies that pentadeca(en)yl and pentyl alkyl side chains exhibit the different inhibitory mechanism of tyrosinase (since both molecules share the same resorcinol moiety).

Effect of Cardols on L-DOPA Oxidation

The effect of cardols on L-DOPA oxidation was also tested. Both cardols inhibited tyrosinase-catalyzed L-DOPA oxidation. As a result of UV-Vis spectra at 475 nm, dopachrome formation was suppressed with the addition of cardol ($C_{15:3}$) in a dose-dependent manner, but the inhibitory activity was very weak (Figure 31A). 10-19 % of dopachrome formation was disrupted with the addition of cardol ($C_{15:3}$). For the first 5 min, the inhibitory effect was not observed; however, the inhibitory effect was larger at the end of the reaction. This weak inhibitory effect of cardol ($C_{15:3}$), surprisingly, was not observed with the oxygen consumption assay (Figure 31B). The addition of 2.5 μM cardol ($C_{15:3}$) or a lower concentration of cardol ($C_{15:3}$) did not show any inhibition on the consumption of oxygen during tyrosinase-catalyzed L-DOPA oxidation. Thus, it appeared that cardol ($C_{15:3}$) did not inhibit the oxygen consumption of tyrosinase-catalyzed reaction but did inhibit dopachrome formation. With the consecutive UV-Vis assay, cardol (C15:3) showed a weak inhibitory activity on dopachrome formation (Figure 32A and B). In the consecutive spectra, the peak at 320 nm and 475 nm were slightly suppressed, which indicated that dopaquinone and dopachrome formation was reduced. In the case of cardol ($C_{5:0}$), the inhibitory activity was observed with both UV-Vis and oxygen consumption assay. In Figure 33A, cardol ($C_{5:0}$) slightly suppressed L-DOPA oxidation in a concentration-dependent manner. The dopachrome formation was delayed with the addition of cardol ($C_{5:0}$); however, the tyrosinase activity was not completely diminished. In other words, no inactivation of tyrosinase was observed. In the case of cardol ($C_{5:0}$), it showed inhibitory effect on oxygen consumption of tyrosinase-catalyzed reaction unlike

cardol ($C_{15:3}$) (Figure 33B). Similar to Figure 33A, cardol ($C_{5:0}$) dose-dependently inhibited the oxygen consumption of tyrosinase-catalyzed L-DOPA oxidation (Figure 33B). It should be noted that the difference between the assay of UV-Vis and oxygen consumption was experimental condition due to instrumental restriction: static vs. stirring. In UV-Vis assay, there is no option to stir the reaction mixture during the assay; however, oxygen consumption has to be monitored in a stirring condition. It is possible that this physical interruption with a stirrer leads to the difference in the results of inhibition. This postulate was further confirmed using the HPLC assay. Tyrosinase activity was monitored under two conditions: static and stirring. In a stirring condition, the reaction mixture was stirred in an entire reaction period, while, in a static condition, the reaction was proceeded without any mixing. Since the available oxygen in cuvette was about 250 μM, there is enough oxygen for 100 μM L-DOPA oxidation in a static condition. In the case of cardol ($C_{15:3}$), as expected, the inhibitory effect was diminished with the introduction of stirring. In Figure 34A, L-DOPA consumption was suppressed by about 13 % in L-DOPA consumption with the addition of 2.5 μM cardol ($C_{15:3}$); however, tyrosinase-catalyzed L-DOPA consumption in a stirring condition was not inhibited even though 2.5 μM cardol ($C_{15:3}$) was added (Figure 34B). This unique and considerable difference was not observed in the case of cardol ($C_{5:0}$). In a static condition, cardol ($C_{5:0}$) inhibited L-DOPA oxidation about 16.7 %. This inhibitory effect for first 10 min was slightly reduced; however, about 17 % of inhibition was still observed at the end of reaction in a stirring condition (Figure 35A and B). This implied that the secondary effect was involved in the inhibitory effect of cardol ($C_{15:3}$) since the simple competitive binding of resorcinol moiety to binuclear copper cannot be disrupted by stirring. From this point of view, it is now possible to postulate that weak interaction of cardol ($C_{15:3}$) to tyrosinase is required to inhibit its activity. The lipophilicity of cardol ($C_{15:3}$) is relatively high and it is possibly to interact with the hydrophobic region of the enzyme. This postulate is probably not applied to the case of cardol ($C_{5:0}$) since the hydrophobicity of cardol ($C_{5:0}$) is significantly lower than that of cardols ($C_{15:3}$). The difference in log *P* of cardol ($C_{15:3}$) and cardol ($C_{5:0}$) is 6.68 and 3.41, respectively. Thus, the investigation was extended to search for the effect of alkyl chain of resorcinolic lipid on tyrosinase activity.

Effect of Cardols on N-acetyl-L-tyrosine Oxidation

To test our postulate, *N*-acetyl-L-tyrosine was used to examine the "direct" interaction of resorcinolic lipids to tyrosinase. Because of the blockage of intracyclization of *N*-acetyldopaquinone, only the tyrosinase-catalyzed reaction step in melanin synthesis can be examined with *N*-acetyl-L-tyrosine. First, the effect of 1 μM cardol ($C_{15:3}$) on tyrosinase (1.0 μg/mL) was examined with 100 μM *N*-acetyl-L-tyrosine in a stationary phase. HPLC assay was used to determine the tyrosinase activity. Cardol ($C_{15:3}$) suppressed the consumption of *N*-acetyl-L-tyrosine by tyrosinase (Figure 36A). The inhibitory effect of cardol ($C_{15:3}$) was not observed until 30 min, and after 30 min the inhibitory effect was significantly observed, suggesting that inhibitory interaction of cardol ($C_{15:3}$) was *slow* interaction. This inhibitory effect was not observed in a stirring condition as observed with UV-Vis or oxygen consumption assays (Figure 36B).

Similarly, cardol ($C_{5:0}$) showed inhibition on *N*-acetyl-L-tyrosine oxidation in a stationary phase (Figure 37A). The inhibitory effect of cardol ($C_{5:0}$) was observed by the first 15 min, indicating that cardol ($C_{5:0}$) exhibited *fast* interaction. In the case of cardol ($C_{5:0}$), it also showed the inhibitory effect on *N*-acetyl-L-tyrosine consumption in a "stirring" condition (Figure 37B). Based on the result, both cardol ($C_{15:3}$) and cardol ($C_{5:0}$) showed direct inhibition on tyrosinase. Because both cardols inhibit monophenolase activity of tyrosinase, presumably they interact with oxy-tyrosinase; however, the mechanism of the inhibition should be different.

Effect of Cardol ($C_{10:0}$) on Tyrosinase

There is a considerable difference between two tested cardols, and presumably the difference is due to the hydrophobicity of alkyl chain. Hence, the effect of hydrophobicity of alkyl chain on mushroom tyrosinase was examined using cardol ($C_{10:0}$) (**5**). The tyrosinase activity was monitored using HPLC since this instrumental assay allowed to test two different conditions: static and stirring. In Figure 38A, cardol ($C_{10:0}$) showed the significant inhibitory effect on the L-DOPA consumption in a static condition. The inhibitory effect was more potent (55.6 % of inhibition) than the other two cardols, which may indicate that there is an optimal length of hydrophobic alkyl chain for the inhibitory effect. This inhibitory effect, interestingly, was reduced in the case of stirring condition; however, unlike cardol ($C_{15:3}$), cardol ($C_{10:0}$) still inhibited L-DOPA oxidation by 34.4 % (Figure 38B). The inhibitory effect of cardol ($C_{10:0}$) on tyrosinase-catalyzed *N*-acetyl-L-tyrosine oxidation was also examined. Cardol ($C_{10:0}$) suppressed the consumption of *N*-acetyl-L-tyrosine in a stationary phase (data not shown). This inhibitory effect was slightly decreased by the stirring. It appeared that the inhibitory effect of cardols is disrupted as if the cardol has a longer alkyl chain. In other words, cardol with a longer alkyl chain requires *slow* and *weak* interaction, and the interaction is easily disrupted by the stirring.

Preincubational Effect of Cardols

Preincubational effect of cardols on tyrosinase-catalyzed melanin formation was also examined. Cardol ($C_{15:3}$) and cardol ($C_{5:0}$) was first incubated with tyrosinase for 0, 10, or 20 min and then L-DOPA was added as a substrate to start the reaction. All of the reaction was proceeded in a stationary phase, and tyrosinase activity was measured with HPLC assay. Inhibitory effect of cardol ($C_{15:3}$) on dopachrome formation was enhanced with 10 and 20 min of preincubation (Figure 39A) in a time-dependent manner while cardol ($C_{5:0}$) did not enhance its inhibitory activity with 10 or 20 min of preincubation (Figure 39B). It appeared that there is a difference in results of the preincubational effects between pentadeca(en)yl and pentyl alkyl chain of cardols, indicating that there is a correlation between the preincubational effects and hydrophobicity. The enhancement of inhibitory effect by preincubation was increased with the extension of the preincubational period in only the case of cardol ($C_{15:3}$). This suggested that hydrophobic inhibitory interaction requires "time" and this had been shown in previous data (Figure 29, 31, 34, and 36). Moreover, this preincubational effect of cardols were also observed when L-

tyrosine was used as a substrate (data not shown), suggesting that, as described, both cardols interact with oxy-tyrosinase as a monophenol analogue.

Irreversibility of Inhibitory Effect of Cardols

For further proof of our postulate (hydrophobic inhibitory interaction), the irreversibility of the inhibition was examined. Thus, the effect of stirring during the reaction was tested. Cardol ($C_{15:3}$) or cardol ($C_{5:0}$) was added with the mixture of L-DOPA (1000 μM) and tyrosinase (1.0μg/mL). Since the amount of residual oxygen is approximately 250 μM, only 500 μM L-DOPA was able to oxidize for the first 15 min. At 15 min the reaction mixture was mixed with a voltex to add oxygen to help further L-DOPA oxidation. In Figure 40A, cardol ($C_{15:3}$) suppressed L-DOPA oxidation for the first 15 min and further oxidation of L-DOPA was not observed even though the mixture was mixed compared to the control. However, further oxidation of L-DOPA was observed for the last 15 min in the case of cardol ($C_{5:0}$) as well as the first half (Figure 40B). There was no difference in L-DOPA consumption between the sample and control before and after the mixing in the case of cardol ($C_{5:0}$) (the control and sample lines were parallel to each other for 30 min), which is probably due to the continuous competitive binding of cardol ($C_{5:0}$). Thus, cardol ($C_{15:3}$) did inhibit tyrosinase-catalyzed melanin formation irreversibly while cardol ($C_{5:0}$) did it reversibly. In addition to these two cardols, cardol ($C_{10:0}$) was also tested for a comparison (data not shown). In the case of cardol ($C_{10:0}$), the further oxidation of L-DOPA after 15 min was observed, but the amount of consumed L-DOPA after 15 min was in between cardol ($C_{5:0}$) and cardol ($C_{15:3}$). This ultimately suggests that there is a correlation between the length of alkyl side chain and the irreversibility of the inhibitory effect. Combining all of the results obtained, cardol ($C_{15:3}$) irreversibly inhibits tyrosinase activity through the hydrophobic portion of the alkyl chain. On the other hand, cardol ($C_{5:0}$) inhibitory mechanism is simply the competitive binding of resorcinol moiety, in which similar examples have been previously reported (*12-14*). Thus, both hydrophilic resorcinol moiety and hydrophobic pentadeca(en)yl side chain play an important role to inactivate the enzyme activity. More, specifically, the resorcinol moiety first quickly competes with the binuclear copper active site as a substrate analogue, and then the hydrophobic pentadeca(en)yl side chain slowly interacts with the hydrophobic domain proximate to the active site in the enzyme. The inactivation of the enzyme by cardols undergoes without oxygen, indicating that k_{cat} type inactivation (inactivation of the enzyme by products of the reaction) is not involved. This tyrosinase inactivation activity of cardols can be explained by their structural feature.

Effect of Cardols on B16-F10 Melanoma Cells

In a preliminary cell free experiment using mushroom tyrosinase, 5-pentadeca (en)ylresorcinols, cardols ($C_{15:n}$), were found to inactivate the mushroom tyrosinase without being oxidized. Tyrosinase-catalyzed dopachrome formation is a key step in melanogenesis and therefore, inhibitors of dopachrome formation are expected to inhibit cellular melanin production. Thus, the investigation was extended to test for the effects of cardols on murine B16-F10 melanoma cells. The investigation was began with cardol

($C_{15:3}$) (**1**) because cardol ($C_{15:3}$) was placed on the center in cell free experiments due to its highest solubility among the tested cardol ($C_{15:n}$) in water based test solutions. (*10*). It should be also noted that there are no significant differences in cytotoxicity among cardol ($C_{15:3}$), cardol ($C_{15:2}$) (**2**), cardol ($C_{15:1}$) (**3**) and cardol ($C_{15:0}$) (**4**) (See Figure 28 for the structures) in previous studies (*11*), indicating that double bond in the side chain is not essential in eliciting the activity. Cardol ($C_{15:3}$) did not suppress melanin formation in the cultured murine B16-F10 melanoma cells but rather increased it up to 25 μM. The cell viability of cardol ($C_{15:3}$)-treated cells was significantly decreased compared to the control (P <0.01) in the range of 25-50 μM (Figure 41A). Observed IC_{50} was at 28 μM (8.8 μg/mL) and complete lethality was observed at 50 μM. The decrease of cell viability from at 25 μM to at 50 μM was considerably large. This sudden death of cells were observed when the chemical concentration (>25 μM) was exceeded the critical point, which is often observed in the case of surfactant molecule (*15-17*). Total melanin content was slightly suppressed in a dose-dependent manner and the difference from the control was statistically significant (P <0.01) in the range of 12.5-50 μM (Figure 41B). The cellular melanin content, as described above, was slightly enhanced (Figure 41C) in a dose-dependent manner. At 25 μM, the difference from the control was statistically significant (P <0.01).

In the case of cardol ($C_{5:0}$) (**6**), known as olivetol, it also did not suppress melanin production in the cultured murine B16-F10 melanoma cells. Cardol ($C_{5:0}$) showed concentration-dependent suppression in the cell viability and the cell viabilities between 100-800 μM were statistically significant different (P <0.01) (Figure 42A). The IC_{50} was established as 300 μM (54.1 μg/mL) and complete lethality was observed at 800 μM. Total melanin content was also dose-dependently suppressed with the addition of cardol ($C_{5:0}$) (Figure 42B). In the range of 100-800 μM, the difference in the total melanin content from the control was statistically significant (P <0.01). The cellular melanin content was not suppressed but rather enhanced up to 400 μM (Figure 42C) and statistical significance was observed at 400 μM. It should be noted that cellular melanin content at 800 μM is zero; however, this effect was not due to the antimelanogenic effect. Since the number of viable cell is zero at this concentration, the total amount of melanin production at equivalent concentration was suppressed.

Both cardol ($C_{15:3}$) and ($C_{5:0}$) did not inhibit melanogenesis in melanocytes. As described, tyrosinase is the key enzyme in melanin synthetic pathway and hence tyrosinase inhibitors are expected to inhibit cellular melanogenesis; however, paradoxically, the inhibition of mushroom tyrosinase activity was reported not to correlate with that of melanogenesis in cultured melanocytes (*18*). Melanogenesis inhibition in melanocyte is not simply to inhibit tyrosinase but involves more complex biochemical reactions (*19*). Instead of antimelanogenic effect, cardols showed potent cytotoxic effects on B16-F10 melanoma cells. The toxicity mechanism of these resorcinolic lipids is poorly investigated. Clarification of the mechanism of toxicity is valuable for the utilization of cardols as functional phytochemical or simply for scientific purposes. Thus, investigation was now focused on identifying the mechanism of the toxicity of cardols.

Toxic Effect of Cardol ($C_{10:0}$) and Resorcinol

According to the toxicological results of cardol ($C_{15:3}$) and cardol ($C_{5:0}$), there are big gaps between pentadeca(en)yl and pentyl alkyl side chain on the influence on the cell viability. To answer this postulate, cardol ($C_{10:0}$) (**5**) and resorcinol (**7**) (See Figure 28 for the structure) were also comparatively examined in a same manner of cellular experiment. Cardol ($C_{10:0}$) showed concentration-dependent suppression of cell viability (data not shown). Observed IC_{50} was at 42 μM (12.3 μg/mL) and almost complete lethality was observed above 100 μM. In the case of resorcinol, resorcinol dose-dependently suppressed cell viability (data not shown). Observed IC_{50} was at 750 μM , and almost complete lethality was observed at 4000 μM. By comparing the IC_{50}, there is a clear influence of longer alkyl side chain of cardol to cytotoxic effect. In other words, longer alkyl side chain exhibited greater toxicity on B16 melanoma cells. This effect/ phenomenon was previously observed in the case of aliphatic alcohol and aldehyde (*15, 20, 21*). Previous studies showed that the mechanism of toxicity of aliphatic compounds is a result of their nonionic surfactant properties to disrupt the biological functions of plasma membrane. Hence, at least, cardol with a longer alkyl chain, that is to say, the surfactant activity may be involved in the mechanism of toxicity of cardol ($C_{15:n}$).

Recovery from the Toxicity

Further investigation to identify the mechanism of toxicity of cardols was conducted by using vitamin C and butylated hydroxyanisole (BHA). Vitamin C or BHA were added to B16-F10 melanoma cells treated when 25 μM cardol ($C_{15:3}$) (approximately equivalent to IC_{50}) was applied, and the cell viability was examined after 72 hrs of incubation. The cytotoxic effect of cardol ($C_{15:3}$) was suppressed with the addition of both vitamin C and BHA. Vitamin C dose-dependently suppressed the cytotoxicity of cardol ($C_{15:3}$) and the maximal recovery was approximately 40% in cell viability (Figure 43A). Subsequently, BHA was used as a radical scavenger to diminish the single electron oxidation process. BHA suppressed the toxic effect of cardol ($C_{15:3}$) and the highest recovery (approximately 30%) was made with the addition of 25 μM BHA (Figure 43B). It appeared that the recovery of BHA from the cytotoxicity of cardol ($C_{15:3}$) on B16-F10 melanoma cells was not the dose-dependent manner but rather enhanced the toxicity at the higher concentrations. This toxic effect is probably due to the high concentration of BHA. Subsequently, vitamin C and BHA were also examined with cardol ($C_{5:0}$)-treated B16-F10 melanoma cells in the same manner as the case of cardol ($C_{15:3}$). The cytotoxicity of cardol ($C_{5:0}$) at 300 μM (approximately equivalent to IC_{50}) was reversed approximately by 30% in cell viability with the addition of an equivalent vitamin C (Figure 44A). This protective effect against the toxic effect of cardol ($C_{5:0}$) was not dose-dependent. In addition, BHA was also tested. As a result, BHA also showed approximately 20% reversed effect in cell viability with the addition of 100 μM BHA (Figure 44B). Subsequently, same experiments were conducted by using resorcinol as a comparison. B16 melanoma cells are treated with 1000 μM resorcinol and either vitamin C or BHA. The cytotoxicity of resorcinol-treated cells was suppressed with the addition

of vitamin C but not with BHA (data not shown), indicating that resorcinol were more likely to be oxidized by intracellular components such as microsomes. Thus, the cytotoxicity of cardol ($C_{15:3}$), cardol ($C_{5:0}$) and resorcinol were partly prevented; however the mechanism of cardols and resorcinol was presumably different. More specifically, both vitamin C and BHA showed controversial effects on the cytotoxicity of both cardol ($C_{15:3}$) and cardol ($C_{5:0}$) in murine B16-F10 melanoma cells. Since BHA does acts as a two-electron reducing agent (Vitamin C can act either single or two electron reductant), the cytotoxicity of both cardol ($C_{15:3}$) and cardol ($C_{5:0}$) may not be affected by their intracellular oxidation. However, the cytotoxicity of resorcinol was prevented with vitamin C and it appeared that resorcinol is intracellularly oxidized, which implies that alkyl side chain bring the big impact on the mechanism of toxicity, although a more thorough studies of their mechanism are beyond the scope of the present work.

Intracellular Oxidative Stress

Intracellular oxidative stress was measured with 2',7'-dichlorodihydrofluorescin diacetate (DCFH-DA) assay. After 1hr of incubation with cardols and DCFH-DA, B16-F10 melanoma cells were assayed to measure intracellular ROS. Cardol ($C_{15:3}$) enhanced the formation of intracellular ROS without affecting cell viability. Within 3.125-30 μM, the total ROS were increased even though cellular viability did not change (Figure 45A and B). The cellular ROS generation above 3.125 μM was enhanced in a concentration-dependent manner and is significantly different from the control (P <0.01) (Figure 45C). The highest increase of ROS was observed when 50 μM cardol ($C_{15:3}$) was applied to the cells. Approximately five times the higher amount of ROS than control was generated. As a result, cardol ($C_{15:3}$) increases intracellular ROS; however, it seemed that the involvement of ROS in toxic activity of cardol ($C_{15:3}$) was not observed in 1 hr of incubation (Figure 45A and B). Cardol ($C_{5:0}$) was also examined with the same manner of DCFH-DA experiment. As expected, cardol ($C_{5:0}$) also showed a prooxidant effect on B16-F10 melanoma cells. The highest total ROS content was observed at 50 μM and the total amount of ROS formed was reduced from the highest amount at the higher concentrations (100-800 μM) whereas cell viability was dose-dependently reduced (Figure 46A and B). The cellular ROS content enhanced with the addition of cardol ($C_{5:0}$), and the highest ROS formation was observed at approximately 50 and 100 μM (Figure 46C). Different from cardol ($C_{15:3}$), the cell viability of cardol ($C_{5:0}$)-treated cells were suppressed with the increase of intracellular ROS, indicating that at least, the generation of free radical involved in the mechanism of toxicity of cardol ($C_{5:0}$). On the other hand, resorcinol showed similar result as cardol ($C_{15:3}$) but not as cardol ($C_{5:0}$). B16 melanoma cells treated with 2000 μM resorcinol showed no toxicity after 1 hr of exposure; however, cellular ROS content were dose-dependently increased (data not shown). Thus, the primary toxic mechanism of resorcinol is presumably due to intracellular oxidation to corresponding toxic metabolites. Subsequently, the effect of 6-[8(Z)-pentadecenyl]salicylic acid, commonly known as anachardic acid monoene (**8**; see Figure 28 for the structure), on intracellular ROS generation was examined for a comparison. In the case of anachardic acid, any influences on both cell viability and

cellular ROS content was not observed (data not shown). As seen in the structure in Figure 28, *ortho*-position of hydroxyl OH to carbonyl group is usually known to form intramolecular hydrogen bonding. Thus, this prevents the formation of phenoxy radical corresponding to anachardic acid. In addition, anachardic acid is known to act as a chelator, indicating that, in cells, it could remove the active metal-related ROS generations (*11, 22*), which suggested that ROS generation is due to the structural features of resorcinol moiety but not due to the effect of alkyl side chain.

2.1.3 DISCUSSION

The inhibitory mechanism of tyrosinase is classified in several types. Both cardol ($C_{15:3}$) and cardol ($C_{5:0}$) inhibited tyrosinase-catalyzed melanin formation (both L-DOPA and L-tyrosine) but the mechanism of inhibition was different from each other even though they share the hydrophilic resorcinol moiety (hydrophilic head). The only difference is the length of alkyl chain, and it makes significant difference in inhibitory mechanism. The hydrophobic portion of cardols showed noticeable impact on the inhibition of tyrosinase activity. Furthermore, both L-DOPA and L-tyrosine oxidation were inhibited by all cardols, which suggested that shared resorcinol moiety of cardols are more likely to bind to oxy-tyrosinase as a substrate analogue (because only oxy-tyrosinase binds to L-tyrosine or other monophenols). It is now logical to conclude, based on the preliminary and current results, that cardol ($C_{15:3}$) inhibits tyrosinase activity with a two-step inactivating process. First, resorcinol moiety of cardol ($C_{15:3}$) interacts with copper site of tyrosinase, especially oxy-tyrosinase, as well as other resorcinol derivatives (*12-14, 23, 24*), and then hydrophobic alkyl chain slowly interacts with hydrophobic portion of proximate to active site of tyrosinase. Because of this hydrophobic interaction, the cardol ($C_{15:3}$) is stabilized at the active site of tyrosinase with the binding of resorcinolic OH to binuclear copper of tyrosinase. Furthermore, the hydrophobicity of alkyl side chain may interact hydrophobically with other cardol ($C_{15:3}$) molecules of hydrophobic portion, which leads to the complex binding/interactions of cardol ($C_{15:3}$) molecules to tyrosinase (*13, 25-27*). As a result of this stabilization, this inhibition process of cardol ($C_{15:3}$) seems to be irreversible. In addition, this interaction is presumably slow process, and thus, preincubational experiments enhanced the inhibitory effect of cardol ($C_{15:3}$). Once this hydrophobic interaction established, cardol ($C_{15:3}$) irreversibly disrupt the quaternary structure of tyrosinase and, as a result, inactivate the enzyme. Since native proteins form a sort of intramolecular micelle in which their nonpolar side chains are largely out of contact with the water based-test solution. The hydrophilic head part binds with an intermolecular hydrogen bond to hydrophilic portion of the enzyme, and then the hydrophobic portion of the molecule is able to disrupt the quaternary structure. The low conformational stabilities of native proteins make them easily susceptible to denaturation by altering the balance of the weak nonbonding forces that maintain the native conformation. On the other hand, cardol ($C_{5:0}$), or olivetol, inhibits tyrosinase reversibly, which is due to the competitive binding of resorcinol

moiety on the basis of previous and current studies (*12, 13, 23, 28*). Because of less hydrophobicity of pentyl side chain of cardol ($C_{5:0}$), the secondary process is not applied to the case of cardol ($C_{5:0}$). Cardol ($C_{10:0}$) also showed similar inhibitory results of tyrosinase to that of cardol ($C_{15:3}$); however, the inhibitory effect was surprisingly more potent than other cardols by comparing the result of the consumption of L-DOPA (Figure 38). As a result, the inhibitory mechanism of cardol ($C_{10:0}$) on tyrosinase-catalyzed dopachrome formation is a two-step inactivation as well as cardol ($C_{15:3}$). It should be noted that the higher lipophilicity does not simply exhibit greater degree of inhibition on tyrosinase. The detailed influence of length of alkyl chain of resorcinolic lipid is discussed in the following section (Chapter 2.2).

Based on the IC_{50} result, the difference between cardol ($C_{15:3}$) and cardol ($C_{5:0}$) in cytotoxicity is more likely due to the difference in length of alkyl chains (C15 vs. C5). This difference directly affects the mechanism of toxicity. As a basis of the results from our preliminary and current studies, the cytotoxicity of cardols obtained by the assays estimated the following increasing order; $C_{15:3} \approx C_{15:2} \approx C_{15:1} \approx C_{15:0} > C_{10:0} > C_{5:0}$ (olivetol) > resorcinol (*11*). Consequently, the head and tail balanced concept of activity may be applicable to the cardols. Thus, cardols are amphipathic molecules and therefore their hydrophobic properties dominate the properties of these molecules. Presumably, the pentadeca(en)yl hydrocarbon chain may act as an anchor by interacting with the hydrophobic portion of the cellular membrane to disrupt membrane fluidity and ultimately burst the cell wall, which would suggest that the cytotoxic effects observed seems most likely due to its ability to act as a surfactant. A similar moderate cytotoxicity activity of cardols against several cancerous cell lines was previously reported (*29*). As a results of biochemical (addition of vitamin C and BHA) and intracellular reactive oxygen species (ROS) measurement, it is possible to assume that both cardol ($C_{15:3}$) and cardol ($C_{5:0}$) act as a prooxidant in B16-F10 melanoma cells while resorcinol could be intracellularly oxidized to toxic metabolites. All cardols and resorcinol significantly enhanced the level of intracellular oxidative stress; however, cardol ($C_{15:3}$) and resorcinol did not affect cell viability while cardol ($C_{5:0}$) dose-dependently suppressed. This suggests that prooxidative effect of cardol ($C_{15:3}$) and resorcinol is not directly linked to the mechanism of the cytotoxicity of cardol ($C_{15:3}$) and resorcinol. In the case of cardol ($C_{5:0}$), prooxidative effect is more likely the main mechanism of toxic effect. Moreover, the prooxidative effect is due to the effect of resorcinol moiety but not due to the effect of alkyl side chain. Combining this fact and sequential order of cytotoxicity (or simply IC_{50}) due to the length of alkyl chain, the primary toxic mechanism should be the surfactant action by hydrophobic alkyl side chain. Thus, in a conclusion, pentadeca(en)yl side chain of cardols ($C_{15:n}$) possibly act as an anchor to disrupt the cellular membrane whereas pentyl side chain of cardol ($C_{5:0}$) is not long enough to disrupt the plasma membrane. However, cardol ($C_{5:0}$) is passively absorbed into cell, and causes oxidative stress. In the case of resorcinol, possibility of surfactant is diminished; however, *ortho*-position of hydroxyl group is less steric hindrance compared to other cardols, which suggest that resorcinol should be metabolized (*30, 31*). Moreover, the difference in length of alkyl chain also greatly affects their solubility. Because cardol ($C_{5:0}$) has lower molecular

weight and higher hydrophilicity than cardol ($C_{15:n}$), cardol ($C_{5:0}$) is more likely to penetrate plasma membrane and to enter into cytoplasmic domain of the cells. On the other hand, higher molecular weight and lipophilicity of cardol ($C_{15:3}$) interacts with phospholipids in cellular membrane, indicating that surfactant mechanism is more favorable than others.

Cardols are isolated from many edible plants and food protection agents isolated from regularly consumed edible plants may be superior to non-natural products. Cardols ($C_{15:n}$) can be obtained in quantities, as described, from the cashew nut shell liquid (CNSL) (*32, 33*). Although, CNSL is available in greater tonnage, it is neglected in commercial terms, and thus, there is thus considerable potential for further exploitation. During the lipoxygenase kinetic study of cardols, we became aware that cardol ($C_{15:3}$) and cardol ($C_{15:2}$) were oxidized as substrates at lower concentrations (<40 μM) because both possess a (1Z,4Z)-pentadiene system in their C15-alkenyl side chain, although both exhibited inhibitory activity at higher concentrations (>40 M) (*34*). However, in the case of tyrosinase and B16-F10 melanoma cell assays, there is no considerable difference between saturated and unsaturated C15-alkyl side chains of cardols. In addition, cardols are known to exhibit broad antibacterial activity (*35*), and inhibit lipid peroxidation (*8*) and lipoxygenase activity (*36*). On the other hand, it is not clear if ingested cardols are absorbed into the system through the intestinal tract and delivered to the place where these beneficial biological activities are needed without being metabolized. Their further valuation is needed from not only one aspect, but also from a whole and dynamic perspective.

2.1.4 FIGURES & TABLES

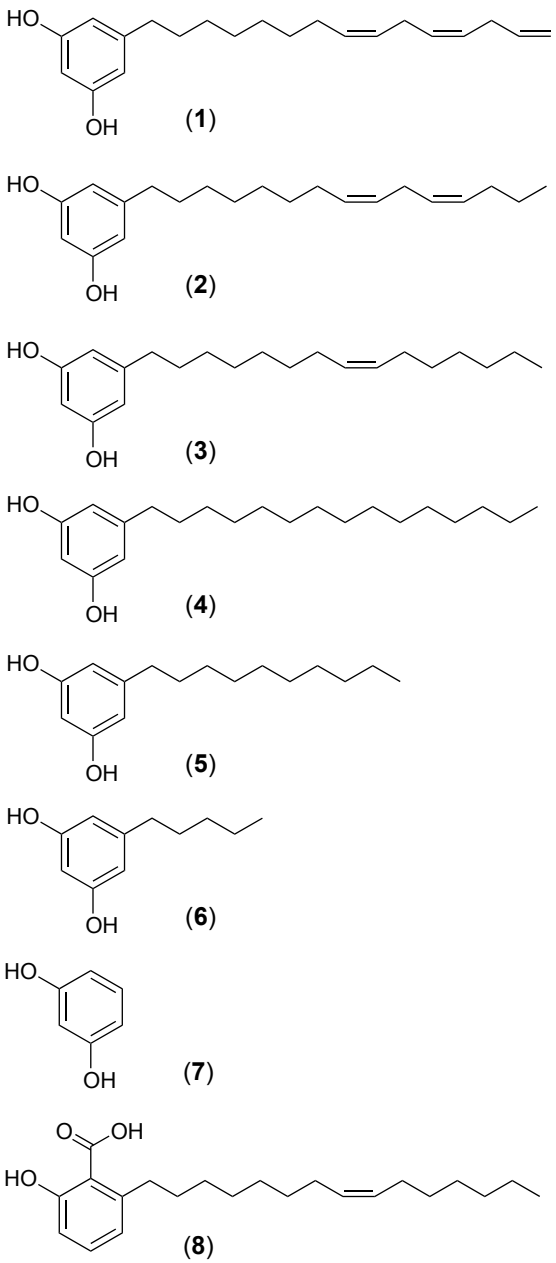

Figure 28. Chemical structures of cardol ($C_{15:3}$) (**1**), cardol ($C_{15:2}$) (**2**), cardol ($C_{15:1}$) (**3**), cardol ($C_{15:0}$) (**4**), cardol ($C_{10:0}$) (**5**), cardol ($C_{5:0}$) (**6**), resorcinol (**7**), and anachardic acid ($C_{15:1}$) (**8**).

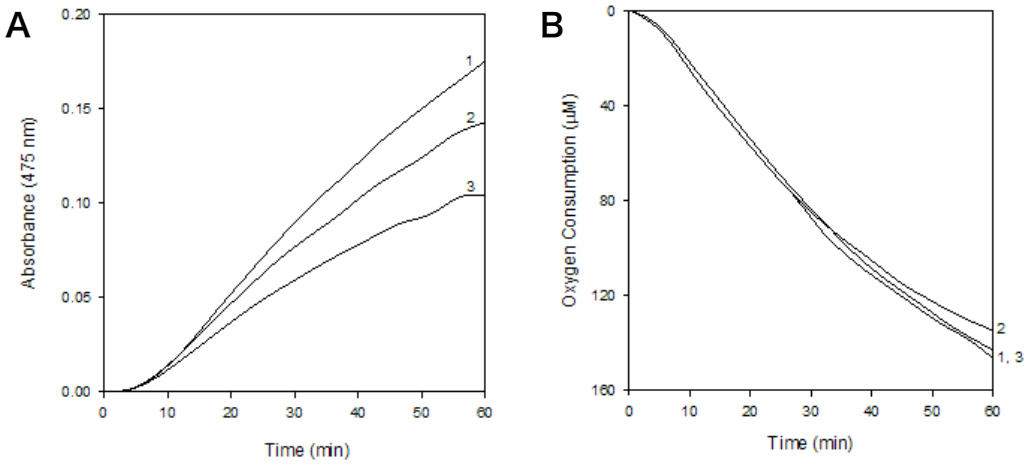

Figure 29. (**A**) UV-Vis spectra at 475 nm obtained in oxidation of 100 µM of L-tyrosine by mushroom tyrosinase in presence of cardol ($C_{15:3}$) for 60 min. Concentrations of cardol ($C_{15:3}$) were selected at 1 µM (2) and 2.5 µM (3). Line 1 represents oxidation of L-tyrosine by mushroom tyrosinase in absence of cardol ($C_{15:3}$). (**B**) The oxygen consumption of oxidation of L-tyrosine (100 µM) by mushroom tyrosinase in absence or presence of cardol ($C_{15:3}$) for 60 min. The concentrations of cardol ($C_{15:3}$) were selected at 1 µM (2) and 2.5 µM (3). Line 1 represents the oxygen consumption of oxidation of 100 µM of L-tyrosine by mushroom tyrosinase in absence of cardol ($C_{15:3}$).

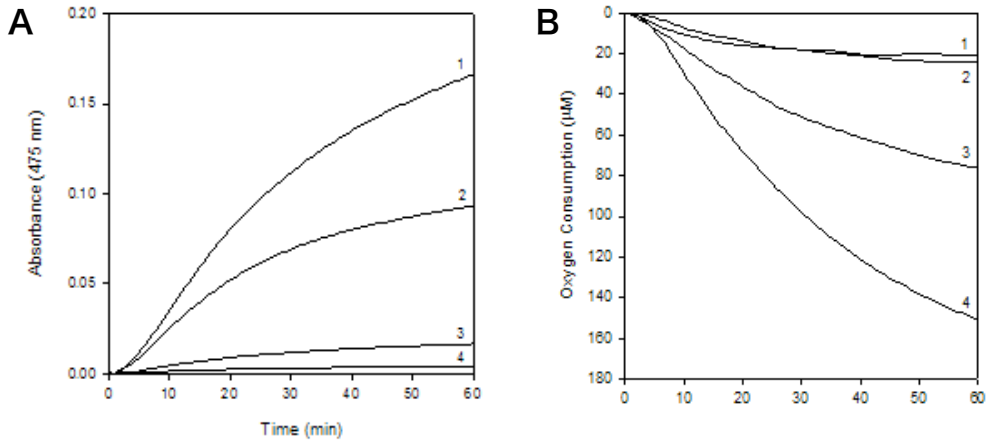

Figure 30. (**A**) UV-Vis spectra at 475 nm obtained from the oxidation of 100 µM L-tyrosine by mushroom tyrosinase in presence of cardol ($C_{5:0}$) for 60 min. Concentrations of cardol ($C_{5:0}$) were selected at 10 µM (2), 100 µM (3) and 200 µM (4). Line 1 represents oxidation of L-tyrosine by mushroom tyrosinase in absence of cardol ($C_{5:0}$). (**B**) Oxygen consumption of 100 µM of L-tyrosine oxidation by mushroom tyrosinase in presence of cardol ($C_{5:0}$) for 60 min. Concentrations of cardol ($C_{5:0}$) was selected at 200 µM (1), 100 µM (2) and 10 µM (3). Line 4 represents the oxidation of L-tyrosine in absence of cardol ($C_{5:0}$).

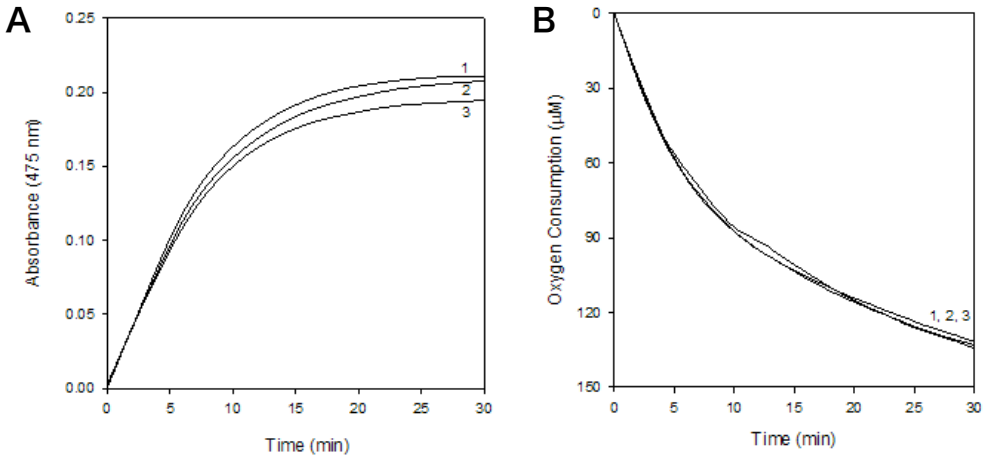

Figure 31. (**A**) UV-Vis spectra at 475 nm obtained from the oxidation of 100 µM L-DOPA by mushroom tyrosinase in presence of cardol ($C_{15:3}$) for 30 min. Concentrations of cardol ($C_{15:3}$) were selected at 1 µM (2) and 2.5 µM (3). Line 1 represents oxidation of L-DOPA by mushroom tyrosinase in absence of cardol ($C_{15:3}$). (**B**) The oxygen consumption of oxidation of L-DOPA (100 µM) by mushroom tyrosinase in absence or presence of cardol ($C_{15:3}$) for 30 min. The concentrations of cardol ($C_{15:3}$) were selected at 1 µM (2) and 2.5 µM (3). Line 1 represents the oxygen consumption of oxidation of 100 µM of L-DOPA by mushroom tyrosinase in absence of cardol ($C_{15:3}$).

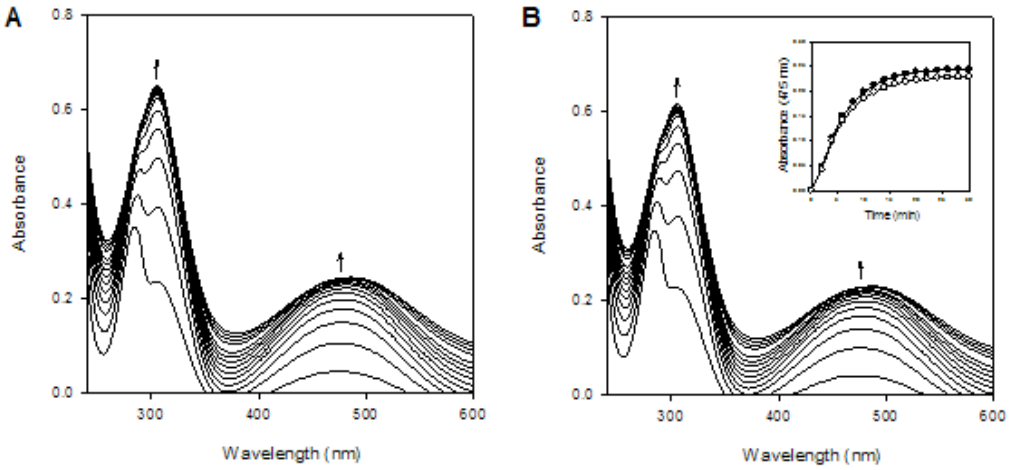

Figure 32. Consecutive UV-Vis spectra obtained in the oxidation of 100 μM of L-DOPA by mushroom tyrosinase in presence of 1 μM of cardol ($C_{15:3}$) for 30min. Change in absorbance of L-DOPA at 475 nm in absence (●) or presence (○) of 1 μM of cardol ($C_{15:3}$). Scan speed was at 2 min intervals for 30 s. the arrows (↑) designate the evolution of the peak.

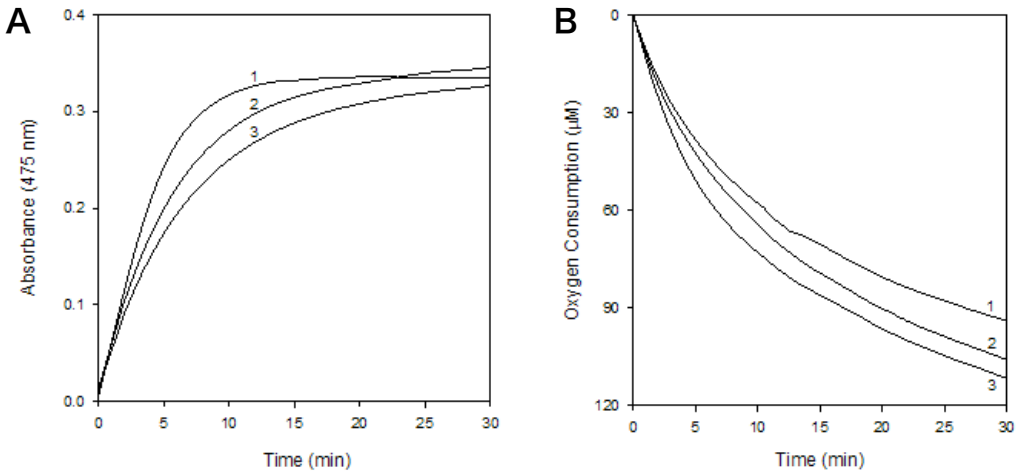

Figure 33. (**A**) UV-Vis spectra at 475 nm obtained in oxidation of 100 μM of L-DOPA by mushroom tyrosinase in presence of cardol ($C_{5:0}$) (olivetol) for 30 min. Concentrations of cardol ($C_{5:0}$) were selected at 100 μM (2) or 200 μM (3). Line 1 represents oxidation of L-DOPA by mushroom tyrosinase in absence of cardol ($C_{5:0}$). (**B**) Oxygen consumption of the oxidation of L-DOPA (100 μM) by mushroom tyrosinase in presence of cardol ($C_{5:0}$) for 30 min. The concentrations of cardol ($C_{5:0}$) were selected at 100 μM (2) or 200 μM (1). Line 3 represents the oxygen consumption of oxidation of 100 μM of L-DOPA by mushroom tyrosinase in absence of cardol ($C_{5:0}$).

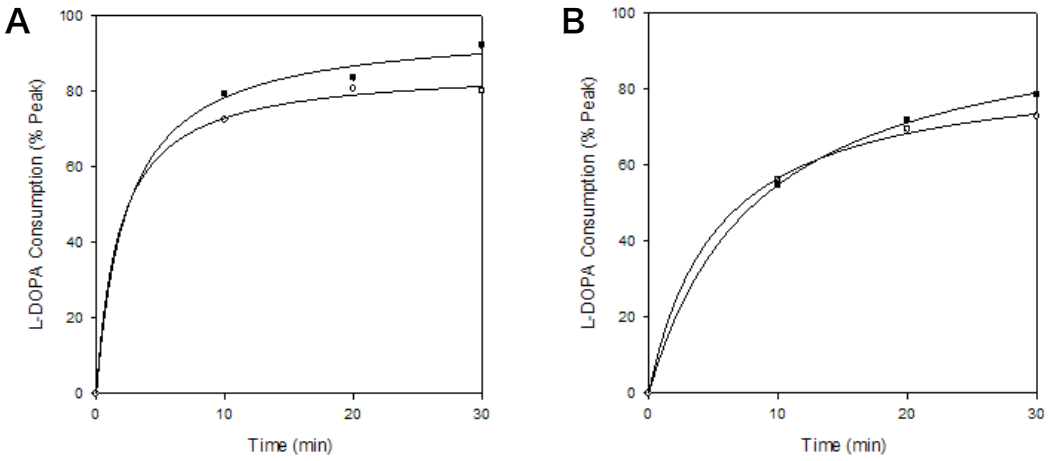

Figure 34. (**A**) HPLC analysis of L-DOPA (100 μM) oxidation by tyrosinase in absence (●) or presence (○) of 2.5 μM cardol ($C_{15:3}$) in a static condition. Sampling time was chosen at 0 min, 10 min, 20 min, and 30 min. (**B**) HPLC analysis of L-DOPA (100 μM) oxidation by tyrosinase in absence (●) or presence (○) of 2.5 μM cardol ($C_{15:3}$). The experiment was done under the stirring condition. Sampling time was chosen at 0 min, 10 min, 20 min, and 30 min. HPLC operating conditions were as follows; Deverosil ODS-UG-5 (Nomura Chemical, CO., LTD., Seto-Shi, Aichi, Japan). Solvent; 7 % MeCN/H_2O containing 0.2 % TFA, Flow rate 1.0 mL/min, detection; UV at 280 nm, 0.02 range, injected amount; 25 μL. Each dot was connected smoothly with SigmaPlot (Systat Software, Inc.).

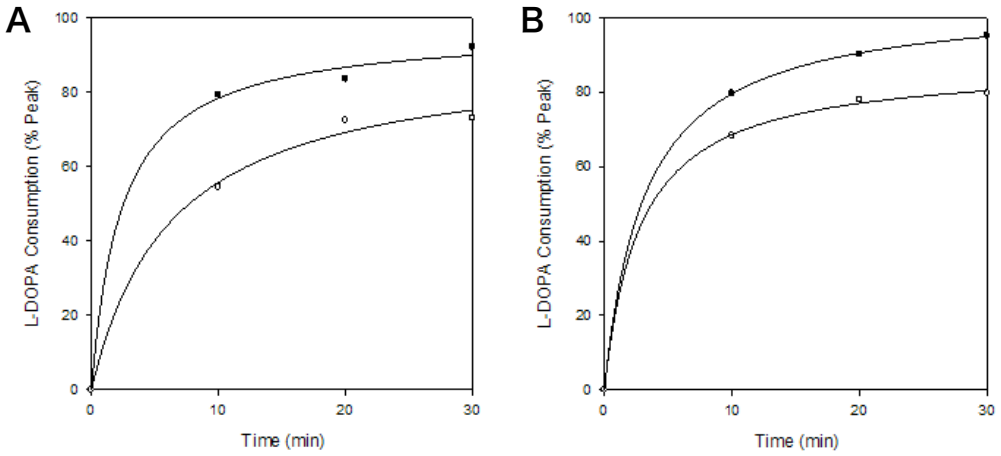

Figure 35. (**A**) HPLC analysis of L-DOPA (100 μM) oxidation by tyrosinase in absence (●) or presence (○) of 2.5 μM cardol ($C_{5:0}$) (olivetol) in a static condition. Sampling time was chosen at 0 min, 10 min, 20 min, and 30 min. (**B**) HPLC analysis of L-DOPA (100 μM) oxidation by tyrosinase in absence (●) or presence (○) of 200 μM cardol ($C_{5:0}$). The experiment was performed in a stirring condition. Sampling time was chosen at 0 min, 10 min, 20 min, and 30 min. HPLC operating conditions were as follows; Deverosil ODS-UG-5 (Nomura Chemical, CO., LTD., Seto-Shi, Aichi, Japan). Solvent; 7 % MeCN/H_2O containing 0.2 % TFA, Flow rate 1.0 mL/min, detection; UV at 280 nm, 0.02 range, injected amount; 25 μL. Each dot was connected smoothly with SigmaPlot (Systat Software, Inc.).

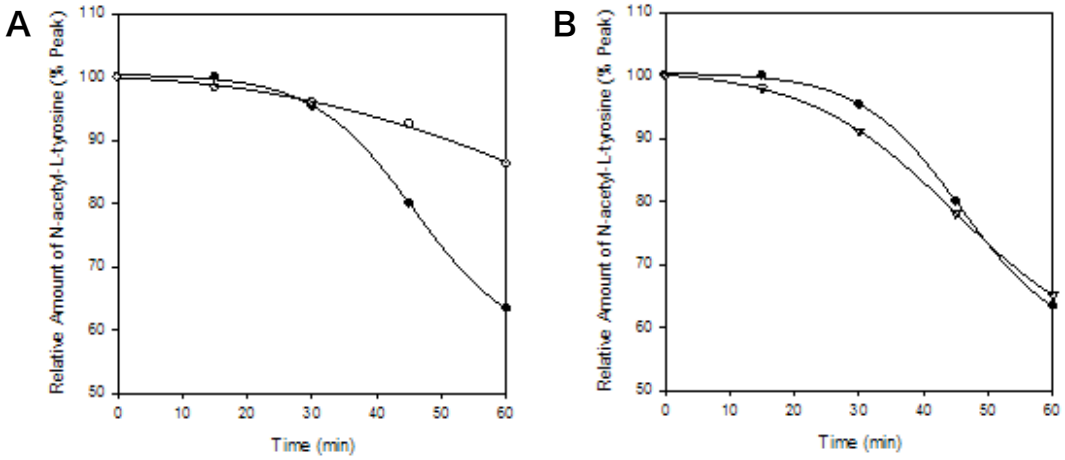

Figure 36. HPLC analysis of N-acetyl-L-tyrosine (100 μM) oxidation by tyrosinase in absence (●) or presence (○, ▽) of cardol ($C_{15:3}$) (1 μM). The reaction was proceeded with either static (**A**) or stirring (**B**) condition. Sampling time was chosen at 0 min, 15 min, 30 min, 45 min and 60 min. HPLC operating conditions were as follows; Deverosil ODS-UG-5 (Nomura Chemical, CO., LTD., Seto-Shi, Aichi, Japan). Solvent; 18 % MeCN/H_2O containing 0.2 % TFA, Flow rate 1.0 mL/min, detection; UV at 280 nm, 0.02 range, injected amount; 25 μL. Curve fitting is done with SigmaPlot (Systat Software, Inc.).

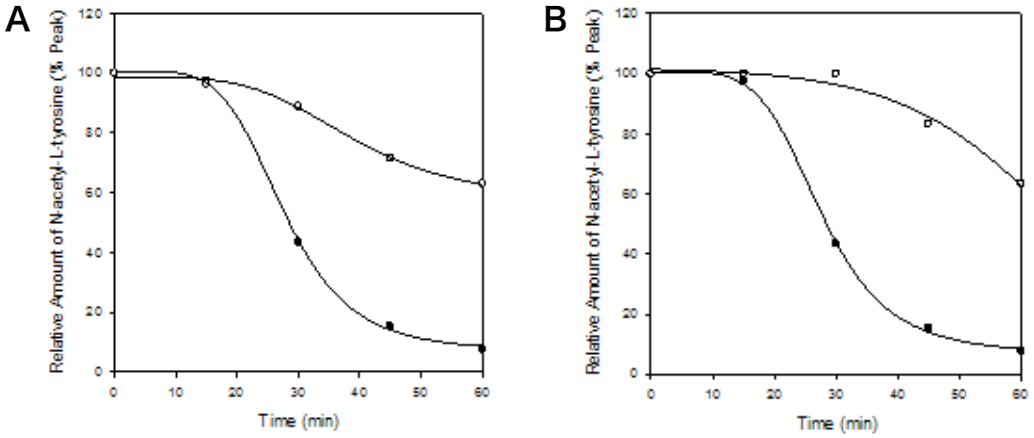

Figure 37. HPLC analysis of *N*-acetyl-L-tyrosine (100 μM) oxidation by tyrosinase in absence (●) or presence (○) of 10 μM cardol ($C_{5:0}$) (olivetol) in a static (**A**) or stirring (**B**) condition. Sampling time was chosen at 0 min, 15 min, 30 min, 45 min and 60 min. HPLC operating conditions were as follows; Deverosil ODS-UG-5 (Nomura Chemical, CO., LTD., Seto-Shi, Aichi, Japan). Solvent; 12 % MeCN/H_2O containing 0.2 % TFA, Flow rate 1.0 mL/min, detection; UV at 280 nm, 0.02 range, injected amount; 25 μL. Curve fitting is done with SigmaPlot (Systat Software, Inc.).

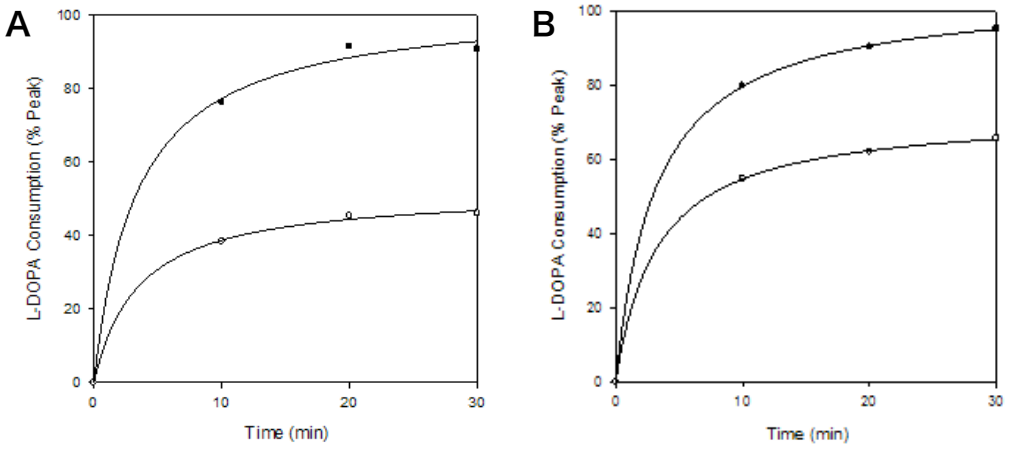

Figure 38. (**A**) HPLC analysis of L-DOPA (100 μM) oxidation by tyrosinase in absence (●) or presence (○) of 25 μM cardol ($C_{10:0}$) in a static condition. Sampling time was chosen at 0 min, 10 min, 20 min, and 30 min. (**B**) HPLC analysis of L-DOPA (100 μM) oxidation by tyrosinase in absence (●) or presence (○) of 2.5 μM cardol ($C_{15:3}$). The experiment was performed in a stirring condition. Sampling time was chosen at 0 min, 10 min, 20 min, and 30 min. HPLC operating conditions were as follows; Deverosil ODS-UG-5 (Nomura Chemical, CO., LTD., Seto-Shi, Aichi, Japan). Solvent; 7 % MeCN/H_2O containing 0.2 % TFA, Flow rate 1.0 mL/min, detection; UV at 280 nm, 0.02 range, injected amount; 25 μL. Each dot was connected smoothly with SigmaPlot (Systat Software, Inc.).

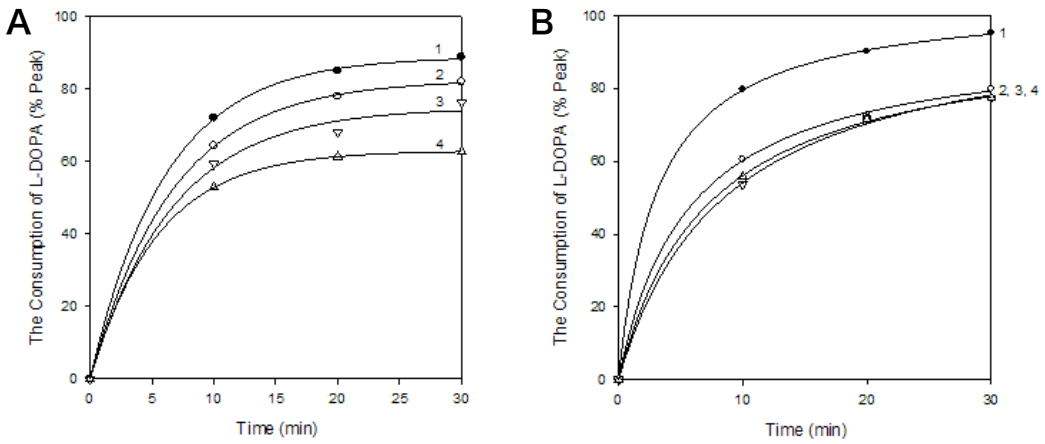

Figure 39. HPLC analysis of L-DOPA (100 μM) oxidation by mushroom tyrosinase in absence (1) or presence (2, 3, 4) of 5 μM cardol ($C_{15:3}$) (**A**) or 200 μM cardol ($C_{5:0}$) (**B**) without (2) or with 10 min (3) or 20 min (4) of preincubation in a static condition. All data were normalized. Sampling time was chosen at 0 min, 10 min, 20 min, and 30 min. HPLC operating conditions were as follows; Develosil ODS-UG-5 (Nomura Chemical, CO., LTD., Seto-Shi, Aichi, Japan). Solvent; 10% MeCN/H2O containing 0.2 % TFA, Flow rate 1.0 mL/min, detection; UV at 280 nm, 0.02 range, injected amount; 25 mL. Peak *a* and *b* represent L-DOPA and dopachrome, respectively.

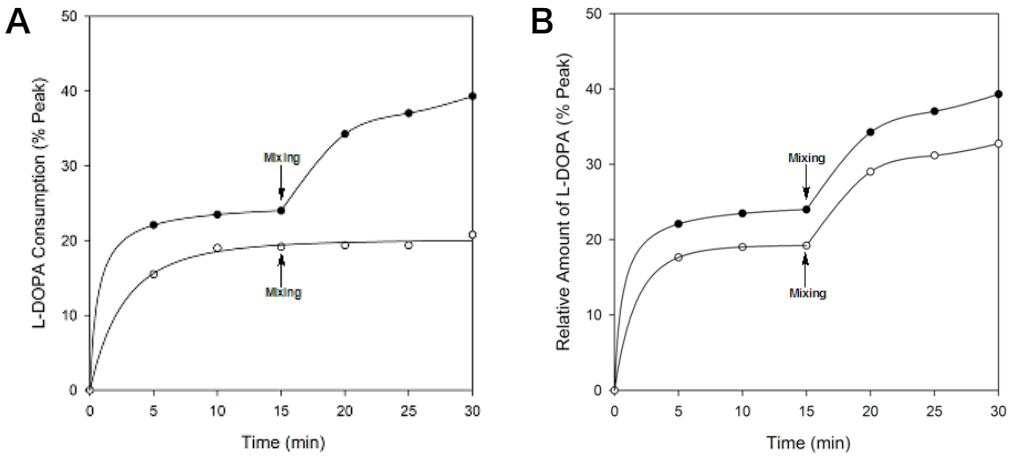

Figure 40. (**A**) HPLC analysis of L-DOPA (1000 μM) oxidation by tyrosinase in absence (●) or presence (○) of cardol ($C_{15:3}$) (1 μM). The reaction mixtures were voltexed at 15 min. Sampling time was chosen at 0 min, 15 min, 30 min, 45 min and 60 min. (**B**) HPLC analysis of L-DOPA (1000 μM) oxidation by tyrosinase in absence (●) or presence (○) of cardol ($C_{5:0}$) (olivetol) (200 μM). The reaction mixtures were voltexed at 15 min. Sampling time was chosen at 0 min, 5 min, 10 min, 15 min, 20 min, 25 min and 30 min. HPLC operating conditions were as follows; Deverosil ODS-UG-5 (Nomura Chemical, CO., LTD., Seto-Shi, Aichi, Japan). Solvent; 10 % MeCN/H_2O containing 0.2 % TFA, Flow rate 1.0 mL/min, detection; UV at 280 nm, 0.02 range, injected amount; 25 μL. Each dot was connected smoothly with SigmaPlot (Systat Software, Inc.).

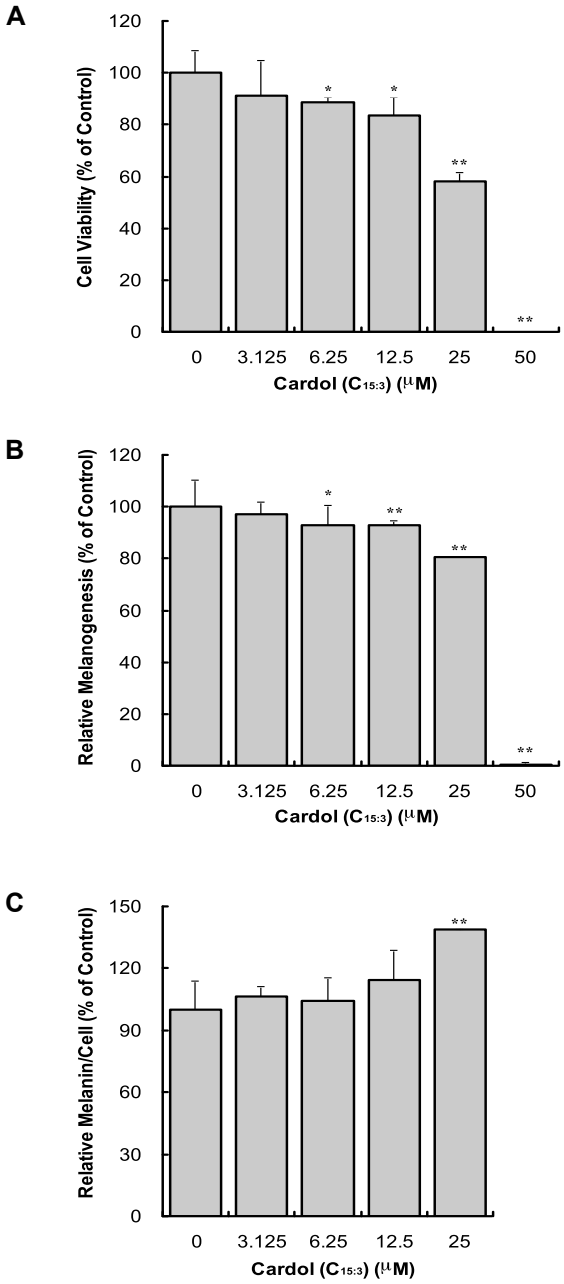

Figure 41. (**A**) Viabilities of B16-F10 melanoma cells following treatment with cardol ($C_{15:3}$) for 72hr; data are expressed as percentage of the number of viable cells observed with the control, and each column represents the mean ± S.D. of at least 4 determinations. (**B**) Total melanin content in B16 melanoma cells following treatment with cardol ($C_{15:3}$) for 72hr; data are expressed as percentage of melanin content per well observed with the control, and each column represents the mean ± S.D. of 4 determinations. (**C**) Cellular melanin content in B16 melanoma cells following treatment with cardol ($C_{15:3}$) for 72hr measured as percentage of melanin content per cell observed with the control, and each column represents the mean ± S.D. of 4 determinations. The statistical significance of differences was evaluated using Student's or Welch's *t*-test. Significantly different from the control value: **p*<0.05, ***p*<0.01.

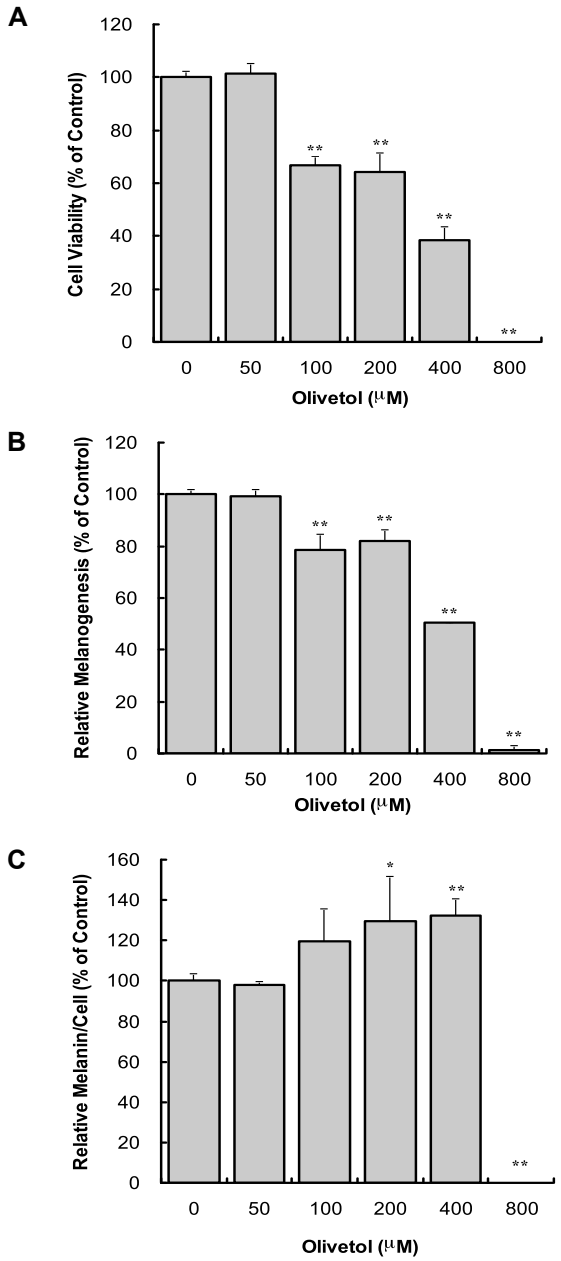

Figure 42. (**A**) Viabilities of B16-F10 melanoma cells following treatment with cardol ($C_{5:0}$) (olivetol) for 72hr; data are expressed as percentage of the number of viable cells observed with the control, and each column represents the mean ± S.D. of at least 4 determinations. (**B**) Total melanin content in B16 melanoma cells following treatment with cardol ($C_{5:0}$) for 72hr; data are expressed as percentage of melanin content per well observed with the control, and each column represents the mean ± S.D. of 4 determinations. (**C**) Cellular melanin content in B16 melanoma cells following treatment with cardol ($C_{5:0}$) for 72hr measured as percentage of melanin content per cell observed with the control, and each column represents the mean ± S.D. of 4 determinations. The statistical significance of differences was evaluated using Student's or Welch's *t*-test. Significantly different from the control value: *p<0.05, **p<0.01.

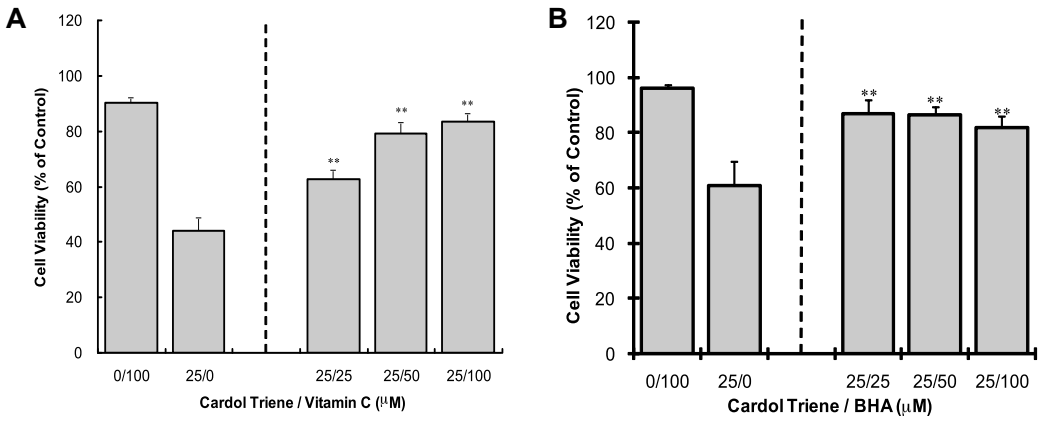

Figure 43. (**A**) Viabilities of B16 melanoma cells following treatment with 25 μM of cardol ($C_{15:3}$) in presence or absence of vitamin C after 72hr of incubation. The concentrations of vitamin C applied to cardol ($C_{15:3}$) treated cells were chosen at 0 μM (25/0), 25 μM (25/25), 50 μM (25/50) and 100 μM (25/100). Cells are also treated with 100μM of vitamin C without cardol ($C_{15:3}$) (0/100). Data are expressed as the percentage of the number of viable cells observed with cardol ($C_{15:3}$) control (0/25), and each column represents the mean ± S.D. of at least 4 determinations. (**B**) Viabilities of B16 melanoma cells following treatment with 25 μM of cardol ($C_{15:3}$) in presence or absence of butylated hydroxyanisol (BHA) after 72 hr of incubation. The concentrations of butylated hydroxyanisol applied to cardol ($C_{15:3}$) treated cells were chosen at 0 μM (25/0), 25 μM (25/25), 50 μM (25/50) and 100 μM (25/100). Cells are also treated with 100 μM of butylated hydroxyanisol without cardol ($C_{15:3}$) (0/100). Data are expressed as the percentage of the number of viable cells observed with cardol ($C_{15:3}$) control (25/0), and each column represents the mean ± S.D. of at least 4 determinations. The statistical significance of differences was evaluated using Student's or Welch's *t*-test. Significantly different from the cardol control value: **p*<0.05, ***p*<0.01.

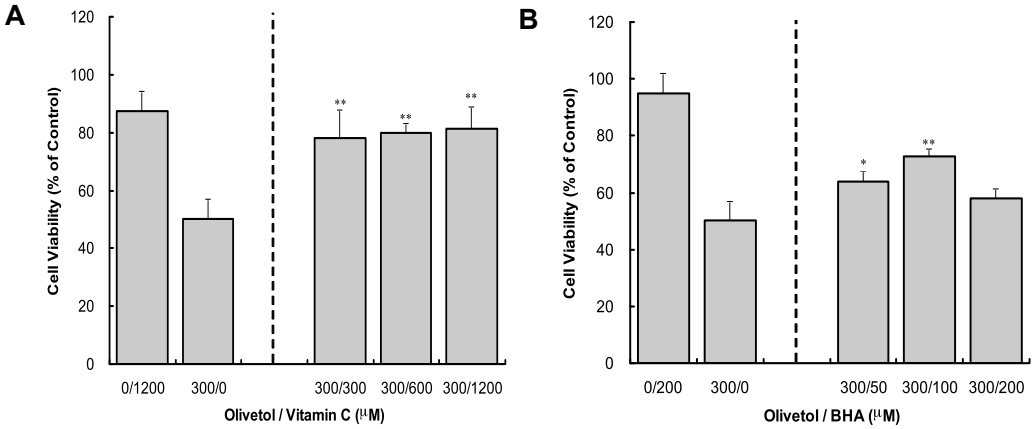

Figure 44. (**A**) Viabilities of B16 melanoma cells following treatment with 300 μM of cardol ($C_{5:0}$) (olivetol) in presence or absence of vitamin C after 72hr of incubation. The concentrations of vitamin C applied to cardol ($C_{5:0}$) treated cells were chosen at 0 μM (300/0), 300 μM (300/300), 600 μM (300/600) and 1200 μM (300/1200). Cells are also treated with 1200μM of vitamin C without cardol ($C_{5:0}$) (0/1200). Data are expressed as the percentage of the number of viable cells observed with cardol ($C_{5:0}$) control (0/300), and each column represents the mean ± S.D. of at least 4 determinations. (**B**) Viabilities of B16 melanoma cells following treatment with 300 μM of cardol ($C_{5:0}$) in presence or absence of butylated hydroxyanisol (BHA) after 72 hr of incubation. The concentrations of BHA applied to cardol ($C_{5:0}$) treated cells were chosen at 0 μM (300/0), 50 μM (300/50), 100 μM (300/100) and 200 μM (300/200). Cells are also treated with 200 μM of BHA without cardol ($C_{5:0}$) (0/200). Data are expressed as the percentage of the number of viable cells observed with cardol ($C_{5:0}$) control (300/0), and each column represents the mean ± S.D. of at least 4 determinations. The statistical significance of differences was evaluated using Student's or Welch's *t*-test. Significantly different from the cardol control value: *p<0.05, **p<0.01.

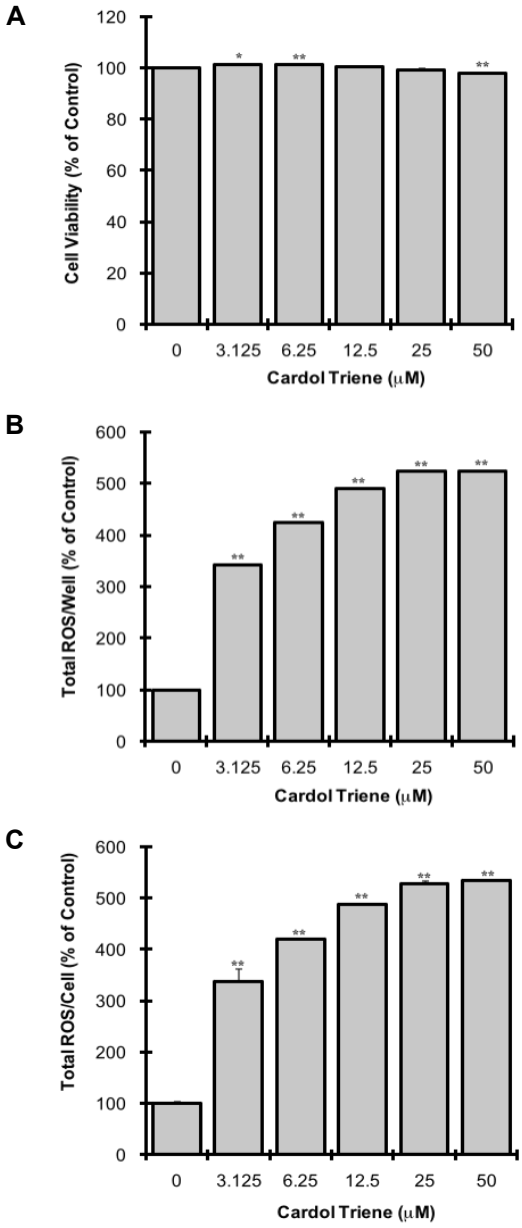

Figure 45. (**A**) Viabilities of B16-F10 melanoma cells following treatment with cardol ($C_{15:3}$) for 1 hr; data are expressed as percentage of the number of viable cells observed with the control, and each column represents the mean ± S.D. of at least 4 determinations. (**B**) Total ROS contents in B16 melanoma cells following treatment with cardol ($C_{15:3}$) for 1 hr; data are expressed as percentage of ROS content per well observed with the control, and each column represents the mean ± S.D. of 4 determinations. (**C**) Cellular ROS contents in B16 melanoma cells following treatment with cardol ($C_{15:3}$) for 1 hr measured as percentage of ROS contents per cell observed with the control, and each column represents the mean ± S.D. of 4 determinations. The statistical significance of differences was evaluated using Student's or Welch's *t*-test. Significantly different from the control value: *p<0.05, **p<0.01.

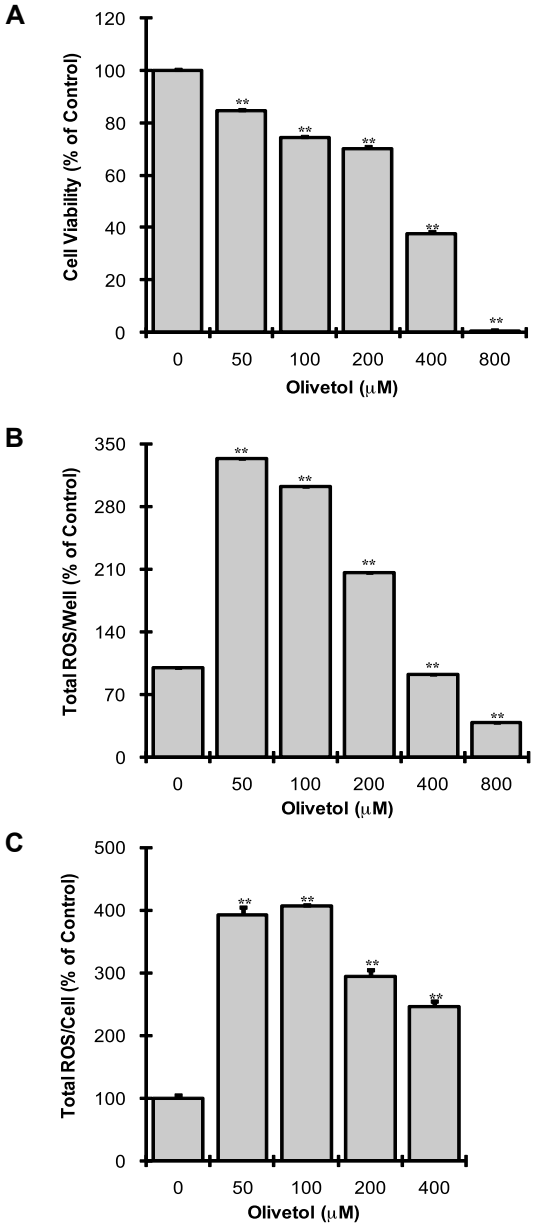

Figure 46. (**A**) Viabilities of B16-F10 melanoma cells following treatment with cardol ($C_{5:0}$) (olivetol) for 1 hr; data are expressed as percentage of the number of viable cells observed with the control, and each column represents the mean ± S.D. of at least 4 determinations. (**B**) Total ROS contents in B16 melanoma cells following treatment with cardol ($C_{5:0}$) for 1 hr; data are expressed as percentage of ROS content per well observed with the control, and each column represents the mean ± S.D. of 4 determinations. (**C**) Cellular ROS contents in B16 melanoma cells following treatment with cardol ($C_{5:0}$) for 1 hr measured as percentage of ROS contents per cell observed with the control, and each column represents the mean ± S.D. of 4 determinations. The statistical significance of differences was evaluated using Student's or Welch's *t*-test. Significantly different from the control value: **p*<0.05, ***p*<0.01.

2.2 Effect of Alkyl-3,5-dihydroxybenzoate and 3,5-dihydroxyphenyl Alkanoate on Mushroom Tyrosinase and B16 Melanoma Cells

2.2.1 INTRODUCTION

In our continuing search for a melanin synthesis inhibitor from the natural sources, cardol ($C_{15:3}$) (**23**) is an active principal. Cardol ($C_{15:3}$) showed a two-step inactivation on tyrosinase leading to the reduction of dopachrome formation (Chapter 2.1). The resorcinol moiety first *quickly* and *reversibly* competes with the binuclear active site as a substrate analogue after which the hydrophobic pentadeca(en)yl side chain *slowly* and *irreversibly* interacts with the hydrophobic domain near the active site (two-step inhibition). On the basis of this concept, we selected a resorcinol moiety as a head portion. Once the head portion is selected, the inhibitory activity can be maximized by the selection of the appropriate tail portions. A series of alkyl moieties can be connected as esters, either -COOR or –OCOR. Thus, a homologous series of alkyl-3,5-dihydroxybenzoates (**1**-**9**) and 3,5-dihydroxyphenyl alkanoates (**16**-**22**) (see Figure 47 for the structures), which are referred to as RA or PLG, respectively for the convenient purposes, were synthesized by one step esterification utilizing *N*,*N*'-dicyclohexylcarbodiimide (DCC) as an activating reagent, similar to the procedure described for alkyl-3,4-dihydroxybenzoates (*37*) and alkyl-3,4,5-trihydroxybenzoates (*38*) (All compounds were synthesized by Dr. K. Nihei in previous studies; see Materials and Methods, and Acknowledgement sections). The aim of the current experiment was to clarify the role of alkyl chain length as well as for further confirmation of the result obtained from cardols.

2.2.2 RESULTS

Effects of Alkyl-3,5-dihydroxybenzoate and 3,5-dihydroxyphenyl Alkanoate on Tyrosinase

Tyrosinase (EC 1.14.18.1) is a key enzyme in melanin synthesis and therefore, tyrosinase inhibitors are expected to inhibit melanin production. Hence, their effects on tyrosinase activity were tested first. A series of alkyl-3,5-dihydroxybenzoates (C6-C14) (**1**-**9**) and 3,5-dihydroxyphenyl alkanoates (C7-C13) (**16**-**22**) were synthesized based on the resorcinol scaffold and tested for their effects on the tyrosinase-catalyzed oxidation of L-DOPA. The reaction mixture consisting of tyrosinase (1 μg/mL) and L-DOPA (100 μM) was used as the standard unless otherwise specified. The initial oxidation rate of L-DOPA was fast and was oxidized within 5 min. The tyrosianse activity was monitored with HPLC analysis since this method was free from the instrumental restrictions; hence, both static and stirring conditions were tested (See chapter 2.1 for the details). Using a HPLC analysis, both alkyl-3,5-dihydroxybenzoates (RA) and 3,5-dihydroxyphenyl octanoate (PLG) with C9 through C12 alkyl chain (RA-9 to RA-12 and PLG-9 to PLG-12) showed noticeable inhibition on tyrosinase-catalyzed L-DOPA oxidation in a

static condition. In Table 3, only RA-9, -10, -11 and -12 inhibited L-DOPA consumption; however, the effect of RA-12 was lower than the other efficacious three RA molecules (RA-9, -10 and -11). It appeared that only the RA molecules containing alkyl chain from C9 to C12 inhibit tyrosinase activity during the 30 min of reaction period. Since their head portion is the same, the observed data is interpreted to mean that the changes in the hydrophobic tail portion correlated to this specific inhibitory activity. Thus, the hydrophobic side chain from C9 to C12 plays an important role to inhibit the enzyme activity. In addition, RA-9 showed the highest inhibitory effect on tyrosinase-catalyzed L-DOPA oxidation, and about 53 % of L-DOPA consumption was diminished in this method. It seemed that there is a correlation between the length of alkyl chain and inhibitory effect but not between the length of alkyl chain and the degree of inhibition. These inhibitory effects of RA-9 through RA-12, importantly, were not observed in the case of stirring condition, as expected from the result of cardols (Chapter 2.1). Among the tested PLG compounds, PLG-9 through PLG-12 showed the inhibition on mushroom tyrosinase in a static condition as well as RA (Table 4). The highest inhibition was observed with PLG-10, and 63 % of L-DOPA consumption was inhibited. Similar to the case of RA, no inhibitory effect was observed with the addition of 100 μM PLG-7 and PLG-8. As well as cardols or RA, the stirring during the tyrosinase assays diminished the inhibitory effects of PLG-9 through PLG-12. According to the data obtained, there is a clear boundary for inhibitory actions between C8 and C9 in both cases of RA and PLG. Moreover, calculated log *P* values and experimental results suggested that there is a correlation between the hydrophobicity of chemicals and inhibitory effect (log *P* column in Table 3 and 4). In other words, this hydrophobicity of synthetic resorcinol lipids is the key for the mode of action of RA and PLG, which implies that the inhibitory mechanism observed with cardols could be applied.

Effect of Nonyl-3-hydroxybenzoate and Nonyl-2,4-dihydroxybenzoate on Tyrosinase

The investigation was first aimed to the involvement of resorcinolic moiety in the mechanism of inhibition of RA and PLG. In order to understand the mode of action, nonyl-3-hydroxybenzoate (**11**) and nonyl-2,4-dihydroxybenzoate (**14**) were obtained from previous studies (*20, 38*). As mentioned, resorcinolic lipid could be considered to have two domains: a hydrophilic head and a hydrophobic tail. Hence, nonyl-3-hydroxybenzoate and nonyl-2,4-dihydroxybenzoate were used to test the effect of hydrophilic head on tyrosinase-catalyzed melanin formation. The tyrosinase activity was tested with HPLC analysis. In Figure 48A, any noticeable changes in L-DOPA consumption were not observed with the addition of 100 μM nonyl-3-hydroxybenzoate. In the case of nonyl-2,4-dihyroxybenzoate, tyrosinase-catalyzed L-DOPA oxidation was also not inhibited (Figure 48B). It should be noted that hydroxyl OH at 2-position of nonyl-2,4-dihydroxybenzoate commonly forms the intramolecular hydrogen bonding with carbonyl group attached to benzene ring. Thus, it is not a “free” resorcinol moiety as well as RA or PLG. Hence, resorcinol moiety is an essential component of resorcinolic lipid as a tyrosinase inhibitor.

Effect of 3,5-dihydroxyphynyl Undecanoate (PLG-10) on Tyrosinase

Among the tested compounds, 3,5-dihydroxyphenyl undecanoate (PLG-10; **19**) was the most efficacious one, and thus, it was further assayed for the identification of the effect on tyrosinase activity using L-DOPA as a substrate. Decyl-3,5-dihydroxybenzoate (RA-10; **5**) were also tested for a comparison; however, similar results were usually obtained in both PLG-10 and RA-10 unless specified. Based on the structural similarity, RA-10 and PLG-10 were expected to have the similar inhibitory action to that of cardol ($C_{15:3}$) (**23**) (Chapter 2.1). Concentrations of PLG-10 were selected at 25 μM and 50 μM. Tyrosinase was incubated with L-DOPA and PLG for 30 min, and the activity was monitored by spectrophotometric or oxygen consumption methods. PLG-10 significantly inhibited the tyrosinase-catalyzed oxidation of L-DOPA at the concentration of 50 μM but not 25 μM. (Figure 49A). The same reaction mixture was incubated and oxygen consumption was monitored for 30 min. Notably, the amount of oxygen consumption was not different from the control, indicating that PLG-10 did not inhibit oxygen consumption (Figure 49B). It should be noted that the difference in the inhibitory activity of PLG-10 observed with L-DOPA by measuring dopachrome formation spectrophotometrically and by measuring oxygen consumption is presumably due to the same reason as to why cardol ($C_{15:3}$) showed inhibitory effects in a static condition but not in a stirring condition (Chapter 2.1). Subsequently, the consecutive UV-Vis spectrum of L-DOPA oxidation was measured with 2 min intervals for 30 min under the same conditions as the oxygen uptake experiment. The changes in the spectrum started increasing in the characteristic broad absorbance, corresponding to dopachrome, with the maximum at around 475 nm. Thus, the evolution of the peak at 475 nm decreased with the addition of PLG-10 (Figure 50B). Thus, PLG-10 suppressed approximately 50% of dopachrome formation. The results were consistent with the spectrophotometric assay but not with the oxygen consumption experiment.

Direct Interaction of Resorcinolic Lipids with Tyrosinase

The enzyme activity was monitored by dopachrome formation at 475 nm even when L-tyrosine was used as a substrate (data not shown). Both PLG-10 and RA-10 inhibited the dopachrome formation but the inhibition mechanism is still largely obscure. However, the inhibitory effect of these molecules was not observed in the case of the oxygen consumption assay. The effect of PLG-10 or RA-10 on the tyrosinase-catalyzed oxidation of *N*-acetyl-L-tyrosine was examined as an alternative substrate. This amino acid can be enzymatically oxidized to *N*-acetyl-dopaquinone but its further intracyclization is blocked because its amino-group is acetylated, and therefore the tyrosinase-catalyzed reaction to dopaquinone can be checked. The reaction mixture consisting tyrosinase (1 μg/mL), *N*-acetyl-L-tyrosine (100 μM) and PLG-10 (100 μM) was incubated and the activity was monitored by HPLC analysis of *N*-acetyl-L-tyrosine (100 μM) consumption. The reaction was proceeded with (**A**) or without (**B**) stirring. Sampling time was selected at 0 min, 15 min, 30 min, 45 min, and 60 min. As a result, most of *N*-acetyl-L-tyrosine remained without being oxidized (Figure 51B), indicating that PLG-10 inhibited the monophenolase activity of tyrosinase. Again, similar result was

observed with RA-10. Thus, it appears that RA and PLG inhibited tyrosinase as a monophenol substrate analogue but could not inhibit completely. The different results between (**A**) and (**B**) indicate that the hydrophobic interaction was disrupted by stirring. According to these results, the inactivation of tyrosinase by both RA and PLG were direct interaction with tyrosinase.

Preincubation Effect of Tyrosinase with Resorcinolic Lipids

The preincubational effect on tyrosinase activity with RA-10 or PLG-10 was further examined in order to test their *slow* hydrophobic inactivation to tyrosinase activity. The effect of 10 min of preincubation of chemical inhibitors with tyrosinase was examined, and the addition of 100 μM L-DOPA initiates the reaction. The tyrosinase activity was monitored as a L-DOPA consumption with HPLC analysis. In Figure 52, PLG-10 inhibits L-DOPA consumption by 67 % at the 30 min of reaction period. The 10 min of preincubation enhanced this inhibitory effect PLG-10, and additional 11 % of L-DOPA consumption was suppressed (Figure 52A). Similar result was also observed with RA-10, and the inhibitory activity was increased by 11 % with 10 min of preincubation (data not shown). It should be noted that none of tested molecules were subjects to be oxidized by tyrosinase, and hence, the mechanism of k_{cat} type inactivation, commonly known as suicide inactivation, was not applied to both cases. Thus, the enhancement of inhibition represents that the *slow* interaction was involved in the mechanism of the inhibition. These enhanced inhibitory effects observed in the cases of PLG-10 and RA-10 were not observed in the cases of PLG-8 and RA-8 (Figure 52B), suggesting that there is a critical difference in the mechanism of inhibition. This is further indication that hydrophobicity of alkyl side chain is involved in the mechanism of inhibition by PLG or RA. Moreover, tyrosinase activity was not completely inactivated with 10 min of preincubation in both cases of RA-10 and PLG-10; therefore, it can be assumed that this inactivation process is a relatively slow process (Presumably, it takes more than 10 min for PLG or RA to inactivate the enzyme).

Irreversibility of Tyrosinase Inhibition by Resorcinolic Lipids

The irreversibility of tyrosinase inhibition by PLG and RA on tyrosinase was further examined in detail with the mixing experiment. The assay was carried out in air-saturated aqueous solutions, though tyrosinase catalyzes a reaction between two substrates, a phenolic compound (L-DOPA) and oxygen. The amount of available oxygen in the cuvette was estimated approximately 250 μM, and therefore, the amount of L-DOPA for this experiment was increased to 1000 μM. As expected, dopachrome formation reached the plateau as all of the available oxygen in the cuvette was consumed (0-15 min). The remaining L-DOPA in the cuvette was oxidized as soon as oxygen became available by mixing in a second (15-30 min). In Figure 53, the remaining L-DOPA in the cuvette containing 50 μM PLG-10 was not oxidized even when oxygen was supplied by mixing (Figure 53), which is similar to the case of cardol ($C_{15:3}$). This observation indicates that tyrosinase irreversibly interacts with an inhibitor over the course of the reaction time, and thus, PLG-10 inactivated the enzyme. In the case of

DMSO control, the remaining L-DOPA in the cuvette was oxidized as soon as oxygen became available by mixing. In the case of RA-10, a similar result was observed with RA-10 (data not shown). Based on the results obtained, the inhibitory effect of PLG and RA were irreversible.

Effect of Longer Alkyl Chain (>C12) of Resorcinolic Lipids

In the case of dodecyl-3,5-dihydroxybenzoate (RA-12; **7**), it showed less inhibitory activity than RA-10 or RA-9 when L-DOPA was used as a substrate. It should be noted, however, that this RA-12 exhibited significant inhibitory activity when *N*-acetyl-L-tyrosine was used as a substrate (data not shown). Similar to RA-10 or RA-9, this inhibitory activity was not visible when the enzyme activity was monitored under the stirring condition (data not shown). In the case of RA-12 or a higher number of alkyl chain containing RA or PLG, their inhibitory activity was not observed presumably because only a low concentration of the chemicals are able to be tested due to the problem in solubility. As testing this postulate, RA-12 and RA-14 (**9**) was subject to examine their preincubation effect on tyrosinase-catalyzed L-DOPA oxidation. Again, both RA-12 and RA-14 did not show any inhibitory effect as if L-DOPA was used as a substrate. However, their inhibitory effects were observed after 10 min of preincubation with tyrosinase. In Figure 54A, the result clearly showed that 10 min of preincubation of RA-12 with tyrosinase, introduces the inhibition against L-DOPA consumption. A similar result was observed in the case of RA-14 (Figure 54B), indicating that RA or PLG with a higher number of carbon containing alkyl chain could inactive tyrosinase as well as effective RA or PLG (>C9). However, because of their high lipophilicity as a molecule, their concentration could not be reached to effective dose (effective dose > saturated concentration). Because of this problem, resorcinolic lipids with a longer alkyl chain exhibit less inhibitory effect. In other words, there is an optimal length of alkyl chain for the inhibitory action, which is observed in the case of cardol ($C_{10:0}$) (Chapter 2.1). Furthermore, there is a clear boundary at C9 to differentiate the inhibitory mechanism of RA and PLG. Therefore, RA and PLG inhibited tyrosinase activity in different ways depending on their alkyl chain lengths.

Effect of Resorcinolic Lipids on Monophenolase Activity

Among the tested compounds including RA, PLG, nonyl-3-dihydroxybenzoate and nonyl-2,4-dihydroxybenzoate, only RA or PLG with the alkyl side chain longer than C9 inhibited the tyrosinase-catalyzed oxidation of L-DOPA (diphenolase activity), indicating that a specific head and tail balance is required for the diphenolase inhibitory activity. The rate of the initial hydrophobic interaction depends on the alkyl chain lengths. As a result, RA and PLG with alkyl side chain shorter than C9 inhibit monophenolase activity (L-tyrosine oxidation) competitively but cannot inhibit completely (no inactivation). If the rate of the initial hydrophobic interaction is faster than the enzymatic oxidation of L-DOPA, its oxidation is presumably inhibited. However, the hydrophobic interaction is not an essential element in inhibiting the monophenolase activity. For example, PLG-8 (**3**) does not form the hydrophobic irreversible interaction but still

inhibit the monophenolase activity with all three analytical methods: UV-Vis, oxygen consumption, and HPLC (data not shown). In the case of higher number of PLG (>C9) they also inhibited monophenolase activity of tyrosinase; however, the effect was observed only when the reaction was in a static condition (data not shown). This also implied that there is significant difference in mechanistic point of view between >C9 and <C9. In these resorcinol structures, the head and tail portions are connected as esters, either -COOR or -OCOR. Thus, the ester groups either an electron withdrawing (-COOR) or an electron donating (-OCOR) group were connected at C-5 position to the resorcinol moiety. However, as a result, the electronegativity of resorcinol moiety is not essential for the inhibition.

Effects of Resorcinolic Lipids on B16-F10 Melanoma Cells

Based on the result obtained from cell free assays, RA and PLG were expected to inhibit melanogenesis on B16-F10 melanoma cells. Therefore, the investigation was extended to cellular experiments including the identification of cytotoxic effect of RA and PLG. Cytotoxic and antimelanogenic effects on B16-F10 melanoma cells with RA or PLG were identified. Interestingly, some of the RA molecules showed antimelanogenic effect on melanoma cells while none of the PLG molecules showed neither toxicity nor antimelanogenic effect (Table 5). For instance, about 35 % of cellular melanin content of RA-9-treated cells was suppressed with low toxic effect, win which the highest examined concentration of RA-9 was 100 μM. RA-9 did not suppressed cell viability up to 25 μM, and at 50 μM, slight reduction of cell viability was observed (Figure 55A). Almost complete lethality was observed at 100 μM. Estimated IC_{50} was 67 μM. Total melanin production was significantly suppressed (P <0.01) up to 200 μM in a concentration-dependent manner (Figure 55B). It came out that total melanin production up to 25 μM was suppressed without any decline of cell viability. Thus, RA-9 showed inhibitory effect on cellular melanin production (Figure 55C). At the concentration between 6.25 μM and 25 μM, the cellular melanin synthesis was significantly suppressed (P <0.01). This U-shaped curve is usually observed when the depigmentation effect is larger than the cytotoxic effects at the certain concentration range. A similar antimelanogenic effect was observed with RA-9, RA-10, RA-12 and RA-14; however, none of the RA molecules that has an alkyl side chain shorter than C9 did not inhibit melanogenesis (Table 5). Interestingly, the cytotoxic effect of RA (IC_{50}) was increased when the alkyl side chain was increased, and the highest IC_{50} was observed with RA-14. It appeared that there is a clear correlation with hydrophobicity of alkyl side chain of RA and both antimelanogenic and cytotoxic effects, which is partly expected from the result obtained in tyrosinase assays. In the case of PLG, among the tested PLG, none of the compounds showed any cytotoxicity and antimelanogenic effects on B16-F10 melanoma cells, different from the case of RA (Table 5). Subsequently, alkyl-3-hydroxybenzoate (**10**-**12**) and alkyl-2,4-dihydroxybenzoate (**13**-**15**) were also tested as a comparison (Table 5). Both alkyl-3-hydroxybenzoate and alkyl-2,4-dihydroxybenzoate did not show any effect on melanogenesis. Moreover, alkyl-3-hydroxybenzoate showed less toxic effect; however, alkyl-2,4-dihydroxybenzoate showed a similar toxic effect to RA. Interestingly, the

cytotoxic effect was increased when the alkyl side chain was extended, which is observed in the case of RA. Thus, hydrophobic portion of the compounds are extremely important for specific biological effect as well as the choice of hydrophilic head.

Toxic Mechanism of Alkyl-3,5-dihydroxybenzoate

For the utilization of RA as a whitening reagent, the clarification of the mechanism of toxicity of RA is essential. As partly discussed above, it seemed that there is a relationship between hydrophobicity of alkyl side chain and mechanism of toxicity. In other words, the more potent cytotoxicity was observed with the increase in the length of alkyl side chain. This phenomenon was often observed when molecules act as a "surfactant" on cellular surface (*11, 15, 16*). The hydrophobic portion of resorcinol head acts as a "hook" in order to interact with plasma membrane, and then the hydrophobic portion of alkyl side chain is slowly diffused into and disrupts the cellular membrane. Thus, higher hydrophobicity is more likely to interact with the lipid portion of plasma membrane. To test this postulate, other possible mechanisms such as intracellular oxidation or prooxidant have to be eliminated. Hence, the effect of vitamin C and butylated hydroxyanisole (BHA) on RA molecule-treated melanoma cells were examined since vitamin C can act as one or two electron reductant while BHA can act one electron reductant. As a result, both vitamin C and BHA did not show any effects on the cytotoxicity of RA on cells. For instance, observed cytotoxicity of RA-9 at 70 μM (approximately equivalent to IC_{50}) was not suppressed with the addition of vitamin C up to 400 μM (Figure 56A). In the case of radical scavenger, BHA, it showed no reversed effect on RA-9-treated melanoma cells (Figure 56B).

As a further supportive evidence to determine that none of the RA molecules are prooxidants, intracellular oxidative stress was measured with 2',7'-dichlorodihydrofluorescin diacetate (DCFH-DA) assay. Intracellular reactive oxygen species (ROS) oxidized the DCFH to a highly fluorescent compound, DCF, after esterase cleaves two acetate groups (*39*). After 1hr of incubation with RA-9 and DCFH-DA, B16-F10 melanoma cells were assayed to measure intracellular ROS. Surprisingly, up to 100 μM, total ROS was slightly but dose-dependently increased. Cell viability of RA-9-treated cells did not show any change in one hour of incubation (Figure 57A). However, total and cellular ROS content was significantly increased with the addition of RA-9 (Figure 57 B and C). Thus, RA-9 showed prooxidative effects, but the effect was presumably not involved in the mechanism of toxicity. These results indicated that the primary mechanism of cytotoxicity by RA is surfactant effect.

Effect of Low Concentration of Decyl-3,5-dihydroxybenzoate (RA-10)

The primary goal of our research was for the development of a depigmenting reagent that does not affect cellular viability. After screening various lengths of RA (Table. 5), RA-10 showed the most potent antimelanogenic effect, which is expected based on the result of tyrosinase assays. Hence, the effect of lower concentration range of RA-10 on melanogenesis was examined. The highest tested concentration of RA-10 was 10 μM, in which almost no cytotoxicity was observed in this range of concentration

(Figure 58A). Total melanin content was dose-dependently suppressed even though cellular viability was not (Figure 58B). In the range between 0.625 μM and 10 μM, total melanin was significantly reduced (P <0.01). Cellular melanin content above 0.625 μM was also reduced dose-dependently without affecting cell growth (Figure 58C). Above 0.625 μM, the suppressive effects on melanogenesis were significant (P <0.01 and 0.05). This result clearly represented that the antimelanogenic effect of RA is not due to the melanocytotoxic effect on melanogenic components of melanoma cells.

Degradation of Resorcinolic Lipids in DMEM

During our continuing efforts to clarify the effects of RA and PLG on a molecular basis, we became aware that the data obtained with the melanoma cells are not the effects of RA or PLG themselves but their decomposed compounds in Dulbecco's modified Eagle's medium (DMEM). Some molecules have high degradability such as gallic acid in this growth medium since the pH of fresh DMEM was relatively basic, and was about pH 9. Thus, RA or PLG might be decomposed in part as soon as it is being mixed with the DMEM containing 10% fetal bovine serum (10% FBS-DMEM) before their application to the cells. This prompted us to examine if RA or PLG decomposed in the same medium. After 60 min of incubation in DMEM, any degradation of 200 μM RA-9 was not observed (data not shown). These results were shared with a series of RA. However, the HPLC analysis showed that the peaks identified as PLG-10 were quickly diminished. The mixture consisted of the medium and 150 μM of PLG-10 was incubated for 60 min and measured at each 15 min. The peak identified as PLG-10 was almost linearly diminished within 60 min (Figure 59). The result was also applied to all other PLG. In the case of PLG, the observed effects in cellular assays are not the effects of the true structure of PLG but that of decomposed PLG. This suggested that there is a possibility for PLG to act as a antimelanogenic reagent if PLG is not decomposed. Based on the results, the specific head and tail portion is required for the antimelanogenic activity. In the current experiment, only the non-branched aliphatic chains having various lengths have been synthesized. It is thus conceivable that optimization of more specific activity is still achievable through a synthetic approach from the aspect of the molecular dimensions, together with the lipophilicity, would have a critical impact on the ability profile of these molecules.

2.2.3 DISCUSSION

Tyrosinase contains a strongly coupled binuclear copper active site and functions, the hydroxylation of a monophenol and the conversion of an *o*-diphenol to the corresponding *o*-quinone as illustrated in Figure 4. The hydroxylation of monophenol demands that this substrate react only with oxy-tyrosinase, giving rise to an ordered sequential mechanism, while the *o*-diphenol is free to bind to the oxy and met forms of the enzyme, producing a random sequential mechanism. Once oxidized to *o*-diols, they were further oxidized to the corresponding *o*-quinone rather quickly. As a result, all of the

series of RA and PLG inhibited tyrosinase-catalyzed L-tyrosine oxidation, indicating that both RA and PLG involve in an ordered sequential mechanism of tyrosinase but not in a random one. Thus, RA and PLG, which share the same resorcinol head, can significantly suppress the initial rate of the dopachrome formation as a monophenol substrate analogue by binding to oxy-tyrosinase. The inactive $E_{oxy}I$ complex subsequently undergoes a slow irreversible inactivation. Because of this slow inactivation, the preincubation allows enough time for the hydrophobic alkyl moiety of RA or PLG to interact with the hydrophobic domain. Once this hydrophobic interaction established, RA or PLG may irreversibly disrupt the quaternary structure of tyrosinase and, as a result, inactivate the enzyme (Chapter 2.1). Thus, the tendency of this slow inactivation is determined by the hydrophobicity of alkyl side chain, indicating that log P higher than 4.4 (ChemBioDraw Ultra12; Cambridge Soft Inc.), at least, is essential for the inhibition of L-DOPA oxidation but not for L-tyrosine oxidation. In fact, because of problem in solubility in resorcinolic lipids with a longer alkyl chain, the optimal length of alkyl chain exhibits more potent inhibitory effect on tyrosinase activity. It should be noted that L-DOPA oxidation is a random sequential event (substrate binds to both oxy and met form), and because of that, the inhibitor has to suppress both oxy and met form or to inactivate tyrosinase itself. Furthermore, the presence of cofactors accelerates the rate of reaction, and hence, inhibition of L-DOPA is extremely difficult. Since native proteins form a sort of intramolecular micelle in which their nonpolar side chains are largely out of contact with the water based-test solution. The hydrophilic head part competitively binds to binuclear copper (*14, 23, 24, 40*), and then the hydrophobic portion of the molecule is able to disrupt the quaternary structure *slowly*. The low conformational stabilities of native proteins make them easily susceptible to denaturation by altering the balance of the weak nonbonding forces that maintain the native conformation.

Based on the results, RA or PLG with alkyl side chain that is longer than C9 showed the potent tyrosinase inhibition, and RA, especially, also showed depigmenting effect without affecting cell growth. In the case of PLG, their activity was limited only with cell free condition due to its instability in growth medium. The -OCOR linkage is decomposed in relative basic medium or buffer. Thus, the application of PLG might be limited; however, the variation of usage of RA would be possible. As well as the result of the cell free experiment, RA showed antimelanogenic effect only with a higher number of carbon alkyl chain. Furthermore, RA showed the antimelanogenic in the non-toxic range. These results indicate that depigmenting effect of RA is not due to melanocytotoxic effect (cytotoxic effect on melanogenic functions) but probably inhibition of tyrosinase activity (based on the cellular and cell free experiments results). At the higher dose, RA tends to show cytotoxicity, which is correlated with the hydrophobicity of alkyl chain (or length of alkyl side chain). Based on further confirmation with vitamin C, BHA and DCFH-DA assays, the hydrophobic alkyl side chain is the active functional domain of the compounds. More specifically, hydrophilic head interacts with negatively charged phospholipids of cellular membrane, and the hydrophobic alkyl side chain possibly and slowly diffuse into the membrane matrix. As a result, the plasma membrane would be disrupted. Thus, RA molecules do not involve in the intracellular components of

melanoma cells. However, RA could make the hole on the cellular membrane with surfactant activity, and then, other RA invade into the cytosol and reach to tyrosinase within melanosomes, which causes antimelanogenic effect. Thus, it is logical to conclude that the depigmenting effect of RA (C9, C10, C12, C14) was due to the inhibition of tyrosinase after entering the cells. As mentioned, PLG was decomposed in the growth medium; however, PLG would suppress melanogenesis if they are not decomposed in the medium, based on the results. Thus, the hydrophilic resorcinol head and hydrophobic alkyl tail inhibit tyrosinase and thus, presumably inhibit melanogenesis. From the point of view of molecular design of tyrosinase and melanogenesis inhibitor, this discovery is critical. Moreover, the chemical features of RA such as lipophilicity, stability, colorlessness and odorlessness, are important aspects for their possible utilization, and also indicate that further improvement of this inhibitor is possible.

Molecular design based on the structure-activity relationship is a common and essential process for a drug design. In the cases of RA and PLG, they are synthesized based on the structure of cardols, and some of the molecules show more potent inhibitory effect compared to an original cardol. Furthermore, based on the valuation of the inhibitory effect of resorcinolic lipids containing various lengths of alkyl chain, we confirmed a novel mechanism of tyrosinase inhibition. Changing of the hydrophilic head to an optimal functional group produce tight binding toward the target active site. Simultaneously, changing of the hydrophobic side chain with an optimal shape could maximize their functions. Hence, the discovery with RA and PLG is critical for future drug development. Further investigation of RA and PLG will offer unique and novel chemotherapeutic medications against severe diseases.

2.2.4 FIGURES & TABLES

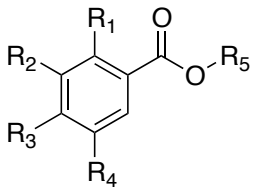

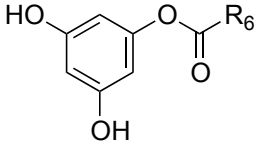

1: $R_1 = R_3 = H$, $R_2 = R_4 = OH$, $R_5 = (CH_2)_5CH_3$
2: $R_1 = R_3 = H$, $R_2 = R_4 = OH$, $R_5 = (CH_2)_6CH_3$
3: $R_1 = R_3 = H$, $R_2 = R_4 = OH$, $R_5 = (CH_2)_7CH_3$
4: $R_1 = R_3 = H$, $R_2 = R_4 = OH$, $R_5 = (CH_2)_8CH_3$
5: $R_1 = R_3 = H$, $R_2 = R_4 = OH$, $R_5 = (CH_2)_9CH_3$
6: $R_1 = R_3 = H$, $R_2 = R_4 = OH$, $R_5 = (CH_2)_{10}CH_3$
7: $R_1 = R_3 = H$, $R_2 = R_4 = OH$, $R_5 = (CH_2)_{11}CH_3$
8: $R_1 = R_3 = H$, $R_2 = R_4 = OH$, $R_5 = (CH_2)_{12}CH_3$
9: $R_1 = R_3 = H$, $R_2 = R_4 = OH$, $R_5 = (CH_2)_{13}CH_3$
10: $R_1 = R_3 = R_4 = H$, $R_2 = OH$, $R_5 = (CH_2)_5CH_3$
11: $R_1 = R_3 = R_4 = H$, $R_2 = OH$, $R_5 = (CH_2)_8CH_3$
12: $R_1 = R_3 = R_4 = H$, $R_2 = OH$, $R_5 = (CH_2)_{11}CH_3$
13: $R_2 = R_4 = H$, $R_1 = R_3 = OH$, $R_5 = (CH_2)_5CH_3$
14: $R_2 = R_4 = H$, $R_1 = R_3 = OH$, $R_5 = (CH_2)_8CH_3$
15: $R_2 = R_4 = H$, $R_1 = R_3 = OH$, $R_5 = (CH_2)_{11}CH_3$
16: $R_6 = (CH_2)_6CH_3$
17: $R_6 = (CH_2)_7CH_3$
18: $R_6 = (CH_2)_8CH_3$
19: $R_6 = (CH_2)_9CH_3$
20: $R_6 = (CH_2)_{10}CH_3$
21: $R_6 = (CH_2)_{11}CH_3$
22: $R_6 = (CH_2)_{12}CH_3$

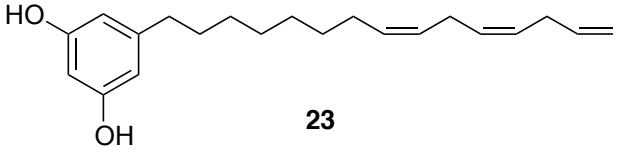

23

Figure 47. Chemical structures of alkyl-3,5-dihydroxybenzoate (**1-9**), alkyl-3-hydroxybenzoate (**10-12**), alkyl-2,4-dihydroxybenzoate (**13-15**), 3,5-dihydroxyphenyl alkanoate (**16-22**), and cardol ($C_{15:3}$) (**23**).

Table 3. Inhibitory effect of alkyl-3,5-dihydroxybenzoate (RA) on tyrosinase-catalyzed L-DOPA oxidation.

		Static	Stirring	log*P*[*]
C6	RA-6	― (100 μM)	― (100 μM)	3.15
C7	RA-7	― (100 μM)	― (100 μM)	3.57
C8	RA-8	― (100 μM)	― (100 μM)	3.99
C9	RA-9	**53 %** (50 μM)	― (50 μM)	4.4
C10	RA-10	**37 %** (25 μM)	― (25 μM)	4.82
C11	RA-11	**45 %** (25 μM)	― (25 μM)	5.24
C12	RA-12	**16 %** (10 μM)	― (10 μM)	5.65
C13	RA-13	― (10 μM)	― (10 μM)	6.07
C14	RA-14	― (5 μM)	― (5 μM)	6.49

[a]Numbers in percentage represent that higher inhibition on L-DOPA oxidation after 30 min of reaction
[b]― indicates that no noticeable inhibitory effect was observed
[c]The numbers in parentheses indicate the highest concentration tested
[*]log *P* was calculated with ChemBioDraw Ultra12 (Cambridge Soft Inc.)

Table 4. The effect of 3,5-dihydroxyphenyl alkanoate (PLG) on tyrosinase-catalyzed L-DOPA oxidation.

		Static	Stirring	log *P*[*]
C7	PLG-7	― (100)	― (100)	3.58
C8	PLG-8	― (100)	― (100)	4.00
C9	PLG-9	**20 %** (100)	― (100)	4.42
C10	PLG-10	**67 %** (50)	― (50)	4.83
C11	PLG-11	**53 %** (25)	― (25)	5.25
C12	PLG-12	**11 %** (10)	― (10)	5.67
C13	PLG-13	― (10)	― (10)	6.08

[a]Numbers in percentage represent that higher inhibition on L-DOPA oxidation after 30 min of reaction
[b]― indicates that no noticeable inhibitory effect was observed
[c]The numbers in parentheses indicate the highest concentration tested
[*]log *P* was calculated with ChemBioDraw Ultra12 (Cambridge Soft Inc.)

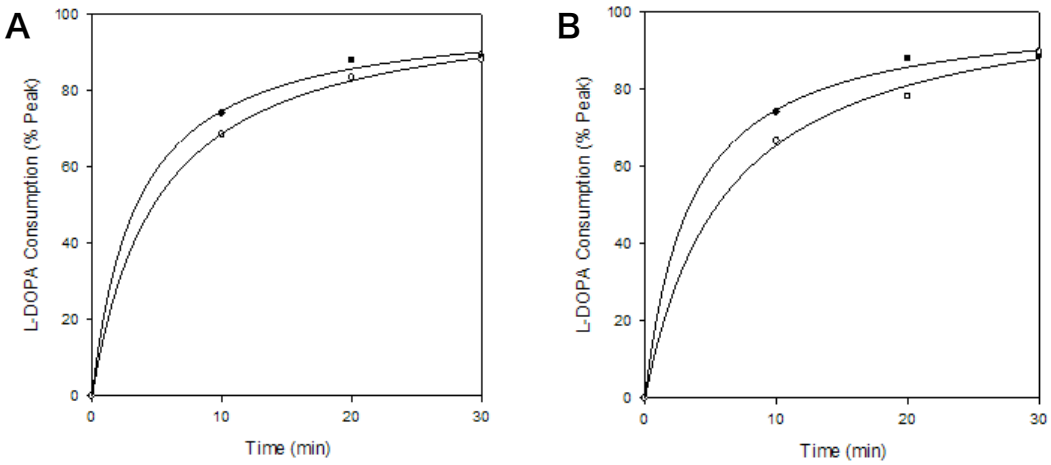

Figure 48. (**A**) HPLC analysis of L-DOPA (100 μM) oxidation by tyrosinase in absence (●) or presence (○) of 100 μM nonyl-3-hydroxybenzoate (3-HB-9) in a static condition. Sampling time was chosen at 0 min, 10 min, 20 min, and 30 min. (**B**) HPLC analysis of L-DOPA (100 μM) oxidation by tyrosinase in absence (●) or presence (○) of 100 μM nonyl-2,4-dihydroxybenzoate (2,4-DHB-9) in a static condition. Sampling time was chosen at 0 min, 10 min, 20 min, and 30 min. HPLC operating conditions were as follows; Deverosil ODS-UG-5 (Nomura Chemical, CO., LTD., Seto-Shi, Aichi, Japan). Solvent; 7 % MeCN/H_2O containing 0.2 % TFA, Flow rate 1.0 mL/min, detection; UV at 280 nm, 0.02 range, injected amount; 25 μL. Each dot was connected smoothly with SigmaPlot (Systat Software, Inc.).

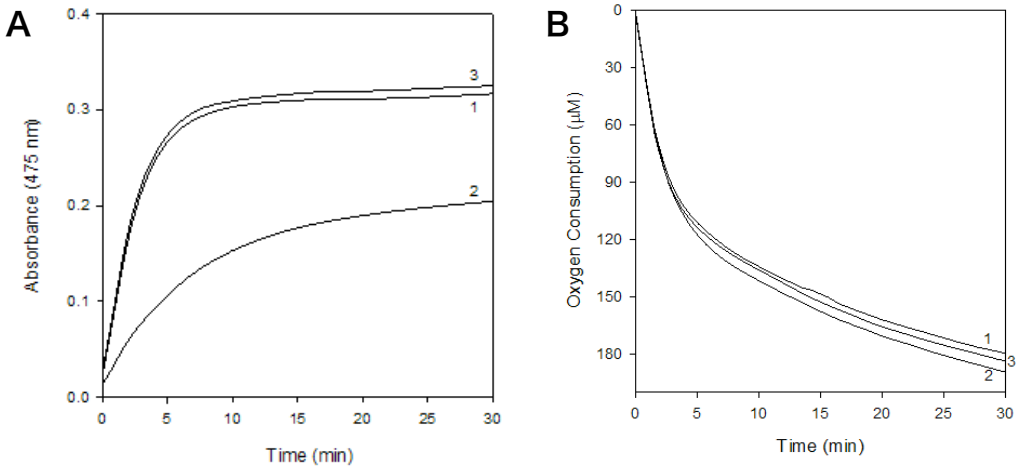

Figure 49. (**A**) UV-Vis spectra at 475 nm obtained in oxidation of 100 μM of L-DOPA by mushroom tyrosinase in presence of 3,5-dihydroxyphenyl undecanoate (PLG-10) for 30 min. Concentrations of PLG-10 were selected at 50 μM (2) and 25 μM (3). Line 1 represents oxidation of L-DOPA by mushroom tyrosinase in absence of PLG-10. (**B**) The oxygen consumption of oxidation of L-DOPA (100 μM) by mushroom tyrosinase in presence of PLG-10 for 30 min. The concentrations of PLG-10 were selected at 25 μM (2) and 50 μM (3). Line 1 represents the oxygen consumption of oxidation of 100 μM of L-tyrosine by mushroom tyrosinase in absence of PLG-10.

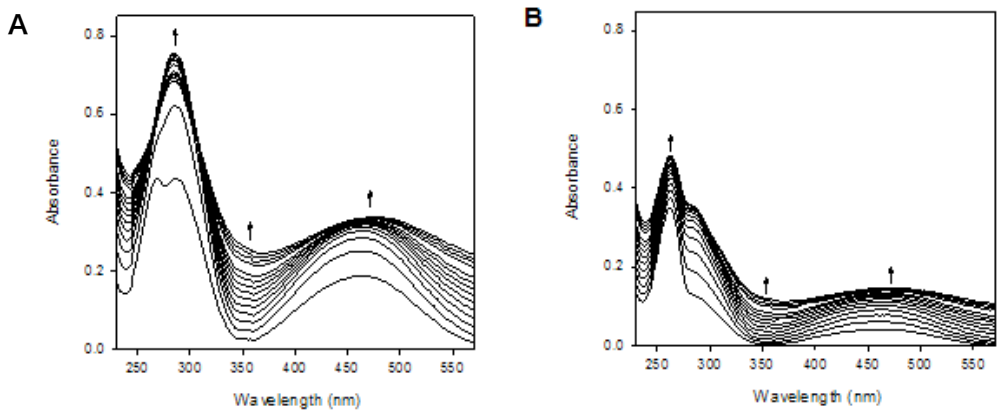

Figure 50. Consecutive UV-Vis-spectra obtained in the oxidation of 100 µM of L-DOPA by mushroom tyrosinase in absence (**A**) or presence (**B**) of 50 µM of 3,5-dihydroxyphenyl undecanoate (PLG-10) for 30min. Scan speed was at 2 min intervals for 30 s. the arrows (↑) designate the evolution of the peak.

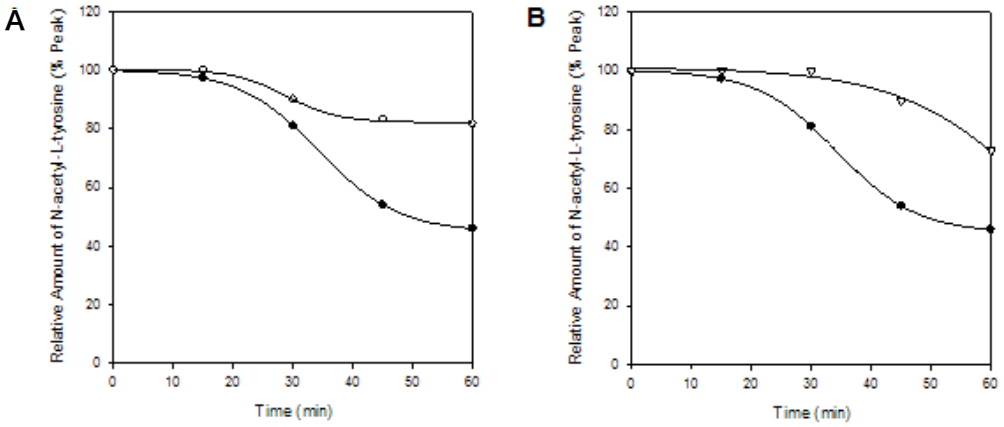

Figure 51. HPLC analysis of *N*-acetyl-L-tyrosine (100 μM) oxidation catalyzed by tyrosinase in absence (●) or presence (○, ▽) of 3,5-dihydroxyphenyl undecanoate (PLG-10) (50 μM). The reaction was proceeded with (**A**) or without (**B**) stirring. Sampling time was chosen at 0 min, 15 min, 30 min, 45 min and 60 min. HPLC operating conditions were as follows; Deverosil ODS-UG-5 (Nomura Chemical, CO., LTD., Seto-Shi, Aichi, Japan). Solvent; 12 % MeCN/H_2O containing 0.2 % TFA, Flow rate 1.0 mL/min, detection; UV at 280 nm, 0.02 range, injected amount; 25 μL. Curve fitting is done with SigmaPlot (Systat Software, Inc.).

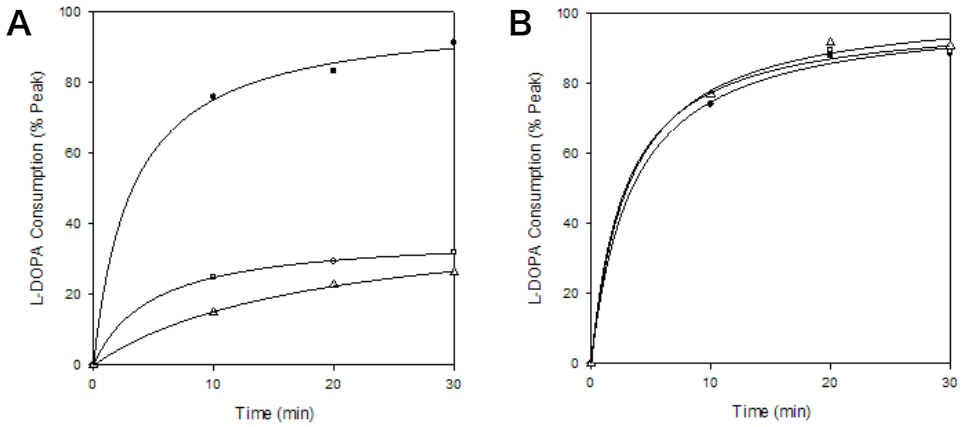

Figure 52. (**A**) HPLC analysis of L-DOPA (100 μM) oxidation by tyrosinase in absence (●) or presence (○, △) of 50 μM 3,5-dihydroxyphenyl undecanoate (PLG-10). Line ○ and △ represent the effect of PLG-10 without or with 10 min of preincubation, respectively. Sampling time was chosen at 0 min, 10 min, 20 min, and 30 min. (**B**) HPLC analysis of L-DOPA (100 μM) oxidation by tyrosinase in absence (●) or presence (○, △) of 100 μM 3,5-dihydroxyphenyl nonanoate (PLG-8). Line ○ and △ represent the effect of PLG-8 without or with 10 min of preincubation, respectively. Sampling time was chosen at 0 min, 10 min, 20 min, and 30 min. HPLC operating conditions were as follows; Deverosil ODS-UG-5 (Nomura Chemical, CO., LTD., Seto-Shi, Aichi, Japan). Solvent; 7 % MeCN/H_2O containing 0.2 % TFA, Flow rate 1.0 mL/min, detection; UV at 280 nm, 0.02 range, injected amount; 25 μL. Each dot was connected smoothly with SigmaPlot (Systat Software, Inc.).

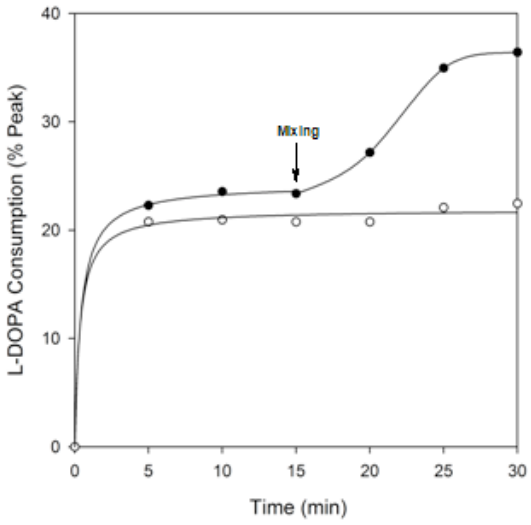

Figure 53. HPLC analysis of L-DOPA (1000 μM) oxidation by tyrosinase in absence (●) or presence (○) of 50 μM 3,5-dihydroxyphenyl undecanoate (PLG-10). Sampling time was chosen at 0 min, 5 min, 10 min, 15 min, 20 min, 25 min and 30 min. The reaction mixture was mixed/voltexed at 15 min. HPLC operating conditions were as follows; Deverosil ODS-UG-5 (Nomura Chemical, CO., LTD., Seto-Shi, Aichi, Japan). Solvent; 3 % MeCN/H_2O containing 0.2 % TFA, Flow rate 1.0 mL/min, detection; UV at 280 nm, 0.02 range, injected amount; 25 μL. Each dot was connected smoothly with SigmaPlot (Systat Software, Inc.).

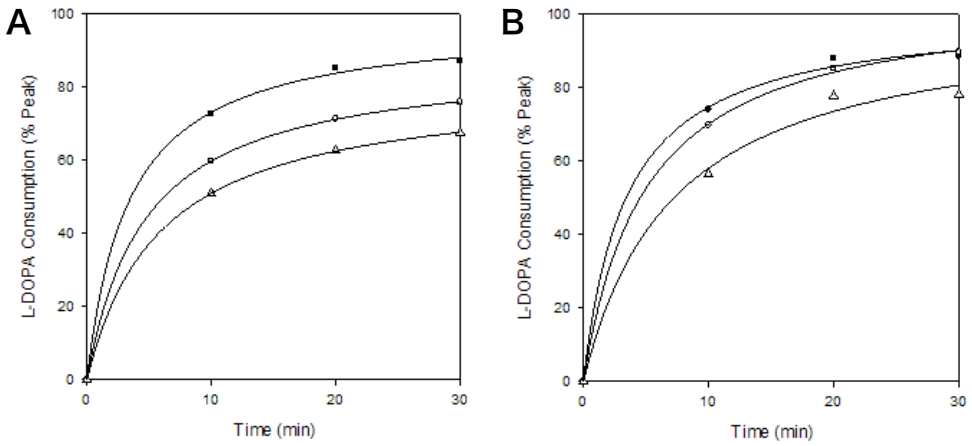

Figure 54. (**A**) HPLC analysis of L-DOPA (100 μM) oxidation by tyrosinase in absence (●) or presence (○, △) of 5 μM dodecyl-3,5-dihydroxybenzoate (RA-12). Line ○ and △ represent the effect of RA-12 without or with 10 min of preincubation, respectively. Sampling time was chosen at 0 min, 10 min, 20 min, and 30 min. (**B**) HPLC analysis of L-DOPA (100 μM) oxidation by tyrosinase in absence (●) or presence (○, △) of 5 μM tetradecyl-3,5-dihydroxybenzoate (RA-14). Line ○ and △ represent the effect of RA-14 without or with 10 min of preincubation, respectively. Sampling time was chosen at 0 min, 10 min, 20 min, and 30 min. HPLC operating conditions were as follows; Deverosil ODS-UG-5 (Nomura Chemical, CO., LTD., Seto-Shi, Aichi, Japan). Solvent; 7 % MeCN/H_2O containing 0.2 % TFA, Flow rate 1.0 mL/min, detection; UV at 280 nm, 0.02 range, injected amount; 25 μL. Each dot was connected smoothly with SigmaPlot (Systat Software, Inc.).

Table 5. Effects of alkyl-3,5-dihydroxybenzoate (RA), 3,5-dihydroxyphenyl alkanoate (PLG), alkyl-3-hydroxybenzoate, and alkyl-2,4-dihydroxybenzoate on B16-F10 melanoma cells

	RA	**PLG**	**3-hydroxybenzoate**	**2,4-dihydroxybenzoate**
C6	252.5	N/A	>200	88
C7	132.5	N/A	N/A	N/A
C8	116	> 200	N/A	N/A
C9	67 (↓)	N/A	66	61.5
C10	62.5 (↓)	> 50	N/A	N/A
C12	28 (↓)	>25	>25	23.5
C14	24.5 (↓)	N/A	N/A	N/A

*The number represents the IC_{50} in μM.
**Down arrow (↓) in parentheses indicate down-regulation of melanogenesis.

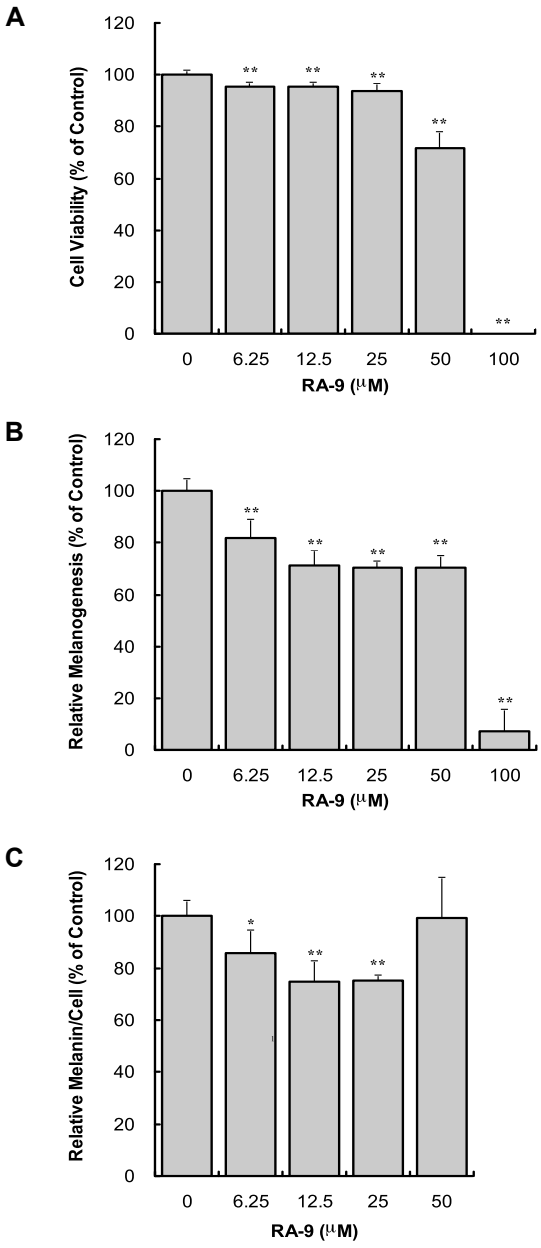

Figure 55. (**A**) Viabilities of B16-F10 melanoma cells following treatment with nonyl-3,5-dihydroxybenzoate (RA-9) for 72hr; data are expressed as percentage of the number of viable cells observed with the control, and each column represents the mean ± S.D. of at least 4 determinations. (**B**) Total melanin content in B16 melanoma cells following treatment with RA-9 for 72hr; data are expressed as percentage of melanin content per well observed with the control, and each column represents the mean ± S.D. of 4 determinations. (**C**) Cellular melanin content in B16 melanoma cells following treatment with RA-9 for 72hr measured as percentage of melanin content per cell observed with the control, and each column represents the mean ± S.D. of 4 determinations. The statistical significance of differences was evaluated using Student's or Welch's *t*-test. Significantly different from the control value: **p*<0.05, ***p*<0.01.

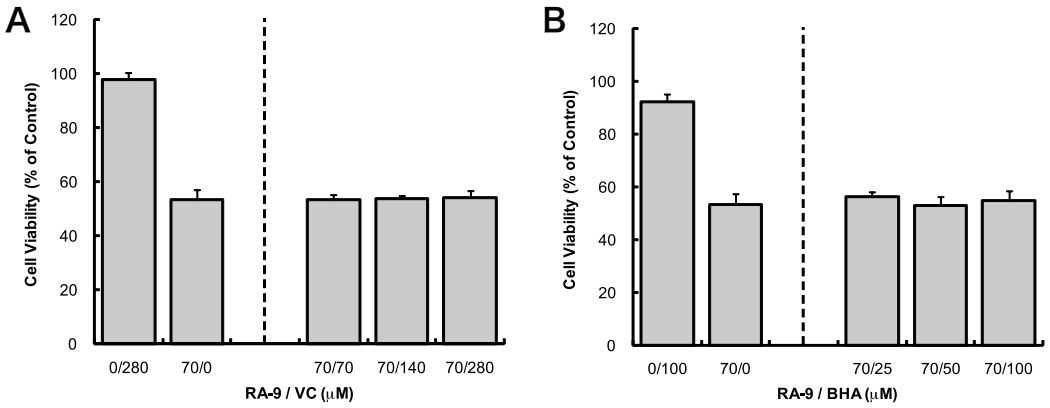

Figure 56. (**A**) Viabilities of B16 melanoma cells following treatment with 70 μM of nonyl-3,5-dihydroxybenzoate (RA-9) in presence or absence of vitamin C for 72hr. The concentrations of vitamin C applied to RA-9 treated cells were chosen at 0 μM (70/0), 70 μM (70/70), 140 μM (70/140) and 70 μM (70/280). Cells are also treated with 280μM of vitamin C without RA-9 (0/280). Data are expressed as the percentage of the number of viable cells observed with RA-9 control (70/0), and each column represents the mean ± S.D. of at least 4 determinations. (**B**) Viabilities of B16 melanoma cells following treatment with 70 μM of RA-9 in presence or absence of butylated hydroxyanisole (BHA) for 72hr. The concentrations of BHA applied to RA-9 treated cells were chosen at 0 μM (70/0), 25 μM (70/25), 50 μM (70/50) and 100 μM (70/100). Cells are also treated with 100μM of BHA without RA-9 (0/100). Data are expressed as the percentage of the number of viable cells observed with RA-9 control (70/0), and each column represents the mean ± S.D. of at least 4 determinations. The statistical significance of differences was evaluated using Student's or Welch's *t*-test. Significantly different from the RA-9 control value: *$p<0.05$, **$p<0.01$.

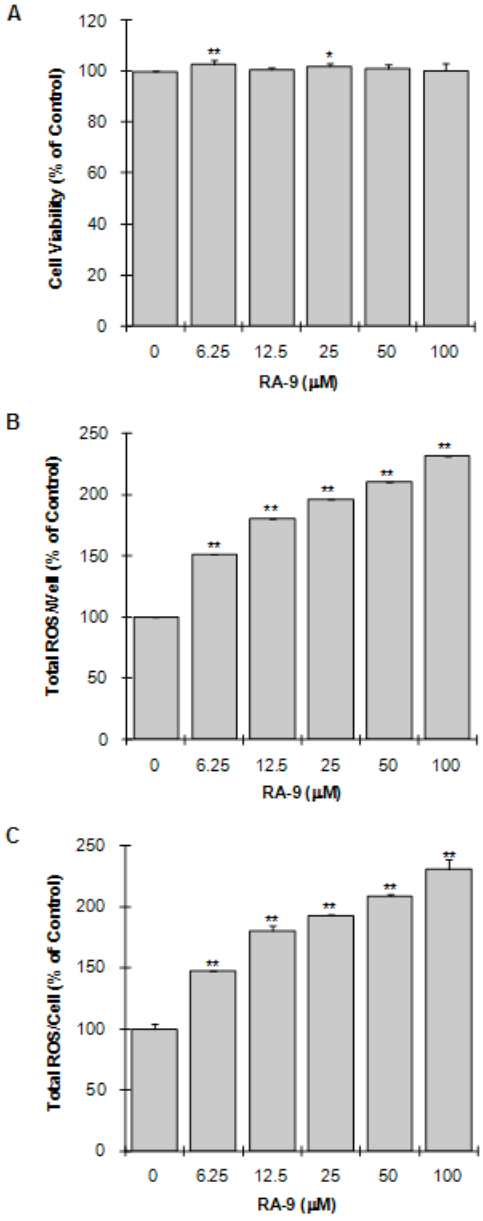

Figure 57. (**A**) Viabilities of B16-F10 melanoma cells following treatment with nonyl-3,5-dihydroxybenzoate (RA-9) for 1 hr; data are expressed as percentage of the number of viable cells observed with the control, and each column represents the mean ± S.D. of at least 4 determinations. (**B**) Total ROS contents in B16 melanoma cells following treatment with RA-9 for 1 hr; data are expressed as percentage of ROS content per well observed with the control, and each column represents the mean ± S.D. of 4 determinations. (**C**) Cellular ROS contents in B16 melanoma cells following treatment with RA-9 for 1 hr measured as percentage of ROS contents per cell observed with the control, and each column represents the mean ± S.D. of 4 determinations. The statistical significance of differences was evaluated using Student's or Welch's *t*-test. Significantly different from the control value: *$p<0.05$, **$p<0.01$.

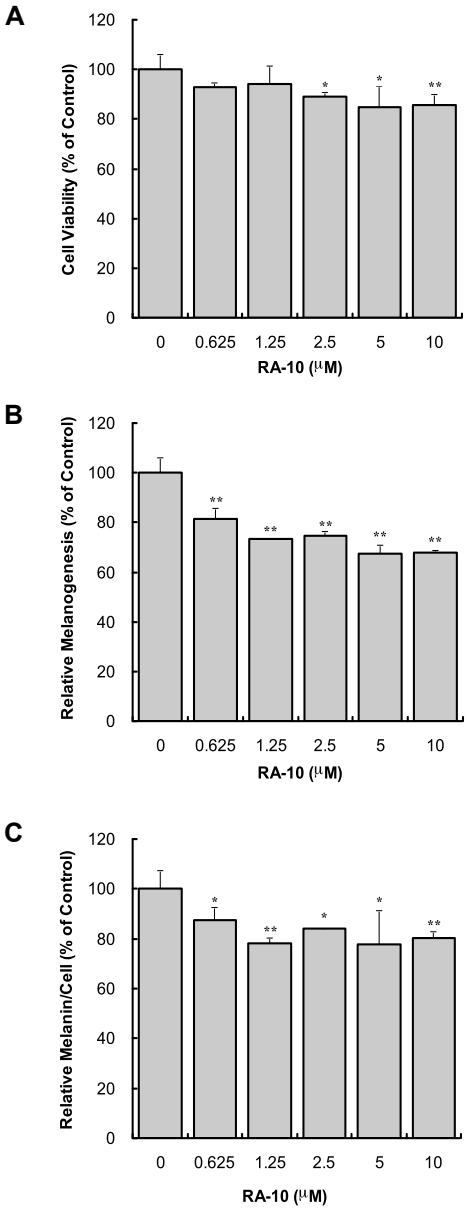

Figure 58. (**A**) Viabilities of B16-F10 melanoma cells following treatment with decyl-3,5-dihydroxybenzoate (RA-10) for 72hr; data are expressed as percentage of the number of viable cells observed with the control, and each column represents the mean ± S.D. of at least 4 determinations. (**B**) Total melanin content in B16 melanoma cells following treatment with RA-10 for 72hr; data are expressed as percentage of melanin content per well observed with the control, and each column represents the mean ± S.D. of 4 determinations. (**C**) Cellular melanin content in B16 melanoma cells following treatment with RA-10 for 72hr measured as percentage of melanin content per cell observed with the control, and each column represents the mean ± S.D. of 4 determinations. The statistical significance of differences was evaluated using Student's or Welch's *t*-test. Significantly different from the control value: **p*<0.05, ***p*<0.01.

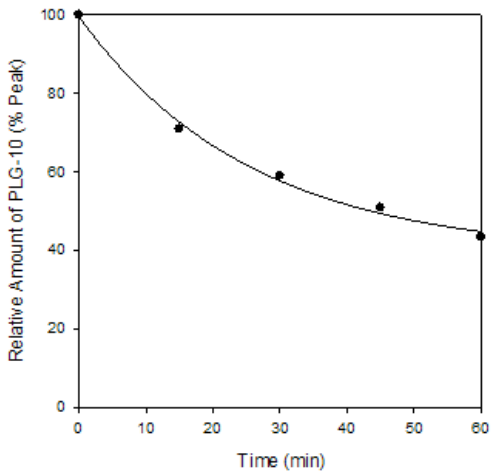

Figure 59. HPLC analysis of 3,5-dihydroxyphenyl undecanoate (PLG-10) in Dulbecco's Modified Eagle Medium (DMEM) containing 10 % of fetal bovine serum. The concentration of sample was set to 150 μM (●). Sampling time was chosen at 0 min, 15 min, 30 min, 45 min and 60 min. HPLC operating conditions were as follows; Deverosil ODS-UG-5 (Nomura Chemical, CO., LTD., Seto-Shi, Aichi, Japan). Solvent; 80 % MeCN/H_2O containing 0.2 % TFA, Flow rate 1.0 mL/min, detection; UV at 230 nm, 0.01 range, injected amount; 25 μL. Curve fitting was done by using SigmaPlot Software (Systat Software Inc.).

2.3 Conclusions and Remarks

Resorcinol moiety is one of the fundamental chemical structure found in many chemical compounds such as flavonoids and stilbenoids. This common functional group has variety of biological effects, and shows inhibitory binding if tyrosinase is a target enzyme. Cardols, RA, and PLG with alkyl chain longer than C9 tend to undergo a two-step inactivation process. The compounds with shorter chain do not inactivate tyrosinase; however, the competitive effect are still observed. Thus, specific hydrophilic and hydrophobic balance is required for the specific mechanism of inhibition. As discussed, this inhibitory effect could be improved by swapping the head and tail portion to optical ones. In addition to the tyrosinase inhibitory effects, the cytotoxic effects is also relied on the balance of hydrophilic and hydrophobic portions. In this studies, only the effect of alkyl chains are identified; however, there are many other possibilities that these inhibitors could improve in the aspects of safety, stability and effectiveness. Further investigations with dynamic and structural perspectives are essential.

2.4 Materials and Methods

General

General procedures were the same in the previous work (*11, 41, 42*). The assays were performed in triplicate on separate occasions. Cells were viewed in 96-well plates approximately 72 hours after the chemical treatment.

Materials

Cardol ($C_{15:n}$) are previously isolated from the cashew *Anacardium occidentale* L. (Anacardiaceae) (*10*). All synthetic resorcinolic lipids were previously synthesized by Dr. K. Nihei during his postdoctoral training at UC Berkeley (*37, 38, 43*). Cardol ($C_{10:0}$) was provided from our contributor, Dr. T. Isobe. Cardol ($C_{5:0}$) and resorcinol were purchased from Aldrich Chemical Co. (Milwaukee, WI). L-Tyrosine, L-DOPA, L-cysteine, L-ascorbic acid (vitamin C), butylated hydroxyanisole, 2',7'-dichlorodihydrofluorescin diacetate (DCFH-DA), and dimethyl sulfoxide (DMSO) were purchased from Sigma Chemical Co. (St. Louis, MO). 4-*tert*-butylcatechol was purchased from Fluka Chemika (Buchs, Switzerland). *N*-acetyl-L-tyrosine was purchased from Tokyo Kasei Kogyo Co. Ltd. (Tokyo, Japan). Fatal bovine serum (FBS) and Dulbecco's modified Eagle's medium (DMEM), and 3-(4,5-dimethylthiazole-2-yl)-2,5-diphenyltetrazolium bromide (MTT) cell proliferation assay kit were purchased from ATCC (Manassas, VA, USA).

Enzyme/Spectrophotometric Assay

General procedures were the same as the previous works (*1, 43*) but slightly modified. All assays were performed in triplicate on separate occasions. The mushroom tyrosinase (EC 1.14.18.1) used for the bioassay was purchased from Sigma Chemical Co. and was purified by anion-exchange chromatography using DEAE-Sepharose Fast Flow (Pharmacia, Uppsala, Sweden) as previously described (*44*). The current experiment was subjected to use the purified tyrosinase. Although mushroom tyrosinase differs somewhat from those of other sources, this fungal enzyme was used for the entire experiment because it is readily available. Throughout the experiment, L-DOPA or L-tyrosine was used as a substrate. In general, L-tyrosine was mainly used as a substrate since it is a natural substrate of tyrosinase. In a spectrophotometric experiment, the enzyme activity was monitored by dopachrome formation at 475 nm with a SpectraMAX Plus Microplate spectrophotometer (Molecular Devices, Sunnyvale, CA) at 30 °C. All samples were first dissolved in DMSO and used for the experiment after dilution. The final concentration of DMSO in the test solution was always 3.3%. The assay was performed as previously reported with slight modifications. First, 100 μL of a 3 mM L-DOPA or L-tyrosine aqueous solution was mixed with 2.1 mL of filtered distilled H_2O and 600 μL of 250 M phosphate buffer (pH 6.8) and incubated at 30 °C for 5 min. Then, 100 μL of the sample solution and 100 μL of the same phosphate buffer solution of the purified mushroom tyrosinase (1 μg/mL) were added in this order to the mixture. Results were expressed as

in absorbance unit with appropriate wavelength (nm), and all data were processed with SigmaPlot 10 software (Systat Software Inc.).

Oxygen Consumption Assay

In general, procedure was previously described (*1, 43*). Briefly, 100 μL of a 3 mM L-DOPA or L-tyrosine aqueous solution was mixed with 2.1 mL of distilled H_2O, 600 μL of 67 mM phosphate buffer (pH 6.8) and 100 μL of sample-DMSO solution was incubated at 30 °C for 5 min. Then, 100 μL of the same phosphate buffer solution of the purified mushroom tyrosinase (1 μg/mL) was added and oxygen consumption was measured with an OBH 100 oxygen electrode and an oxygraph equipped with a water-jacket chamber of YSI 5300 (all from Yellow Springs Instruments Co., Yellow Springs, OH) maintained at 30 °C for 60 min. The results were expressed as the oxygen consumption in μM, and calibration of an oxygen electrode was performed by using 4-*tert*-butylcatechol and excess tyrosinase according to the previous report (*45*). All assays were performed in triplicate on separate occasions.

HPLC analysis

Time-dependent consumption of substrates and/or formation of products were monitored with HPLC analysis. The HPLC analysis was performed on an EYELA LPG-100 (Tokyo Rikakikai Co. Ltd., Tokyo, Japan) with an EYELA UV-7000 detector (Tokyo Rikakikai Co. Ltd., Tokyo, Japan) and Develosil ODS-UG-5 column (4.6 x 150 mm, Nomura Chemical Co., Ltd., Japan). In general, the operating conditions were as follows: solvent; 7% MeCN/H_2O containing 0.2 % TFA, flow rate; 1.0 mL/min, detection; UV at 280 nm, injected amount; 20 μL from above described 3 mL assay system. For analysis, samples were collected from the reaction mixtures described above at certain time points. The peak heights of each chromatographic peak were used to monitor the consumption of substrates and/or formation of products. In appropriate occasions, the results were expressed with the ratio of the height of sample peaks to that of control one, and then points were connected smoothly using the statistical software.

Cell culture

B16-F10 mouse melanoma cells (CRL-6475) were obtained from ATCC (Manassas, VA, USA), and cultured in continuous log phase growth in DMEM containing 10 % FBS. Cells were seeded in 96-well plates (2000 cells/well) and incubated at 37 °C in 5 % CO_2 for about 24 h before chemical treatment. Each chemical was applied in duplicate with a final content of 0.1% DMSO, and treated cells were cultured for 72 h before assays.

Melanin assay

The melanin content was determined as previously described (*46, 47*) with minor modifications. Cells were washed with PBS, harvested by trypsinization, and centrifuged for 10 min at 1500 x *g*. The cell pellets were then dissolved in 1.0 M NaOH containing 10 % DMSO during 2 h incubation at 80 °C. Melanin content was measured at

475 nm using a SpectraMax Plus spectrophotometer and SoftMax Pro software (Molecular Devices, Union City, CA, USA).

Cell viability assays

Cell viability was determined by trypan blue exclusion and MTT cell proliferation assays. Both bioassays basically provided the same results but the concentration leading to 50 % viable cells lost (IC_{50}) was established by trypan blue assay for steady comparison purpose. The appropriate concentrations of the test chemicals were selected by microscopic observation of the preliminary cell viability assay using a Nikon Diaphoto TMD (Nikon, Tokyo, Japan).

Trypan blue method

Cells were washed with PBS, and dispersed by trypsinization. An aliquot of the cells was mixed with a half volume of DMEM containing 10 % FBS, and then mixed with trypan blue solution (final content 0.1 %) at room temperature. Unstained cells (viable cells) were counted using a hemocytometer within 10 min after mixing with trypan blue solution.

MTT method

Cells were washed with PBS, and dispersed with trypsinization, and an aliquot of the cells was seeded in 96-well plates and incubated with DMEM containing 10 % FBS at 37 °C in 5 % CO_2 for 16 to 24 h. At the end of the period, 10 µl of MTT reagent were added to each well, which was then incubated at 37 °C in 5 % CO_2 for 4 h. Then, 100 µl of detergent reagent were added to each well. The plate was kept at room temperature in the dark for 2 h, and a relative amount of MTT reduction was determined based on the absorbance at 570 nm using a SpectraMax Plus spectrophotometer and SoftMax Pro software (Molecular Devices).

DCFH-DA method

The level of intracellular reactive oxygen species (ROS) in B16-F10 melanoma cells was measured by DCFH-DA method. Intracellular ROS oxidized the DCFH to a highly fluorescent compound, DCF, after esterase cleaves two acetate groups (*39*). General procedures are listed as previously described (*48, 49*) with minor modifications. Shortly, the cultured cells were incubated with the sample and DCFH-DA reagent for 60 min at 37 °C in the dark. After the incubation, cells were removed from the plate with trypsinization in order to measure fluorescent. The amount of formed DCF was measured using fluorolog-3 with DataMax (Instruments S.A., Inc. NJ, USA) with the excitation wavelength at 485 nm and the emission wavelength at 520 nm.

Statistical analysis

The statistical significance of differences was evaluated by either Student's or Welch's *t*-test after examining the variances using F test and $^{**}p < 0.01$ was considered to be statistically significant.

2.5 References

1. Kubo, I.; Kinst-Hori, I.; Yokokawa, Y., Tyrosinase inhibitors from Anacardium occidentale fruits. *J. Nat. Prod.* **1994,** 57, (4), 545-551.
2. Cojocaru, M.; Droby, S.; Glotter, E.; Goldman, A.; Gottlieb, H. E.; Jacoby, B.; Prusky, D., 5-(12-Heptadecenyl)-resorcinol, the major component of the antifungal activity in the peel of mango fruit. *Phytochemistry* **1986,** 25, (5), 1093-1095.
3. Clay, J. W., World agriculture and the environment: a commodity-by-commodity guide to impacts and practices. Island Press: 2004.
4. Kubus, G.; Tluscik, F., Alkylresorcinols in grains from plants from the family Gramineae. *Acta Soc. Bot. Pol* **1983,** 52, 223-230.
5. Hladyszowski, J.; Zubik, L.; Kozubek, A., Quantum mechanical and experimental oxidation studies of pentadecylresorcinol, olivetol, orcinol and resorcinol. *Free Radical Res.* **1998,** 28, (4), 359-368.
6. Kozubek, A.; Tyman, J. H. P., Bioactive phenolic lipids. In *Studies in Natural Products Chemistry*, Atta ur, R., Ed. Elsevier: 2005; Vol. Volume 30, pp 111-190.
7. Rea, A. I.; Schmidt, J. M.; Setzer, W. N.; Sibanda, S.; Taylor, C.; Gwebu, E. T., Cytotoxic activity of *Ozoroa insignis* from Zimbabwe. *Fitoterapia* **2003,** 74, (7-8), 732-735.
8. Struski, D. G. J.; Kozubek, A., Cereal grain alk(en)ylresorcinols protect lipids against ferrous ionsinduced peroxidation. *Z. Naturforsch. C.* **1992,** 46, 47–50.
9. Stojanovic, S.; Brede, O., Elementary reactions of the antioxidant action of trans-stilbene derivatives: resveratrol, pinosylvin and 4-hydroxystilbene. *Phys. Chem. Chem. Phys.* **2002,** 4, (5), 757-764.
10. Kubo, I.; Komatsu, S.; Ochi, M., Molluscicides from the cashew *Anacardium occidentale* and their large-scale isolation. *J. Agr. Food Chem.* **1986,** 34, (6), 970-973.
11. Kubo, I.; Nitoda, T.; Tocoli, F. E.; Green, I. R., Multifunctional cytotoxic agents from *Anacardium occidentale*. *Phytother. Res.* **2010,** 25, (1), 38-45.
12. Chang, T. S., An updated review of tyrosinase inhibitors. *IJMS* **2009,** 10, (6), 2440.
13. Khatib, S.; Nerya, O.; Musa, R.; Tamir, S.; Peter, T.; Vaya, J., Enhanced substituted resorcinol hydrophobicity augments tyrosinase inhibition potency. *J. Med. Chem.* **2007,** 50, (11), 2676-81.
14. Shimizu, K.; Yasutake, S.; Kondo, R., A new stilbene with tyrosinase inhibitory activity from Chlorophora excelsa. *Chem. Pharm. Bull.* **2003,** 51, (3), 318-319.
15. Kubo, I.; Fujita, K.; Kubo, A.; Nihei, K.; Ogura, T., Antibacterial activity of coriander volatile compounds against *Salmonella choleraesuis*. *J. Agric. Food Chem.* **2004,** 52, (11), 3329-3332.
16. Kubo, I.; Fujita, K.; Nihei, K.; Kubo, A., Anti-*Salmonella* activity of (2E)-alkenals. *J. Appl. Microbiol.* **2004,** 96, (4), 693-699.

17. Maupas, C.; Moulari, B.; Béduneau, A.; Lamprecht, A.; Pellequer, Y., Surfactant dependent toxicity of lipid nanocapsules in HaCaT cells. *Int. J. Pharm.* **2011.** 411, (1-2), 136-141.
18. Maeda, K.; Fukuda, M., Arbutin: mechanism of its depigmenting action in human melanocyte culture. *J. Pharmacol. Exp. Ther.* **1996,** 276, (2), 765-9.
19. Briganti, S.; Camera, E.; Picardo, M., Chemical and instrumental approaches to treat hyperpigmentation. *Pigm. Cell Res.* **2003,** 16, (2), 101-110.
20. Kubo, I.; Masuoka, N.; Ha, T. J.; Shimizu, K.; Nihei, K., Multifunctional Antioxidant Activities of Alkyl Gallates. *Open Bioact. Comp. J.* **2010,** 3, 1-11.
21. Togashi, N.; Shiraishi, A.; Nishizaka, M.; Matsuoka, K.; Endo, K.; Hamashima, H.; Inoue, Y., Antibacterial activity of long-chain fatty alcohols against Staphylococcus aureus. *Molecules* **2007,** 12, (2), 139-148.
22. Tsujimoto, K., Anacardic acids and ferric ion chelation. *Z. Naturforsch. C.* **2007**.
23. Jiménez, M.; Garcia-Carmona, F., 4-Substituted resorcinols (sulfite alternatives) as slow-binding inhibitors of tyrosinase catecholase activity. *J. Agr. Food Chem.* **1997,** 45, (6), 2061-2065.
24. Shimizu, K.; Kondo, R.; Sakai, K., Inhibition of tyrosinase by flavonoids, stilbenes and related 4-substituted resorcinols: structure-activity investigations. *Planta Med.* **2000,** 66, (1), 11-15.
25. Buskirk, A. R.; Liu, D. R., Creating small-molecule-dependent switches to modulate biological functions. *Chem. Biol.* **2005,** 12, (2), 151-161.
26. Grady, R. W.; Bienen, E. J.; Clarkson Jr, A. B., Esters of 3, 4-dihydroxybenzoic acid, highly effective inhibitors of the sn-glycerol-3-phosphate oxidase of Trypanosoma brucei brucei. *Mol. Biochem. Parasit.* **1986,** 21, (1), 55-63.
27. Kim, C. U.; Lew, W.; Williams, M. A.; Liu, H.; Zhang, L.; Swaminathan, S.; Bischofberger, N.; Chen, M. S.; Mendel, D. B.; Tai, C. Y., Influenza neuraminidase inhibitors possessing a novel hydrophobic interaction in the enzyme active site: design, synthesis, and structural analysis of carbocyclic sialic acid analogues with potent anti-influenza activity. *J. Am. Chem. Soc.* **1997,** 119, (4), 681-690.
28. Kim, Y.; Uyama, H., Tyrosinase inhibitors from natural and synthetic sources: structure, inhibition mechanism and perspective for the future. *Cell Mol. Life Sci.* **2005,** 62, (15), 1707-1723.
29. Kozubek, A.; Tyman, J., Resorcinolic lipids, the natural non-isoprenoid phenolic amphiphiles and their biological activity. *Chem. Rev.* **1999,** 99, (1), 1-26.
30. Gaal, A.; Neujahr, H., Metabolism of phenol and resorcinol in Trichosporon cutaneum. *J. Bacteriol.* **1979,** 137, (1), 13.
31. Kim, Y.; Matthews, H., Comparative metabolism and excretion of resorcinol in male and female F344 rats. *Fund. Appl. Toxicol.* **1987,** 9, (3), 409-414.
32. Kozubek, A.; Tyman, J. H. P., Resorcinolic lipids, the natural non-isoprenoid phenolic amphiphiles and their biological activity. *Chem. Rev.* **1999,** 99, (1), 1-26.
33. Tyman, J., Non-isoprenoid long chain phenols. *Chem. Soc. Rev.* **1979,** 8, (4), 499-537.

34. Ha, T. J.; Kubo, I., Lipoxygenase inhibitory activity of anacardic acids. *J. Agr. Food Chem.* **2005,** 53, (11), 4350-4354.
35. Himejima, M.; Kubo, I., Antibacterial agents from the cashew *Anacardium occidentale* (Anacardiaceae) nut shell oil. *J. Agr. Food Chem.* **1991,** 39, (2), 418-421.
36. Shobha, S.; Ramadoss, C. S.; Ravindranath, B., Inhibition of soybean lipoxygenase-1 by anacardic acids, cardols, and cardanols. *J. Nat. Prod.* **1994,** 57, (12), 1755-1757.
37. Nihei, K.; Nihei, A.; Kubo, I., Rational design of antimicrobial agents: antifungal activity of alk (en) yl dihydroxybenzoates and dihydroxyphenyl alkanoates. *Bioorg. Med. Chem. Lett.* **2003,** 13, (22), 3993-3996.
38. Kubo, I.; Xiao, P.; Nihei, K.; Fujita, K.; Yamagiwa, Y.; Kamikawa, T., Molecular design of antifungal agents. *J. Agr. Food. Chem.* **2002,** 50, (14), 3992-3998.
39. Rhee, S. G.; Chang, T.-S.; Jeong, W.; Kang, D., Methods for detection and measurement of hydrogen peroxide inside and outside of cells. *Mol. Cells* **2010,** 29, (6), 539-549.
40. Shimizu, K.; Kondo, R.; Sakai, K.; Takeda, N.; Nagahata, T.; Oniki, T., Novel vitamin E derivative with 4-substituted resorcinol moiety has both antioxidant and tyrosinase inhibitory properties. *Lipids* **2001,** 36, (12), 1321-1326.
41. Satooka, H.; Kubo, I., Effects of Thymol on Mushroom Tyrosinase-Catalyzed Melanin Formation. *J. Agr. Food. Chem.* **2011,** 59, (16), 8908-8914.
42. Kubo, I.; Hori, I.; Nihei, K.; Satooka, H.; Cespedes, C. L.; Calderon, J. S., Insect Growth Inhibitory Activity and Cytotoxicity of Tannic Acid from Gallae Rhois. *Biopestic. Int.* **2008,** 4, (1), 6-14.
43. Kubo, I.; Chen, Q. X.; Nihei, K., Molecular design of antibrowning agents: antioxidative tyrosinase inhibitors. *Food Chem.* **2003,** 81, (2), 241-247.
44. Espin, J. C.; Wichers, H. J., Slow-binding inhibition of mushroom (*Agaricus bisporus*) tyrosinase isoforms by tropolone. *J. Agric. Food Chem* **1999,** 47, (7), 2638-2644.
45. Rodriguez-López, J. N.; Ros-Martínez, J. R.; Varón, R.; García-Cánovas, F., Calibration of a Clark-Type oxygen electrode by tyrosinase-catalyzed oxidation of 4-tert-butylcatechol. *Anal. Biochem.* **1992,** 202, (2), 356-60.
46. Kageyama, A.; Oka, M.; Nakamura, S.; Ueyama, T.; Saito, N.; Hearing, V. J.; Ichihashi, M.; Nishigori, C., Down-regulation of Melanogenesis by Phospholipase D2 through Ubiquitin Proteasome-mediated Degradation of Tyrosinase. *J. Biol. Chem.* **2004,** 279, (26), 27774-27780.
47. Venkatasamy, R.; Faas, L.; Young, A. R.; Raman, A.; Hider, R. C., Effects of piperine analogues on stimulation of melanocyte proliferation and melanocyte differentiation. *Bioorg. Med. Chem.* **2004,** 12, (8), 1905-1920.
48. Galati, G.; Lin, A.; Sultan, A. M.; O'Brien, P. J., Cellular and in vivo hepatotoxicity caused by green tea phenolic acids and catechins. *Free Radical Biol. Med.* **2006,** 40, (4), 570-80.

49. Tsoncheva, V. L.; Milchev, G. I., Delayed reproductive death and ROS levels in the progeny of irradiated melanoma cells. *Z Naturforsch. C.* **2004,** 59, (3-4), 297-301.

Chapter 3

Polyphenolic Compounds

3.1 Resveratrol as a k_{cat} type Inhibitor for Tyrosinase: Potentiated Melanogenesis Inhibitor

3.1.1 INTRODUCTION

Resveratrol, 3,5,4'-trihydroxy-*trans*-stilbene (**1**; see Figure 60 for the structure), is a widely distributed natural stilbenoid in nature such as in grapes. Resveratrol is currently the subject of many research investigations due to its health beneficial effects including antioxidative, antifungal, anticarcinogenic, cardioprotective, and anti-aging actions (*1-4*). Antioxidant effect of resveratrol has been extensively studied, and the mechanism of action involves the recruitment of antioxidant defense enzymes in the cells (*5-9*). In addition to antioxidant effect, resveratrol is known to have anti-cancerous and apoptotic actions (*2, 10, 11*). Despite of wide beneficial biological functions, its effects on melanogenesis and on tyrosinase have been limitedly studied. Inhibitory effect of resveratrol on tyrosinase activity has been reported previously (*12, 13*). Newton *et al*., also previously reported that antimelanogenic effect on human melanocyte through affecting the post-transcriptional synthesis of tyrosinase (*14*). However, the detailed mechanism of tyrosinase inhibition is not fully understood. Furthermore, the effects of resveratrol on monophenol oxidation of tyrosinase and on cellular melanogenesis as a potentiated drug have not been studied yet.

k_{cat} type inhibitors possess reactive groups selectively activated by target enzyme at its active site (*15*). They are also often described as suicide inhibitors. The enzyme sometimes undergoes inactivating processes by bioactivating their substrates; in the case of tyrosinase, the reactive oxidation product(s) was converted from unreactive tyrosinase substrate to inactivate enzyme (*16, 17*). Several compounds including natural products are known to be a suicide inhibitor; for example, 7,8,4'-trihydroxyisoflavone and 5,7,8,4'-tetrahydroxyflavone are recently reported as one of the potent suicide inhibitors of tyrosinase (*18*). The investigation of k_{cat} type inhibitors is important in functional design of enzymatic inhibitors for pharmaceutical and therapeutic purposes. In the case of tyrosinase, functional inhibitors are not used only in pharmaceutical field but also used in food industry and for cosmetic users. These problems motivate us to find the inhibitory mechanism of resveratrol on tyrosinase activity and on melanogenesis.

3.1.2 RESULTS

Oxidation of Resveratrol by Mushroom Tyrosinase

The investigation was begun with finding whether tyrosinase oxidized resveratrol or not since the previous data suggested that *para*-4-hydroxyl unit with no steric hindrance was often oxidized by tyrosinase. Resveratrol (100 μM) was incubated with tyrosinase for 60 min, and its conversion at each time point was monitored with reverse-phase HPLC system. Resveratrol (peak ***a***; t_R = 9.0 min) was oxidized by

tyrosinase in a time-dependent manner (Figure 61). Most of the oxidation of resveratrol occurred for the first 30 min, and, at the end of the reaction period, about 90% of resveratrol (peak high ratio) was oxidized. Various tyrosinase-catalyzed reaction products (peak ***b***, ***c***, ***d***) were observed; however, these oxidation product(s), unfortunately, were not stable enough to identify the structure as Espin and Wichers described in their previous investigation (*19*). The effect of the oxidation of resveratrol on mushroom tyrosinase is poorly understood; hence, further investigation was conducted.

Effects of Resveratrol on L-tyrosine Oxidation

L-Tyrosine is an endogenous substrate of tyrosinase in nature, and the examination of the effect of resveratrol on tyrosinase-catalyzed L-tyrosine oxidation is significant in the biological point of view. Tyrosinase activities were examined with three different approaches: UV-vis spectrum at 475 nm, oxygen consumption, and HPLC. Dopachrome formation was measured with UV-vis spectrum at 475 nm, and resveratrol did not exhibit inhibitory effect on tyrosinase-catalyzed formation of dopachrome for 60 min in this assay (Figure 62A). The formations of dopachrome (absorbance at 475 nm) were significantly increased in a concentration-dependent manner (curve 2, 3, and 4 in Figure 62A) with the addition of resveratrol. The shape of the sample curves was significantly different from that of the control. With resveratrol, the absorbance at 475 nm was sharply increased within 20 min and then decreased, while the curve without resveratrol (DMSO control) was almost linearly increased during the entire reaction period. The extension of lag phase, which is commonly observed when compounds act as a monophenol analogue, was also observed in the case of resveratrol. Resveratrol dose-dependently extended the lag phase of oxidation of L-tyrosine. Tyrosinase activity was measured by monitoring the consumption of another substrate, oxygen. Oxygen consumption was not suppressed with the addition of resveratrol but was rather enhanced in a concentration-dependent manner (Figure 62B). After the addition of resveratrol, the rate of oxygen consumption, interestingly, was accelerated; however, the oxygen consumption after 20 min became a stationary phase. Both UV and oxygen consumption results indicated resveratrol to be oxidized during the reaction. However, it appeared that, after 20 min, tyrosinase activities were inhibited. Thus, resveratrol requires the time (20-30 min in this condition) to inhibit tyrosinase. Subsequently, L-tyrosine consumption was monitored with HPLC analysis (Figure 63). L-tyrosine was time-dependently decreased without the addition of resveratrol (control) while L-tyrosine consumption was significantly suppressed with 100 μM resveratrol. Almost all L-tyrosine oxidation was diminished with the addition of resveratrol for 60 min. Furthermore, the effect of resveratrol on L-tyrosine was measured with consecutive UV-vis spectra assay (Figure 64). The formation of dopachrome and dopaquinone was corresponding to the evolution of the peak at 475 and 350 nm, respectively, during the tyrosinase-catalyzed oxidation of L-tyrosine. The incubation of L-tyrosine and tyrosinase allowed to elevate the peak at 475 and 375 nm, and decreased the peak at 280 nm (Figure 64A). Interestingly, tyrosinase-assayed resveratrol showed similar spectra to the case of L-tyrosine and resveratrol (Figure 64B & C). In Figure 64B, 100 μM resveratrol (280 nm) was quickly

oxidized and corresponding quinone compounds (320 nm) were formed in first 10 min; however, the spectra also showed further oxidation of oxidized products of resveratrol (460 nm region). Figure 64C indicated that even though L-tyrosine was contained in the mixture, it seemed that dopachrome corresponding to L-tyrosine oxidation was not formed. This phenomenon was further supported by creating Figure 64D, which represented that simulated spectra which created from the addition of spectra A and B. In simulated graph, the dopachrome formation was about 0.25 in absorbance unit; however, the actual observed absorbance in Figure 64C was about 0.125. This suggested that most of dopachrome formation was suppressed by the addition of resveratrol as well as the result of HPLC analysis.

Effects of Resveratrol on L-DOPA Oxidation

To find the inhibitory mechanism of resveratrol on tyrosinase activity, the effect of resveratrol on the tyrosinase-catalyzed L-DOPA oxidation was examined. L-DOPA was used as a substrate in order to determine the effect of resveratrol on diphenolase activities of tyrosinase. Tyrosinase activity against L-DOPA was also measured with three different methods described above. With UV-vis spectra at 475 nm, resveratrol did not show significant inhibition on L-DOPA oxidation but rather enhanced as well as in the result observed with L-tyrosine with 30 min of reaction period (Figure 65A). In Figure 65A, resveratrol was oxidized and newly oxidized compound(s) was observed at 475 nm (curve 3), and the mixture of L-DOPA and resveratrol significantly enhanced the absorbance at 475 nm (curve 1 and 2). The similar results were obtained with the oxygen consumption assay (Figure 65B). In the case of tyrosinase-catalyzed "resveratrol" oxidation, the induction phase was observed in both UV-vis spectra and oxygen consumption assays; however, this lag phase was eliminated with the addition of L-DOPA due to the effect of a cofactor. Subsequently, the L-DOPA consumption was measured with HPLC assay. The rate of oxidation of L-DOPA became slower when resveratrol was added, but at the end of the reaction, most of the L-DOPA was consumed in both cases (data not shown). It should be pointed out that resveratrol was not oxidized before L-DOPA oxidation while resveratrol was oxidized before the oxidation of L-tyrosine. Thus, resveratrol acted as a monophenol substrate and resveratrol itself did not inhibit tyrosinase, but the oxidized product(s) potentially inhibited tyrosinase activities.

Effect of Preincubation on Inhibitory Activity of Resveratrol

Based on the results of the effect of resveratrol on L-tyrosine or L-DOPA oxidation, oxidized product(s) of resveratrol may be the key of inhibitory activity against tyrosinase. Hence, the effect of resveratrol after its oxidation was examined; preincubational experiments were performed for this purpose. First, 100 μM resveratrol was oxidized with tyrosinase for 30 min (preincubational process), and then either 100 μM L-tyrosine or L-DOPA was added to the mixture to measure tyrosinase activity. Tyrosinase activity on L-tyrosinase oxidation was examined first. As expected, L-tyrosine oxidation was not observed in both UV-vis and oxygen consumption assays (Figure 66). In Figure 66A, dopachrome was formed with DMSO while it was not with resveratrol,

and the activity of tyrosinase on L-tyrosinase oxidation was nearly lethal. A similar result was obtained from the oxygen consumption assay (Figure 66B). Secondly, the preincubational effect was tested on tyrosinase-catalyzed L-DOPA oxidation. While without preincubation, resveratrol did not inhibit L-DOPA oxidation, with preincubation, resveratrol strongly suppressed L-DOPA oxidation (Figure 67). Dopachrome formation in 30 min was strongly suppressed (Figure 67A) as well as the oxygen consumption (Figure 67B). Almost 90-100% of L-DOPA oxidation was inhibited with this preincubational experiment. These experiment results were further supported with HPLC analysis (Figure 68). In Figure 68-1, L-DOPA (peak ***a***; t_R = 6.2 min) was quickly oxidized by tyrosinase (up to 95% of L-DOPA) and dopachrome (peak ***b***; t_R = 4.8 min) was newly formed. However, after the 30 min of preincubation, only 10% of L-DOPA was oxidized for 30 min, and a small peak of dopachrome was observed (Figure 68-2). Thus, it is logical to conclude that resveratrol undergoes enzymatic activation prior to the inhibition of tyrosinase (k_{cat} type inhibition).

Recovery from the Preincubational Effects

Further detail of the mechanism of inhibition of resveratrol was examined by using L-cysteine. The inhibitory effect on tyrosinase-catalyzed L-DOPA oxidation was enhanced with 30 min of preincubation; however, the effect was reduced with the addition of 200 μM L-cysteine (Figure 69). About 20% of inhibition was reduced by introducing 200 μM L-cysteine (Curve 1 and 2 in Figure 69). In the presence of resveratrol, L-DOPA oxidation was not observed without L-cysteine (Curve 1 in Figure 69). This suggested that L-cysteine disrupted the inhibitory effect of resveratrol on tyrosinase activity. During the oxidation of resveratrol, resveratrol is converted to *o*-quinone. L-cysteine undergoes nucleophilic addition to react with the quinone, which leads to the removal of the metabolite(s) of resveratrol. Thus, this reduction of inhibitory effect with the addition of L-cysteine explains that inhibitory action of resveratrol is due to the formation of reactive electrophile(s) such as *o*-quinone.

Resveratrol as a Melanogenesis Inhibitor on B16-F10 Melanoma Cells

From the results of cell-free investigations, resveratrol showed the potent inhibitory effect on tyrosinase activity. Thus, the investigations were extended to cellular experiments. The initial goal was to test whether resveratrol inhibits melanogenesis in cultured melanocytes without affecting cell growth. Hence, their cell viability was examined first. In this regard, cell viability was determined on the third day for melanocytes using both trypan blue dye exclusion and 3-(4,5-dimethylthiazole-2-yl)-2,5-diphenyltetrazolium bromide (MTT) colorimetric assays. The same result was usually observed by both assays, but the concentration leading to 50% viable cells lost (IC_{50}) was established by trypan blue assay for steady comparison purpose. The specificity of melanogenesis inhibition was assessed by dividing the melanin content by the number of cells determined by trypan blue exclusion. The appropriated concentrations of the test chemicals were selected by microscopic observation of the preliminary cell viability assay.

Cytotoxic and antimelanogenic effects of resveratrol were identified. The highest examined concentration of resveratrol was 200 μM. Resveratrol slightly suppressed cell viability in a dose-dependent manner (Figure 70A), and IC_{50} was not observed up to 200 μM. About only 10% of cell viability was suppressed with 200 μM resveratrol. The cell viability above 200 μM was significantly different (P <0.01) from the control. Total melanin production above 25 μM was significantly suppressed (P <0.01) in a concentration-dependent manner (Figure 70B). It came out that the total melanin production was reduced without affecting the cell growth; hence, cellular melanin production is dose-dependently suppressed. The significant difference from the control (P< 0.01) was observed when 200 μM resveratrol was applied (Figure 70C). Furthermore, other stilbenoids, namely, *trans*-pinosylvin (**2**), *cis*-pinosylvin (**3**), dihydropinosylvin (**4**) were tested for the comparisons (data not shown). None of these compounds suppressed cellular viability in a concentration-dependent manner. Only *trans*-pinosylvin showed the significant difference is observed at 400 μM. Cellular melanin content was not suppressed but rather increased with the addition of *trans*-, *cis*- or dihydropinosylvin. Cellular morphological changes of resveratrol-treated melanoma cells were also microscopically observed (data not shown). The cellular morphology of control (DMSO treated) cells was almost exactly the same as that of resveratrol-treated cells. Thus, resveratrol is a unique potentiated melanogenesis inhibitor with less/no cytotoxic effects.

3.1.3 DISCUSSION

Tyrosinase inhibitor can be used in variety of ways including cosmetic products and food antibrowning reagents. Because of this purpose, several antimelanogenic reagents have been developed and discovered nowadays. However, only a few of the inhibitors have been able to introduce and use because of the problems in cytotoxicity (affecting the cell growth), selectivity, solubility, and stability. Resveratrol is a naturally occurring polyphenol, and is commonly taken in foods or beverages. Hence, it is no doubt that resveratrol is more applicable as a melanogenesis drug than any other synthetic chemicals (if the biological effects of resveratrol are inappropriate). Based on the data obtained, it appeared that resveratrol inhibits tyrosinase activities through the mechanism of k_{cat} type inhibition. According to Robert Rando, k_{cat} inhibitors can be constructed to possess latent reactive grouping that is selectively activated by the target enzyme at its active site (*17*). Usually, highly reactive product(s) are synthesized, and once generated, they react with the enzyme, which leads to its irreversible inhibition. Thus, activation of resveratrol thorough the oxidation by tyrosinase is the key process of the mode of action. Interestingly, resveratrol-4-*O*-methyl ether showed less inhibitory activity against mushroom tyrosinase and B16 melanoma cells (*13*), which is confirmed by our conclusions. This helps understanding that 4'-hydroxyl group is essential for the inhibition. Furthermore, based on the previous studies, resorcinolic moiety has high inhibitory potency to tyrosinase while 4-hydroxyl group is the subject of the oxidation,

for instance, arbutin (**5**) or methyl *p*-coumarate (**6**) (*20-24*). As Espin studied using polyphenol oxidase (PPO) (*19*), resveratrol is converted to *ortho*-diol and further oxidized to quinone-derivatives (Scheme 5). As they commented in their previous study, oxidation product(s) of resveratrol was unstable, and it could not reach to the steady state. Their result was confirmed by our HPLC, UV-vis and oxygen consumption assays (Figure 61, 64B, and 65B line3). The instability of oxidation product(s) also suggested the mechanism of suicide inhibition by resveratrol. Comparing the data from L-tyrosine and L-DOPA, resveratrol is relatively easy to be oxidized; the order of the rate of oxidation is the following: L-DOPA > resveratrol > L-tyrosine. Hence, L-DOPA oxidation was not inhibited by resveratrol without preincubation. It is not clear if the suicide inactivation of tyrosinase is due to one of either 1) the formation of reactive oxygen species that attack on the active site of enzyme (*25*), 2) "cresolase-type mechanism of tyrosinase" to inactivate active copper of tyrosinase to be a copper(0) (*26*), or 3) formation of oxidized product(s) of resveratrol such as quinone (*27*). However, in the case of resveratrol, it seems the last case (case 3) is true. Figure 69 represented that the addition of L-cysteine prevents the tyrosinase from its inactivation. L-cysteine reacts with quinone (or maybe other metabolites) of resveratrol and diminished the inactivation. Furthermore, Kubo *et al*. have suggested the mechanism of melanogenesis inhibition on B16 mouse melanoma cells due to methyl *p*-coumarate (*21*), a potent melanin formation inhibitor, is caused by the metabolite(s) of the compound but not by the compound itself. Based on our results and the structural similarities, it is understandable that resveratrol acts as a suicide inhibitor.

Antioxidants have variety of activities, including direct quenching of reactive oxygen species (ROS), inhibition of enzymes involved in the production of ROS, chelation of low-valent metal ions such as Fe^{2+} or Cu^{2+}, and regeneration of membrane-bound antioxidants such as α-tocopherol (*28*). Resveratrol is a known antioxidant and extensive investigations have been done. Including radical scavenging activities (*29*), in several reports, resveratrol induces cardioprotective effect, anti-aging, apoptotic effect and anticarcinogenesis (*3, 6, 11, 30*). Antimelanogenic effect could be added to one of the biological function of resveratrol and this natural polyphenol could be developed as a multifunctional drug.

Safety is the primary concern for any purposes including cosmetic products or chemotherapeutic reagents. Resveratrol is oxidized by tyrosinase and the metabolite(s) would inhibit tyrosinase activity and reduce the cellular melanin content; however, the effects/functions of these metabolites to other biological systems are still unclear. Resveratrol is found in many natural sources, and hence, it may be the alternate choice to non-natural chemical reagents. Despite clarification of the mechanism of anti-tyrosinase effect, the detail of inhibitory mechanism of cellular melanogenesis by resveratrol is still under investigations.

DISCLOSURE

This work has been accepted to publish in *Bioorganic & Medicinal Chemistry.*

3.1.4 FIGURES & TABLES

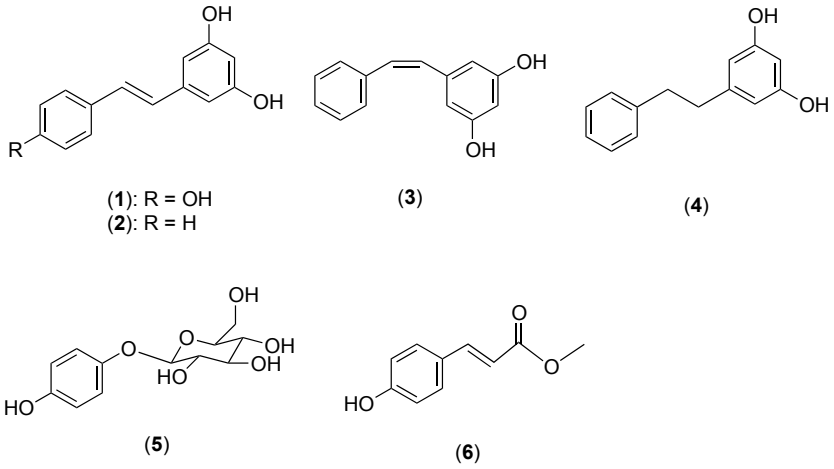

Figure 60. Chemical structures of resveratrol and the related compounds.

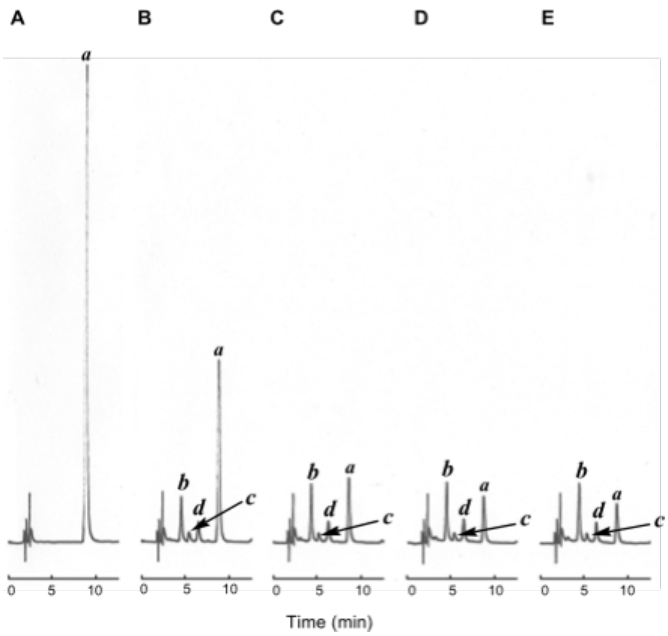

Figure 61. HPLC analysis of resveratrol (100 μM) oxidation by tyrosinase. Sampling time was chosen at 0 min (**A**), 15 min (**B**), 30 min (**C**), 45 min (**D**) and 60 min (**E**). HPLC operating conditions were as follows; Deverosil ODS-UG-5 (Nomura Chemical, CO., LTD., Seto-Shi, Aichi, Japan). Solvent; 25% MeCN/H_2O containing 0.2% TFA, Flow rate 1.0 mL/min, detection; UV at 280 nm, 0.04 range, injected amount; 25 μL. Peak ***a*** represents resveratrol. Peak ***b***, ***c***, and ***d*** indicate oxidation products of resveratrol.

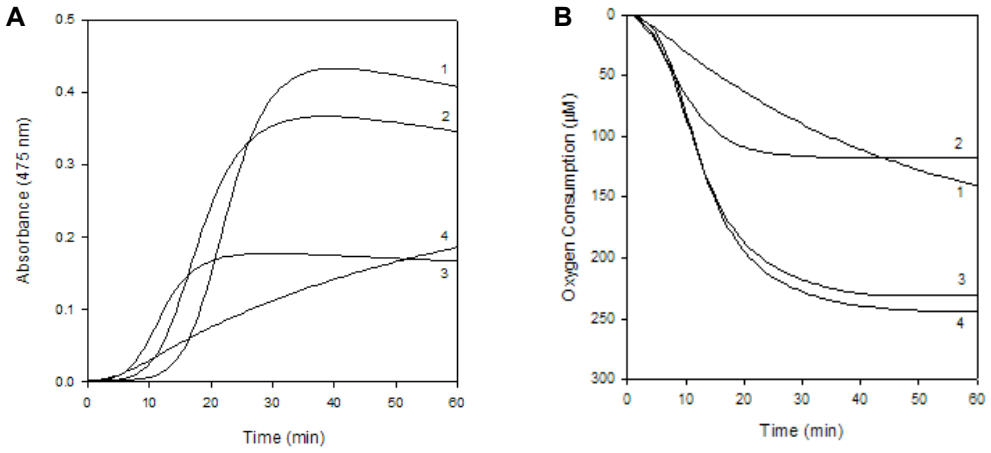

Figure 62. (**A**) UV-vis spectra at 475 nm obtained in oxidation of 100 μM L-tyrosine by mushroom tyrosinase in presence of resveratrol for 60 min. Concentrations of resveratrol were selected at 1000 μM (1), 500 μM (2), and 100 μM (3). Line 4 represents oxidation of L-tyrosine by mushroom tyrosinase in absence of resveratrol. (**B**) Oxygen consumption of oxidation of L-tyrosine (100 μM) by mushroom tyrosinase in presence of resveratrol for 60 min. The concentrations of resveratrol were 100 μM (2), 500 μM (3), and 1000 μM (4). Line 1 represents the oxygen consumption of oxidation of 100 μM L-tyrosine by mushroom tyrosinase in absence of resveratrol.

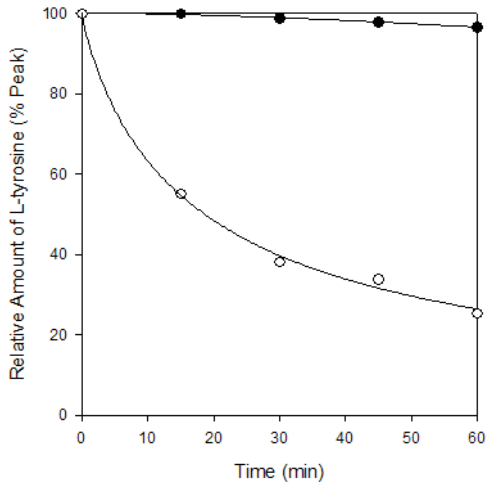

Figure 63. HPLC analysis of L-tyrosine (100 μM) oxidation by tyrosinase in absence (○) or presence (●) of 100 μM resveratrol. Sampling time was chosen at 0 min, 15 min, 30 min, 45 min, and 60 min. HPLC operating conditions were as follows; Develosil ODS-UG-5 (Nomura Chemical, CO., LTD., Seto-Shi, Aichi, Japan). Solvent; 7% MeCN/H_2O containing 0.2% TFA, Flow rate 1.0 mL/ min, detection; UV at 280 nm, 0.02 range, injected amount; 25 μL. SigmaPlot (Systat Software, Inc.) was used for curve fitting.

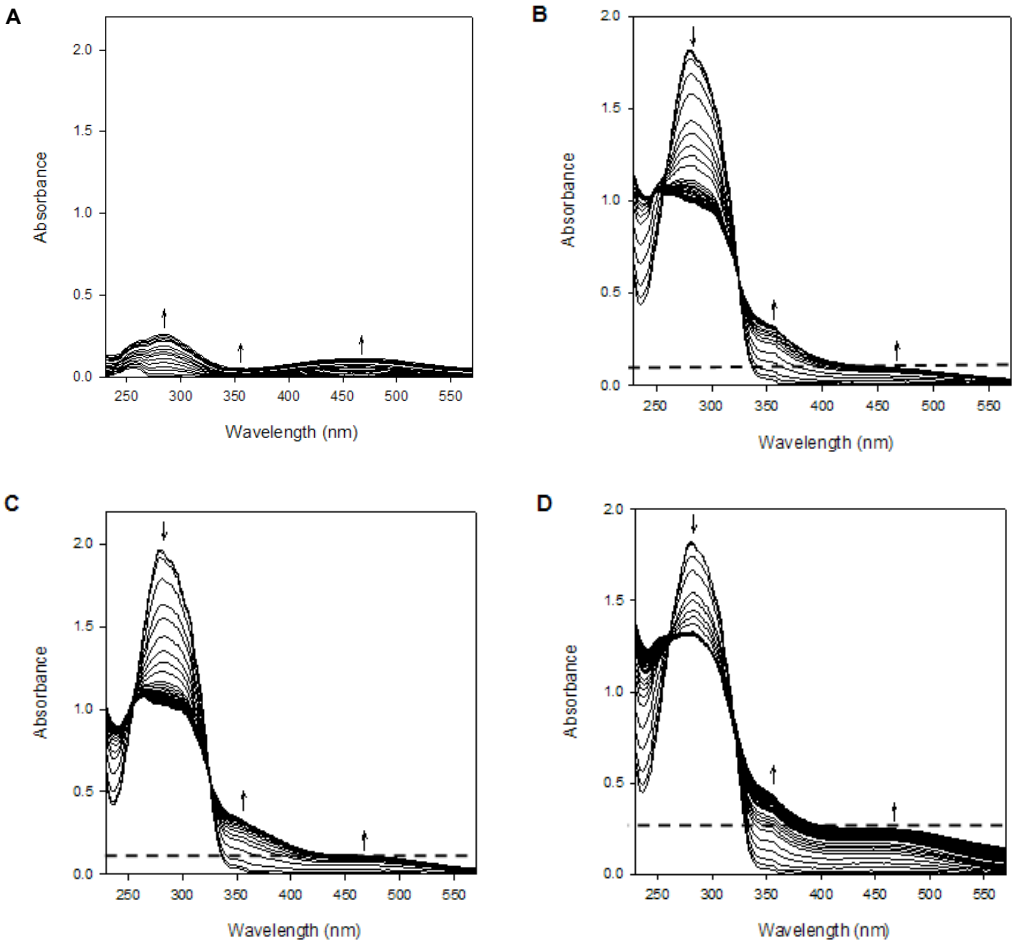

Figure 64. Consecutive UV-Vis spectra obtained in the oxidation of 100 μM L-tyrosine by mushroom tyrosinase in absence (**A**) or presence (**C**) of 100 μM resveratrol for 60min. **B** represents the oxidation of 100 μM resveratrol by mushroom tyrosinase. **D** indicates that simulated spectrum that is obtained from the sum of spectrum of L-tyrosine oxidation and of resveratrol oxidation (i.e., **A** + **B**). Scan speed was at 2 min intervals for 30 sec. the arrows (↑) designate the evolution of the peak.

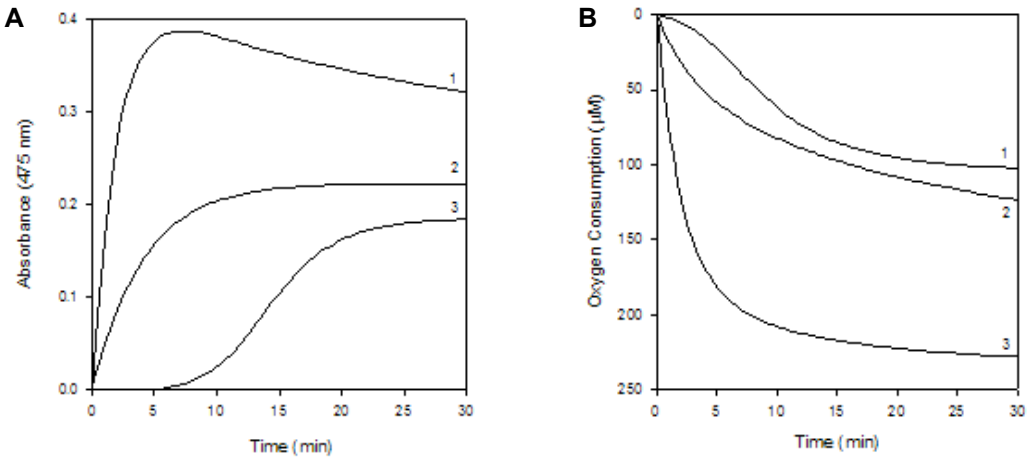

Figure 65. (**A**) UV-bis spectra at 475 nm obtained in oxidation of 100 μM L-DOPA by mushroom tyrosinase in presence (1) or absence (2) of resveratrol for 30 min. Concentrations of resveratrol were selected at 100 μM. Line 3 represents oxidation of resveratrol by mushroom tyrosinase without L-DOPA. (**B**) Oxygen consumption of oxidation of L-DOPA (100 μM) by mushroom tyrosinase in absence (2) or presence (3) of resveratrol for 30 min. The concentrations of resveratrol were 100 μM. Line 1 represents the oxygen consumption of oxidation of 100 μM resveratrol by mushroom tyrosinase without L-DOPA.

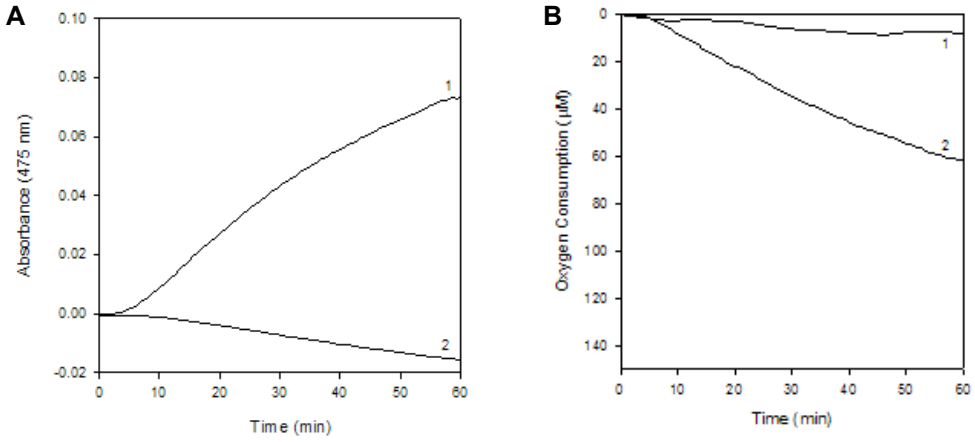

Figure 66. (**A**) UV-bis spectra at 475 nm obtained in oxidation of 100 µM L-tyrosine by mushroom tyrosinase in absence (1) or presence (2) of resveratrol for 60 min after 30 min of preincubation. Concentrations of resveratrol were selected at 100 µM. (**B**) Oxygen consumption of 100 µM L-tyrosine oxidation by mushroom tyrosinase in presence (1) or absence (2) of resveratrol for 60 min after 30 min of preincubation. Concentrations of resveratrol were selected at 100 µM.

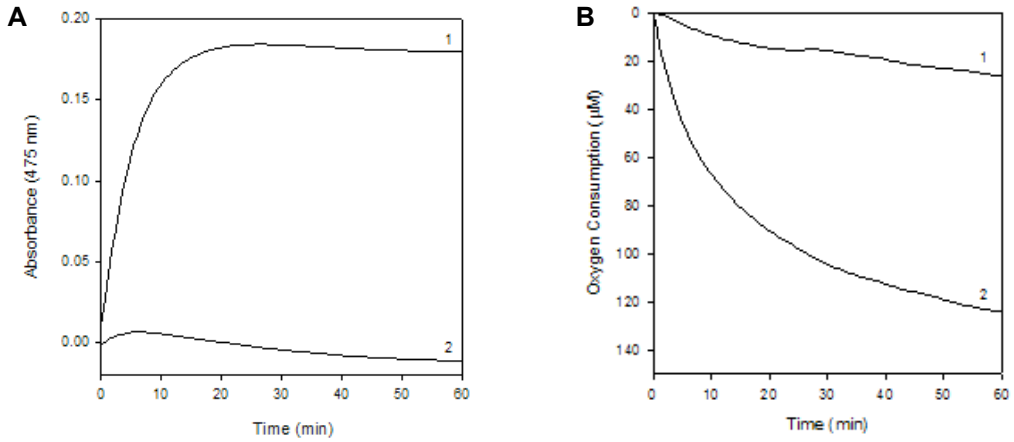

Figure 67. (**A**) UV-bis spectra at 475 nm obtained in oxidation of 100 µM L-DOPA by mushroom tyrosinase in absence (1) or presence (2) of resveratrol for 60 min after 30 min of preincubation. Concentrations of resveratrol were selected at 100 µM. (**B**) Oxygen consumption of 100 µM L-DOPA oxidation by mushroom tyrosinase in presence (1) or absence (2) of resveratrol for 60 min after 30 min of preincubation. Concentrations of resveratrol were selected at 100 µM.

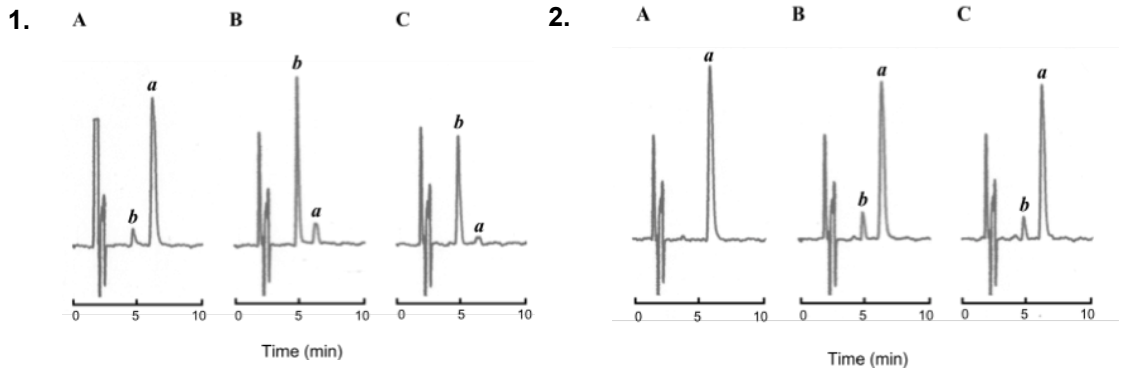

Figure 68. HPLC analysis of L-DOPA (100 μM) oxidation by mushroom tyrosinase in absence (1) or presence (2) of 100 μM resveratrol after 30 min of preincubation. Sampling time was chosen at 0 min (**A**), 15 min (**B**), 30 min (**C**). HPLC operating conditions were as follows; Develosil ODS-UG-5 (Nomura Chemical, CO., LTD., Seto-Shi, Aichi, Japan). Solvent; 7% MeCN/H2O containing 0.2% TFA, Flow rate 1.0 mL/min, detection; UV at 280 nm, 0.02 range, injected amount; 25 mL. Peak *a* and *b* represent L-DOPA and dopachrome, respectively.

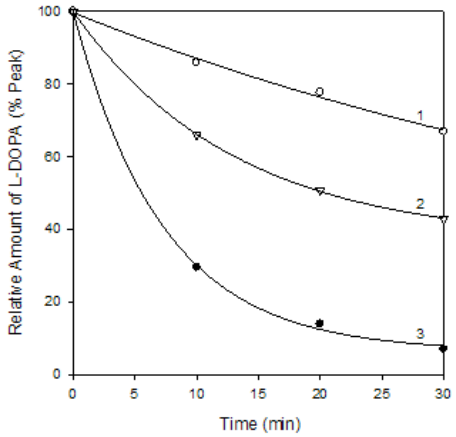

Figure 69. HPLC analysis of L-DOPA (100 μM) oxidation by mushroom tyrosinase in presence of 100 μM resveratrol with or without L-cysteine after 30 min of preincubation. Line 1 and 2 represent that the tyrosinase-catalyzed oxidation of L-DOPA in presence of both 100 μM resveratrol and 0 μM (1) or 200 μM (2) L-cysteine. Line 3 indicates L-DOPA oxidation by tyrosinase in absence of both resveratrol and L-cysteine. Sampling time was chosen at 0 min, 10 min, 20 min, and 30 min. HPLC operating conditions were as follows; Develosil ODS-UG-5 (Nomura Chemical, CO., LTD., Seto-Shi, Aichi, Japan). Solvent; 10% MeCN/H2O containing 0.2% TFA, Flow rate 1.0 mL/min, detection; UV at 280 nm, 0.02 range, injected amount; 25 mL. SigmaPlot (Systat Software, Inc.) was used for curve fitting.

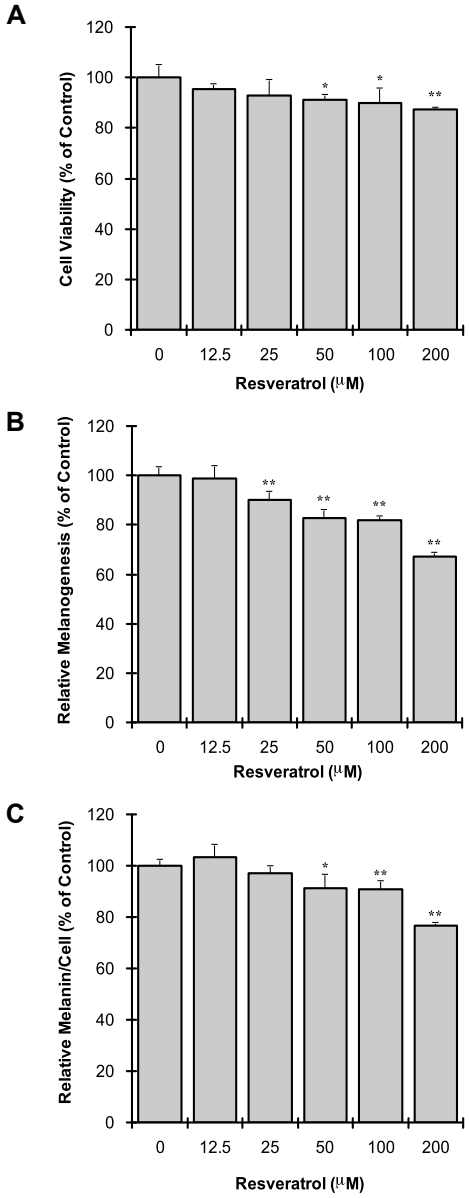

Figure 70. (**A**) Viabilities of B16-F10 melanoma cells following treatment with resveratrol for 72hr; data are expressed as percentage of the number of viable cells observed with the control, and each column represents the mean ± S.D. of at least 4 determinations. (**B**) Total melanin content in B16 melanoma cells following treatment with resveratrol for 72hr; data are expressed as percentage of melanin content per well observed with the control, and each column represents the mean ± S.D. of 4 determinations. (**C**) Cellular melanin content in B16 melanoma cells following treatment with resveratrol for 72hr measured as percentage of melanin content per cell observed with the control, and each column represents the mean ± S.D. of 4 determinations. The statistical significance of differences was evaluated using Student's or Welch's *t*-test. Significantly different from the control value: **p*<0.05, ***p*<0.01

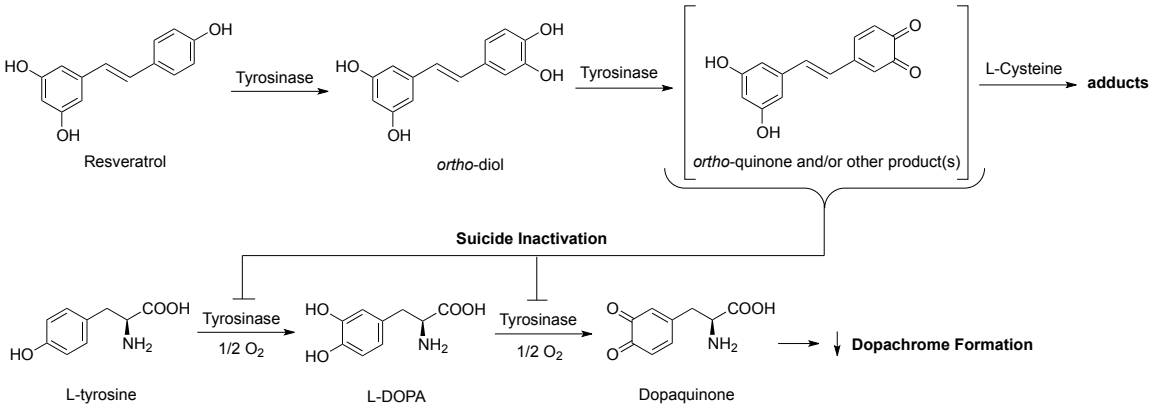

Scheme 5. Potentiated mechanism of k_{cat} type inhibition by resveratrol on tyrosinase activity.

3.2 Luteolin as a Redox Cycler Enhancing Melanin Formation

3.2.1 INTRODUCTION

Flavones are one of the chemical classes which are abundant in nature. Wide variety of beneficial effects of flavones has been reported including antioxidative, anti-cancerous, anti-aging, anti-inflammatory effects (*31-33*). In our continuing search for tyrosinase inhibitors from plants, quercetin (**1**) was isolated as the principal inhibitor from the dried flower of *Heterotheca inuloides* (Compositae), locally known as "arnica" in Mexico (*34*). Quercetin was found to be a competitive inhibitor for tyrosinase-catalyzed L-DOPA oxidation with the short-term kinetic assay (*35, 36*). The mechanism of inhibitory action was reported as a chelation of binuclear copper of tyrosinase since γ-pyrone moiety seemed to preferentially chelate copper, described by Kubo and Kinst-Hori (*37*). This chelation mechanism was described to be specific to flavones as long as the 3-hydroxyl group is free (*38*). However, further investigation showed that quercetin was actually oxidized to the corresponding *o*-quinone and subsequent isomerization to *p*-quinone methide type intermediate, followed by the addition of water on C-2 yielding a relatively stable intermediate, 2-(3,4-dihydroxybenzoyl)-2,4,6-trihydroxy-3(2*H*)-benzofuranone (Scheme 6) (*22*). This is because catechol moiety in the B-ring tends to be recognized by tyrosinase and subject to be oxidized. On the other hand, luteolin (5,7,3', 4'-tetrahydroxyflavone) (**2**), a quercetin analogue, was previously reported to inhibit tyrosinase-catalyzed oxidation of L-DOPA noncompetitively using the commercial mushroom tyrosinase (*36*). This flavone possesses the resorcinol moiety in the A-ring, and catechol moiety in the B-ring, and hence, could be oxidized similarly as reported for quercetin. Aim of current study is the identification of the effect of tyrosinase on luteolin, and the mechanism of the effect. Hence, the effect of luteolin and related analogues on the tyrosinase activity was reexamined using the purified tyrosinase (*39*).

3.2.2 RESULTS

Oxidation of Luteolin by Purified Mushroom Tyrosinase

Inhibitory effects of luteolin (**2**; see Figure 71 for structure) on the oxidation of L-3,4-dihydroxyphenylalanine (L-DOPA) catalyzed by mushroom tyrosinase (EC 1.14.18.1) were previously reported by several researchers (*38, 40, 41*). The enzyme activity was monitored by measuring dopachrome formation at 475 nm and luteolin was reported to inhibit this enzymatic oxidation noncompetitively. Dopachrome is a relatively stable intermediate but is gradually oxidized further, and hence, the spectrophotometric assay measures only the very initial rate of dopachrome formation to avoid involvement of the secondary reaction (*42*). Thus, the inhibition kinetic data are usually obtained within 1 min. Because of this restriction, notably, the long-term (> 5min) effects of luteolin on tyrosinase activities rather than short-period kinetics have not been

investigated. Hence, the enzyme activity was reexamined using the purified enzyme for 30 min. Tyrosinase is known to catalyze a reaction between two substrates, a phenolic compound and oxygen, but the discussion previously described was based on the experiment using L-DOPA as a substrate. As the need arises, L-tyrosine and *N*-acetyl-L-tyrosine were also assayed to see when the inhibitors characterized were effective on monophenolase activity. In all cases, the enzyme activity was monitored by dopachrome formation at 475 nm. The assay was carried out in air-saturated aqueous solution and, as a result, oxygen, the other substrate, was disregarded. The enzyme activity was also monitored by measuring oxygen consumption and this polarographic method was linked to consecutive spectrum and HPLC analyses as the need arose.

The effects of the purified mushroom tyrosinase on luteolin without L-DOPA were examined first. The mixture consisting of tyrosinase (1 μg/mL) and luteolin (100 μM) was incubated for 30 min. The results obtained are illustrated as line 1 in Figure 72. Luteolin consumed oxygen as soon as it was mixed with the enzyme. More specifically, oxygen was rapidly consumed within the first 5-10 minutes and then slowed down thereafter, but almost all of the available oxygen in the cuvette was consumed when 200 μM of luteolin was added (data not shown). The consecutive UV-Vis spectrum was subsequently examined for 30 min (Figure 73). The notable changes in the spectrum started in decreasing in the absorbance around at 360 nm. The peak corresponding to luteolin (100 μM) at 360 nm was decreased in a time-dependent manner. After the first 20 min of reaction, the rate of degradation of luteolin was slowed down. Apparently, luteolin was oxidized as a substrate even without a cofactor to the corresponding *o*-quinone after the abstraction of $2e^-$ and $2H^+$ from the hydroxyl groups at C-3' and C-4' (*22*). This result is consistent with the observation that one molecule of luteolin consumed 1/2 molecule of oxygen. In other words, 50 μM of oxygen molecules are required to oxidize 100 μM luteolin. Based on the result and the stoichiometric observation, the corresponding quinone of luteolin is not further oxidized up to 30 min. This postulate was further confirmed with HPLC analysis. Chromatographic analyses in the tyrosinase reaction on 100 μM luteolin with each 15 min intervals, showed the peak ***a*** (t_R = 7 min) identified as luteolin, was decreased time-dependently as soon as it was mixed with the enzyme as illustrated in Figure 74 (Top). The peak was diminished within the first 15 min and then slowed down thereafter, similar to that observed for oxygen consumption. The peak ***b*** (t_R = 6 min) that newly appeared after 15 min is likely the oxidized product, presumably the corresponding *o*-quinone. It is evident that luteolin was rather quickly oxidized as a substrate even without a cofactor in the preincubation experiment.

Effect of Luteolin on Tyrosinase-catalyzed L-DOPA Oxidation

Subsequently, the effect of luteolin on the tyrosinase-catalyzed oxidation of L-DOPA was examined. When both luteolin and L-DOPA coexist in the reaction mixture, the available oxygen in the cuvette was used for the oxidation of both luteolin and L-DOPA. In Figure 72, the oxygen consumption of the mixture of L-DOPA (100 μM) and luteolin (100 μM) was purely an additive result of the two oxygen consumptions: L-DOPA and that of luteolin (line 3 in Figure72). This implied that luteolin was oxidized by

tyrosinase when L-DOPA was coexisted. The reaction mixture consisting of tyrosinase (1 μg/mL), luteolin (100 μM) and L-DOPA (100 μM) was incubated and HPLC analysis was performed after each 15 min interval as shown in Figure 74 (Bottom). In the current experiment, the consumption of luteolin identified as the peak ***a*** (t_R = 7 min) was time-dependently decreased for 60 min. Compared to Figure 74 (Top; No L-DOPA), the luteolin oxidation was significantly suppressed. Concurrently, the corresponding oxidation product(s) identified as the peak ***b*** (t_R = 6 min) was quickly diminished after 15 min, indicating that there is a possible interaction between the oxidation product(s) and L-DOPA (or maybe metabolites of L-DOPA). This result was further confirmed with consecutive UV-Vis spectra assay. The oxidation of L-DOPA (50, 100 & 200 μM) and luteolin (100 μM) were monitored for 30 min in the presence of tyrosinase (Figure 75). The peak at 360 nm, corresponding to luteolin was not diminished for 30 min of the reaction period, which was different from the results in Figure 72 and 73. In the case of the presence of both L-DOPA and luteolin, the peaks at 320 nm and at 475 nm were noticeably elevated, corresponding to quinone and dopachrome formation, respectively. It should be noted that the elevation of the peaks at 320 nm and 475 nm was not observed in the case of luteolin only (Figure 73). This suggested that the peak evolutions at 320 nm and 475 nm were due to the oxidation of L-DOPA but not to luteolin oxidation. By comparing the Figure 75B (100 μM L-DOPA + 100 μM luteolin) and simulational consecutive UV-Vis spectra obtained from the addition of spectra of the oxidation of 100 μM luteolin (Figure 73) and that of 100 μM DOPA in the presence of mushroom tyrosinase for 30min (Figure 76), the difference was found at 360 nm. The peak at 360 nm, corresponding to luteolin was decreased in the case of simulation. This explained that the peak at 360 nm corresponding to luteolin would be diminished if luteolin was tyrosinase-assayed individually. In other words, luteolin oxidation was not observed when L-DOPA was coexisted. Furthermore, about 0.4-0.45 absorbance unit of dopachrome (475 nm) was quickly formed in “the first 8 min” (fourth spectra from the bottom) in the simulational spectra (Figure 76) while only 0.2-0.25 absorbance unit of dopachrome was formed in the case of the actual experiment (Figure 75B), indicating that the available oxygen in the cuvette was preferentially used for the oxidation of luteolin. Similar phenomenon was observed at 320 nm. In fact, there is a contradiction between the result of the consecutive UV-Vis assay and that of the oxygen consumption. More specifically, L-DOPA seemed to prevent the oxidation of luteolin (Figure 75); however, luteolin is more likely to consume oxygen in the presence of L-DOPA (Figure 72). Based on the result, tyrosinase oxidizes luteolin; however, “the consumption of luteolin” due to this oxidation is not observed, indicating that luteolin quinone should be reduced back to luteolin immediately when it formed. Luteolin quinone presumably reacts with L-DOPA or leukodopachrome for a redox reaction. Thus, consumption of luteolin was not observed in the presence of L-DOPA. Furthermore, in a short-term kinetic assay, tyrosinase activity was suppressed (because luteolin is oxidized prior to L-DOPA); however, the overall dopachrome formation was not inhibited. Thus, during the entire reaction period, luteolin did not inhibit the tyrosinase-catalyzed oxidation of L-DOPA. In addition, fisetin (**3**) behaves the same as luteolin (data not shown). None of them inhibit

the tyrosinase-catalyzed oxidation of L-DOPA and all were oxidized as substrates wherever the catechol moiety is located. It should be noted, however, that rutin, or quercetin 3-*O*-rutinoside (**4**), does not act as either an inhibitor or a substrate; this is because the bulky sugar moiety blocks the enzyme approach (*43*).

Effect of Luteolin on N-acetyl-L-tyrosine Oxidation

The effect of luteolin on tyrosinase activity was also further examined by using *N*-acetyl-L-tyrosine. *N*-acetyl-L-tyrosine was oxidized by tyrosinase to form corresponding *ortho*-diol and *ortho*-quinone; however, the intramolecular cyclization was prevented because of the presence of acetyl group linking to the amino group of the compound. The consumption of luteolin (peak ***a***; t_R = 7 min) in the presence of *N*-acetyl-L-tyrosine was not noticeably different from the consumption of luteolin in the absence of *N*-acetyl-L-tyrosine (Figure 77). In both cases, corresponding *o*-quinone (peak ***b***; t_R = 6 min) was formed. Thus, the redox effect which was observed in the case of L-DOPA was not observed. The consumption of *N*-acetyl-L-tyrosine was subsequently examined and the consumption of *N*-acetyl-L-tyrosine was not noticeably enhanced (data not shown). It should be noted that the lag phase during *N*-acetyl-L-tyrosine oxidation was diminished with the addition of luteolin; however, this is due to a cofactor effect since the catechol moiety of luteolin reduce the state of tyrosinase from met to oxy. Even though the activity of enzyme was enhanced by the cofactor effect, the overall consumption of *N*-acetyl-L-tyrosine was still the same in both cases.

L-DOPA was oxidized to dopaquinone catalyzed by tyrosinase and this enzymatically oxidized quinone undergoes an intramolecular 1,4-addition to the benzene ring, which causes its intramolecular cyclization into leukodopachrome (Figure 1 in Introduction). This intermediate is quickly oxidized to dopachrome by another molecule of dopaquinone, which is reduced back to L-DOPA (*44*). Based on the results described above and the previous findings, in the case when L-DOPA and luteolin coexist, both are oxidized. When both compounds are oxidized, the corresponding *o*-quinone seems to be reduced back to luteolin as a redox cycler, and thus, leukodopachrome itself is oxidized to dopachrome by the redox reaction (Scheme 6). Reduced back luteolin should be enzymatically oxidized again (redox cycle). As a result, the rate of oxidation of luteolin was seemingly decreased when it coexists with L-DOPA. Moreover, in the case of *N*-acetyl-L-tyrosine, because of the lack of formation of leukodopachrome, the luteolin *o*-quinone would be failed to reduce back to luteolin (Scheme 7). Thus, *o*-quinone of luteolin specifically reacts with leukodopachrome but not L-DOPA or other intermediates. All of the results explain that *o*-quinone of luteolin was reduced back to luteolin if the leukodopachrome was present in the reaction mixture.

Luteolin as a Redox Cycle Reagent

This redox capability of luteolin was further examined using rutin (**4**), which is not oxidized by tyrosinase (*43*). As described above, the hydrophilic sugar moiety may prevent the substrate binding and hence, rutin is not a substrate of tyrosinase even if it has a catechol moiety on B-ring. However, if luteolin and rutin are coexisted in the reaction

mixture, the oxidation product of luteolin by tyrosinase successfully oxidized rutin. 100 μM luteolin and 100 μM rutin were incubated with tyrosinase (1.0 μg/mL), and the consumption of rutin was monitored with HPLC method. After the addition of tyrosinase to the mixture of luteolin and rutin, the peak corresponding to rutin (peak ***a***; t_R = 8 min) was time-dependently decreased (Figure 78). In contrast to the decrease of peak ***a***, the peak(s) around t_R = 3 min was newly formed during the reaction. They are presumably oxidation product(s) of rutin. In addition to the case of rutin, the luteolin quinone was also able to oxidize esculetin or gallic acid (data not shown). As a result, the capability of luteolin as a redox cycler is relatively strong enough to oxidize several compounds, and hence, further utilization would be possible.

Effect of Luteolin on B16-F10 Melanoma Cells

Tyrosinase is a key enzyme in melanin synthetic pathway and therefore tyrosinase inhibitors are expected to inhibit melanin production. However, the inhibition of mushroom tyrosinase activity was reported not to correlate with that of cellular tyrosinase or melanin production in cultured melanocytes (*45*). In fact, some compounds show potent inhibitory effect on cellular melanogenesis after the bioactivating metabolism. For instance, *o*-phenylphenol, which is known as a depigmenting agent, has little depigmenting action while its metabolite, phenylhydroquinone is a potent depigmenting agent affecting melanocytes (*46*). This prompted us to see whether luteolin is oxidized to the corresponding *o*-quinone (Scheme 6 and 7) in melanocytes and whether this metabolite blocks melanin biosynthesis. Hence, the effect of luteolin on melanin formation in murine B16-F10 melanoma cells was examined. In this regard, cell viability was determined on the third day for melanocytes using both trypan blue dye exclusion and 3-(4,5-dimethylthiazole-2-yl)-2,5-diphenyltetrazolium bromide (MTT) colorimetric assays. The same results were usually observed by both assays, but the concentration leading to 50% viable cells lost (IC_{50}) was established by the trypan blue assay for steady and reliable comparison purposes. The appropriate concentrations to be used in the experiment were selected by microscopic observation of the preliminary cell viability assay, and the highest concentration of luteolin tested was 20 μM (Figure 79). The specificity of melanogenesis inhibition was assessed by dividing the melanin content by the number of cells determined by the trypan blue exclusion. Preliminary results of luteolin showed that melanin production was not suppressed but increased slightly as murine B16-F10 melanoma cells were cultured with luteolin. However, luteolin was noted to exhibit potent cytotoxicity in a concentration-dependent manner (Figure 79). The IC_{50} was established as up to 6 μM (1.7 μg/mL) and almost complete lethality was observed at 20 μM by trypan blue assay.

Toxic Mechanism of Luteolin on B16 Melanoma Cells

Luteolin is known to show diverse biological activities (*47*). To express the biological activities, luteolin has to enter into cells by passive diffusion across the membrane. Once inside cells, luteolin may be oxidized to the corresponding *o*-quinone. This chemically highly reactive *o*-quinone presumably binds with various cellular

materials similar to those described for quercetin (*48, 49*). To test this hypothesis, biochemical approach with vitamin C and butylated hydroxyanisole (BHA) was examined. Observed cytotoxicity of luteolin at 10 μM (approximately equivalent to IC_{50}) was suppressed in cell viability in a dose-dependent manner. The greatest reduction of cytotoxicity by luteolin (40 % in cell viability) was observed when 40 μM vitamin C was added (Figure 80A). Vitamin C could act as either a two-oxidation reductant or a single-radical scavenger; hence, the additional experiment was required by using a well-known radical scavenger, BHA. In the case of BHA, noticeable change in observed cytotoxicity with 10 μM luteolin was not observed (Figure 80B). The highest applied BHA concentration applied was 40 μM, and there was no change in cell viability in any tested-concentration of BHA. As a result of the recovery with vitamin C but not with BHA, cytotoxicity of luteolin is preferably due to the formation of *o*-quinone by intracellular two-electron oxidation (probably by tyrosinase) rather than the formation of radicals and oxidative stress.

This result was further confirmed by using a 2',7'-dichlorodihydrofluorescin diacetate (DCFH-DA) assay. Intracellular reactive oxygen species (ROS) oxidized the DCFH to a highly fluorescent compound, DCF, after esterase cleaves two acetate groups (*50*). After 1hr of incubation with luteolin and DCFH-DA, B16-F10 melanoma cells were assayed to measure intracellular ROS. After 1 hr of exposure of cells to luteolin, it did not affect the cell viability (Figure 81A). Total ROS were slightly but significantly increased in the range of 0.625-10 μM luteolin (Figure 81B). Thus, cellular ROS was increased in this range since the cellular viability did not change but total ROS formation was enhanced (Figure 81C). The highest cellular ROS (30% relative to the control) was observed when 2.5 μM luteolin was applied. Even though the cellular ROS was slightly increased with the addition of luteolin (Figure 81C), the no effect on cell viability (Figure 81A) implied that primary mechanism of cytotoxicity of luteolin is not due to the formation of intracellular oxidative stress.

3.2.3 DISCUSSION

Tyrosinase contains a strongly coupled binuclear copper active site and functions, the hydroxylation of a monophenol and the conversion of an *o*-diphenol to the corresponding *o*-quinone as illustrated in Figure 4. The hydroxylation of monophenol demands that this substrate react only with oxy-tyrosinase, giving rise to an ordered sequential mechanism, while the diphenol is free to bind to the oxy, deoxy, and met forms of the enzyme, producing a random sequential mechanism. It appears that luteolin is oxidized as soon as it is mixed with tyrosinase. Luteolin contains resorcinolic moiety (*m*-diphenol) in A-ring and catechol moiety (*o*-diphenol) in B-ring. Based on the structural similarity to quercetin, tyrosinase is more likely to recognize and bind to catechol moiety of B-ring rather than A-ring (*22, 43, 44*). Hence, the oxidation of luteolin is preferred to occur at the hydroxyl group at C-3' and C-4', indicating that luteolin is enzymatically converted to corresponding *o*-quinone (Scheme 6 and 7). The oxidation product of

luteolin seems relatively stable compared to the case of its structural analogue, quercetin. In the case of quercetin, the *o*-quinone product of quercetin is formed as a intermediate by tyrosinase-catalyzed oxidation at C-3' and C-4' catechol moiety. This structure of *o*-quinone is further modified through *p*-quinone methide type intermediate; followed by the addition of water on C-2 position yielding a relatively stable intermediate, 2-(3,4-dihydroxybenzoyl)-2,4,6-trihydroxy-3(2*H*)-benzofuranone. However, in the case of luteolin which lacks the C-3 hydroxyl group, the formation of *p*-quinone methide is prevented; hence, further oxidation of luteolin is not observed after the formation of *o*-quinone.

When both luteolin and L-DOPA coexist, tyrosinase oxidizes both luteolin and L-DOPA. Once *o*-quinone of luteolin was formed, this *o*-quinone undergoes a redox reaction with leukodopachrome (not with L-DOPA). The luteolin quinone reduced back to the original structure of luteolin and leukodopachrome was further oxidized to form dopachrome (Scheme 6). Because of this redox effect, the formation of dopachrome, at a glance, was enhanced. Thus, luteolin is not either an enzyme activator or enzyme inhibitor, but a redox cycler. Moreover, when luteolin and rutin are coexisted, luteolin oxidized initially, and then the formed *o*-quinone oxidizes rutin with a redox reaction. A redox cycler may be useful in many fields in order to oxidize the enzymatically non-oxidizable chemicals such as rutin. This redox cycling process with luteolin is a biological and presumably a non-hazardous process. Moreover, because the conversion of luteolin to quinone is an enzymatic step, this redox cycle is theoretically interminable. Hence, the redox cycle with luteolin could be developed as a prospective method in industrial fields.

The cytotoxic effects of flavones towards tumor cells have been explained in terms of many reasons. (*32, 51-54*). Quercetin (**1**), for example, the mechanism of toxicity has been extensively studied; necrotic toxicity including genotoxicity, prooxidative toxicity, and apoptosis-induced toxicity (*55, 56*). Despite of the wide variety of toxic mechanism of quercetin, the predicative mechanism(s) of cytotoxicity has not been identified yet. In fact, luteolin have been reported to exhibit similar mechanism of toxicity (*54, 57, 58*). However, at least, in the case of tyrosinase induced cell line such as B16-F10 murine melanoma cells, the intracellular oxidation of luteolin by tyrosinase (or maybe other oxidases such as peroxidase) is presumably involved based on the results obtained from cellular experiments. Metabolic activation to reactive intermediates contributes to the cytotoxic mechanism as luteolin can act as substrates for peroxidases and tyrosinase, yielding quinones. Once inside cells, luteolin is oxidized to the corresponding quinone and this chemically highly reactive quinone binds with various cellular materials. Flavones are commonly existed in many food sources. Thus, the bioavailability of these flavones is important; however, it is not clear if the orally ingested flavones are absorbed into the biological system through the intestinal tract and delivered to the places where they are needed. The colonic microfloras convert most of these ingested flavonoids into metabolites that then reach the circulation. Further biological evaluation of the flavones is needed from not only one aspect, but from a whole and dynamic perspective.

3.2.4 FIGURES & TABLES

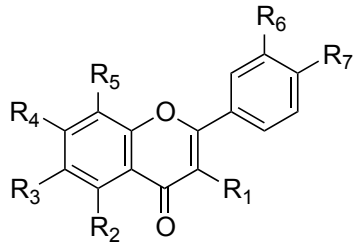

1: $R_1 = R_2 = R_4 = R_6 = R_7 = OH$, $R_3 = R_5 = H$
2: $R_2 = R_4 = R_6 = R_7 = OH$, $R_1 = R_3 = R_5 = H$
3: $R_1 = R_4 = R_6 = R_7 = OH$, $R_2 = R_3 = R_5 = H$
4: $R_1 = R_2 = R_4 = R_6 = R_7 = OH$, $R_5 = H$, $R_3 = OGluc^6\text{-}Rha$

Figure 71. Chemical structures of luteolin and other flavones.

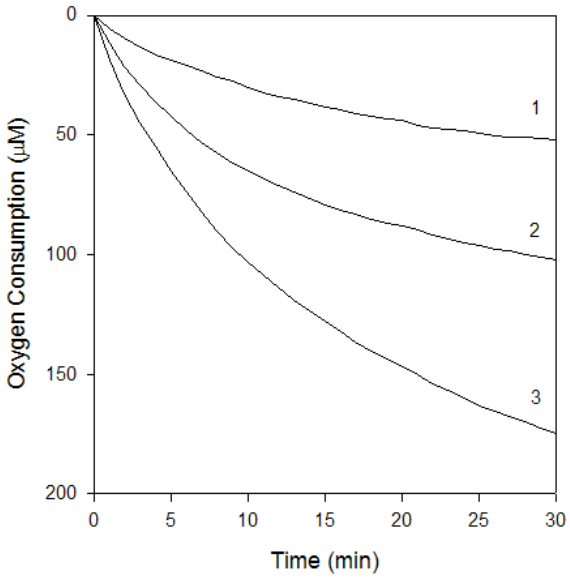

Figure 72. Oxygen consumption of tyrosinase-catalyzed L-DOPA oxidation in absence or presence of luteolin for 30 min. Line 1 represents 100 μM of luteolin in absence of L-DOPA. Line 2 indicates 100 μM of DOPA in absence of luteolin. In line 3, L-DOPA and luteolin were coexisted.

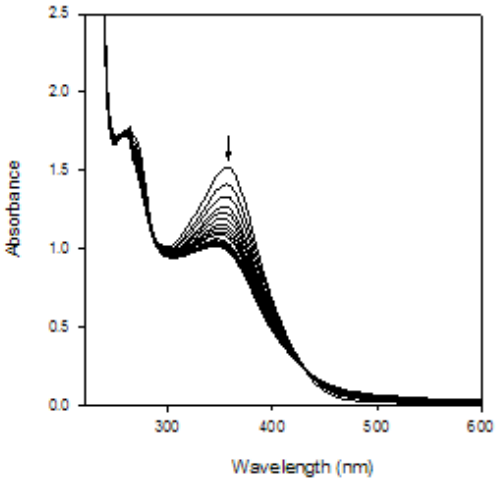

Figure 73. Consecutive UV-Vis spectra obtained in the oxidation of 100 μM of luteolin in presence of mushroom tyrosinase for 30min. Scan speed was at 2 min intervals for 30 s. the arrows (↑) designate the evolution of the peak.

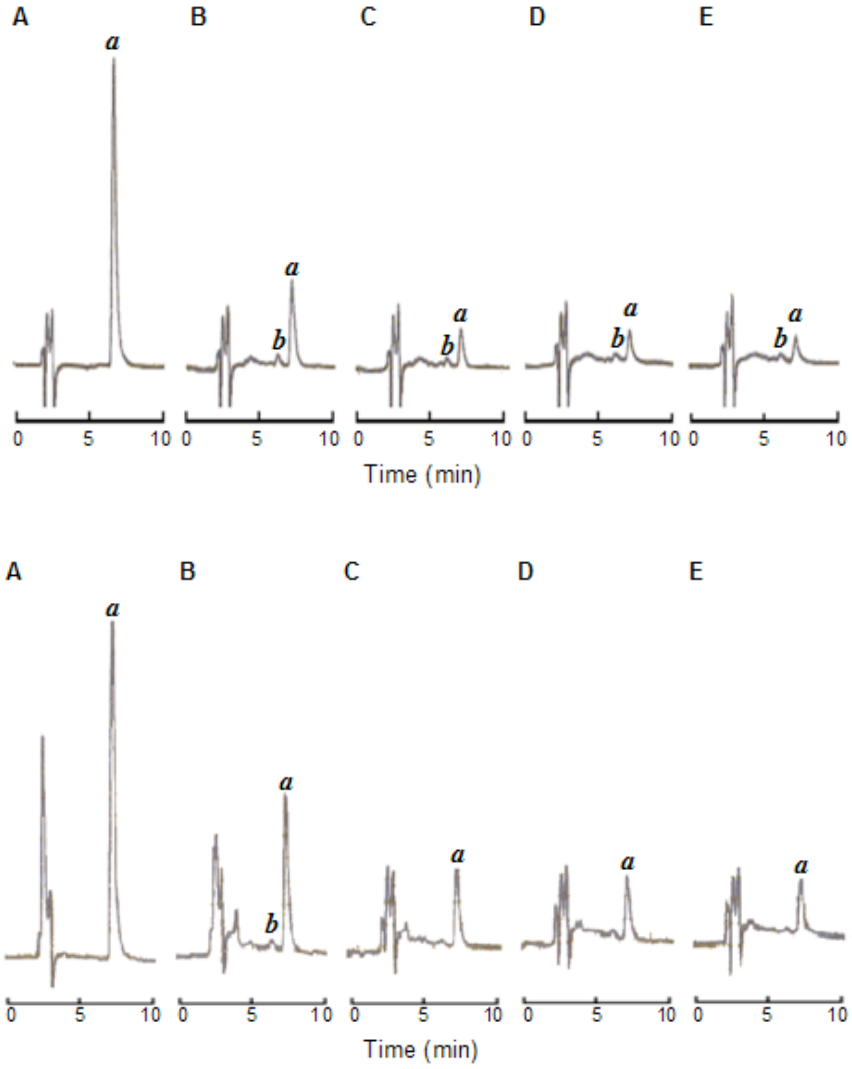

Figure 74. HPLC analysis of luteolin (100 μM) oxidation by tyrosinase in absence (**Top**) or presence (**Bottom**) of L-DOPA (100 μM). Sampling time was chosen at 0 min, 15 min, 30 min, 45 min and 60 min. HPLC operating conditions were as follows; Deverosil ODS-UG-5 (Nomura Chemical, CO., LTD., Seto-Shi, Aichi, Japan). Solvent; 40 % MeCN/H_2O containing 0.2 % TFA, Flow rate 1.0 mL/min, detection; UV at 280 nm, 0.02 range, injected amount; 25 μL. Peak ***a*** and ***b*** indicate luteolin and the oxidation product of luteolin, respectively.

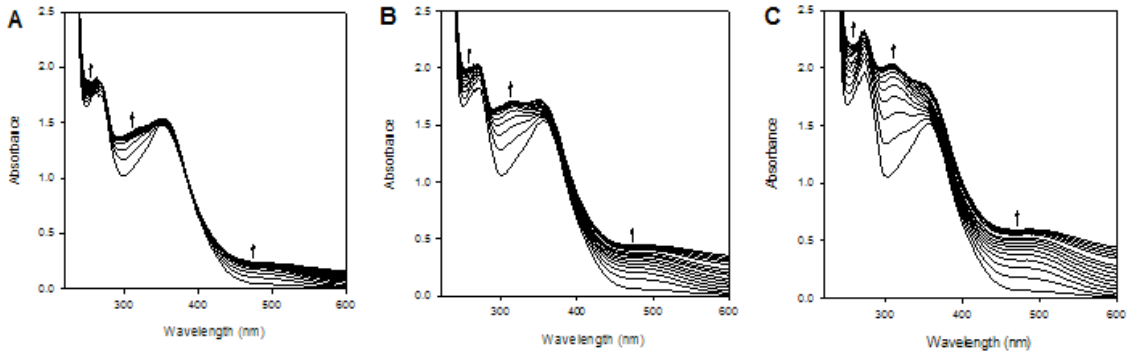

Figure 75. Consecutive UV-Vis spectra obtained in the oxidation of L-DOPA by mushroom tyrosinase in the presence of luteolin (100 μM) for 30min. Concentrations of L-DOPA were selected at 50 μM (**A**), 100 μM (**B**) and 200 μM (**C**). Scan speed was at 2 min intervals for 30 s. the arrows (↑) designate the evolution of the peak.

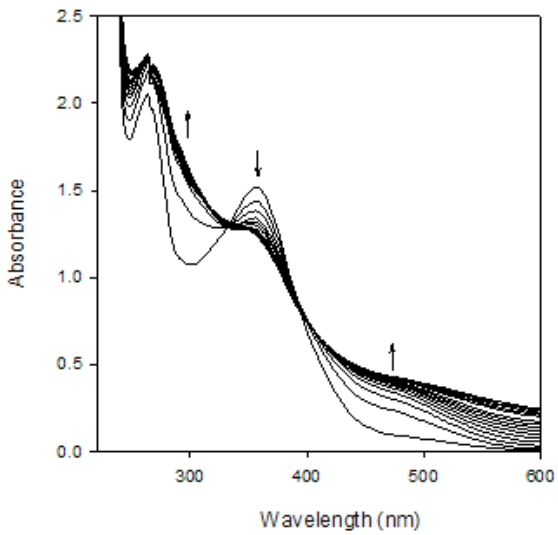

Figure 76. Simulational consecutive UV spectra obtained by the addition of spectra of the oxidation of 100 μM of luteolin and that of 100 μM of DOPA in presence of mushroom tyrosinase for 30min. Scan speed was at 2 min intervals for 30 s. the arrows indicate the change of the peak.

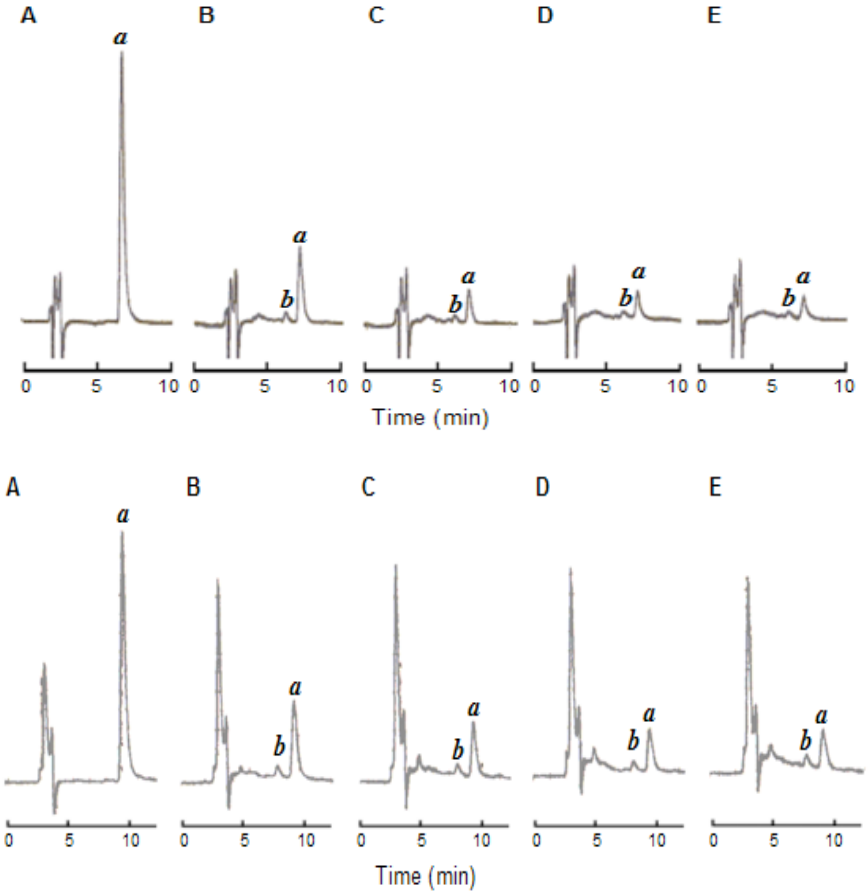

Figure 77. HPLC analysis of luteolin (100 μM) oxidation by tyrosinase in absence (**Top**) or presence (**Bottom**) of *N*-acetyl-L-tyrosine (100 μM). Sampling time was chosen at 0 min, 15 min, 30 min, 45 min and 60 min. HPLC operating conditions were as follows; Deverosil ODS-UG-5 (Nomura Chemical, CO., LTD., Seto-Shi, Aichi, Japan). Solvent; 40 % MeCN/H_2O containing 0.2 % TFA, Flow rate 1.0 mL/min, detection; UV at 280 nm, 0.02 range, injected amount; 25 μL. Peak ***a*** and ***b*** indicate luteolin and oxidation product of luteolin, respectively.

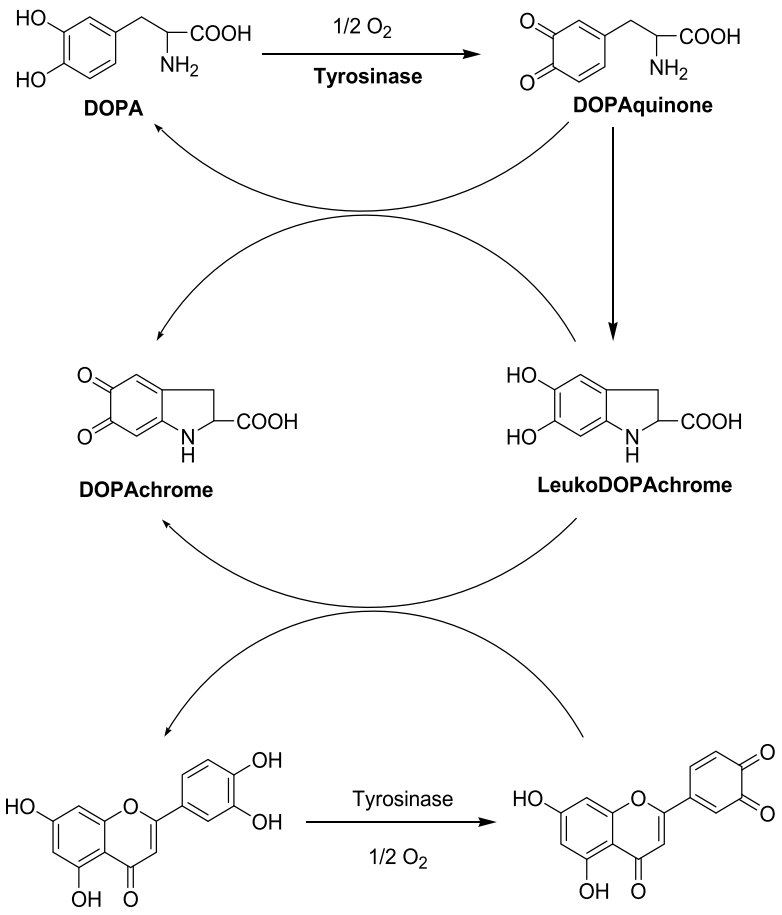

Scheme 6. Redox reaction of luteolin involved in melanin synthetic pathway.

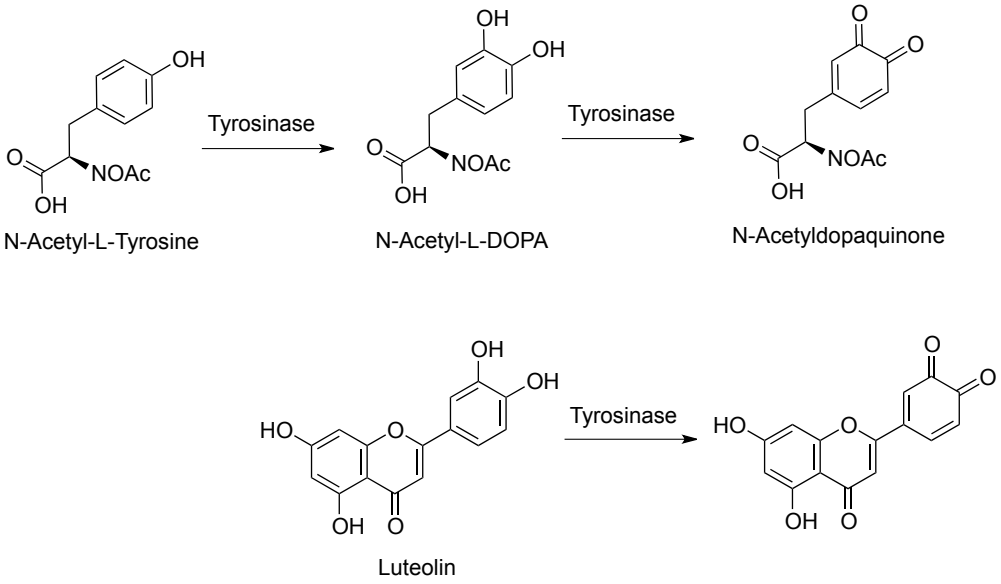

Scheme 7. No redox reaction of luteolin with *N*-acetyl-L-tyrosine oxidation.

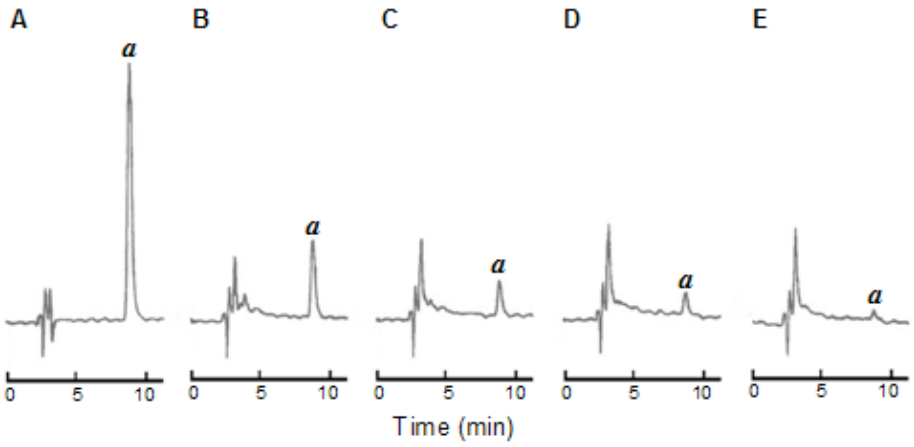

Figure 78. HPLC analysis of rutin (100 μM) oxidation by redox reaction with oxidized product(s) of luteolin (100 μM) by mushroom tyrosinase. Sampling time was chosen at 0 min (**A**), 15 min (**B**), 30 min (**C**), 45 min (**D**) and 60 min (**E**). HPLC operating conditions were as follows; Deverosil ODS-UG-5 (Nomura Chemical, CO., LTD., Seto-Shi, Aichi, Japan). Solvent; 20 % MeCN/H_2O containing 0.2 % TFA, Flow rate 1.0 mL/min, detection; UV at 280 nm, 0.08 range, injected amount; 25 μL. Peak ***a*** indicates rutin.

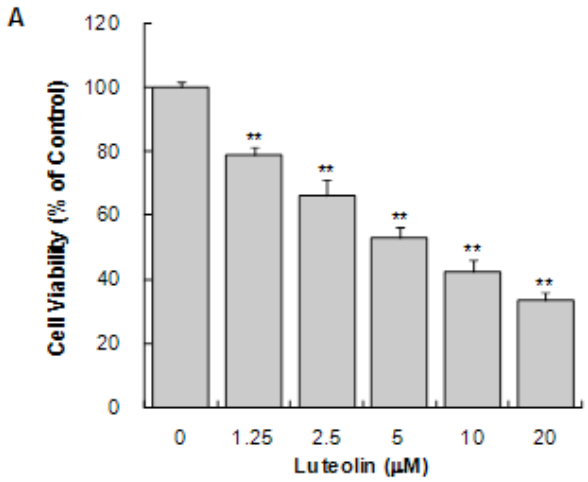

Figure 79. Viabilities of B16-F10 melanoma cells following treatment with luteolin for 72hr; data are expressed as percentage of the number of viable cells observed with the control, and each column represents the mean ± S.D. of at least 4 determinations. The statistical significance of differences was evaluated using Student's or Welch's *t*-test. Significantly different from the control value: **p*<0.05, ***p*<0.01.

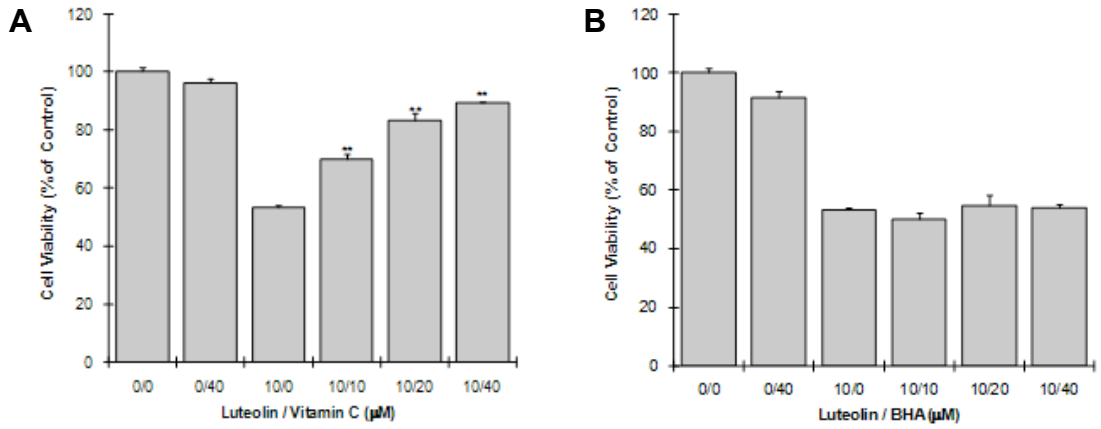

Figure 80. (**A**) Viabilities of B16 melanoma cells following treatment with 10 μM of luteolin in presence or absence of vitamin C after 72hr of incubation. The concentrations of vitamin C applied to luteolin treated cells were chosen at 0 μM (10/0), 10 μM (10/10), 20 μM (10/20) and 40 μM (10/40). Cells are also treated with 40μM of vitamin C without luteolin (0/40). Data are expressed as the percentage of the number of viable cells observed with luteolin control (0/10), and each column represents the mean ± S.D. of at least 4 determinations. (**B**) Viabilities of B16 melanoma cells following treatment with 10 μM of luteolin in presence or absence of butylated hydroxyanisole (BHA) after 72 hr of incubation. The concentrations of BHA applied to luteolin treated cells were chosen at 0 μM (10/0), 10 μM (10/10), 20 μM (10/20) and 40 μM (10/40). Cells are also treated with 40 μM of BHA without luteolin (0/10) for the comparison. Data are expressed as the percentage of the number of viable cells observed with luteolin control (10/0), and each column represents the mean ± S.D. of at least 4 determinations. The statistical significance of differences was evaluated using Student's or Welch's *t*-test. Significantly different from the control value: *$p<0.05$, **$p<0.01$.

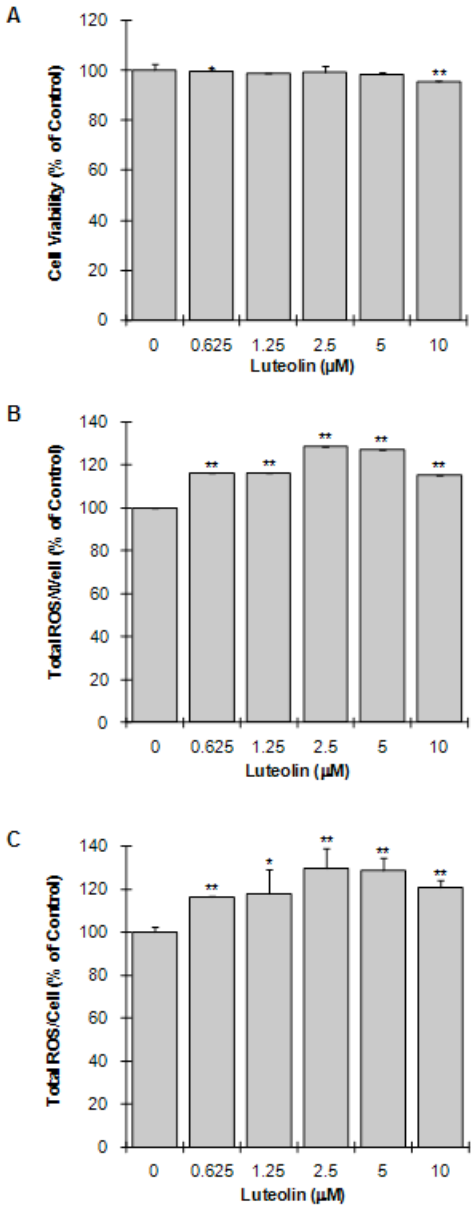

Figure 81. (**A**) Viabilities of B16-F10 melanoma cells following treatment with luteolin for 1 hr; data are expressed as percentage of the number of viable cells observed with the control, and each column represents the meanS.D. of at least 4 determinations. (**B**) Total ROS contents in B16 melanoma cells following treatment with luteolin for 1 hr; data are expressed as percentage of ROS content per well observed with the control, and each column represents the meanS.D. of 4 determinations. (**C**) Cellular ROS contents in B16 melanoma cells following treatment with luteolin for 1 hr measured as percentage of ROS contents per cell observed with the control, and each column represents the meanS.D. of 4 determinations. The statistical significance of differences was evaluated using Student's or Welch's *t*-test. Significantly different from the control value: **p*<0.05, ***p*<0.01.

3.3 Conclusions and Remarks

Polyphenols containing resorcinol moiety is found in many plant sources. In addition to the abundance in nature, polyphonlic compounds also show the several biological activities. In the cases of resveratrol and luteolin, these polyphenols are subjects to be oxidized by mushroom tyrosinase, and their metabolites exhibit the specific activities on melanin sysnthesis. Both compounds are oxidized to corresponding *o*-quinone; however, in each case, the outcome and its mechanism is different. Resveratrol are actively oxidized and the reactive electrophile(s) is generated, which negatively interacts with tyrosinase to inactivate the enzyme. Thus, k_{cat} type inactivation is applied for the mechanism of the regulation. On the other hand, luteolin *o*-quinone acts as a redox cycler instead of an inhibitor. This effect is specific to luteolin but not applied to the luteolin analogue, quercetin. Therefore, small structural change offers wide variety of biological outcomes. However, the mechanism-based activities of naturally occurring small compounds including polyphenol are still poorly understood. The identification of biological behavior of small molecule is challenging. Various scientific approaches including synthetic valuations, molecular biology, computational methods, and any other reliable methods would be possible choices. As an overall conclusion, the evaluation is needed from not only one aspect, but from a whole and dynamic perspective.

3.4 Materials and Methods

General

General procedures were the same in the previous work (*37, 59, 60*). The assays were performed in triplicate on separate occasions. Cells were viewed in 96-well plates approximately 72 hours after the chemical treatment.

Materials

Resveratrol and arbutin were purchased from Aldrich Chemical Co. (Milwaukee, WI). Quercetin, rutin, L-Tyrosine, L-cysteine, L-DOPA, butylated hydroxyanisole (BHA) and dimethyl sulfoxide (DMSO) were purchased from Sigma Chemical Co. (St. Louis, MO). Luteolin and fisetin were purchased from Indofine Chemical Company Inc (Hillsborough, NJ) *N*-acetyl-L-tyrosine was purchased from Tokyo Kasei Kogyo Co. Ltd. (Tokyo, Japan). *trans*-pinosylvin, *cis*-pinosylvin, dihydropinosylvin, methyl *p*-coumarate were synthesized and obtained from the previous studies. Fatal bovine serum (FBS) and Dulbecco's modified Eagle's medium (DMEM), and 3-(4,5-dimethylthiazole-2-yl)-2,5-diphenyltetrazolium bromide (MTT) cell proliferation assay kit were purchased from ATCC (Manassas, VA, USA).

Enzyme/Spectrophotometric Assay

General procedures were the same as the previous work (*21, 37*) but slightly modified. The mushroom tyrosinase (EC 1.14.18.1) used for the bioassay was purchased from Sigma Chemical Co. and was purified by anion-exchange chromatography using DEAE-Sepharose Fast Flow (Pharmacia, Uppsala, Sweden) as previously described (*39*). The current experiment was subjected to use the purified tyrosinase. Although mushroom tyrosinase differs somewhat from those of other sources, this fungal enzyme was used for the entire experiment because it is readily available. Throughout the experiment, L-DOPA or L-tyrosine was used as a substrate. In a spectrophotometric experiment, the enzyme activity was monitored by dopachrome formation at 475 nm with a SpectraMAX Plus Microplate spectrophotometer (Molecular Devices, Sunnyvale, CA) at 30 °C. All samples were first dissolved in DMSO and used for the experiment after dilution. The final concentration of DMSO in the test solution was always 3.3%. The assay was performed as previously reported with slight modifications. First, 100 μL of a 3 mM L-DOPA or L-tyrosine aqueous solution was mixed with 2.1 mL of filtered distilled H_2O and 600 μL of 67 mM phosphate buffer (pH 6.8) and incubated at 30 °C for 5 min. Then, 100 μL of the sample solution and 100 μL of the same phosphate buffer solution of the purified mushroom tyrosinase (1 μg/mL) were added in this order to the mixture. The assays were performed in triplicate on separate occasions. Arbutin was also tested as a comparison. Results were expressed as in absorbance unit with appropriate wavelength (nm), and all data were processed with SigmaPlot 10 software (Systat Software Inc.).

Oxygen Consumption Assay

In general, procedure was previously described (*21, 37*). Briefly, 100 μL of a 3 mM L-DOPA or L-tyrosine aqueous solution was mixed with 2.1 mL of distilled H_2O, 600 μL of 67 mM phosphate buffer (pH 6.8) and 100 μL of sample-DMSO solution was incubated at 30 °C for 5 min. Then, 100 μL of the same phosphate buffer solution of the purified mushroom tyrosinase (1 μg/mL) was added and oxygen consumption was measured with an OBH 100 oxygen electrode and an oxygraph equipped with a water-jacket chamber of YSI 5300 (all from Yellow Springs Instruments Co., Yellow Springs, OH) maintained at 30 °C for 60 min. The results were expressed as the oxygen consumption in μM, and calibration of an oxygen electrode was performed by using 4-*tert*-butylcatechol and excess tyrosinase according to the previous report (*61*). All assays were performed in triplicate on separate occasions.

HPLC analysis

Time-dependent consumption of substrates and/or formation of products were monitored with HPLC analysis. The HPLC analysis was performed on an EYELA LPG-100 (Tokyo Rikakikai Co. Ltd., Tokyo, Japan) with an EYELA UV-7000 detector (Tokyo Rikakikai Co. Ltd., Tokyo, Japan) and Develosil ODS-UG-5 column (4.6 x 150 mm, Nomura Chemical Co., Ltd., Japan). In general, the operating conditions were as follows: solvent; 7% MeCN/H_2O containing 0.2% TFA, flow rate; 1.0 mL/min, detection; UV at 280 nm, injected amount; 20 μL from above described 3 mL assay system. For analysis, samples were collected from the reaction mixtures described above at certain time points. The peak heights of each chromatographic peak were used to monitor the consumption of substrates and/or formation of products. In appropriate occasions, the results were expressed with the ratio of the height of sample peaks to that of control one, and then points were connected smoothly using the statistical software.

Cell culture

B16-F10 mouse melanoma cells (CRL-6475) were obtained from ATCC (Manassas, VA, USA), and cultured in continuous log phase growth in DMEM containing 10% FBS. Cells were seeded in 96-well plates (2000 cells/well) and incubated at 37 °C in 5% CO_2 for about 24 h before chemical treatment. Each chemical was applied in duplicate with a final content of 0.1% DMSO, and treated cells were cultured for 72 h before assays.

Melanin assay

The melanin content was determined as previously described (*62, 63*) with minor modifications. Cells were washed with PBS, harvested by trypsinization, and centrifuged for 10 min at 1500 x *g*. The cell pellets were then dissolved in 1.0 M NaOH containing 10% DMSO during 2 h incubation at 80 °C. Melanin content was measured at 475 nm using a SpectraMax Plus spectrophotometer and SoftMax Pro software (Molecular Devices, Union City, CA, USA).

Cell viability assays

Cell viability was determined by trypan blue exclusion and MTT cell proliferation assays. Both bioassays basically provided the same results but the concentration leading to 50% viable cells lost (IC_{50}) was established by trypan blue assay for steady comparison purpose. The appropriate concentrations of the test chemicals were selected by microscopic observation of the preliminary cell viability assay using a Nikon Diaphoto TMD (Nikon, Tokyo, Japan).

Trypan blue method

Cells were washed with PBS, and dispersed by trypsinization. An aliquot of the cells was mixed with a half volume of DMEM containing 10% FBS, and then mixed with trypan blue solution (final content 0.1%) at room temperature. Unstained cells (viable cells) were counted using a hemocytometer within 10 min after mixing with trypan blue solution.

MTT method

Cells were washed with PBS, and dispersed with trypsinization, and an aliquot of the cells was seeded in 96-well plates and incubated with DMEM containing 10% FBS at 37 °C in 5% CO_2 for 16 to 24 h. At the end of the period, 10 µl of MTT reagent were added to each well, which was then incubated at 37 °C in 5% CO_2 for 4 h. Then, 100 µl of detergent reagent were added to each well. The plate was kept at room temperature in the dark for 2 h, and a relative amount of MTT reduction was determined based on the absorbance at 570 nm using a SpectraMax Plus spectrophotometer and SoftMax Pro software (Molecular Devices).

DCFH-DA method

The level of intracellular reactive oxygen species (ROS) in B16-F10 melanoma cells was measured by DCFH-DA method. Intracellular ROS oxidized the DCFH to a highly fluorescent compound, DCF, after esterase cleaves two acetate groups (*50*). General procedures are listed as previously described (*64, 65*) with minor modifications. Shortly, the cultured cells were incubated with the sample and DCFH-DA reagent for 60 min at 37 °C in the dark. After the incubation, cells were removed from the plate with trypsinization in order to measure fluorescent. The amount of formed DCF was measured using fluorolog-3 with DataMax (Instruments S.A., Inc. NJ, USA) with the excitation wavelength at 485 nm and the emission wavelength at 520 nm.

Statistical analysis

The statistical significance of differences was evaluated by either Student's or Welch's *t*-test after examining the variances using F-test and $^{**}p < 0.01$ was considered to be statistically significant.

3.5 References

1. Alarcón De La Lastra, C.; Villegas, I., Resveratrol as an anti-inflammatory and anti-aging agent: Mechanisms and clinical implications. *Mol. Nutr. Food Res.* **2005,** 49, (5), 405-430.
2. Athar, M.; Back, J. H.; Kopelovich, L.; Bickers, D. R.; Kim, A. L., Multiple molecular targets of resveratrol: Anti-carcinogenic mechanisms. *Arch. Biochem. Biophys.* **2009,** 486, (2), 95-102.
3. Hung, L. M.; Chen, J. K.; Huang, S. S.; Lee, R. S.; Su, M. J., Cardioprotective effect of resveratrol, a natural antioxidant derived from grapes. *Cardiovasc. Res.* **2000,** 47, (3), 549.
4. Weber, K.; Schulz, B.; Ruhnke, M., Resveratrol and its antifungal activity against Candida species. *Mycoses* **2010,** 54, (1), 30-33.
5. Jackson, J. R.; Ryan, M. J.; Hao, Y.; Alway, S. E., Mediation of endogenous antioxidant enzymes and apoptotic signaling by resveratrol following muscle disuse in the gastrocnemius muscles of young and old rats. *AM. J. Physiol-Reg. I.* **2010,** 299, (6), R1572-R1581.
6. Lodovici, M.; Bigagli, E.; Luceri, C.; Manni…, E., Protective Effect of Resveratrol against Oxidation Stress Induced by 2-Nitropropane in Rat Liver. *Pharmacol. Pharm.* **2011**.
7. Mokni, M.; Elkahoui, S.; Limam, F.; Amri, M.; Aouani, E., Effect of Resveratrol on Antioxidant Enzyme Activities in the Brain of Healthy Rat. *Neurochem. Res.* **2007,** 32, (6), 981-987.
8. Wagner, A. E.; Boesch-Saadatmandi, C.; Breckwoldt, D.; Schrader, C.; Schmelzer, C.; Döring, F.; Hashida, K.; Hori, O.; Matsugo, S.; Rimbach, G., Ascorbic acid partly antagonizes resveratrol mediated heme oxygenase-1 but not paraoxonase-1 induction in cultured hepatocytes - role of the redox-regulated transcription factor Nrf2. *BMC Complement. Altern. Med.* **2011,** 11, (1), 1.
9. Zheng, Y.; Liu, Y.; Ge, J.; Wang, X.; Liu, L.; Bu, Z.; Liu, P., Resveratrol protects human lens epithelial cells against H_2O_2-induced oxidative stress by increasing catalase, SOD-1, and HO-1 expression. *Mol. Vis.* **2010,** 16, 1467.
10. Aziz, M. H., Resveratrol-caused apoptosis of human prostate carcinoma LNCaP cells is mediated via modulation of phosphatidylinositol 3'-kinase/Akt pathway and Bcl-2 family proteins. *Mol Cancer Ther* **2006,** 5, (5), 1335-1341.
11. Dong, Z., Molecular mechanism of the chemopreventive effect of resveratrol. *Mutat. Res-Fund. Mol. M.* **2003,** 523, 145-150.
12. Bernard, P.; Berthon, J. Y., Resveratrol: an original mechanism on tyrosinase inhibition. *Int. J. Cosmet. Sci.* **2000,** 22, (3), 219-26.
13. Kim, Y.; Yun, J.; Lee, C.; Lee, H.; Min, K.; Kim, Y., Oxyresveratrol and hydroxystilbene compounds - Inhibitory effect on tyrosinase and mechanism of action. *J. Biol. Chem.* **2002,** 277, (18), 16340-16344.
14. Newton, R. A.; Cook, A. L.; Roberts, D. W.; Leonard, J. H.; Sturm, R. A., Post-Transcriptional Regulation of Melanin Biosynthetic Enzymes by cAMP and

Resveratrol in Human Melanocytes. *J. Invest. Dermatol.* **2007,** 127, (9), 2216-2227.
15. Rando, R., Chemistry and Enzymology of k_{cat} Inhibitors. *Science* **1974,** 185, (4148), 320-324.
16. Muñoz-Muñoz, J. L.; Garcia-Molina, F.; Varon, R.; Garcia-Ruíz, P. A.; Tudela, J.; Garcia-Cánovas, F.; Rodríguez-López, J. N., Suicide inactivation of the diphenolase and monophenolase activities of tyrosinase. *IUBMB life* **2010,** 62, (7), 539-547.
17. Rando, R. R., Mechanisms of action of naturally occurring irreversible enzyme inhibitors. *Accounts Chem. Res.* **1975,** 8, (8), 281-288.
18. Chang, T. S., Two potent suicide substrates of mushroom tyrosinase: 7, 8, 4'-trihydroxyisoflavone and 5, 7, 8, 4'-tetrahydroxyisoflavone. *J. Agr. Food Chem.* **2007,** 55, (5), 2010-2015.
19. Espín, J. C.; Wichers, H. J., Study of the oxidation of resveratrol catalyzed by polyphenol oxtoase. Effect of polyphenol oxidase, laccase, and peroxidase on the antiradical capacity of resveratrol. *J. Food Biochem.* **2000,** 24, (3), 225-250.
20. Khatib, S.; Nerya, O.; Musa, R.; Tamir, S.; Peter, T.; Vaya, J., Enhanced substituted resorcinol hydrophobicity augments tyrosinase inhibition potency. *J. Med. Chem.* **2007,** 50, (11), 2676-81.
21. Kubo, I.; Nihei, K.; Tsujimoto, K., Methyl *p*-coumarate, a melanin formation inhibitor in B16 mouse melanoma cells. *Bioorg. Med. Chem.* **2004,** 12, (20), 5349-5354.
22. Kubo, I.; Nihei, K.; Shimizu, K., Oxidation products of quercetin catalyzed by mushroom tyrosinase. *Bioorg. Med. Chem.* **2004,** 12, (20), 5343-5347.
23. Nihei, K.; Kubo, I., Identification of oxidation product of arbutin in mushroom tyrosinase assay system. *Bioorg. Med. Chem. Lett.* **2003,** 13, (14), 2409-2412.
24. Shimizu, K.; Kondo, R.; Sakai, K.; Takeda, N.; Nagahata, T.; Oniki, T., Novel vitamin E derivative with 4-substituted resorcinol moiety has both antioxidant and tyrosinase inhibitory properties. *Lipids* **2001,** 36, (12), 1321-1326.
25. Seiji, M.; Sasaki, M.; Tomita, Y., Nature of tyrosinase inactivation in melanosomes. *Tohoku J. Exp. Med.* **1978,** 125, (3), 233.
26. Land, E. J.; Ramsden, C. A.; Riley, P. A., The mechanism of suicide-inactivation of tyrosinase: a substrate structure investigation. *Tohoku J. Exp. Med.* **2007,** 212, (4), 341-348.
27. Ingraham, L. L.; Corse, J.; Makower, B., Enzymatic browning of fruits. III. Kinetics of the reaction inactivation of polyphenoloxidase. *J. Am. Chem. Soc.* **1952,** 74, (10), 2623-2626.
28. Rice-Evans; Packer, C. A., In Flavonoids in Health and Disease. **1998**.
29. Shang, Y. J.; Qian, Y. P.; Liu, X. D.; Dai, F.; Shang, X. L.; Jia, W. Q.; Liu, Q.; Fang, J. G.; Zhou, B., Radical-scavenging activity and mechanism of resveratrol-oriented analogues: influence of the solvent, radical, and substitution. *J. Org. Chem.* **2009,** 74, (14), 5025-5031.

30. Robb, E. L.; Page, M. M.; Wiens, B. E.; Stuart, J. A., Molecular mechanisms of oxidative stress resistance induced by resveratrol: Specific and progressive induction of MnSOD. *Biochem. Bioph. Res Co.* **2008,** 367, (2), 406-412.
31. Cai, Y.-Z.; Sun, M.; Xing, J.; Luo, Q.; Corke, H., Structure-radical scavenging activity relationships of phenolic compounds from traditional Chinese medicinal plants. *Life Sci.* **2006,** 78, (25), 2872-88.
32. Nijveldt, R. J.; van Nood, E.; van Hoorn, D. E. C.; Boelens, P. G.; van Norren, K.; van Leeuwen, P. A. M., Flavonoids: a review of probable mechanisms of action and potential applications. *Am. J. Clin. Nutr.* **2001,** 74, (4), 418.
33. Wang, L.; Tu, Y. C.; Lian, T. W.; Hung, J. T.; Yen, J. H.; Wu, M. J., Distinctive antioxidant and antiinflammatory effects of flavonols. *J. Agr. Food Chem.* **2006,** 54, (26), 9798-9804.
34. Haraguchi, H.; Ishikawa, H.; Sanchez, Y.; Ogura, T.; Kubo, Y.; Kubo, I., Antioxidative constituents in Heterotheca inuloides. *Bioorg. Med. Chem.* **1997,** 5, (5), 865-871.
35. Chen, Q. X.; Kubo, I., Kinetics of mushroom tyrosinase inhibition by quercetin. *J. Agr. Food Chem.* **2002,** 50, (14), 4108-4112.
36. Xie, L. P.; Chen, Q. X.; Huang, H.; Wang, H. Z.; Zhang, R. Q., Inhibitory effects of some flavonoids on the activity of mushroom tyrosinase. *Biochemistry-Moscow* **2003,** 68, (4), 487-491.
37. Kubo, I.; Kinst-Hori, I., Flavonols from saffron flower: tyrosinase inhibitory activity and inhibition mechanism. *J. Agr. Food Chem.* **1999,** 47, (10), 4121-4125.
38. Kubo, I.; Kinst-Hori, I.; Chaudhuri, S. K.; Kubo, Y.; Sánchez, Y.; Ogura, T., Flavonols from Heterotheca inuloides: tyrosinase inhibitory activity and structural criteria. *Bioorg. Med. Chem.* **2000,** 8, (7), 1749-1755.
39. Espin, J. C.; Wichers, H. J., Slow-binding inhibition of mushroom (*Agaricus bisporus*) tyrosinase isoforms by tropolone. *J. Agric. Food Chem.* **1999,** 47, (7), 2638-2644.
40. Kim, Y.; Uyama, H., Tyrosinase inhibitors from natural and synthetic sources: structure, inhibition mechanism and perspective for the future. *Cell Mol. Life Sci.* **2005,** 62, (15), 1707-1723.
41. Saewan, N.; Koysomboon, S.; Chantrapromma, K., Anti-tyrosinase and anti-cancer activities of flavonoids from *Blumea balsamifera* DC. *J. Med. Plants Res.* **2011,** 5, (6), 1018-1024.
42. Mayer, A. M.; Harel, E., Polyphenol oxidases in plants. *Phytochemistry* **1979,** 18, (2), 193-215.
43. Kubo, I.; Nitoda, T.; Nihei, K.-i., Effects of quercetin on mushroom tyrosinase and B16-F10 melanoma cells. *Molecules* **2007,** 12, (5), 1045-56.
44. Sanchez-Ferrer, A.; Rodriguez-Lopez, J.; Garcia-Canovas, F.; Garcia-Carmona, F., Tyrosinase - a comprehensive review of its mechanism. *Bba-Protein Struct. M.* **1995,** 1247, (1), 1-11.
45. Maeda, K.; Fukuda, M., Arbutin: mechanism of its depigmenting action in human melanocyte culture. *J. Pharmacol. Exp. Ther.* **1996,** 276, (2), 765-9.

46. Tayama, K.; Takahama, M., Depigmenting Action of Phenylhydroquinone, an o-Phenylphenol Metabolite, on the Skin of JY-4 Black Guinea-Pigs. *Pigm. Cell Res.* **2002,** 15, (6), 447-453.
47. Samejima, K.; Kanazawa, K.; Ashida, H.; Danno, G., Luteolin: a strong antimutagen against dietary carcinogen, Trp-P-2, in peppermint, sage, and thyme. *J. Agr. Food Chem.* **1995,** 43, (2), 410-414.
48. Awad, H. M.; Boersma, M. G.; Boeren, S.; van der Woude, H.; van Zanden, J.; van Bladeren, P. J.; Vervoort, J.; Rietjens, I. M. C. M., Identification of o-quinone/quinone methide metabolites of quercetin in a cellular in vitro system. *Febs Lett.* **2002,** 520, (1-3), 30-34.
49. Boots, A. W.; Kubben, N.; Haenen, G. R. M. M.; Bast, A., Oxidized quercetin reacts with thiols rather than with ascorbate: implication for quercetin supplementation. *Biochem. Bioph. Res. Co.* **2003,** 308, (3), 560-565.
50. Rhee, S. G.; Chang, T.-S.; Jeong, W.; Kang, D., Methods for detection and measurement of hydrogen peroxide inside and outside of cells. *Mol. Cells* **2010,** 29, (6), 539-549.
51. Elingold, I.; Isollabella, M. P.; Casanova, M. B.; Celentano, A. M.; Pérez, C.; Cabrera, J. L.; Diez, R. A.; Dubin, M., Mitochondrial toxicity and antioxidant activity of a prenylated flavonoid isolated from Dalea elegans. *Chem. Biol. Interact.* **2008,** 171, (3), 294-305.
52. Middleton Jr, E.; Kandaswami, C.; Theoharides, T. C., The effects of plant flavonoids on mammalian cells: implications for inflammation, heart disease, and cancer. *Pharmacol. Rev.* **2000,** 52, (4), 673-751.
53. Narayana, K. R.; Reddy, M. S.; Chaluvadi, M.; Krishna, D., Bioflavonoids classification, pharmacological, biochemical effects and therapeutic potential. *Indian J. Pharmacol.* **2001,** 33, (1), 2-16.
54. Czeczot, H.; Kusztelak, J., A study of the genotoxic potential of flavonoids using short-term bacterial assays. *Acta Biochem. Pol.* **1993,** 40, 549-549.
55. Marcarini, J. C.; Tsuboy, M. S. F.; Luiz, R. C.; Ribeiro, L. R.; Hoffmann-Campo, C. B.; Mantovani, M. S., Investigation of cytotoxic, apoptosis-inducing, genotoxic and protective effects of the flavonoid rutin in HTC hepatic cells. *Exp. Toxicol. Pathol.* **2010**, 1-7.
56. Nam, T. W.; Yoo, C. I.; Kim, H. T.; Kwon, C. H.; Park, J. Y.; Kim, Y. K., The flavonoid quercetin induces apoptosis and inhibits migration through a MAPK-dependent mechanism in osteoblasts. *J. Bone Miner. Metab.* **2008,** 26, (6), 551-560.
57. Lin, Y.; Shi, R.; Wang, X.; Shen, H. M., Luteolin, a flavonoid with potentials for cancer prevention and therapy. *Curr. Cancer Drug Targets* **2008,** 8, (7), 634.
58. Yang, S. F.; Yang, W. E.; Chang, H. R.; Chu, S. C.; Hsieh, Y. S., Luteolin induces apoptosis in oral squamous cancer cells. *J. Dent. Res.* **2008,** 87, (4), 401-406.
59. Kubo, I.; Nitoda, T.; Tocoli, F. E.; Green, I. R., Multifunctional cytotoxic agents from Anacardium occidentale. *Phytother. Res.* **2010,** 25, (1), 38-45.

60. Satooka, H.; Kubo, I., Effects of Thymol on Mushroom Tyrosinase-Catalyzed Melanin Formation. *J. Agr. Food Chem.* **2011,** 59, (16), 8908-8914.
61. Rodriguez-López, J. N.; Ros-Martínez, J. R.; Varón, R.; García-Cánovas, F., Calibration of a Clark-Type oxygen electrode by tyrosinase-catalyzed oxidation of 4-tert-butylcatechol. *Anal. Biochem.* **1992,** 202, (2), 356-60.
62. Kageyama, A.; Oka, M.; Nakamura, S.; Ueyama, T.; Saito, N.; Hearing, V. J.; Ichihashi, M.; Nishigori, C., Down-regulation of Melanogenesis by Phospholipase D2 through Ubiquitin Proteasome-mediated Degradation of Tyrosinase. *J. Biol. Chem.* **2004,** 279, (26), 27774-27780.
63. Venkatasamy, R.; Faas, L.; Young, A. R.; Raman, A.; Hider, R. C., Effects of piperine analogues on stimulation of melanocyte proliferation and melanocyte differentiation. *Bioorg. Med. Chem.* **2004,** 12, (8), 1905-1920.
64. Galati, G.; Lin, A.; Sultan, A. M.; O'Brien, P. J., Cellular and in vivo hepatotoxicity caused by green tea phenolic acids and catechins. *Free Radical Biol. Med.* **2006,** 40, (4), 570-80.
65. Tsoncheva, V. L.; Milchev, G. I., Delayed reproductive death and ROS levels in the progeny of irradiated melanoma cells. *Z. Naturforsch C.* **2004,** 59, (3-4), 297-301.